Eidgenössische Technische Hochschule Zürich
Swiss Federal Institute of Technology Zurich

SED
Schweizerischer Erdbebendienst
Swiss Seismological Service

NAGRA-Net Site Characterization

Project overview

Poggi Valerio, Donat Fäh

Last modified - 26 / 12 / 2014

1. Introduction

In cooperation with the National Cooperative for the Disposal of Radioactive Waste (Nagra), the Swiss Seismological Service (SED) has recently completed the installation of ten new seismological observation stations (**Figure 1**), three of them including a co-located borehole sensor. The ultimate goal of the project is to densify the existing Swiss Digital Seismic Network (SDSNet) in Northern Switzerland, in order to increase the sensitivity to very-low magnitude events and to improve the accuracy of future location solutions. This is strategic for unbiased monitoring of micro seismicity at the places of proposed nuclear waste repositories.

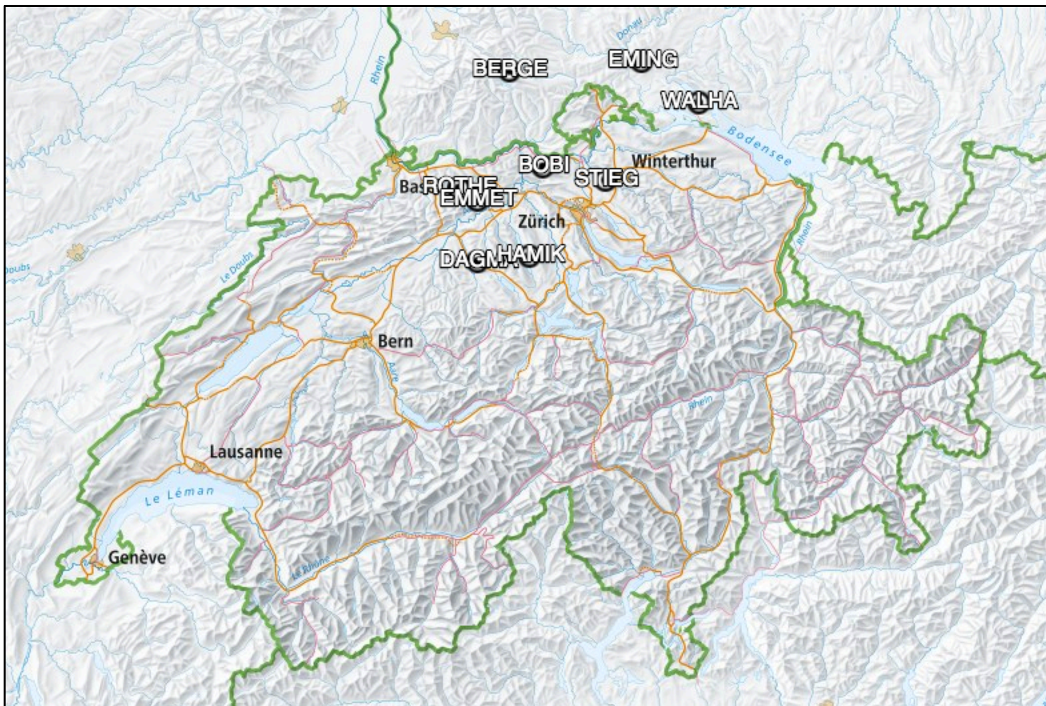

Figure 1 – *Location of the NAGRA stations characterized within the project.*

At each site, to further improve the quality and usability of the recordings, a seismic characterization of the area surrounding the installation area was performed. The investigation consisted of a preliminary geological and geotechnical study, followed by a seismic site response analysis by means of state-of-art geophysical techniques. For the borehole stations (STIEG, HAMIK and BOBI) in particular, the characterization was performed by combining different types of active seismic methods (P-S refraction tomography, surface wave analysis, Vertical Seismic Profiling - VSP) with ambient vibration based approaches (wavelet decomposition, H/V spectral ratio, polarization analysis, three-component f-k analysis). All remaining stations - with exception of station METMA - were characterized by the sole use of ambient vibration techniques.

Results of all analysis converged to the definition a mean velocity profile for the site (e.g. **Figure 2**), later used for the computation of the engineering parameters (travel time average velocity in Table 1 and quarter-wavelength parameters) and the analytical SH-wave transfer function. For each characterized station a summary report is provided, describing the main characteristics of the sites, the performed surveys, analysis results and final interpretations.

	Averaging Depth (m)							
	5	**10**	**20**	**30**	**40**	**50**	**100**	**200**
STIEG	229.55	292.77	382.21	453.01	500.99	556.49	786.21	1105.71
BERGE	1356.45	1416.48	1514.8	1703.22	1833.41	1939.84	2204.53	2371.5
DAGMA	701.25	729.08	823.92	913.7	982.23	1051.84	1263.87	1515.05
METMA	336.62	442.72	640.81	817.94	969.04	1098.2	1602.18	2124.63
ROTHE	611.92	665.97	843.89	954.4	1024.6	1074.3	1202.77	1294.47
HAMIK	238.33	314.41	407.08	487.58	552.09	616.4	834.86	1060.17
BOBI	279.96	350.94	486.23	590.02	668.27	736	955.85	1212.99
WALHA	397.93	464.16	642.18	766.06	851.3	933.78	1165.62	1380.97
EMING	220.99	306.21	489.82	659.08	803.27	932	1392.32	1895.09
EMMET	468.12	571.58	672.68	800.73	892.53	960.55	1140.8	1316.13

Table 1 – *Summary of average travel-time velocities at different depths for all the investigated NAGRA stations. Vs30 is highlighted.*

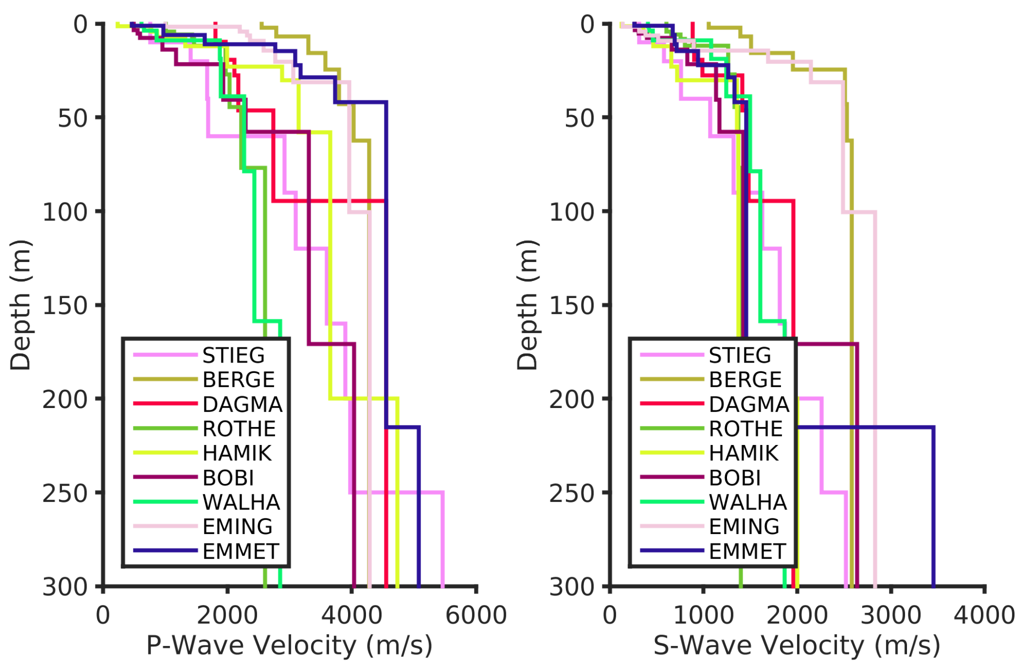

Figure 2 – *Summary of P- and S-wave profiles of all NAGRA stations investigated using ambient vibration analysis.*

REPORTS

Eidgenössische Technische Hochschule Zürich
Swiss Federal Institute of Technology Zurich

SED
Schweizerischer Erdbebendienst
Swiss Seismological Service

Report on site characterization

Stiegenhof, Switzerland (STIEG)

Poggi Valerio, Clotaire Michel, Donat Fäh

Last modified - 24 / 12 / 2014

1. Introduction

In the framework of the NAGRA seismic network project, an array measurement of the ambient vibration wave-field was performed on 24/01/2013 at the location of the SED borehole station STIEG (Stiegenhof, Oberembrach). The scope of the survey is the seismic characterization of the area surrounding the installation, which consists in a short-period borehole sensor at about 100m depth, with a collocated strong motion sensor at the surface. Ambient vibration analysis has been used to infer the characteristics of the underground structure of the site, with special regard to the shear-wave velocity at the site. Such profile was later compared with the results from active seismic measurements and used to assess the local seismic response of the station.

For the analysis, different spectral analysis techniques were implemented, consisting in both single and array methods which are listed below:

- Time-frequency wavelet analysis
- Power-spectral density estimation
- Conventional horizontal to vertical spectral ratios
- Directional horizontal to vertical spectral ratios
- Wavelet polarization analysis
- Three-component high-resolution f-k analysis.

In the following, the main results of these investigations are summarized and a final interpretation of the velocity profile is given. From this interpretation, engineering parameters are finally derived, e.g. the Qwl-Vs average velocity, VsZ (including Vs30) and the seismic amplification from the analytical SH-transfer function of the one-dimensional soil column.

2. Survey description

To characterize the seismic response of the site, an array measurement of ambient vibration has been performed (**Figure 1**). The array consisted in two measuring configurations (A and B) of 14 sensors each and different diameters of 100m and 200m respectively. The two configurations were planned to partially overlap, by sharing 9 common sensors, with the aim of providing a continuous resolution of the frequency range between the two geometries. Configuration A recorded for a total of 1h40m, while configuration B for 2h15m. The differences in the recording length are due to the different resolution characteristics of the two geometries. As a general rule, larger arrays require longer recording time to produce a reasonable statistics of the ambient vibration processing results. For the larger configuration, a penetration depth of 80-100m was expected.

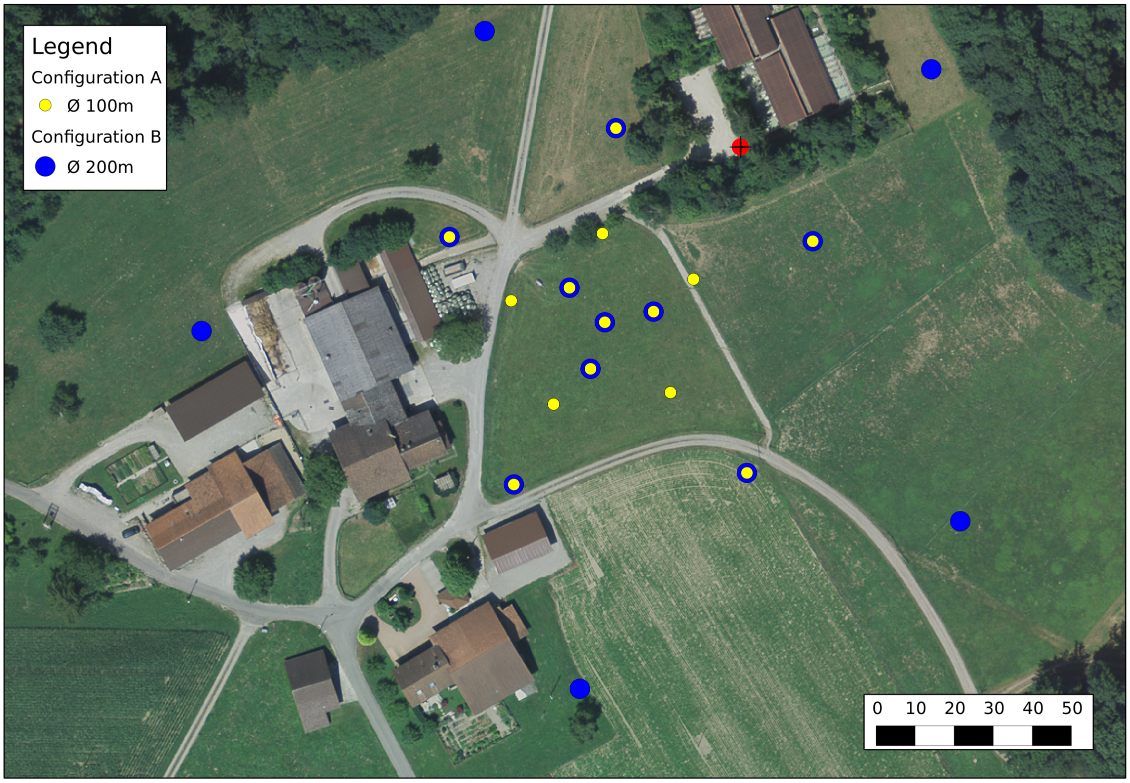

Figure 1 - *Geometry of the ambient vibration arrays in Stiegenhof (SED station STIEG). Two concentric configurations of increasing diameter were used. The borehole station location is shown in red.*

3. Soil type, topography and geology

The array has been set in open field conditions, in a rural area (**Figure 1**). Influence of buildings and anthropogenic disturbances is virtually negligible. Sensors have been mostly deployed on free soil conditions. Good coupling with the ground was assured by means of digging small holes at the sensor's places, and by using a special support (Trihedron) that facilitates the leveled accommodation of the device even in difficult soil conditions. The measurement area is located on a gentle slope toward southeast. However, no topographic correction has been accounted before processing.

From the geological points of view (**Figure 2**), the target area is located within the Molasse basin, surrounded by few moranic deposits, clearly identifiable from the surface topography. The bedrock probably consists of siltstone and marl, with intercalations of some under-consolidated sandstone and occasionally conglomerates. The site can be geotechnically classified as of rock ground-type A. The drilling log report of the borehole can be found in the appendix.

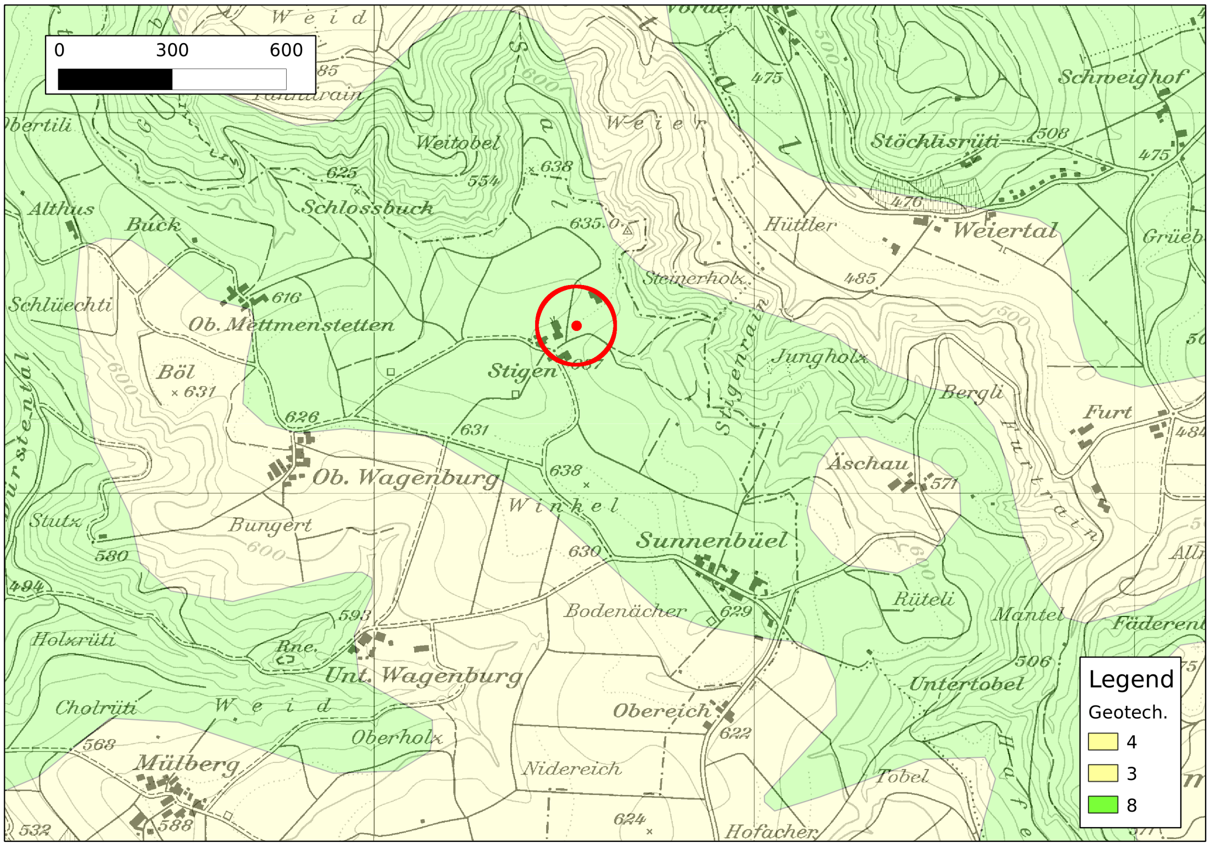

Figure 2 - *Geological map of the area of the array measurement in Stiegenhof (Legend: 3, morain; 4, fluvio-lacustrine deposits; 8, marl and conglomerates; from SWISSTOPO).*

4. Acquisition equipment

Each acquisition point within the array consisted of a three components seismometer (Lennarz 3C with 5s eigenperiod, **Figure 3**) and a 24 bit data logger (Quanterra Q330). Synchronization between stations was assured by standard GPS, while a more accurate differential GPS (Leica Viva system) was used to precisely locate the sensor's coordinates with a tolerance of less than 5cm.

5. Weather conditions

The weather conditions were stable during the whole measurement, with no precipitations and an average (over the whole day) temperature of -2 degrees. It has to be notice the presence of few centimeters of frozen snow on the ground. The cold temperature and the snow cover may be considered an advantage in this case, due to the increase in the stiffness of the soil's top cover, which consequently improves the coupling between sensors and ground.

Figure 3 - *Single acquisition point of the array, consisting in a Q330 datalogger (gray box on the right) and a Lennartz 5s velocity seismometer (blue, on the left). The coupling of the sensor is assured by removing the uppermost part of the frozen soil and by means of a special support (Trihedron).*

6. Pre-processing and preliminary data-quality control

The three-component recording has been filtered prior to analysis using a high-pass 6^{th} order causal Butterworth filter with corner at 0.2Hz. Although it is not a strict requirement for spectral analysis techniques, such filtering was applied in order to facilitate the preliminary visual inspection of the noise traces (**Figure 4**).

To assess the quality of the ambient vibration recordings, spectral analysis has then to be performed. Because of the stochastic nature of the ambient vibration wave-field, a statistical approach has to be used, such as the estimation of the power spectral density (*PSD*). This approach is useful to evaluate the average energy level of the recordings in the analyzed frequency range, and to access the presence of spurious spectral peaks, which might be related to human activity (machinery, pumps). By inspecting the PSD of the three-component recordings at the central station (e.g. **Figure 5**), no relevant spurious peak is visible in the range between 0.5 and 40Hz. The average noise level is quite low and within the minimum and maximum bounds of the USGS noise model.

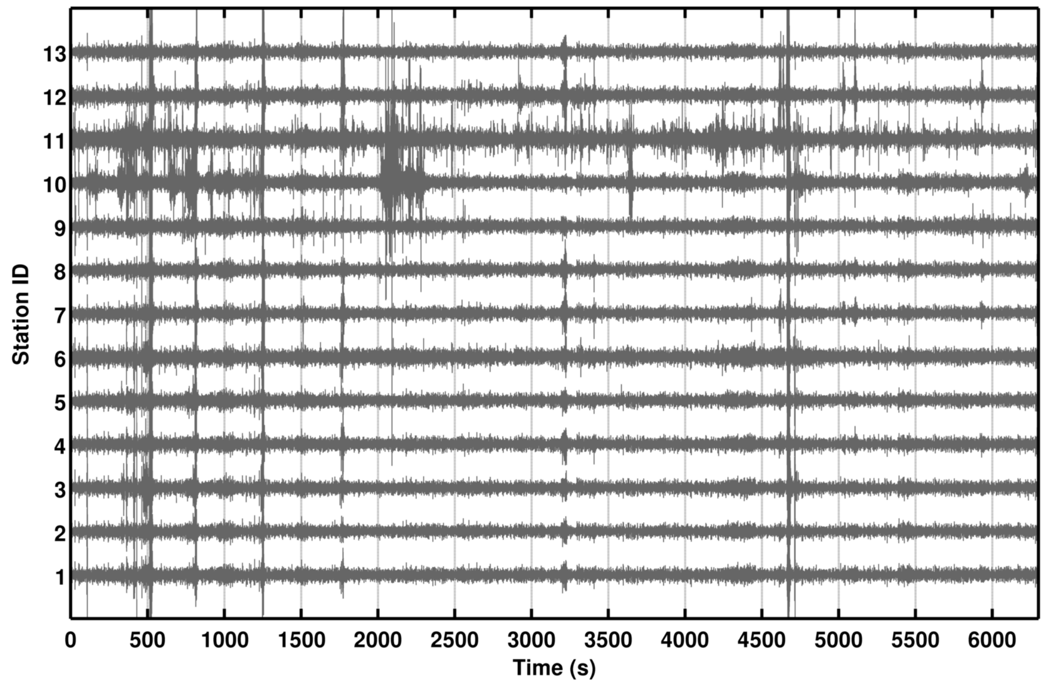

Figure 4 - *Inspection of the useful part of the ambient vibration recording of the array STIEG (configuration A). Several impulsive high-frequency transients of anthropogenic origin (usually > 40Hz) are visible, but the overall quality of the recording is good.*

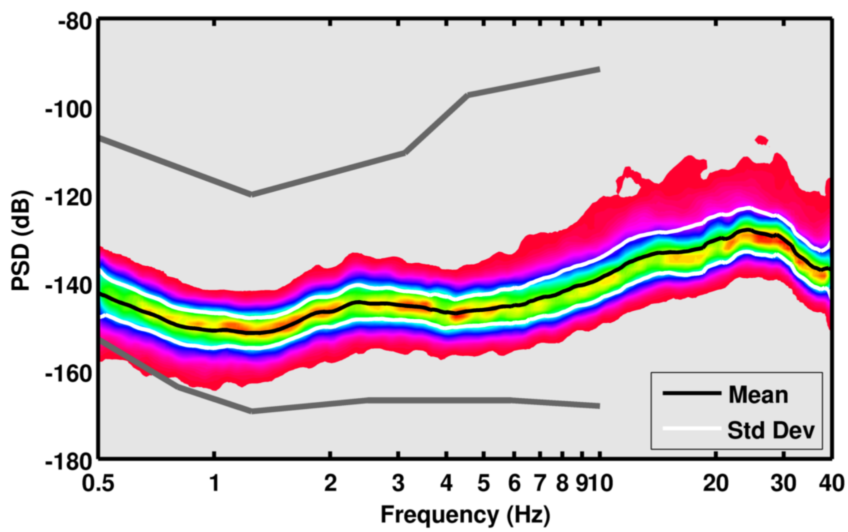

Figure 5 - *Power spectral density (PSD) computed for 1h recording at the central station of the array (here the vertical component is presented). In gray are the minimum and the maximum bounds of the USGS noise model, for comparison.*

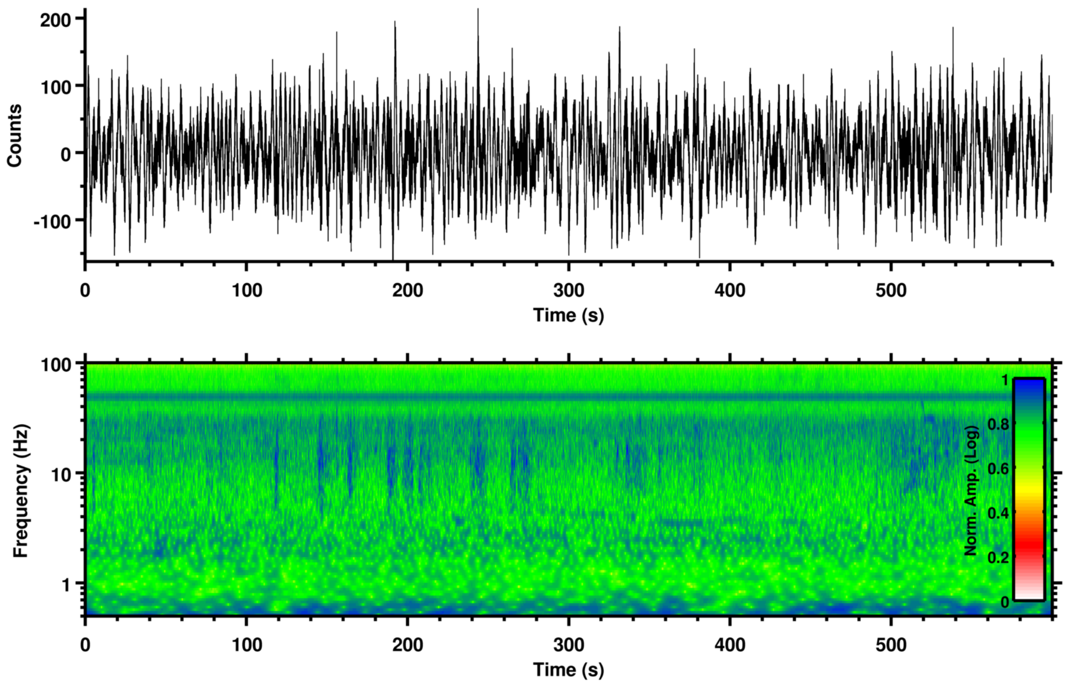

Figure 6 - *Example of spectrogram from 600s of recording of the array central station (A1, vertical component). For the analysis, the cosine wavelet is used (wavelet parameter = 12).*

Complementary to statistical methods, then, a spectral decomposition approach is more suitable to assess the stationarity of the ambient vibration wave-field over time. The wavelet time-frequency analysis was then performed over the whole recording time. From such analysis (**Figure 6**) an overall stability of the ambient-vibration wave-field over time is evident. The only clear disturbance is the 50Hz signal from the electric power line, which is nevertheless not an issue because of the frequency outside the range of interest, and its narrow and well-defined localization in the spectrum.

7. Conventional H/V spectral ratios

The horizontal-to-vertical (H/V) Fourier spectral ratio is a technique widely used in seismic site characterization because of its ability to provide an estimate of the SH wave fundamental frequency of resonance (f_0) of the site. Other than that, H/V ratios are useful to provide information on the Rayleigh wave ellipticity function, which is used in the inversion procedure to constrain the major velocity contrasts at depth. In this study, we use the technique also to map the variability of the subsoil structure along the investigated area; this is necessary to verify the fulfillment of the 1D structure assumption, which is necessary for the f-k method applied later.

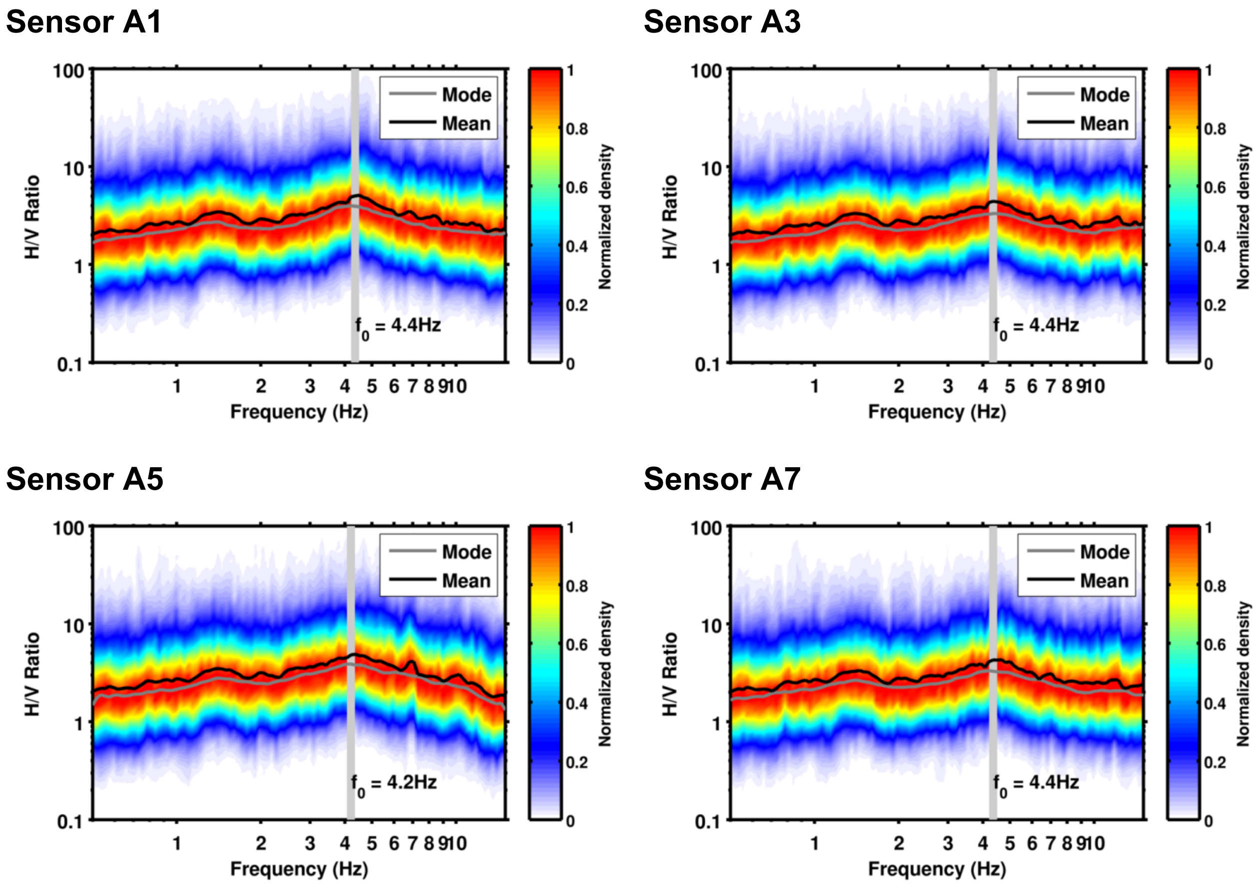

Figure 7 - *Example of H/V spectral ratios at four stations of the array configuration A. The picked fundamental frequency is indicated with a light gray line.*

H/V spectral ratios have been computed for the recordings at each station of the two array configurations (e.g. **Figure 7**). The behavior of the noise wave-field at the different stations location is comparable (**Figure 8**). For the first ring, no strong variation of the fundamental frequency is observed across the area, with an average value of about 4.4Hz. Also the shape of the spectral ratios is very similar, with the only exception of the station A13 (from the external border) that shows a slight decrease in the spectral amplitude below f_0. This can be due to a small change of the velocity in the deeper part of the profile toward south-west. The second ring provides similar results, even if the fundamental frequency is less precisely localized at 4.4Hz, and a small amplitude peak is visible at 1.2Hz. The behavior of the site can be considered laterally homogeneous for the f-k analysis.

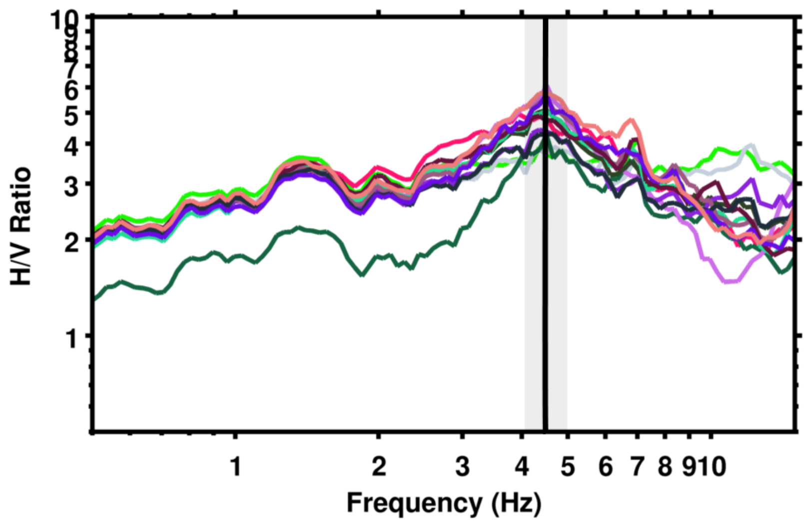

Figure 8 - *Comparison of the H/V spectral ratio curves of all the stations of the array configuration A. Only one station (A13) shows a different behavior at low frequencies, while the fundamental frequency does not change.*

8. Direction H/V spectral ratios

The computation of directional H/V spectral ratios is useful to reveal asymmetries in the ambient vibration wave-field. Such a behavior can be induced by several reasons: 2D/3D structure, topographic effects or a not homogeneous distribution of the noise sources. If a strong directionality is found by the analysis, it is generally recommended to carry out further investigations to properly address the origin of polarization.

By processing the directional H/Vs at all the recording stations of the array (e.g. **Figure 9**) it is possible to observe a very small directionality of the main resonance peak at 4.4Hz. The observed direction is rather stable over the whole array, at about 160°N. Considering that this effect is mostly visible at f_0, we interpret it as an influence of the topographic slope or a small 3D effect. A non-homogenous distribution of the noise sources should be excluded, even if such interpretation has to be validated by the subsequent results of the f-k analysis.

The result of the directional analysis is also confirmed by applying the wavelet polarization analysis techniques as described in Burjanek et al. (2008) to the central station of the array. Also in this case the fundamental frequency shows a moderate directionality (**Figure 10**a), but not a significant polarization (**Figure 10**b).

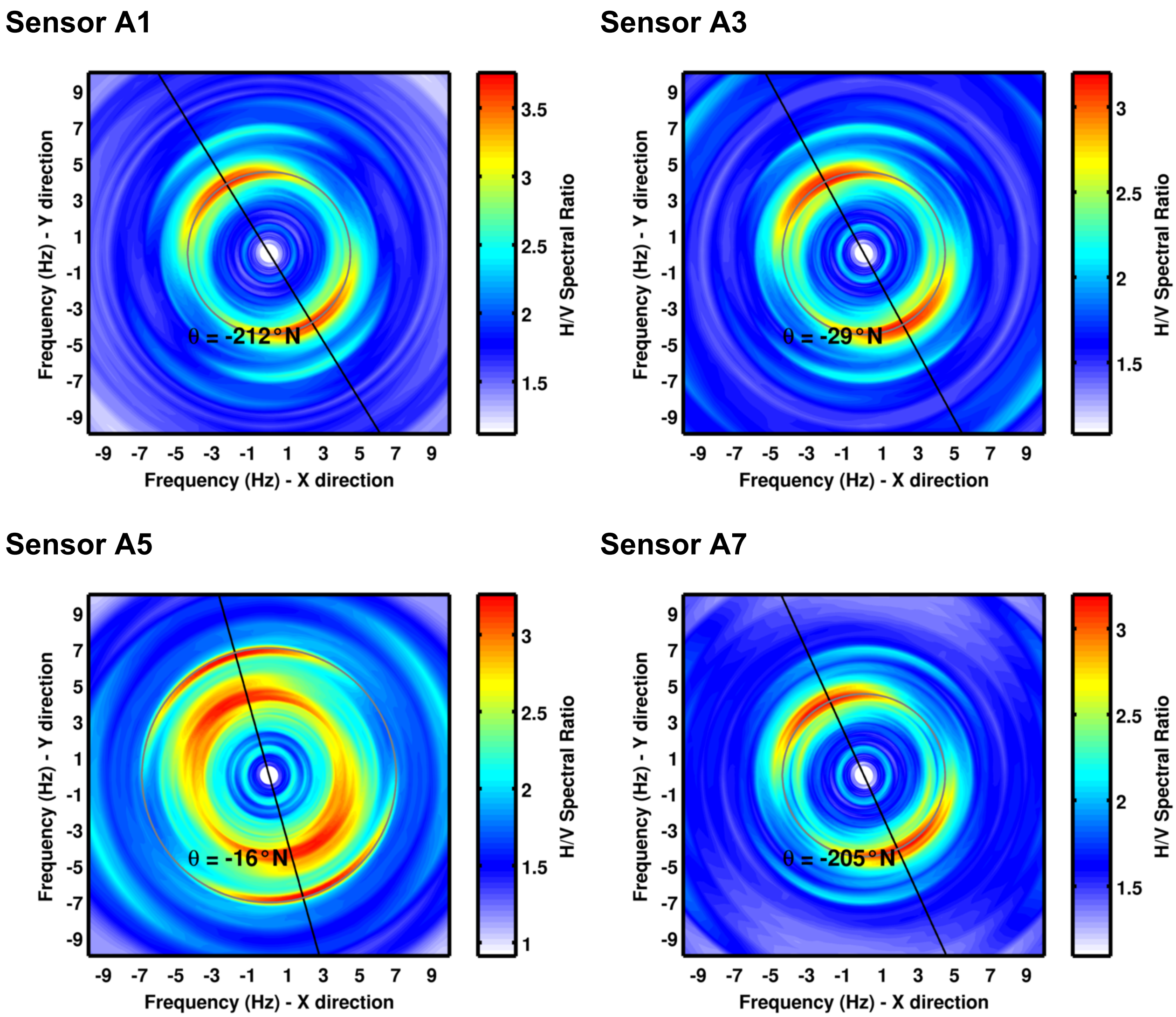

Figure 9 - *Example of directional H/V spectral ratios at four stations of the array configuration A. The fundamental frequency shows some very small directionality effect along NNW-SSE. This might be related to the moderate topography slope.*

a)

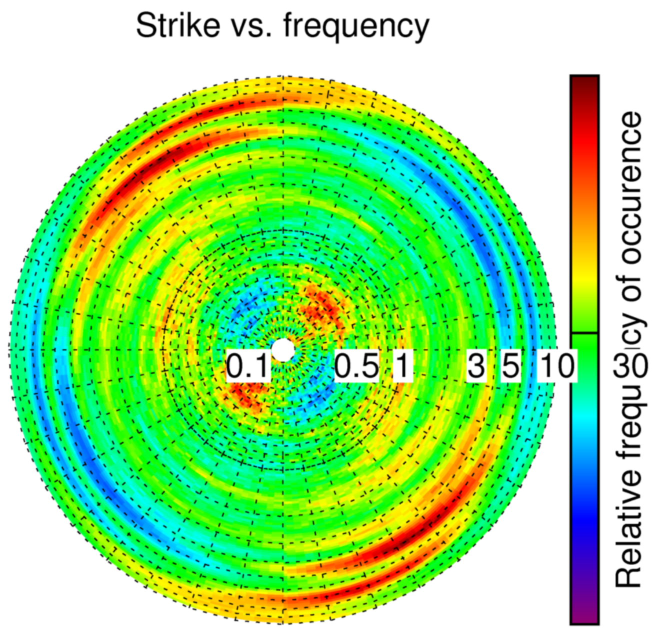

b)

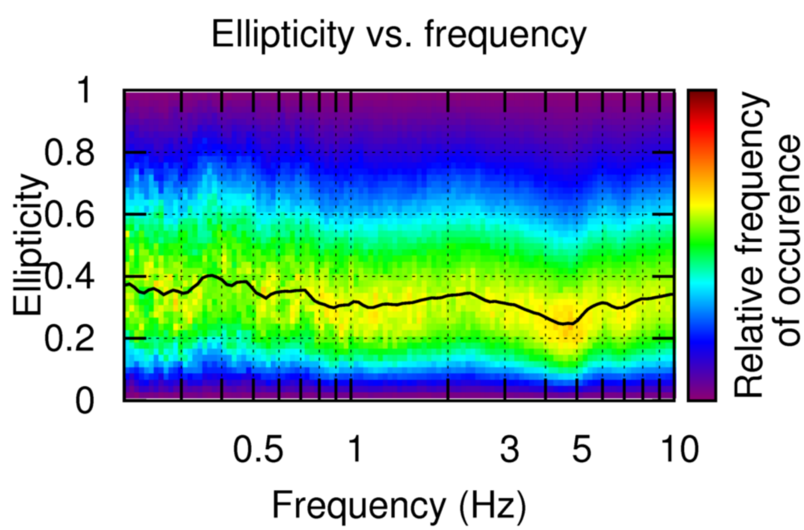

Figure 10 - *Wavelet-based polarization analysis at the central station of the array. By analyzing the polarization over strike (a) and the particle motion ellipticity plot (b), only a moderate directional effect is visible at the resonance frequency.*

9. Three-component f-k analysis

The frequency-wavenumber analysis is a spectral technique based on seismic array recordings that allows retrieving the direction and the dispersion characteristics of the surface wave-field. We apply here this technique to three-component ambient vibration recordings using a modification of the high-resolution method of Capon (1969) as described in Poggi et al. (2010). Using all the three-components of motion gives the possibility to retrieve information about the propagation of the Rayleigh waves (vertical and radial processing direction) as well as of the Love waves (transversal direction).

As in the case of the previous methods, the ambient vibration recordings are treated statistically by subdividing the traces in sub-windows. For each consecutive window a separated f-k analysis is performed, and the results are then averaged over the whole recording, to strength the robustness of the final estimation.

a) 4.4 Hz (Resonance frequency)

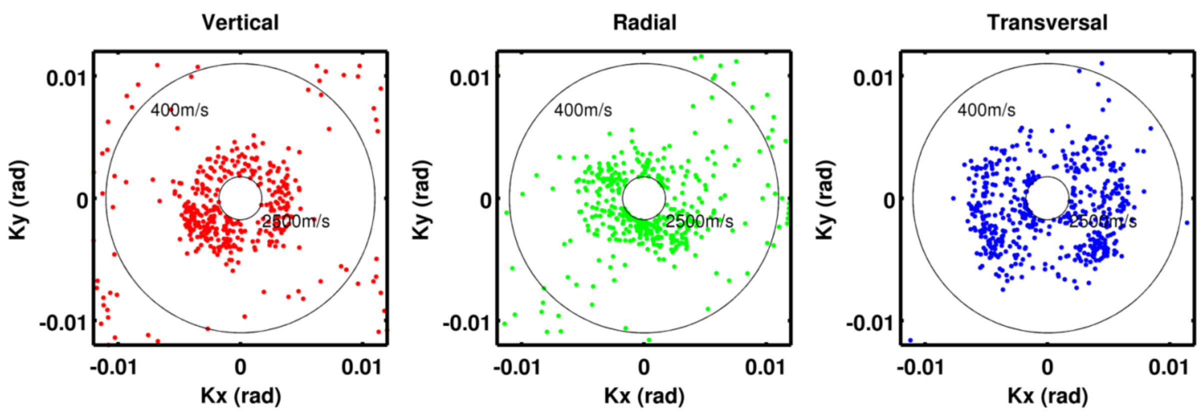

b) 6 Hz

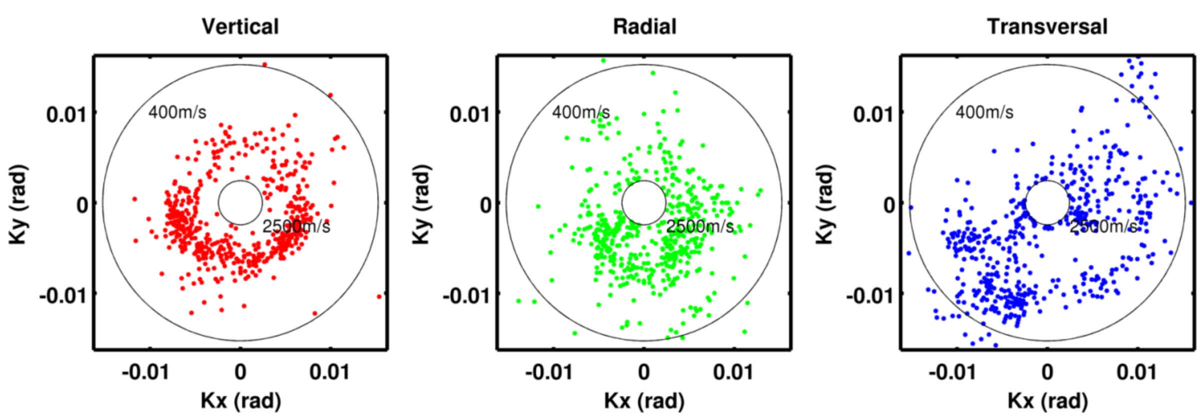

Figure 11 - *Example of distribution of noise sources at 6Hz over the three components of the f-k analysis (here for array configuration B). Distribution is homogeneous for the vertical and radial directions, with only some moderate directionality on the transversal direction at 6Hz.*

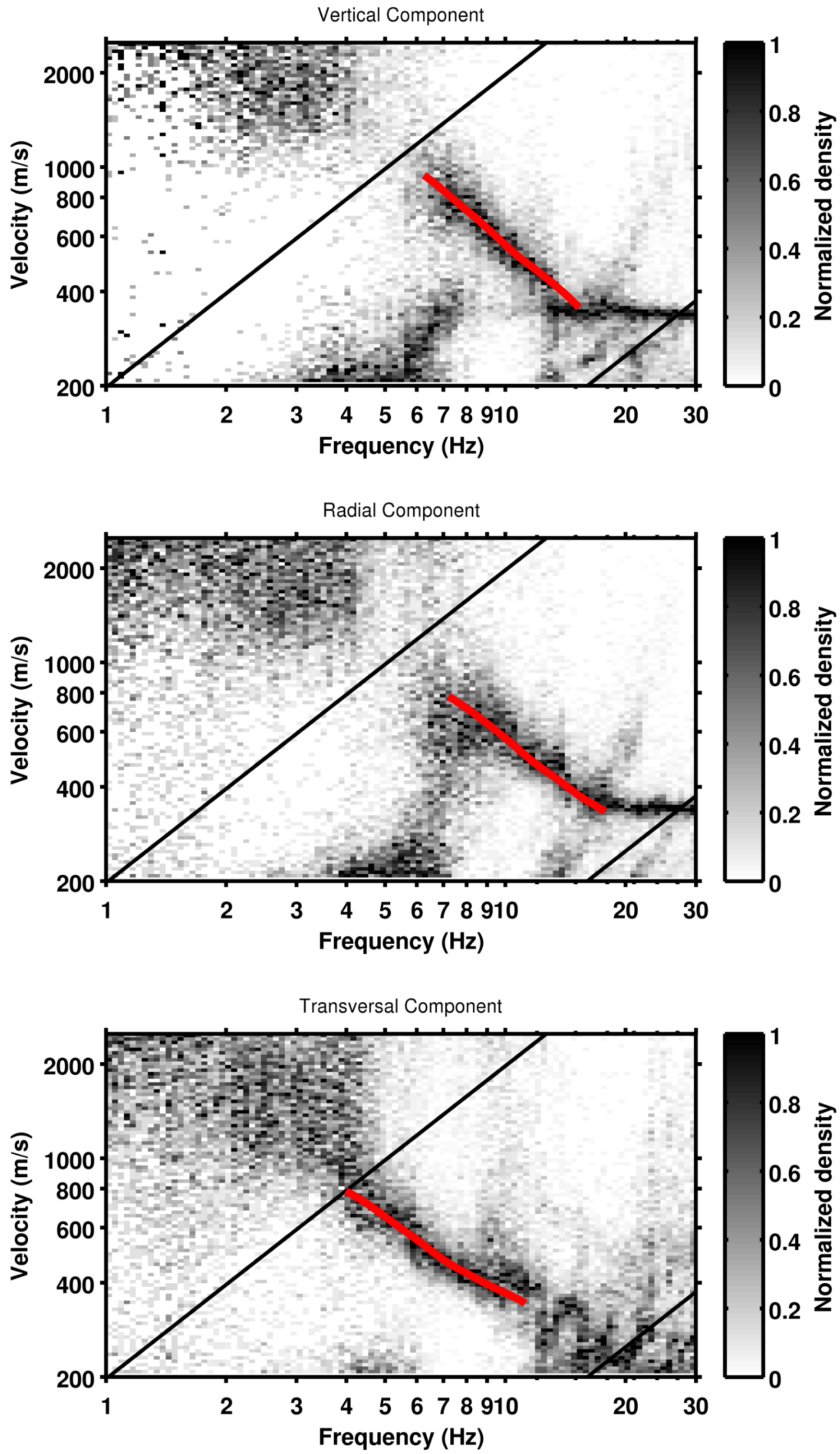

Figure 12 - *Density distribution of all the surface wave signals obtained from the whole recording of array configuration A using f-k analysis. In red is the interpreted dispersion curve (manually selected).*

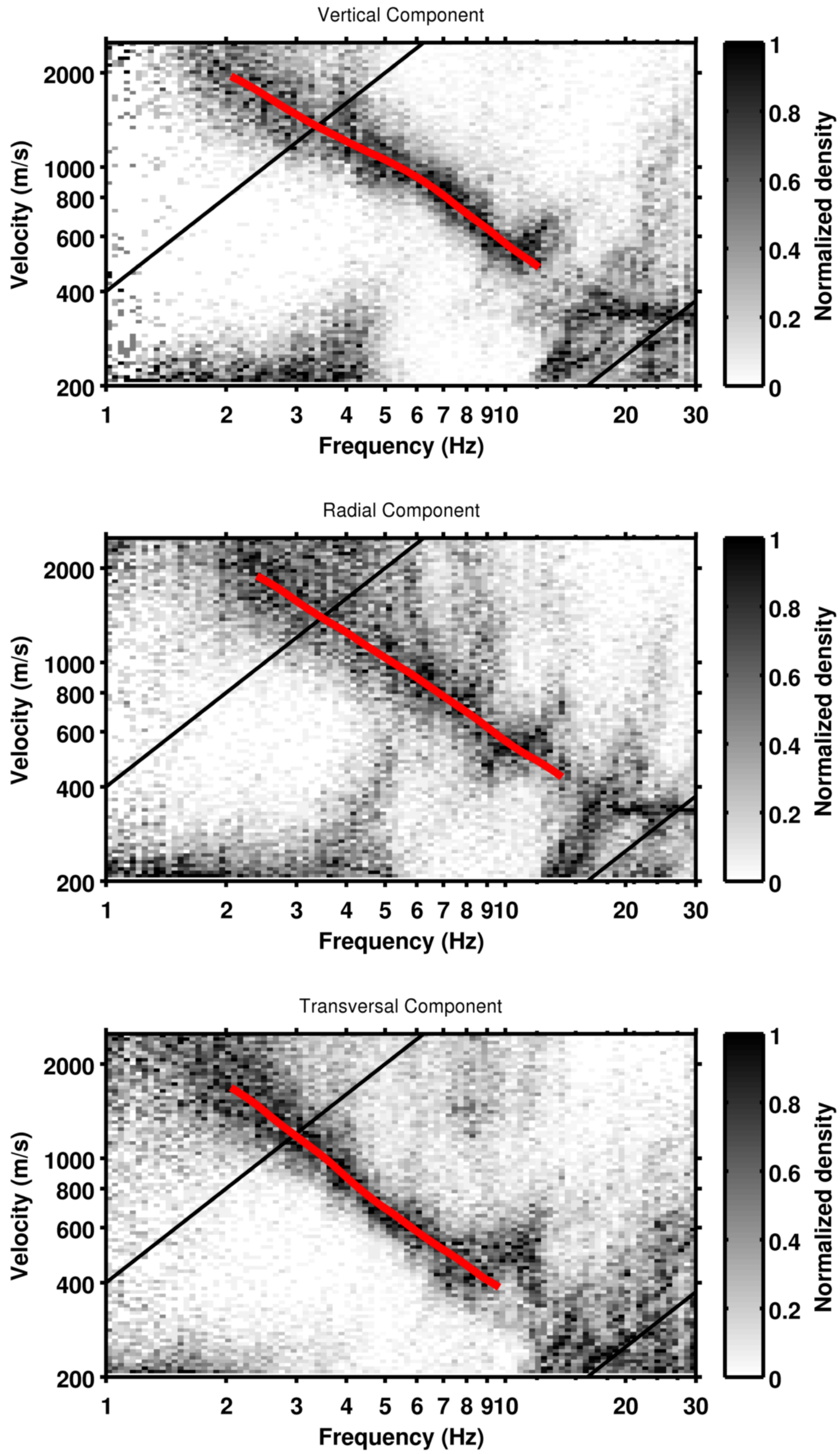

Figure 13 - *Density distribution of all the surface wave signals obtained from the whole recording of array configuration B using f-k analysis. In red is the interpreted dispersion curve (manually selected).*

As first step, from the f-k analysis it was possible to assess the noise source distribution over broad range of analyzed frequencies (e.g. **Figure 11**) for the vertical, the radial and the transversal component. A rather uniform (isotropic) distribution is observed, and particularly at f_0, confirming then the independency of the noise source distribution to the directional behavior observed in the H/V spectral ratio. Subsequently, the surface wave dispersion curves have been extracted by visual inspection and manual picking of the f-k density plots (**Figure 12** and **Figure 13**). It has to be noticed that the two array configurations provided comparable results, but in different frequency bands (which is consequence of the array geometry), which are nevertheless overlapping. The final interpretation of the modal dispersion pattern is presented in **Figure 14** for both the Rayleigh and Love waves.

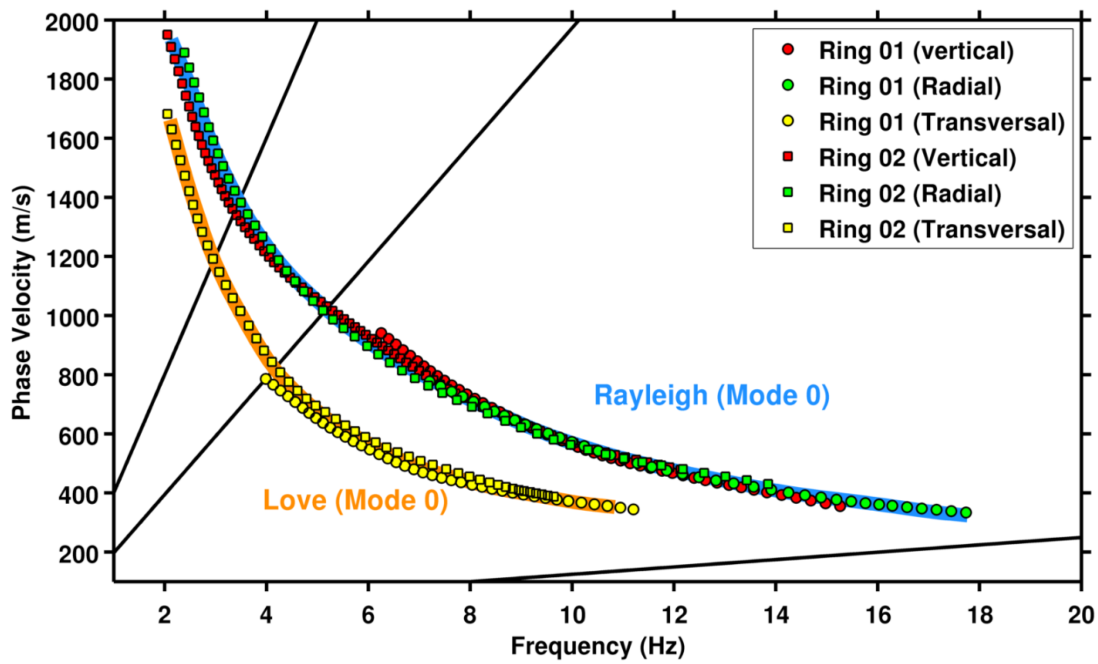

Figure 14 - *Final interpretation of the Rayleigh and Love dispersion modal pattern from the two concentric array configurations.*

10. Inversion of the dispersion curves

The surface wave dispersion curves (Rayleigh and Love) obtained from the three-component f-k analysis of the ambient vibrations were inverted to obtain an estimation of the velocity profile of the site (mainly S-wave velocity as function of depth, and to a lesser extend the P-wave velocity, due to the lower sensitivity). The analysis was performed using the software *Dinver* (www.geopsy.org), which implements a direct search approach (**Figure 15**) based on a conditional version of the neighborhood algorithm (Sambridge 1999).

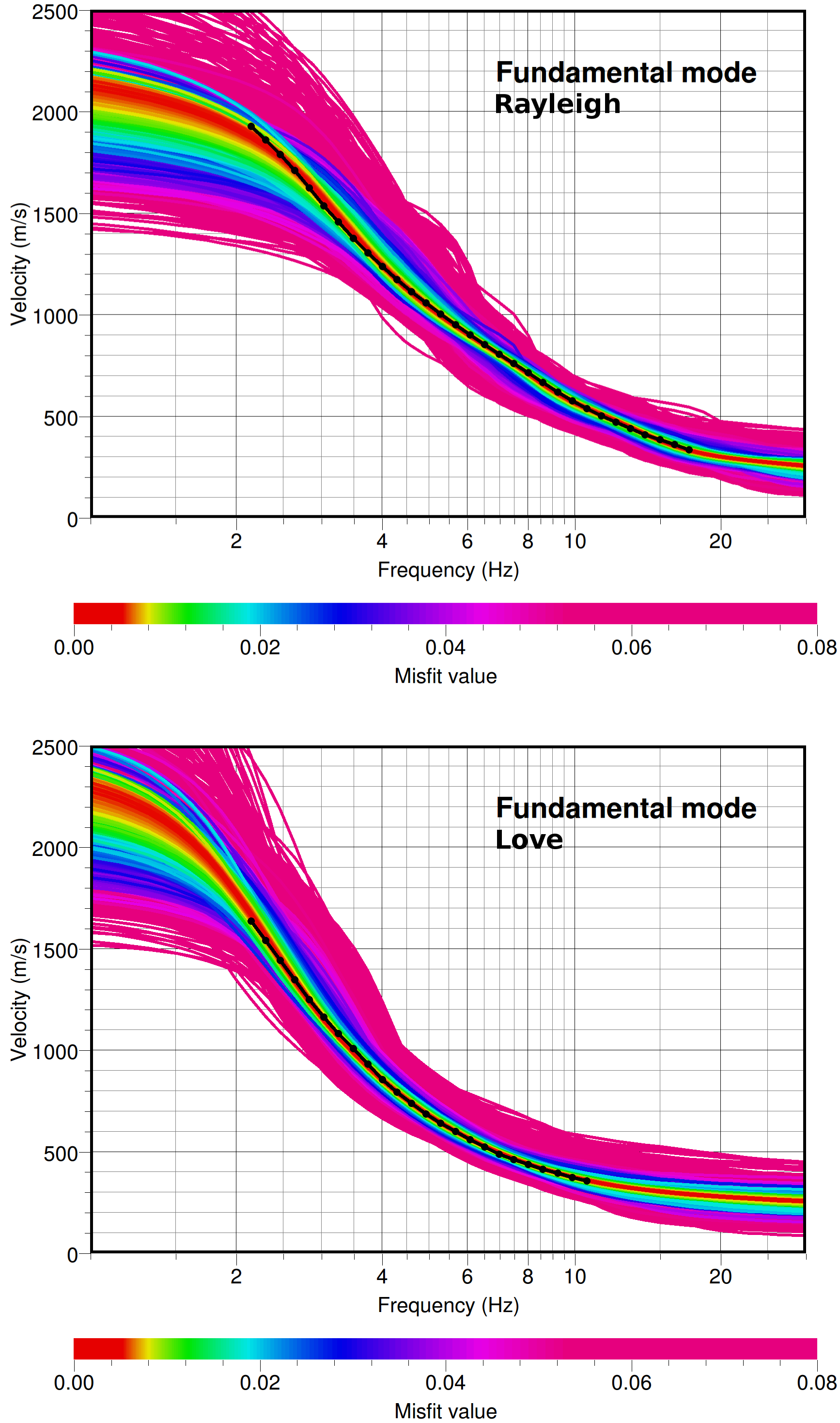

Figure 15 - *Fitting the surface dispersion data within the global optimization procedure. Different colors represent different misfit between the observed (in black) and the modeled dispersion curves.*

Together with the dispersion curves, the fundamental frequency of the Rayleigh-wave ellipticity function obtained from the H/V spectral ratio was used as constraint for the inversion. Using such additional information is advantageous to improve the resolution on the larger velocity interfaces of the model. To parameterize the velocity model, two different approaches were implemented. The first one consisted in setting up an eight-layer model with free interface depths (**Figure 16**). In such a case the free inversion parameters are then the velocities (P and S) and layer thicknesses. In the second case, a fixed-thickness layer approach was used (**Figure 17**). The advantage of the former method stays in the possibility to better resolve sharp velocity interfaces, while the second is less unique and better constraints the seismic velocity. The two approaches have to be nevertheless considered complementary, and they should provide consistent results.

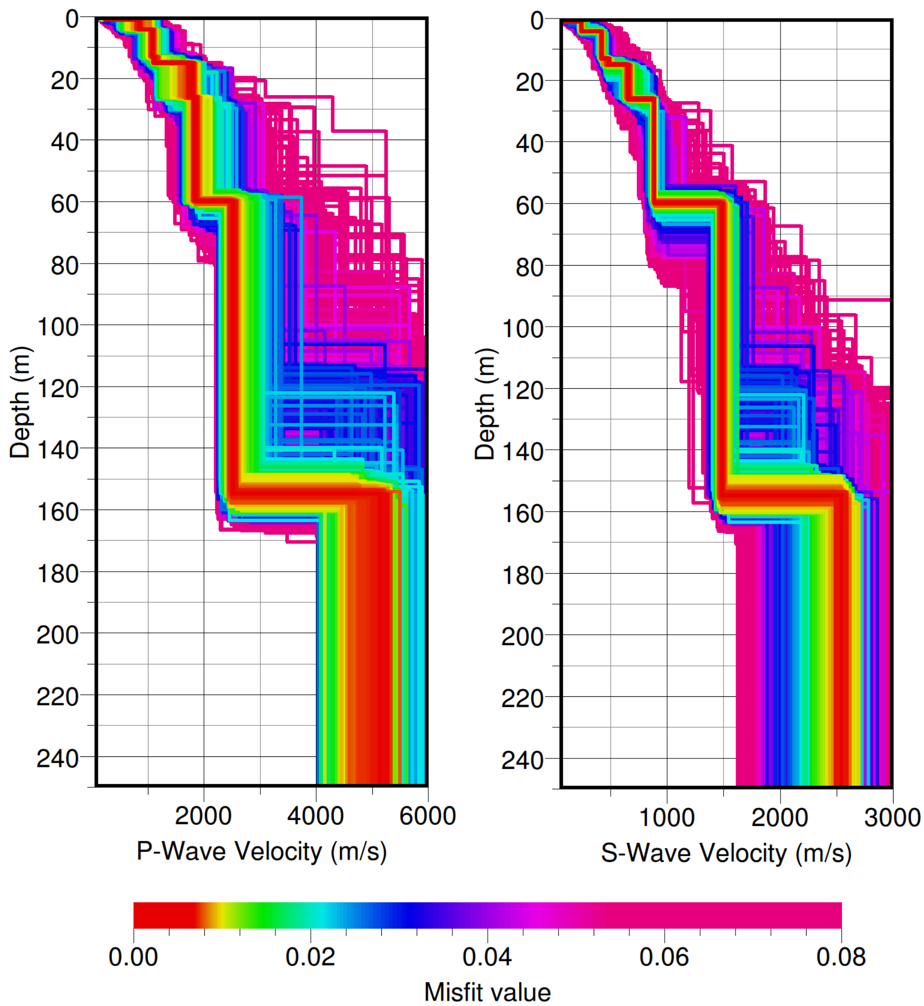

Figure 16 - *Distribution of the free-layer velocity models generated during the inversion process and ordered by decreasing misfit, according to the color scheme of* **Figure 15**.

Eight inversion tests (*runs*) have been performed for each of the two model schemes (**Figure 18**). This in order to minimize the effect related to a possible unfavorable initial randomization of the space parameter. The best fitting models from of each run are then collected and used later on for the computation of the derived soil parameters.

The inverted velocity models (Vs and Vp) are gradient like, with a faster increase in velocity in the first 10~20m, followed by a more smoothed part. This is expected for a rock velocity profile. By considering the minimum available frequency of the surface-wave dispersion curves, and by analyzing the scattering of the inverted models (**Figure 19**), it is realistic to assume the velocity profiles to be reliable down to a depth of about 100~120m. Below this value no direct constrain is available, and the velocity are obtained by pure extrapolation.

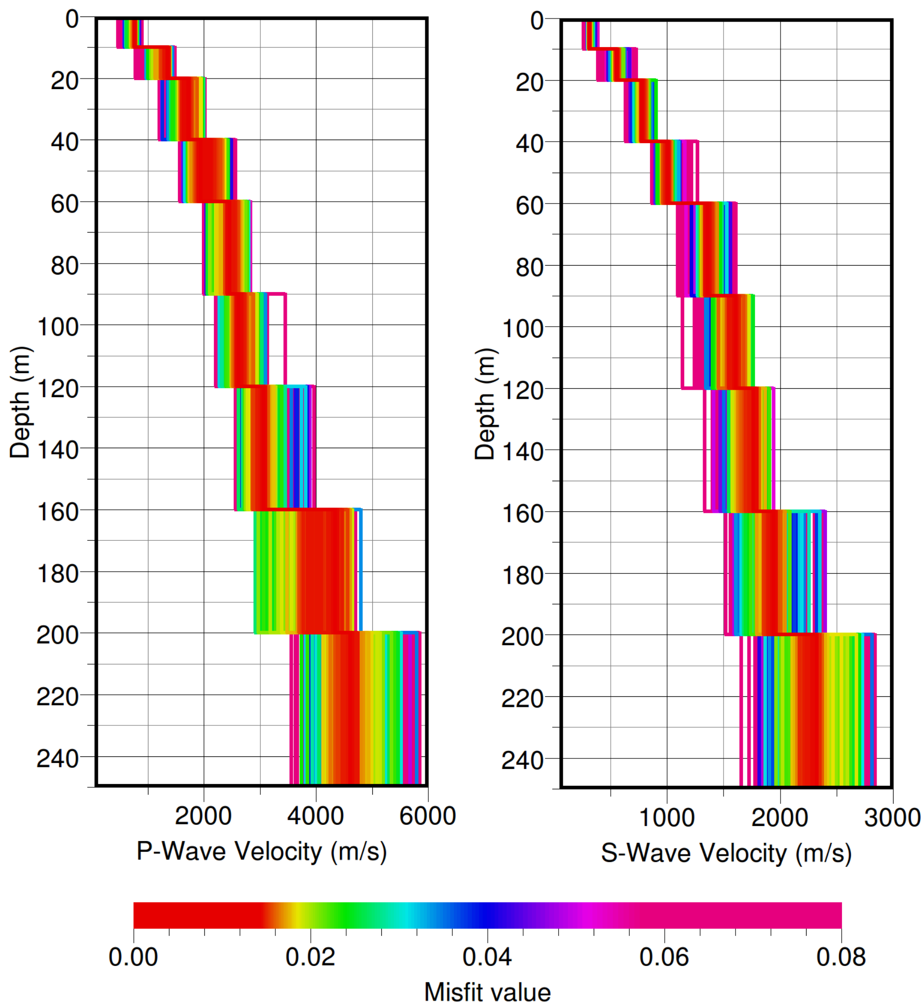

Figure 17 - *Distribution of the fix-layer velocity models generated during the inversion process, and ordered by decreasing misfit according to the color scheme of* **Figure 15**.

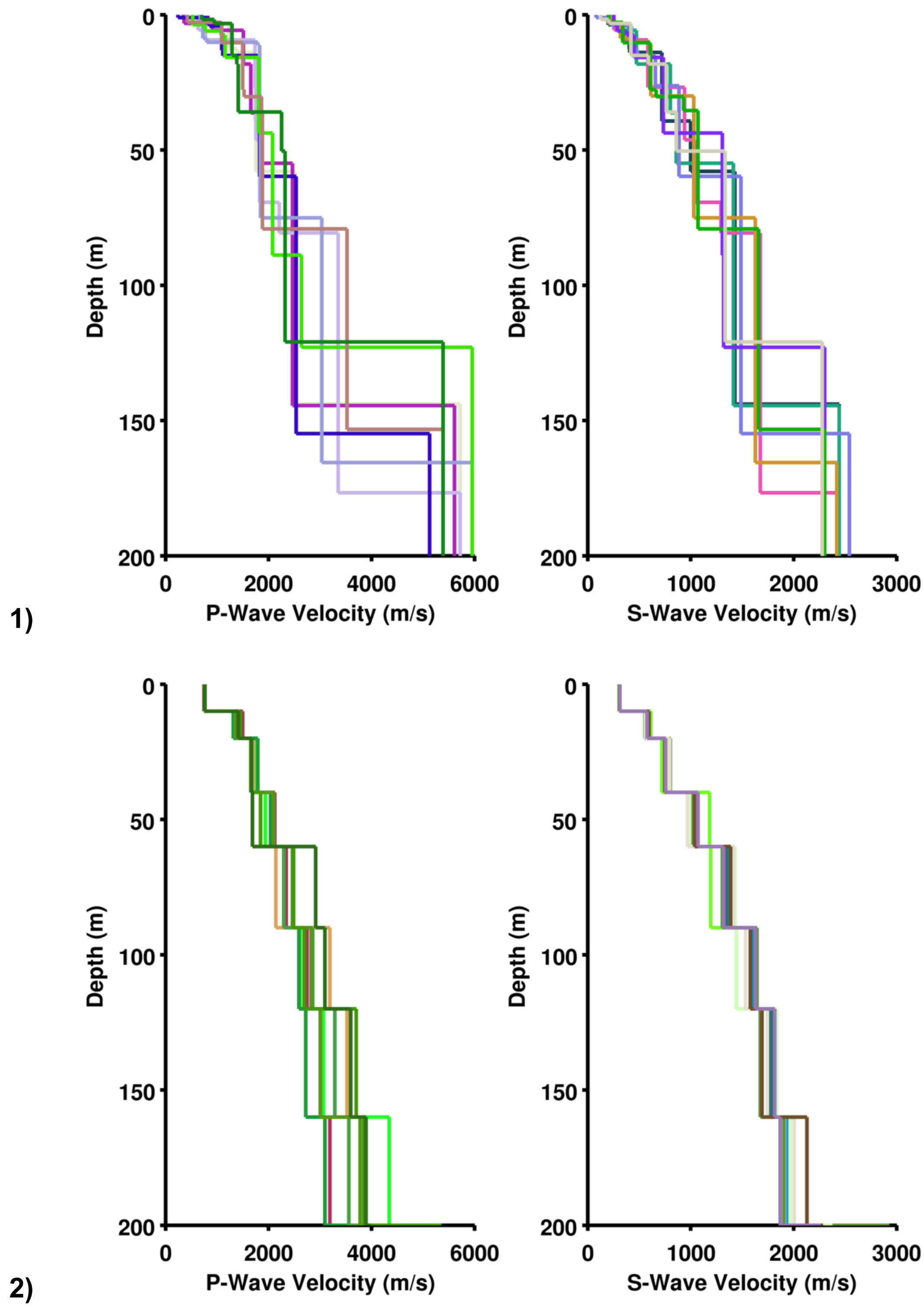

Figure 18 - *Collecting the best fitting models from the eight separated inversion runs using the free-layers (1) and fixed-layers (2) parameterization schemes.*

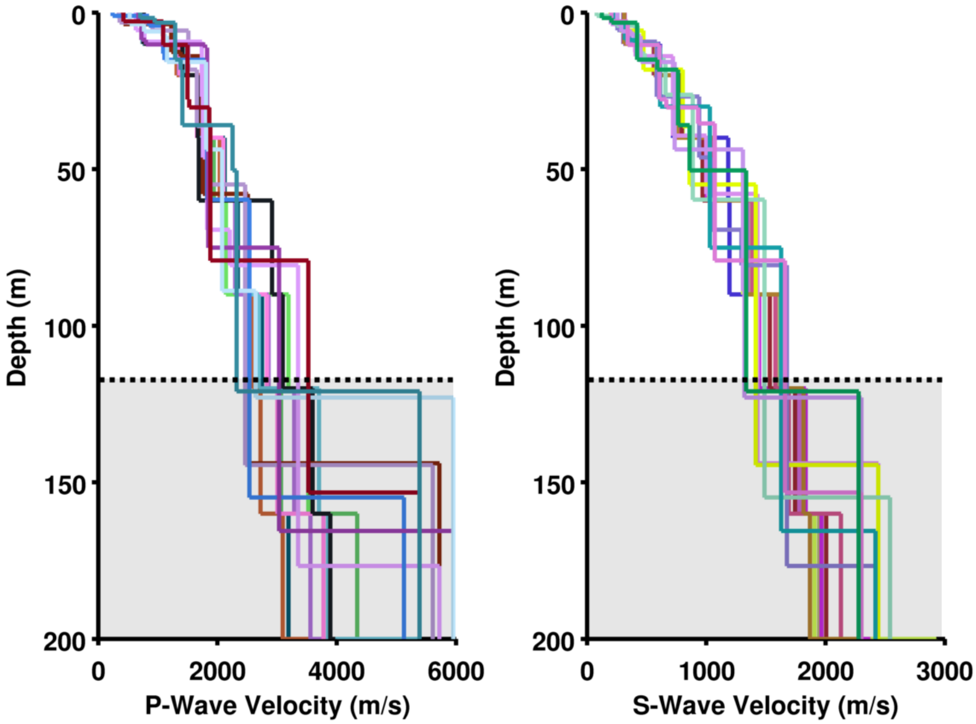

Figure 19 - *Comparison of all the best models from the two parameterization schemes (free and fixed layers). The two approaches are consistent down to a depth of about 100~120m, which can be considered the maximum resolved depth.*

11. Engineering soil parameters

The ensemble of all the best inverted velocity profiles is then used to derive average soil parameters like the VsZ (average travel-time S-wave velocity over the depth Z, including Vs30, Table 1) and the quarter-wavelength (QWL) average velocities (Joyner et al., 1984) for a range of frequencies between 0.8 and 15Hz (**Figure 20**). The former is a standard parameter for the classification of ground-types in most building codes and in ground motion prediction equations. The latter is a parameter useful for the empirical estimation of the site-response and to assess the sensitivity of the seismic wave-field to the different depths. It has to be noticed that these two parameters are derived separately from all the best S-wave velocity models obtained from the inversion, and the results is finally averaged to improve statistics.

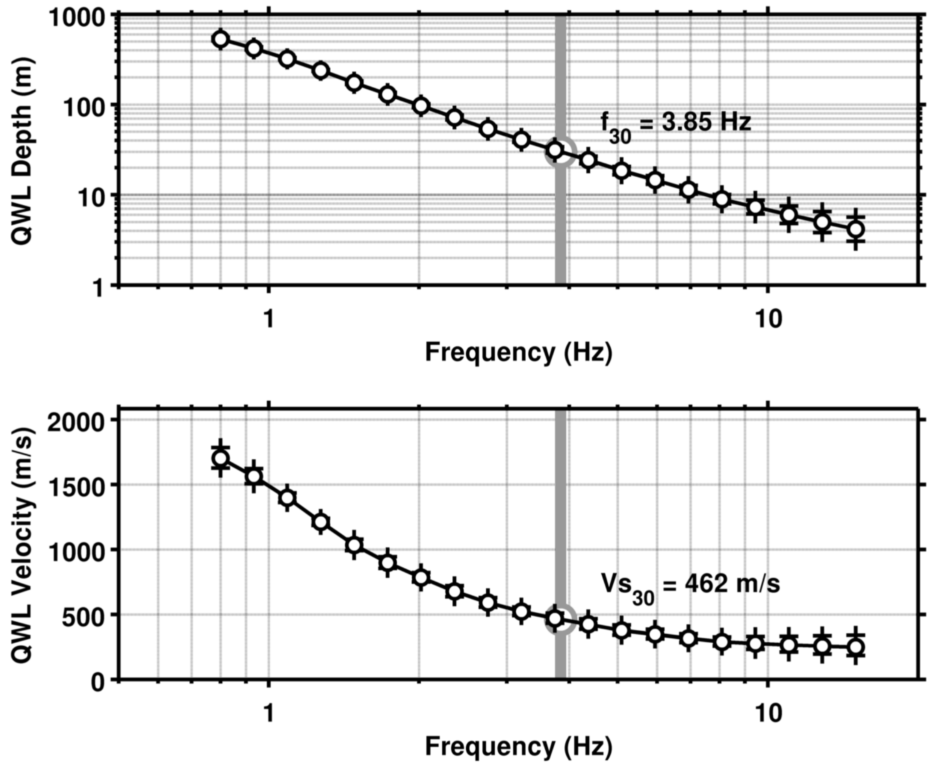

Figure 20 - *Quarter-wavelength representation of the inverted S-wave velocity profiles. On top the depth-frequency dependency. On bottom the QWL average velocity.*

12. Amplification models

Site amplification functions have been computed using two different approaches: the S-wave transfer function for vertical propagation and the quarter-wavelength amplification (Figure 21). In general the first method is used to evaluate the resonance characteristics of the site, while the second is more useful to assess the effect of the velocity contrasts between the lowermost rock layer (as reference) and the different QWL averaging depths. The results from the two methods are comparable, even if the transfer function provides a slightly larger amplification between 1 and 10Hz, because of the presence of some weak resonance in this frequency band. At high frequencies (the plateau regions) both methods provides a maximum average amplification of about 3. It has to be notice that the amplification functions do not include attenuation at this stage of the analysis, as the quality factors of the site are unknown.

Averaging depth	Vs-mean (m/s)	S.D.
5	271.96	46.21
10	299.67	18.05
15	350.92	23.40
20	391.02	19.77
25	430.45	21.15
30	**463.08**	**21.30**
40	518.25	17.19
50	573.15	20.12
75	692.52	19.21
100	795.89	18.62
150	961.33	24.26
200	1107.69	17.56

Table 1 - *Average travel time velocities at different depths. Vs30 is highlighted.*

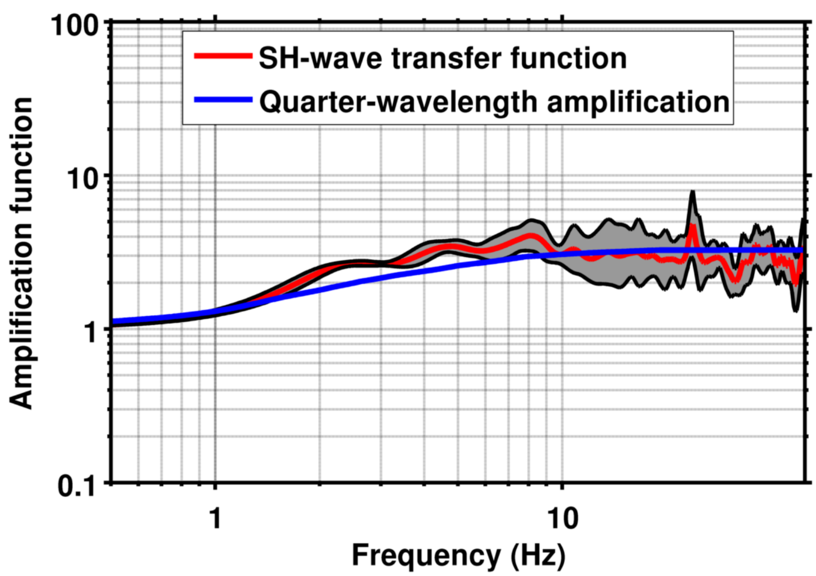

Figure 21 - *Comparison of amplification functions computed using the SH-wave transfer function and the quarter-wavelength formalism on the inverted velocity models. The functions are referenced to lowermost velocity layer.*

The SH-wave transfer function was then corrected for the Swiss rock reference velocity profile as defined in Poggi et al. (2011), according to the procedure described in Edwards et al. (2013). Given the lower velocities in the uppermost part of the Stiegenhof profile compared to the Swiss reference, the final corrected amplification function results in a general deamplification, with a maximum factor of about 0.6 at the plateau region (**Figure 22**).

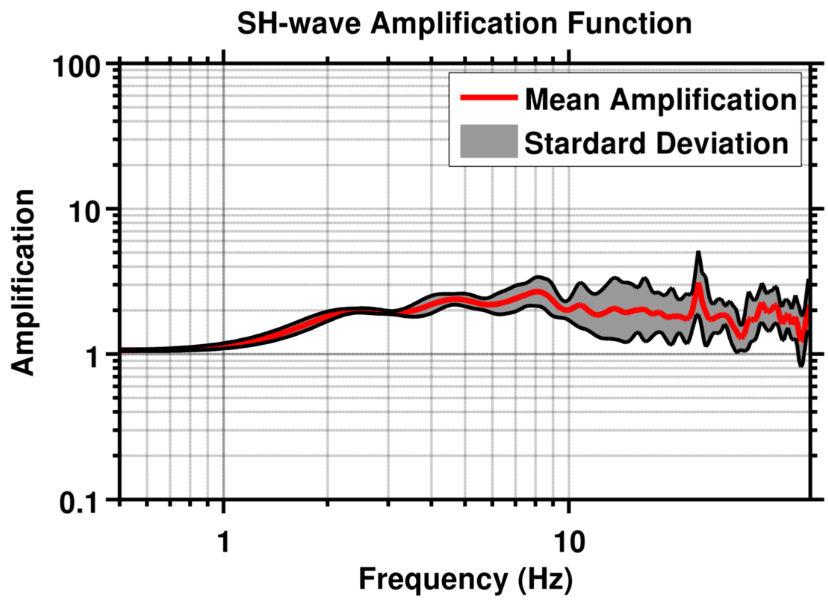

Figure 22 - *Correcting the SH-wave transfer function for the Swiss (rock) reference conditions (Poggi et al. 2011). The final corrected function shows a clear deamplification, with a maximum factor of about 0.6 at high frequencies.*

13. Comparing active and passive seismic results

The best model obtained from the inversion of surface waves from ambient vibration analysis has been finally compared with independent results from different active seismic techniques, including borehole VSP analysis, MASW, and refraction tomography (see attached report). At shallow depths, all the models from the different methods are consistent (**Figure 23**). Particularly, the VSP model shows the best match with the passive seismic result, with the exception of the first 10m, where VSP cannot resolve the details but only the average Vs velocity. Also MASW provided comparable models, but only down to a depth of about 25~30m, which has to be considered the maximum resolving depth of the method. This can be seen when comparing the dispersion curves obtained with ambient vibration array measurements and MASW, which overlap between 8Hz and 15Hz (**Figure 24**). Active MASW cannot excite surface waves at lower frequencies.

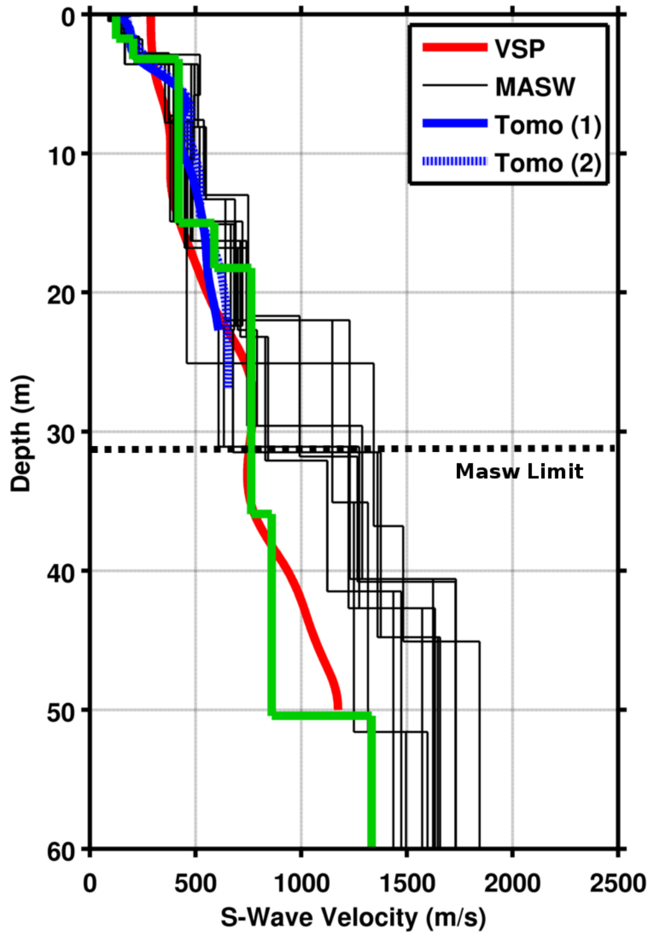

Figure 23 - *Comparison between the best fitting model (in green) from the inversion of passive surface waves with the results from different independent active seismic methods. The reliability region of the MASW method is explicitly presented, to account for the resolution limits of the method.*

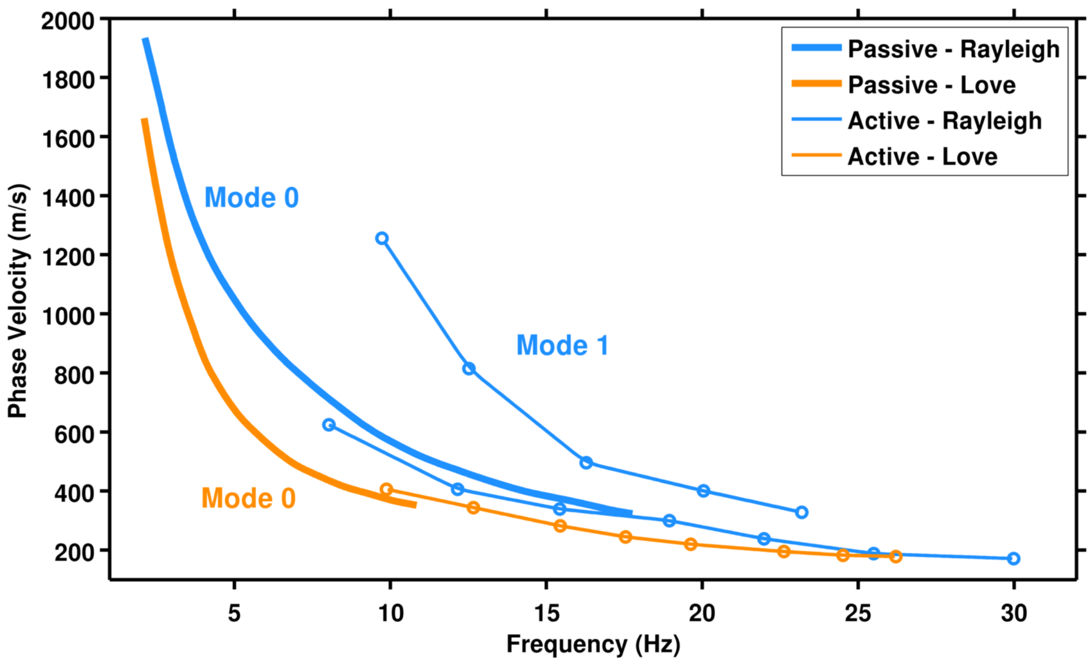

Figure 24 - *Comparison between the dispersion curves (Rayleigh and Love) from active and passive surface waves analysis. The lower resolution limit of MASW is roughly 8~10Hz in this case.*

REFERENCES

Capon, J., 1969. High resolution frequency wavenumber spectrum analysis, Proc. IEEE, 57, 1408-1418.

Burjanek, J., G. Stamm, V. Poggi, J.R. Moore, and D. Fäh [2010], "Ambient vibration analysis of an unstable mountain slope", Geophys. J. Int., Vol. 180, pp. 820-828.

Edwards, B., C. Michel, V. Poggi and D. Fäh (2013). Determination of Site Amplification from Regional Seismicity: Application to the Swiss National Seismic Networks. Accepted for publication in Seismological Research Letters.

Joyner, W. B., R. E. Warrick and T. E. Fumal (1981). The Effect of Quaternary Alluvium on Strong Ground Motion in the Coyote Lake, California, Earthquake of 1979, Bulletin of the Seismological Society of America, 71, 1333-1349.

Poggi, V., B. Edwards and D. Fäh (2011). Derivation of a Reference Shear-Wave Velocity Model from Empirical Site Amplification, Bulletin of the Seismological Society of America, 101, 258-274.

Poggi, V. and Fäh D., 2010. Estimating Rayleigh wave particle motion from three-component array analysis of ambient vibrations. Geophys. J. Int., 180-1, 251-267.

APPENDIX A

Borehole log

Bohrung Stiegenhof STI-1, 8495 Oberembrach ZH
Geologisches Profil 1:500

Koordinaten: 691'578/261'495 (gemäss E-Mail Nagra, Herwig Müller, 11.10.2012)
Höhenlage: Oberkante Terrain Bohrung ca. 635 m (aus LK 1:25'000 herausgelesen)
Bohrfirma: Hastag St. Gallen
Bohrart: ~~Rotary-Spülbohrung, Spülmedium Luft, z.T. Wasser~~
Ausführung: 5./16.10.2012
Bohraufsicht: Herwig R. Müller, Nagra
Probenentnahme: Melissa Schwab, Nagra
Geologische Aufnahme: 17./18.10.2012, Thomas Gubler, magma AG, 8005 Zürich

Legende

- Feinsandstein
- silitiger Feinsandstein
- feinsandiger Siltstein, Siltstein (z.T. tonig)
- toniger Siltstein

US: Überschwemmungsablagerungen
RG: Rinnengürtel
DFR: Durchbruchsfächer
LAK: Seeablagerungen
H: Hörnli-Schüttung
E–W-Gls: E–W-Glimmersand-Schüttung

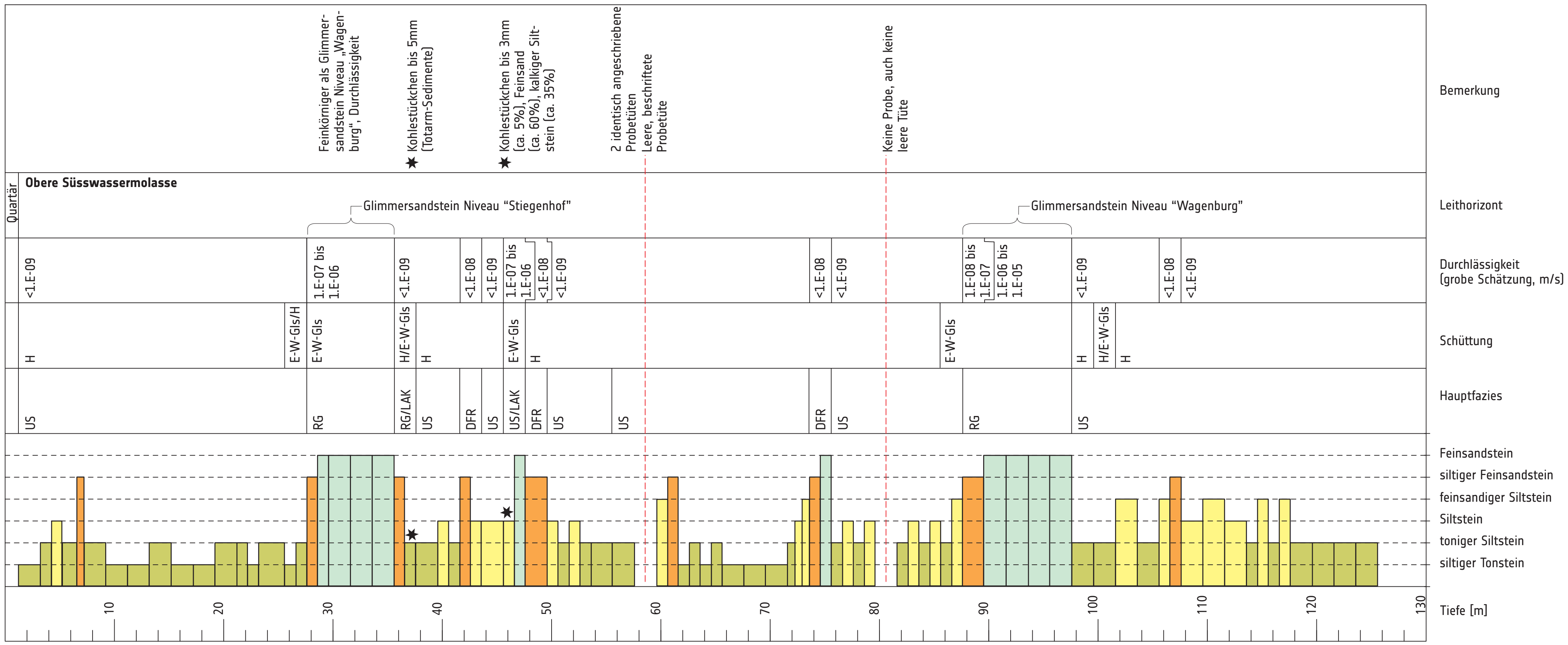

Eidgenössische Technische Hochschule Zürich
Swiss Federal Institute of Technology Zurich

SED
Schweizerischer Erdbebendienst
Swiss Seismological Service

Report on site characterization

Lenzkirch, Germany
(BERGE)

Poggi Valerio, Ulrike Kleinbrod, Donat Fäh

Last modified - 24 / 12 / 2014

1. Introduction

In the framework of the NAGRA seismic network project, an array measurement of the ambient vibration wave-field was performed at the location of the SED station BERGE (Lenzkirch, Germany). The scope of the survey is the seismic characterization of the area surrounding the installation (**Figure 1**), which consists in a broadband seismometer (Trillium Compact) with a high-resolution digitizer (Taurus 24Bit @200sps). Ambient vibration analysis has been used to infer the characteristics of the underground structure of the site, with special regard to the one-dimensional shear-wave velocity. Such profile was later used to assess the local seismic response of the station.

For the analysis, different spectral analysis techniques were implemented, consisting in both single and array methods, which are listed below:

- Time-frequency wavelet analysis
- Power-spectral density estimation
- Conventional horizontal to vertical spectral ratios
- Directional horizontal to vertical spectral ratios
- Wavelet polarization analysis
- Three-component high-resolution f-k analysis.

The results of all these analyses conformed to the definition of the final velocity model. In the following, the main results of these investigations are summarized and a final interpretation of the velocity profile is given. From this interpretation, engineering parameters are finally derived, e.g. the Qwl-Vs average velocity, VsZ (including Vs30) and the seismic amplification from the analytical SH-transfer function of the one-dimensional soil column.

2. Survey description

To characterize the seismic response of the site, a first array measurement of ambient vibration was performed on 22/03/2013. This array consisted in two measuring configurations of 14 sensors each and increasing diameters of 100m and 200m respectively. The two configurations were planned to partially overlap, by sharing 9 common sensors, with the aim of providing a continuous resolution of the frequency range between the two geometries. Unfortunately, the first experiment was unsuccessful, mostly due to unfavorable survey conditions (**Figure 2**A); the acquisition was performed one day after a moderate snowfall, during the melting phase of the snow cover. This created considerable side problems: soil saturation, disturbances induced by the underground water flow and bad coupling/tilting of the sensors at the surface. No results were then obtained from these recordings, as no evidence of coherency of the ambient vibration wave-field was present in the resolvable frequency band (**Figure 3**A).

The survey was then repeated (19/06/2013), with better weather and soil conditions (**Figure 2**B). For this second measurement, given the acquired information about the possible subsurface geology of the area (see following section), it was decided not to implement the small configuration anymore, but to only perform the large geometry of 200m in size (**Figure 1**). This decision was taken on the base of the expected very high phase-velocities of the surface waves for hard rock sites (mostly gneiss and high-grade metamorphic units), which usually require larger array to be successful. A prior estimation of the possible maximum penetration depth was however not possible in this case, due to the large uncertainty of the bedrock velocity.

During the survey, a total of about two hours of recordings has been acquired. By band-pass filtering, the presence of coherency in the ambient vibration wave-field is now evident (**Figure 3**B). However, not all the stations recorded properly for the entire time. One station stopped working unexpectedly due to a failure of the battery; one station had GPS synchronization problems at the beginning; the baler of one station did not properly flush data, leading to a loss of about 20min of recordings. To face these problems and in order to achieve the best compromise between available stations and recording length, two different processing sub-configurations have been tested (**Figure 4**). The configuration named "*Selection 1*" was nevertheless the most successful in term of f-k resolution; the results in the following sections are then based on that geometry.

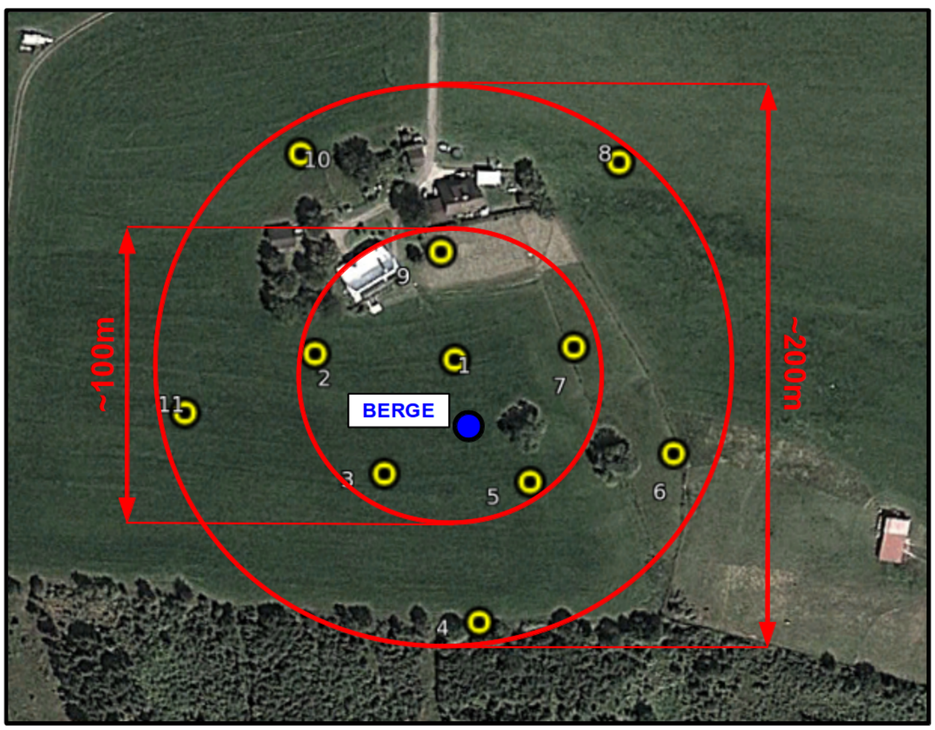

Figure 1 - *Geometry of the second ambient vibration array survey performed in Lenzkirch (SED station BERGE) on 19/06/2013. Two concentric rings of increasing diameter were used. The location of the seismic station is shown in blue.*

A)

B)

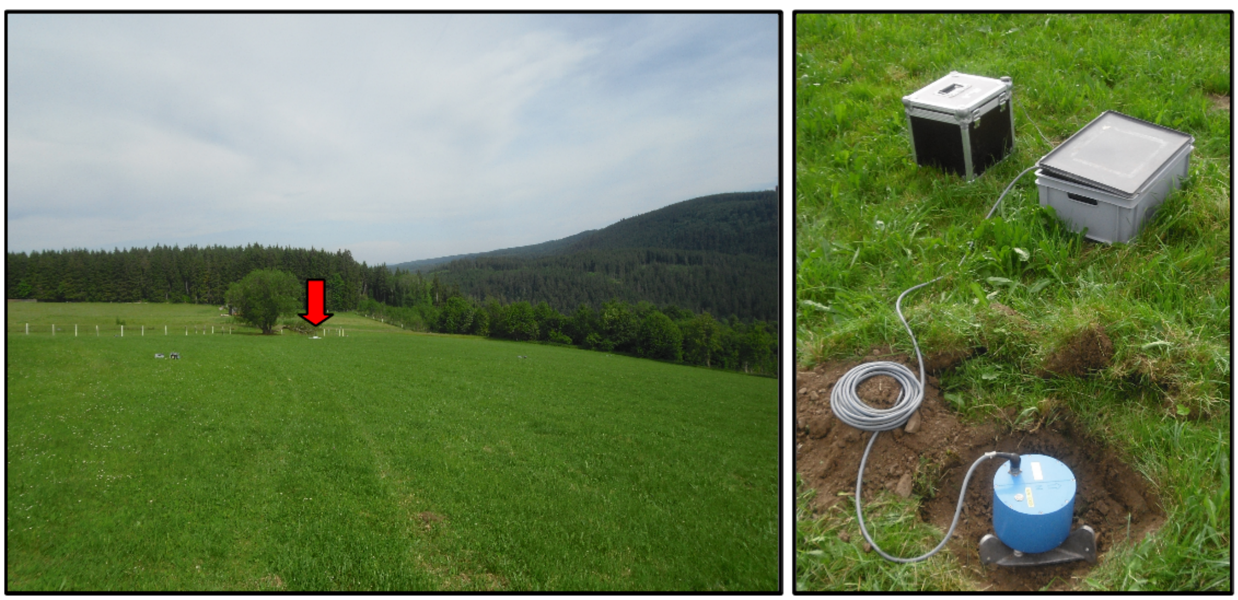

Figure 2 - *Comparison of the general measuring conditions between the two experiments performed respectively in March (A) and June (B) 2013. The red arrow indicates the location of the SED station installation. On the right side, details of single acquisition points of the array, consisting of a Q330 datalogger (in the gray box) and a Lennartz 5s velocity seismometer. The coupling of the sensor is assured by removing the uppermost part of the soil and by means of a special support (Trihedron).*

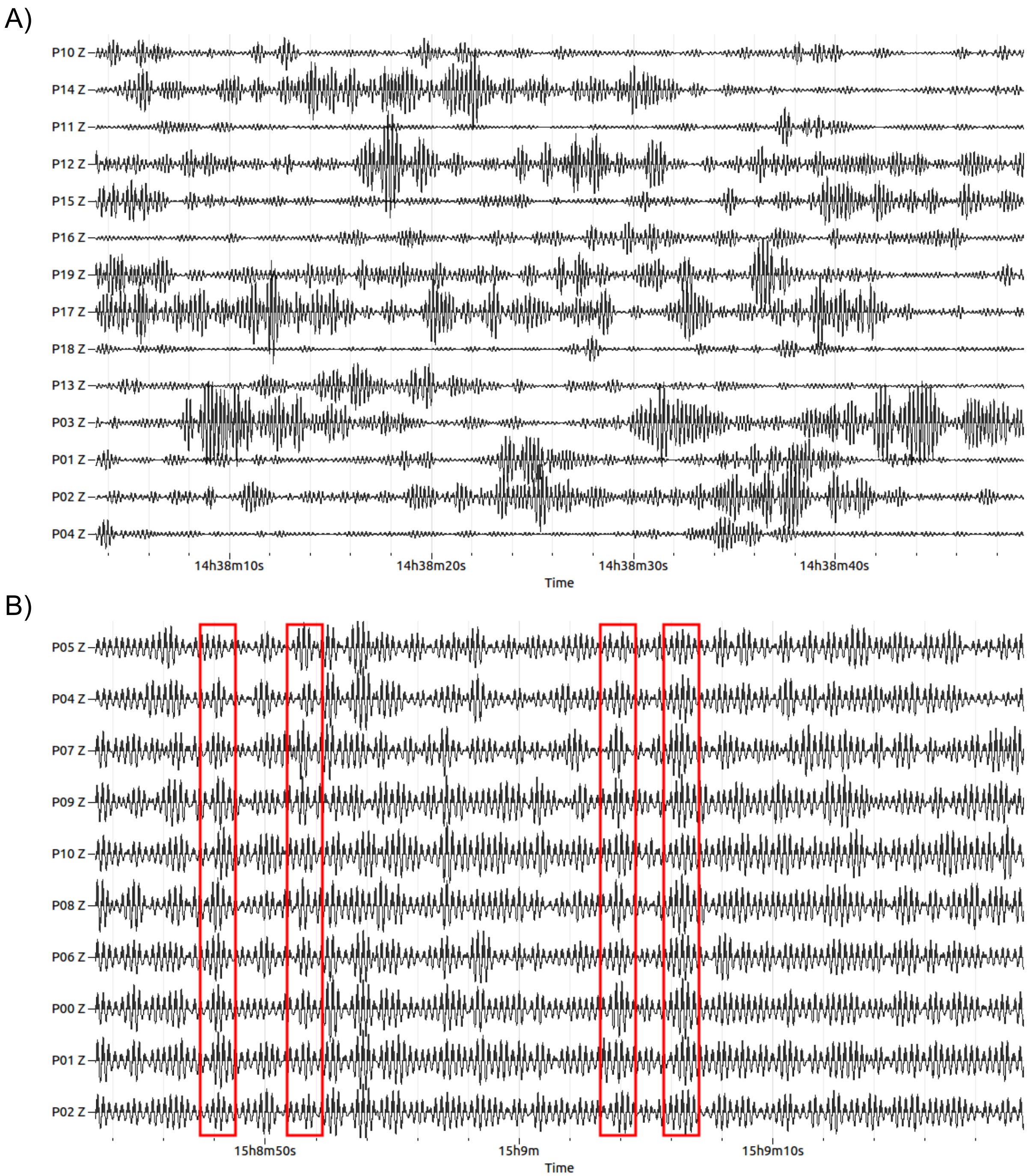

Figure 3 - *Comparison between the recordings from the two surveys performed in March (A) and June (B) 2013 at the station BERGE. For better comparison, the signal's windows are of the same duration and band-pass filtering (4-6Hz, 6^{th} order causal Butterworth). The wave-field in A did not show any sign of coherency, while it is evident in B the presence of numerous correlated signals (e.g. marked with red boxes).*

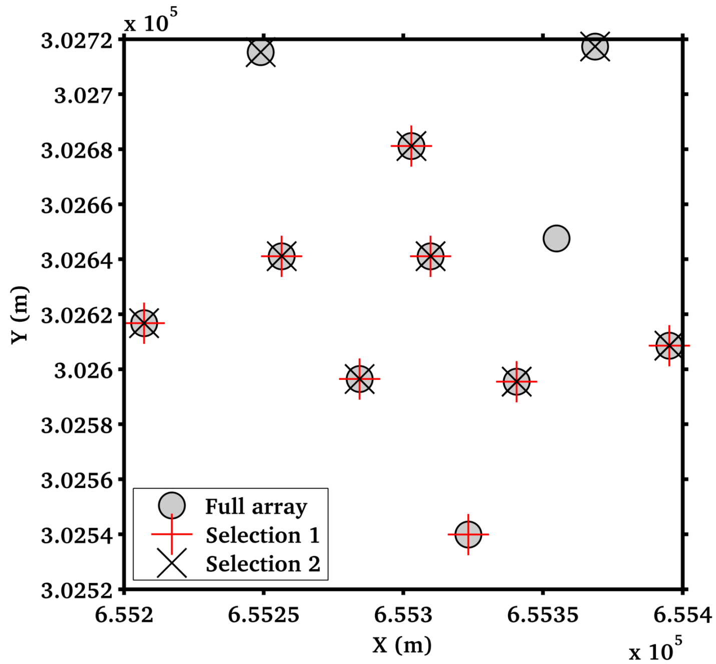

Figure 4 - *Geometry of the two sub-selections obtained from the full array performed on March 2013 in Lenzkirch. Selection 1 consisted of eight stations and about 1h10m of recordings, while for the selection 2 nine stations were included with 40m recording duration.*

3. Soil type, topography and geology

The array has been set in open field conditions, in a rural area (**Figure 1**, **Figure 2**). The influence of buildings and anthropogenic disturbances is virtually negligible. Sensors have been deployed on free soil conditions. Good coupling with the ground was assured by means of digging small holes at the sensor's places, and by using a special support (*Trihedron*) that facilitates the leveling of the device even for difficult soil conditions. The measurement area is located on a moderate slope dipping toward south. However, no topographic correction has been taken into account before processing.

From the geological points of view (**Figure 5**), the target area is located within the Feldberg massif, a relevant geological unit of the Black Forest area. It mostly consists in granite and gneiss of different metamorphic degree. The bedrock is very shallow at the measuring location, but never exposed across the area. The surface morphology is considerably smooth and modeled by the action of glaciers during the Pleistocene. Such site can be classified as of rock ground-type A.

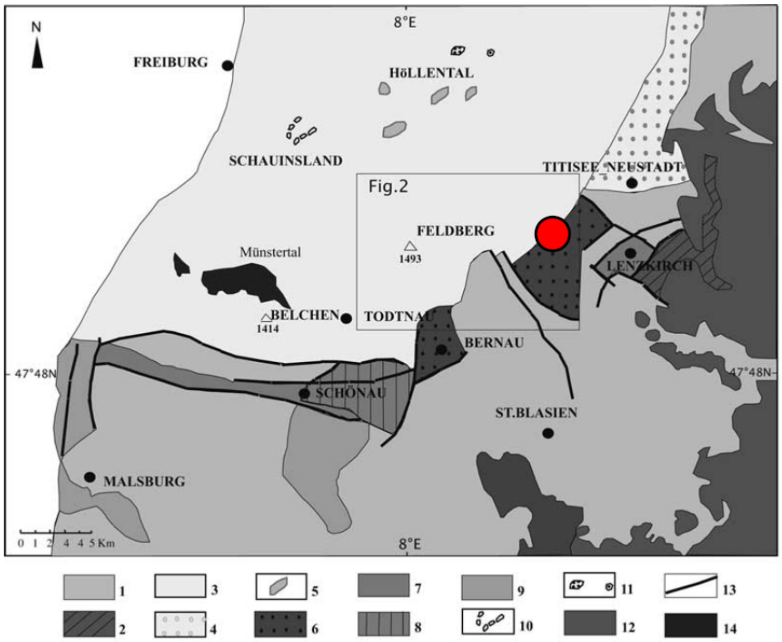

1: granite;
2: rhyolite;
3: gneiss;
4: gneiss with quartzite;
5: orthogneiss;
6: other metamorphic units;
7: Palaeozoic sediments;
8: metamorphosed greywackes;
9: blastites;
10: calcareous silicate rock;
11: Permian sediments;
12: Triassic sandstones;
13: fault;
14: Permian rhyolites.

Figure 5 - *Simplified geological map of the Feldberg massive area (from Huguet 2007, modified). In red the approximate location of the array measurement in Lenzkirch is marked.*

4. Acquisition equipment

Each acquisition point within the array consisted of a three components seismometer (Lennartz 3C with 5s eigenperiod, **Figure 2**) and a 24 bit data logger (Quanterra Q330). Synchronization between stations was assured by standard GPS, while a more accurate differential GPS (Leica Viva system) was used to precisely locate the sensor's coordinates with a tolerance of less than 5cm.

5. Weather conditions

The first measurement (22/03/2013) was performed one day after a moderate snowfall. The average temperature was however above zero at around noon, which caused the partial melt of the snow cover. The ground was consequently saturated with water during the acquisition, which caused coupling/tilting problems to the sensors and the generation of considerable local (uncorrelated) noise disturbances. Conversely, the weather conditions were stable during the second measurement (19/06/2013), with no precipitations and an average (over the whole day) temperature of 25 degrees.

6. Pre-processing and preliminary data-quality control

The three-component recording has been preliminary band-pass filtered using a high-pass 6^{th} order causal Butterworth filter in the bands 0.2-1Hz, 1-4Hz, 4-6Hz and 6-10Hz. Although it is not a requirement for spectral analysis techniques, such filtering was applied in order to facilitate the preliminary visual inspection of the noise traces (e.g. **Figure 3**) and to evaluate the coherency of the wave-field in the different frequency bands. Such procedure gives essential information for the subsequent interpretation of the f-k analysis results.

To assess the quality of the ambient vibration recordings, spectral analysis was subsequently performed. Because of the stochastic nature of the ambient vibration wave-field, a statistical approach has to be used, such as the estimation of the power spectral density (*PSD*). This approach is useful to evaluate the average energy level of the recordings in the analyzed frequency range, and to access the presence of spurious spectral peaks, which might be related to human activity (machinery, pumps). By inspecting the PSD of the three-component recordings at the central station in the range between 0.5 and 40Hz (e.g. **Figure 6**, separately for the three components), only one spurious peak is visible at about 4.2Hz, but more pronounced on the vertical direction. The peak - very narrow - is most likely of anthropogenic origin (from the nearby farm) and should be rejected from interpretation. The average energy level is nevertheless very low, close to the minimum bound of the USGS noise model.

Complementary to the aforementioned statistical methods, a spectral decomposition approach is more suitable to assess the stationarity of the ambient vibration wave-field over time. The wavelet time-frequency analysis was then performed over the whole recording time. From such analysis (**Figure 7**) an overall stability of the ambient-vibration wave-field over time is evident. The disturbance at 4.2Hz is confirmed to be a nearly harmonic contribution, steady over the whole recording window. This provides an additional confirmation of its possible anthropogenic origin. The disturbance is nevertheless very weak and well localized in frequency; therefore it won't affect the following processing steps.

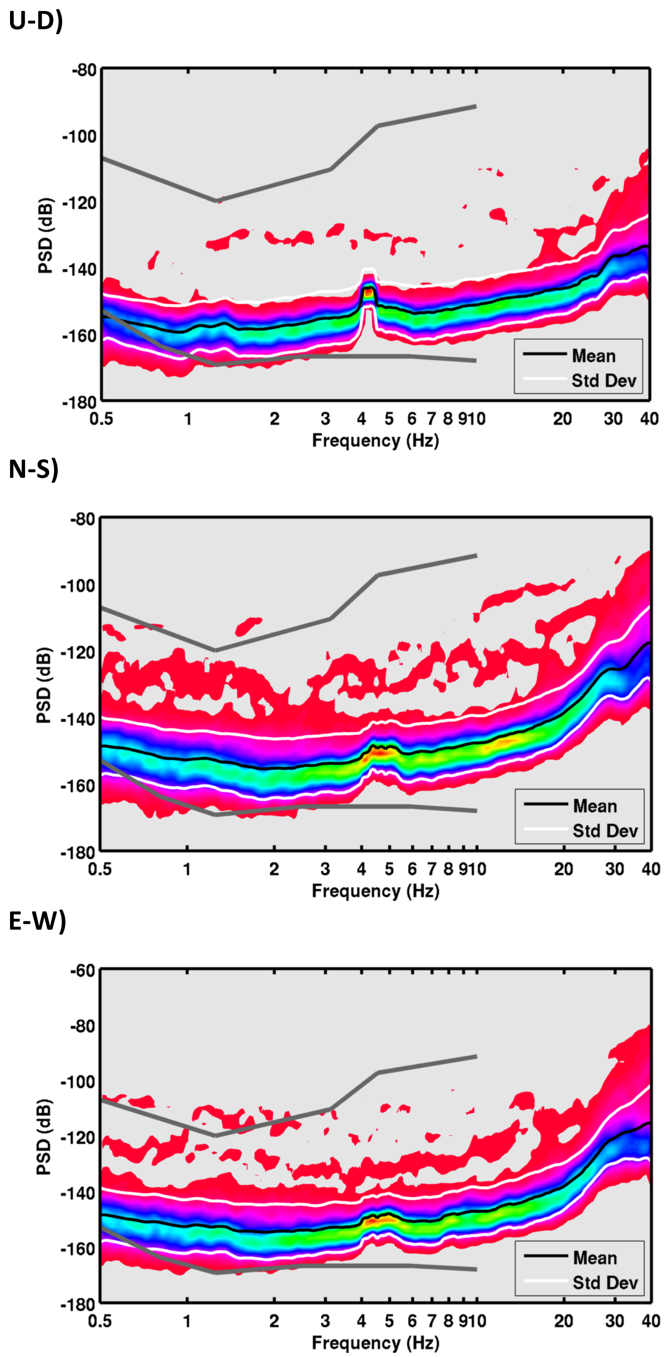

Figure 6 - *Power spectral density (PSD) computed for 1h10m recording at the central station of the array (point P0). Similar results were obtained from the other stations of the array. In gray lines are the minimum and the maximum bounds of the USGS noise model, for comparison.*

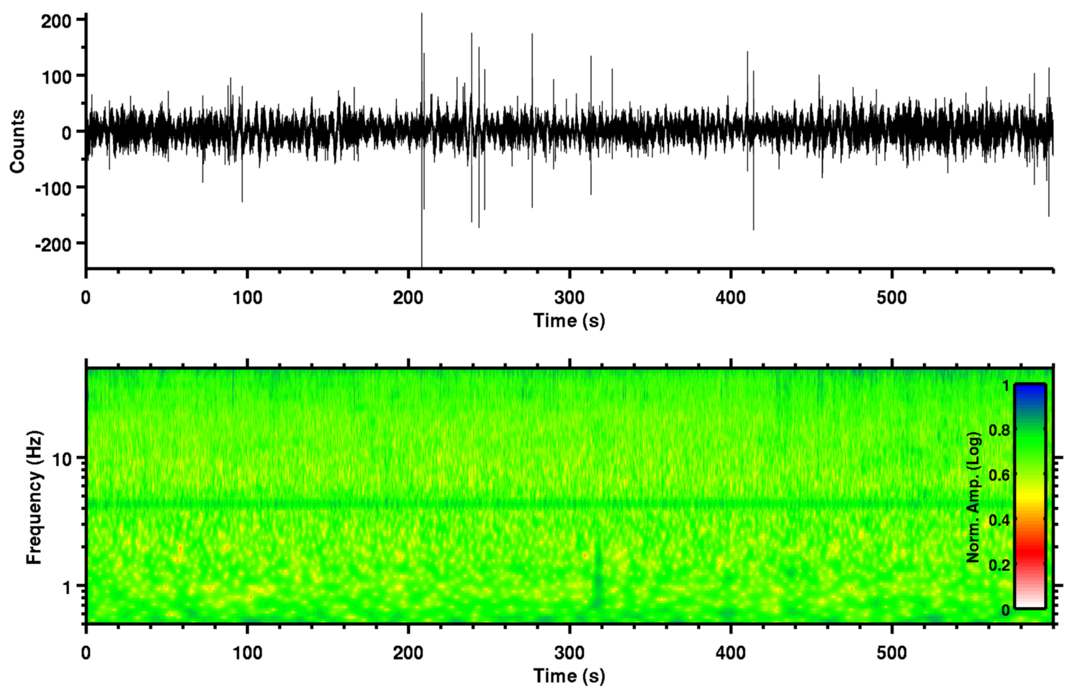

Figure 7 - *Example of spectrogram from 600s of recording of the central station of the array (P0, vertical component). For the analysis, the cosine wavelet is used (wavelet parameter = 12). It is visible on the whole spectrogram the harmonic disturbance at about 4.2Hz, which is nevertheless not particularly energetic.*

7. Conventional H/V spectral ratios

The horizontal-to-vertical (H/V) Fourier spectral ratio is a technique widely used in seismic site characterization because of its ability to provide an estimate of the SH wave fundamental frequency of resonance (f_0) of the site. Other than that, H/V ratios are useful to provide information on the Rayleigh wave ellipticity function, which can be used in the inversion procedure to constrain large velocity contrasts at depth. In this study, we use the H/V technique also to map the variability of the subsoil structure along the investigated area; this is necessary to verify the fulfillment of the 1D structure assumption, which is necessary for the f-k method applied later.

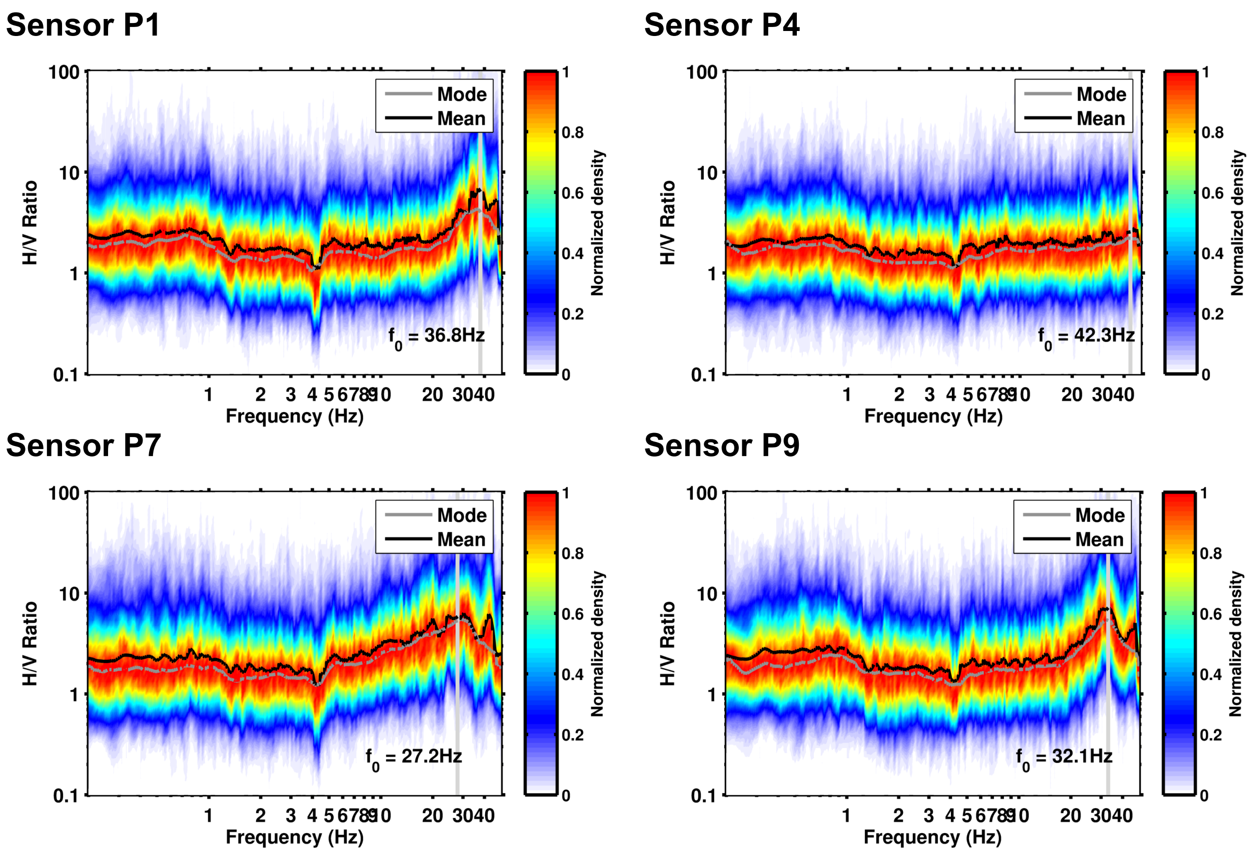

Figure 8 - *Example of H/V spectral ratios at four stations of the array (Selection 1). The resonance frequency of the soil cover is indicated with a light gray line (between 25~50Hz).*

H/V spectral ratios have been computed for the recordings at each station of the array (e.g. **Figure 8**). The behavior of the noise wave-field at the different stations location is comparable (**Figure 9**). A weak maximum on the H/V curves is present at about 0.8Hz, and might be addressed as the resonance frequency of the sites due to a velocity contrast in the rock profile. The peak is very stable over the array, but very low in amplitude. Considering the characteristic of a generic rock site, such maximum might be induced by a change in lithology within the profile at depth, which causes a moderate contrast of seismic impedance. The effect of the topmost soil cover is visible at high frequencies (> 20Hz), where large amplitude resonance peaks are noticeable. The peaks are nevertheless not comparable across the array (in amplitude and frequency), as confirmation of the heterogeneity of the very thin soil cover. The behavior of the site can be considered laterally homogeneous for the f-k analysis.

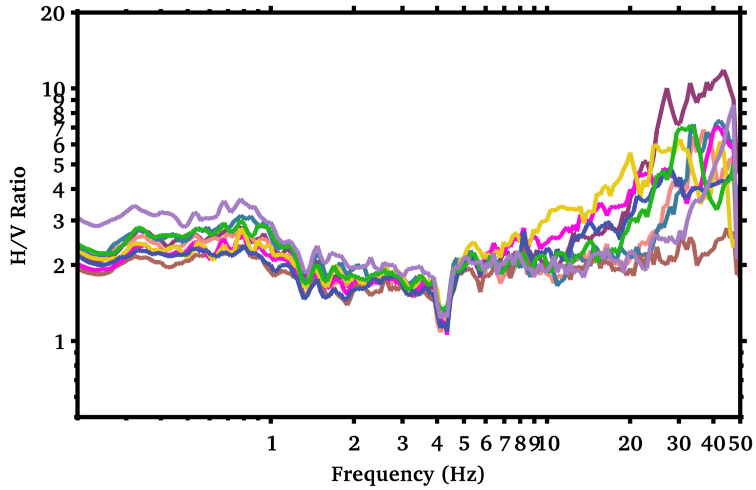

Figure 9 - *Comparison of the H/V spectral ratio curves of all the stations of the array (Selection 1). The curves are stable up to at least 20Hz, confirming the lateral homogeneity of the velocity structure of the site. A low frequency peak is visible at about 0.8Hz, which might be considered the fundamental frequency of the site.*

8. Directional H/V spectral ratios

The computation of directional H/V spectral ratio or polarization analysis is useful to reveal asymmetries in the ambient vibration wave-field. Different effects can induce such a behavior: 2D/3D structure, topographic effects or a non-homogeneous distribution of the noise sources. If a strong directionality is found by the analysis, it is generally recommended to carry out further investigations to properly address the origin of polarization.

By processing the directional H/Vs at all the recording stations of the array (e.g. **Figure 10**) it is possible to observe an isotropy of the wave-field in the low frequency range, roughly below 20Hz. At high frequencies, however, the variability of the H/V peak is noticeable also in their directionality. This can be explained by the variability of the uppermost soil cover layer over the study area, and it cannot be interpreted as an effect of non-homogenous distribution of the noise sources. This issue is later investigated through f-k analysis. The topographic slope seems to have no effect on the ambient vibration wave-field.

The result of the directional analysis is also confirmed by applying the wavelet polarization analysis techniques as described in Burjanek et al. (2008) to the central station of the array. Also in this case no significant directionality (**Figure 11**a) and polarization (**Figure 11**b) of the wave-field are observable.

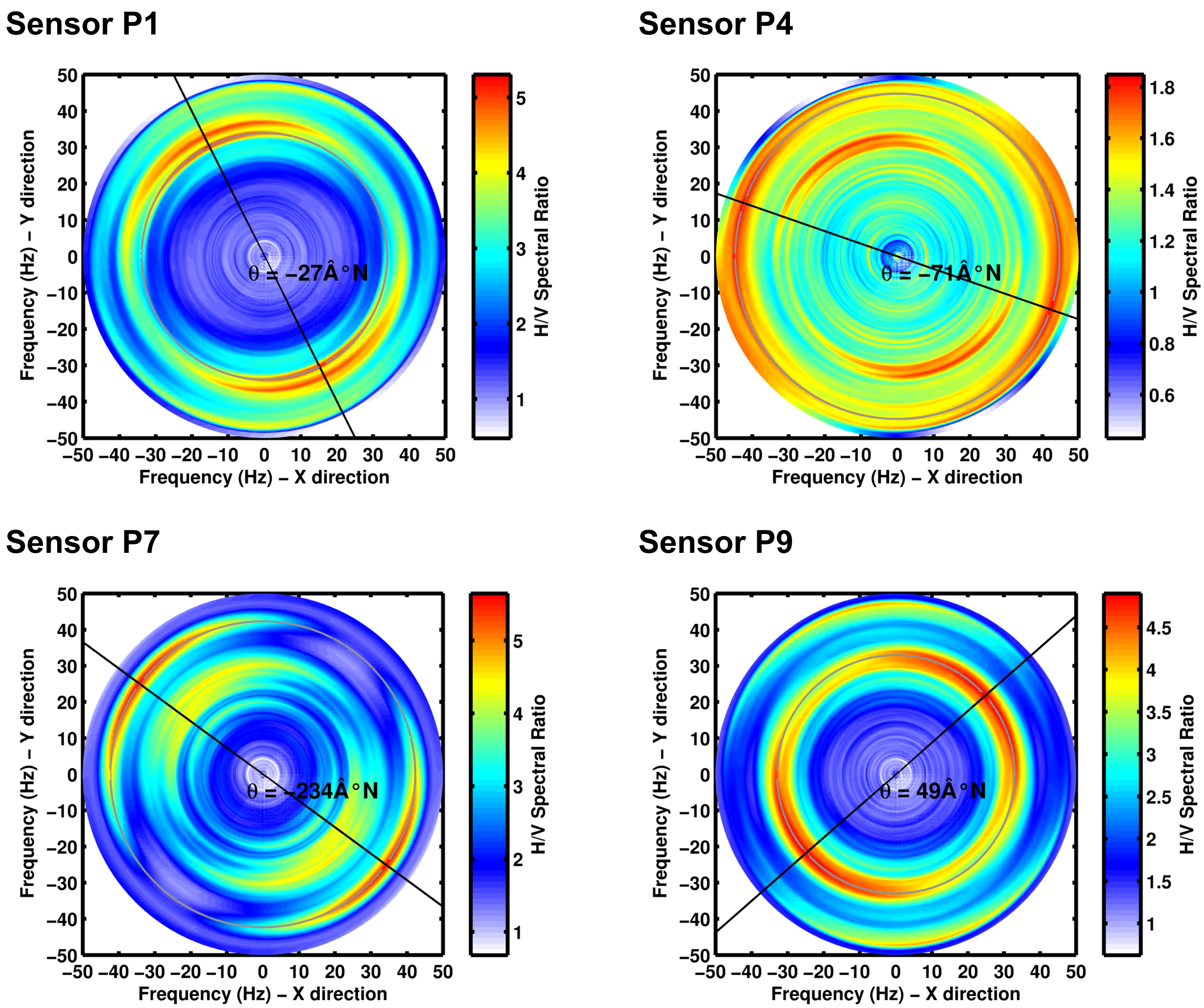

Figure 10 - *Example of directional H/V spectral ratios at four stations of the array configuration A. No consistent evidence of wave-field anisotropy is present below 20Hz.*

a)

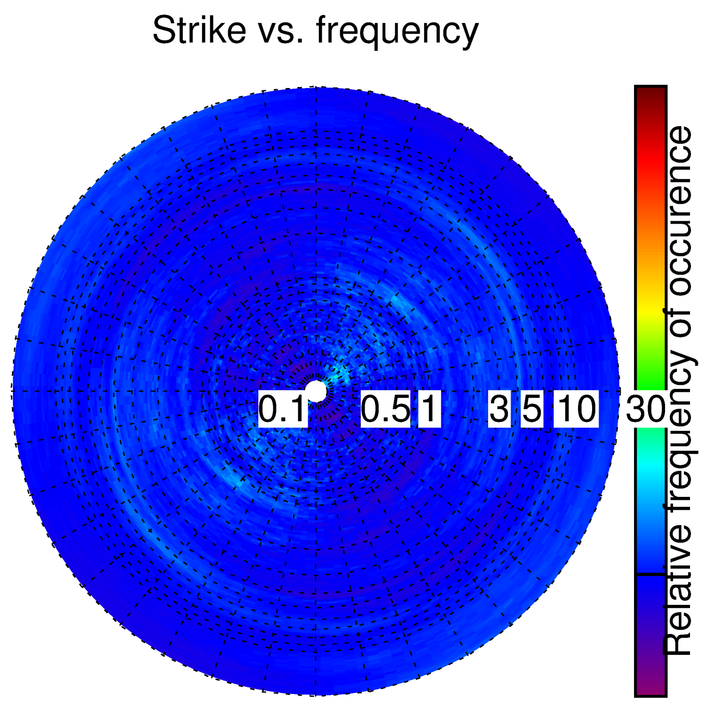

b)

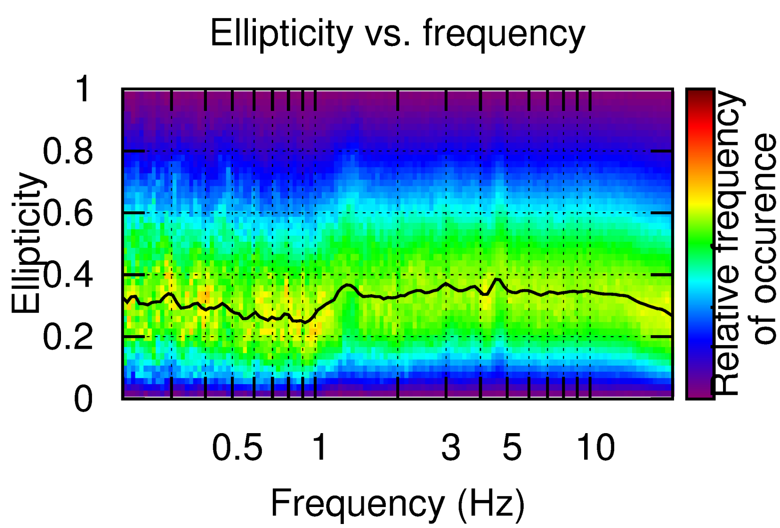

Figure 11 - *Wavelet-based polarization analysis at the central station of the array. By analyzing the polarization over strike (a) and the particle motion ellipticity plot (b), no directional effect is visible in the frequency range of interest.*

9. Three-component f-k analysis

The frequency-wavenumber analysis is a spectral technique based on seismic array recordings that allows retrieving the direction and the dispersion characteristics of the surface waves. We apply here this technique to three-component ambient vibration recordings using a modification of the high-resolution method of Capon (1969) as described in Poggi et al. (2010). Using all the three-components of motion gives the possibility to retrieve information about the propagation of the Rayleigh waves (vertical and radial processing direction) as well as of the Love waves (transversal direction).

As in the case of the previous methods, the ambient vibration recordings are treated statistically by subdividing the traces in sub-windows. For each consecutive window a separated f-k analysis is performed, and the results are then averaged over the whole recording, increasing the robustness of the final estimation.

a) 6-10Hz Hz

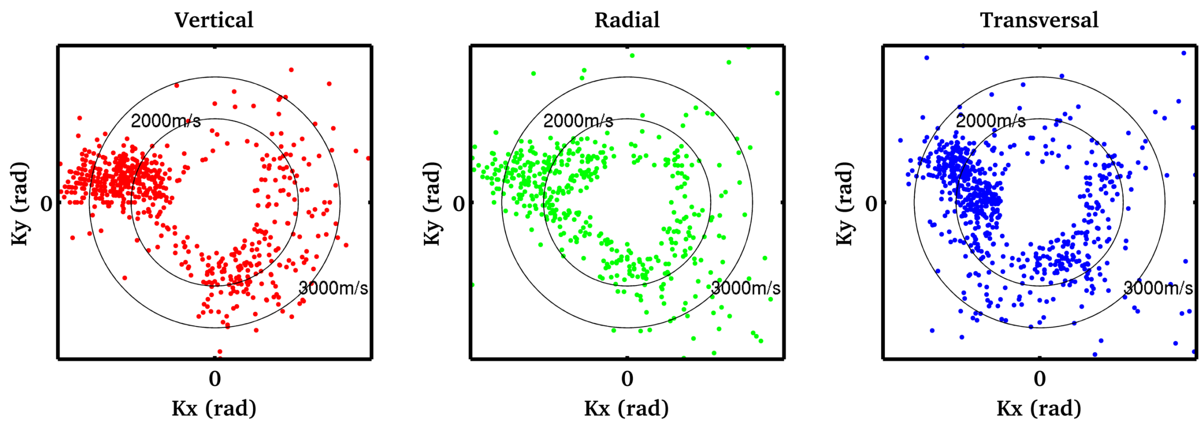

b) 15-20 Hz

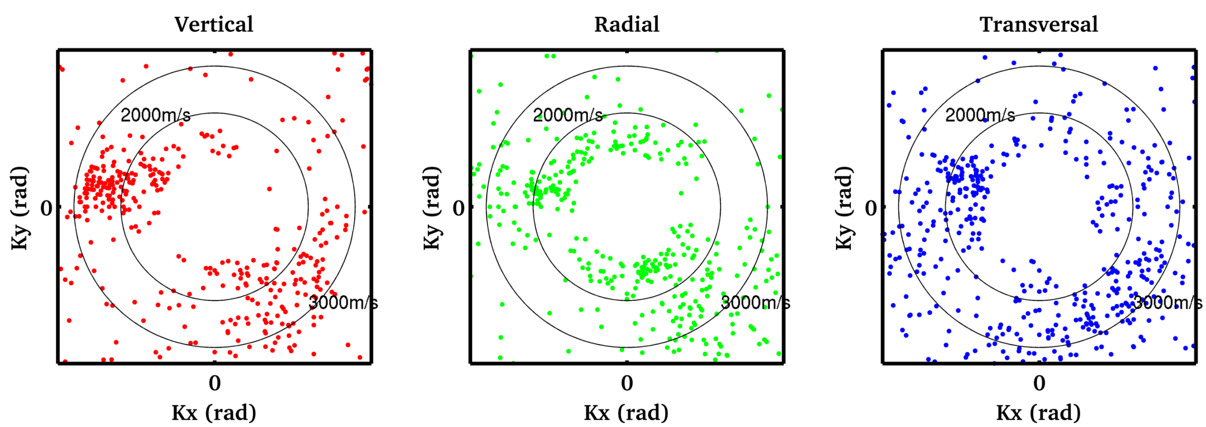

Figure 12 - *Example of distribution of noise sources in the intermediate frequency range (6-10Hz) and at high frequencies (15-20Hz), obtained from three-components f-k analysis (Station selection 1).*

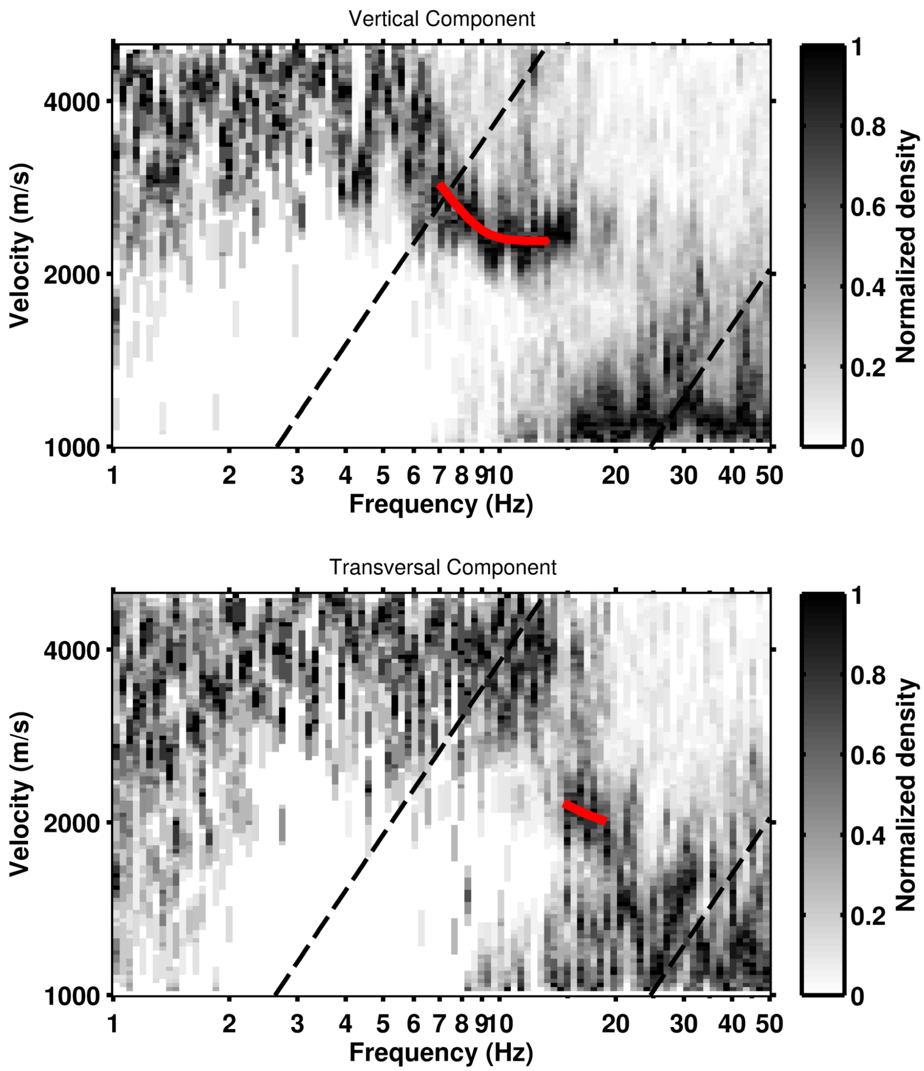

Figure 13 - *Density distribution of all the surface wave signals obtained from the whole recording of the BERGE array (Selection 1) using f-k analysis. Top: result from the analysis of the vertical component (Rayleigh waves); Bottom: result for the transverse component (Love waves). In red the interpreted dispersion curves are given (manually selected).*

As first step, from the f-k analysis it was possible to assess the noise source distribution over broad range of analyzed frequencies (e.g. **Figure 12**) for the vertical, the radial and the transversal component. In particular, in the intermediate frequency range (6-10Hz) the source distribution show a remarkable cluster in NWW direction on all the components. This is not surprising, because this direction is consistent with the location of the farmer house with respect to the array; this is probably the strongest source of noise in the area.

Subsequently, the surface-wave dispersion curves have been extracted by visual inspection and manual picking of the f-k density plots (**Figure 13**). The Rayleigh wave dispersion can be tracked between about 6 and 14Hz, while for Love waves only a limited frequency band has sufficient energy for an interpretation. The phase velocities are in both cases very high, as expected for hard metamorphic rock. The final interpretation of the modal dispersion pattern is then presented in **Figure 14** for both the Rayleigh and Love waves, for comparison.

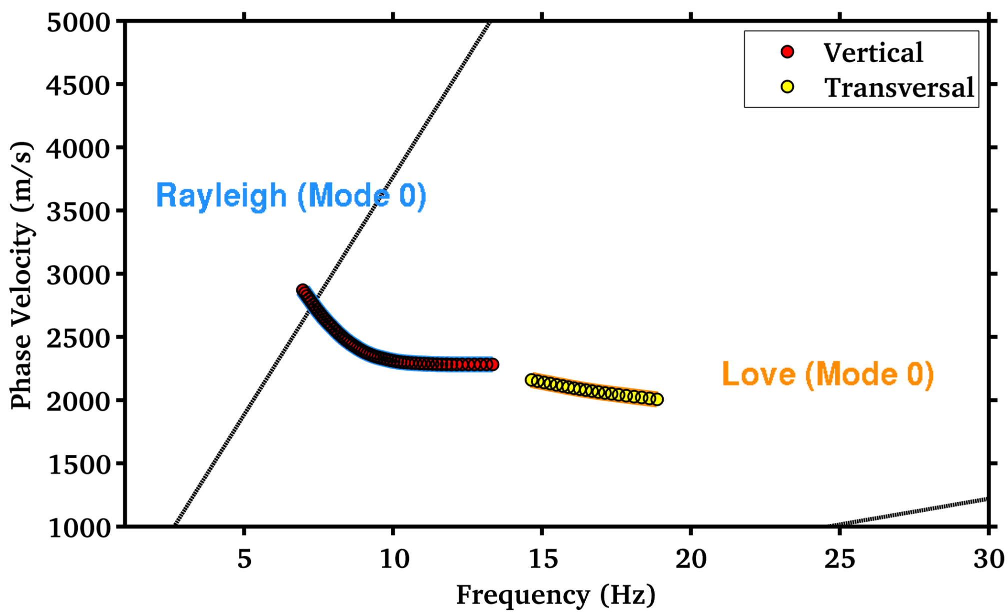

Figure 14 - *Final interpretation of the Rayleigh and Love dispersion curves from the station selection 1 of the BERGE array.*

10. Inversion of the dispersion curves

The surface wave dispersion curves (Rayleigh and Love) obtained from the three-component f-k analysis of the ambient vibrations were inverted to obtain an estimation of the velocity profile of the site (mainly S-wave velocity as function of depth, and to a lesser extend the P-wave velocity, due to the lower sensitivity). The analysis was performed using the software *Dinver* (www.geopsy.org), which implements a direct search approach (**Figure 15**) based on a conditional version of the neighborhood algorithm (Sambridge, 1999).

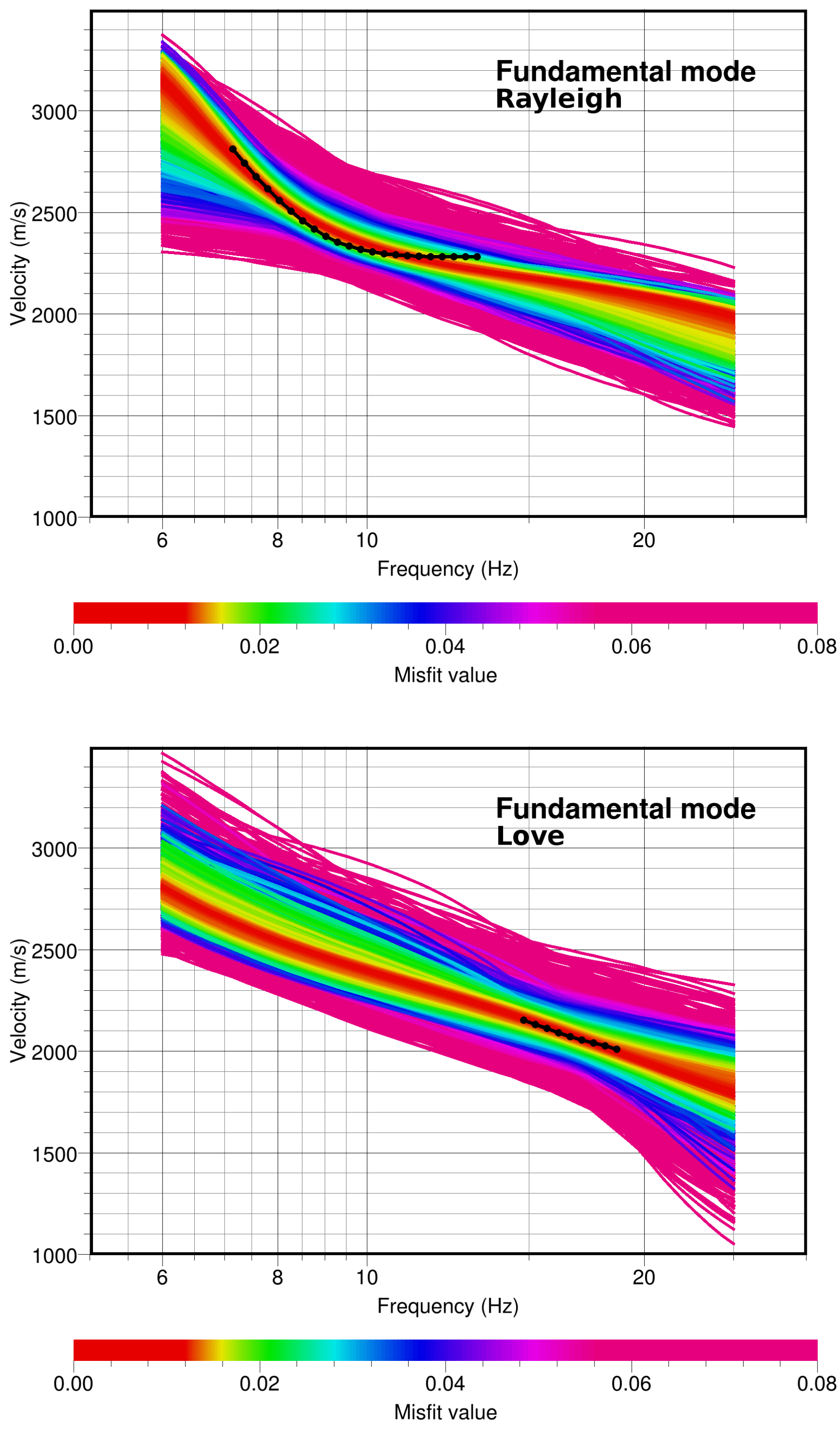

Figure 15 - *Fitting the surface dispersion data within the global optimization procedure. Different colors represent different misfit between the observed (in black) and the modeled dispersion curves during the search.*

To parameterize the velocity model, two different approaches were implemented. The first one consisted in setting up an eight-layer model with free interface depths (**Figure 16**). In such a case the free inversion parameters are then the velocities (P and S) and layer thicknesses. In the second case, a fixed-thickness layer approach was used (**Figure 17**). The advantage of the former method stays in the possibility to better resolve sharp velocity interfaces, while the second is less unique and better constraints the seismic velocity. The two approaches have to be nevertheless considered complementary, and they should provide consistent results.

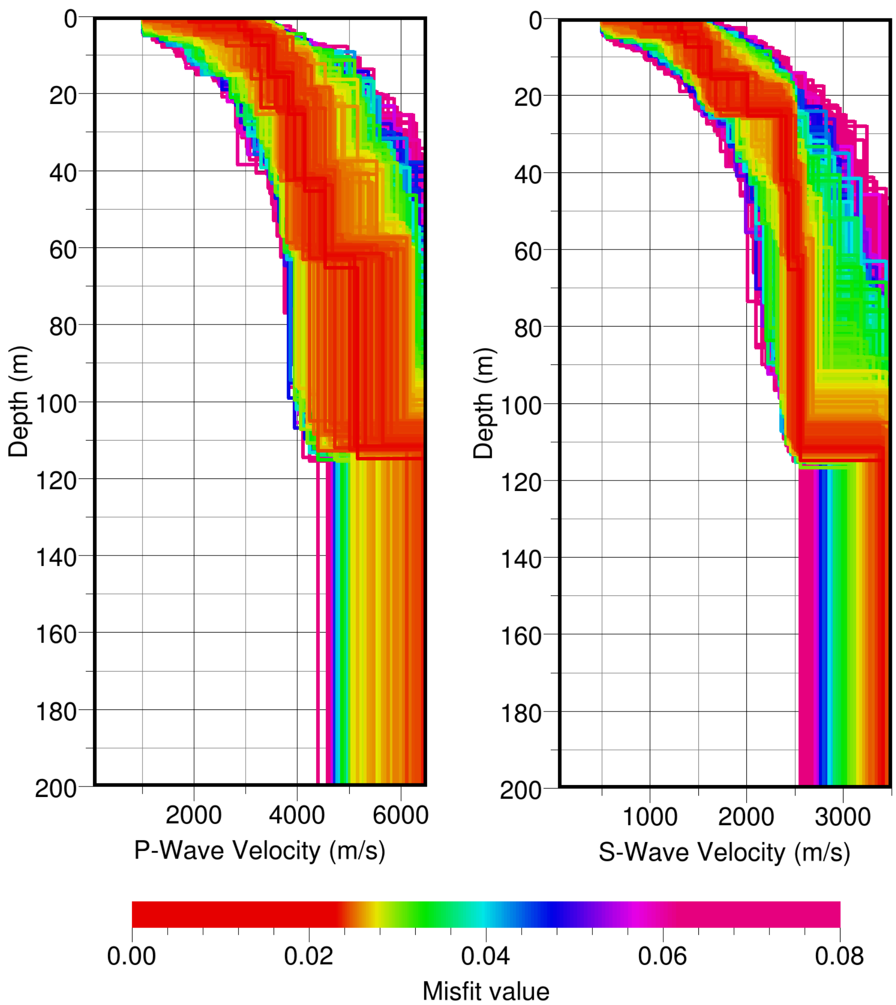

Figure 16 - *Distribution of the free-layer velocity models generated during the inversion process and ordered by decreasing misfit, according to the color scheme of* **Figure 15***.*

Eight inversion tests (*runs*) have been performed for each of the two model schemes (**Figure 18**), in order to minimize the effect related to a possible unfavorable initial randomization of the space parameter. The best fitting models from of each run are then collected and used later on for the computation of the derived soil parameters.

The inverted velocity models (Vs and Vp) are gradient-like, with a faster increase in velocity in the first 10m, followed by a more smoothed part. This is expected for a rock velocity profile. By considering the minimum available frequency of the surface-wave dispersion curves, and by analyzing the scattering of the inverted models (**Figure 19**), it is realistic to assume the velocity profiles to be reliable down to a depth of about 80~100m. Below this value no direct constrain is available, and the velocity are obtained by pure extrapolation.

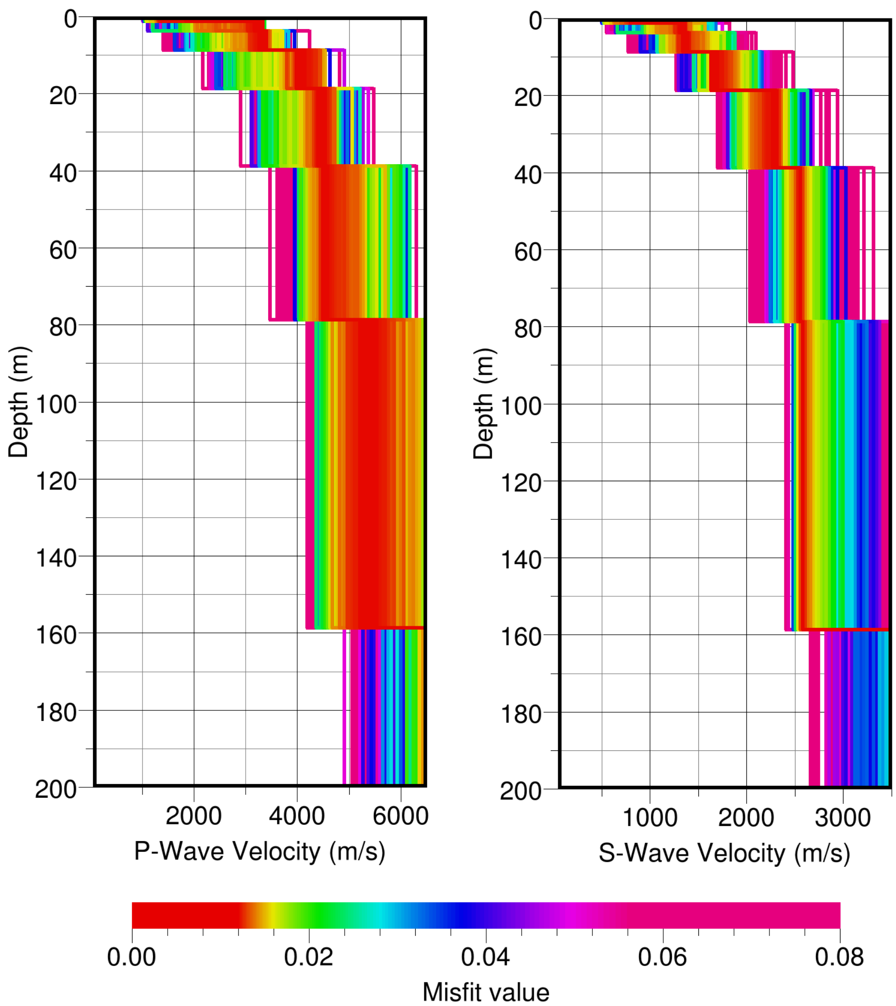

Figure 17 - *Distribution of the fix-layer velocity models generated during the inversion process, and ordered by decreasing misfit according to the color scheme of* **Figure 15**.

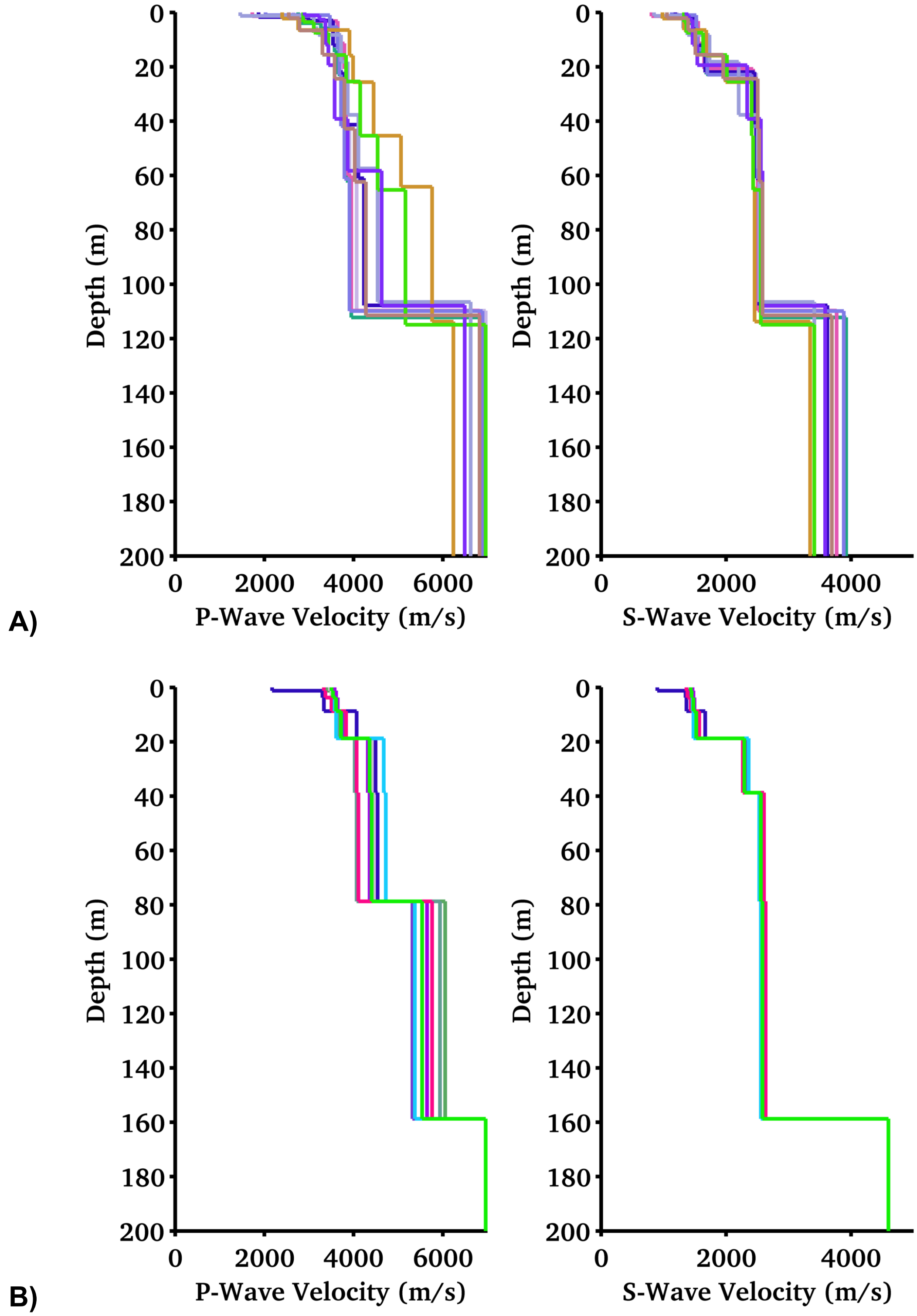

Figure 18 - *Collecting the best fitting models from the eight separated inversion runs using the free-layers (A, top) and fixed-layers (B, bottom) parameterization schemes.*

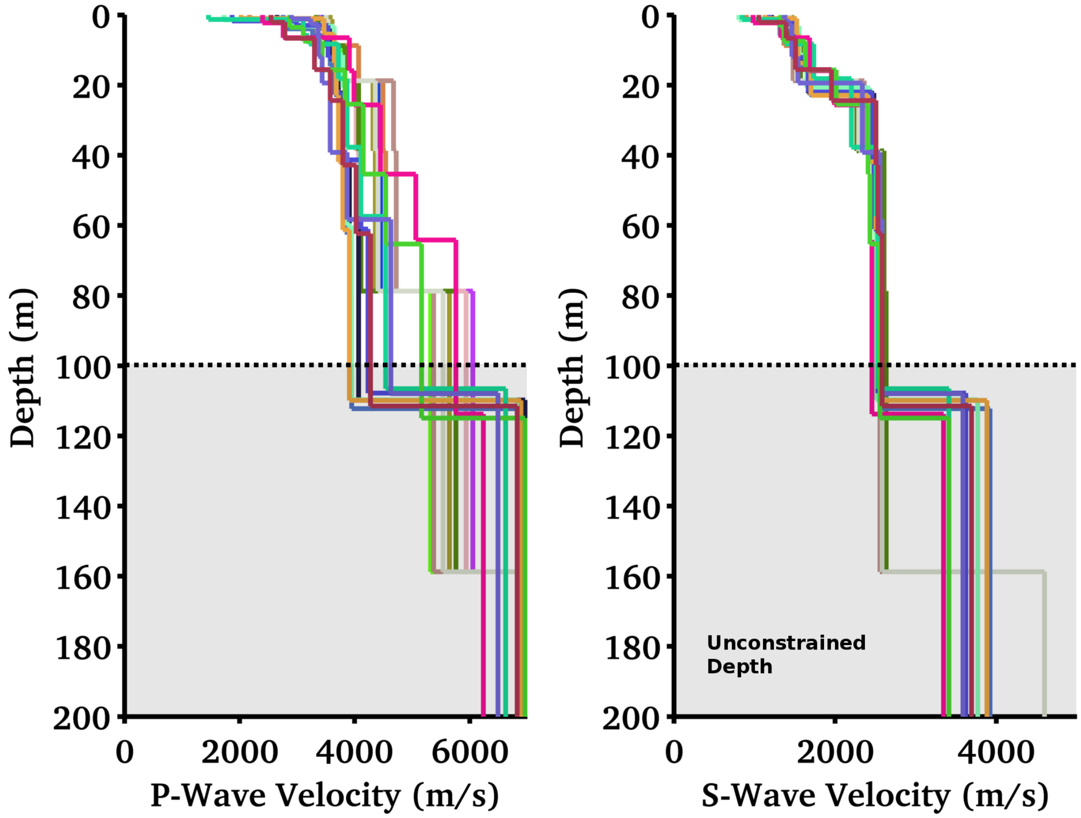

Figure 19 - *Comparison of all the best models from the two parameterization schemes (free and fixed layers). The two approaches are consistent down to a depth of about ~100m, which can be considered the maximum resolved depth.*

11. Engineering soil parameters

The ensemble of all the best inverted velocity profiles is then used to derive average soil parameters like the VsZ (average travel-time S-wave velocity over the depth Z, including Vs30, Table 1) and the quarter-wavelength (QWL) average velocities (Joyner et al., 1984) for a range of frequencies between 1 and 30Hz (**Figure 20**). The former is a standard parameter for the classification of ground-types in most building codes and in ground motion prediction equations. The latter is a parameter useful for the empirical estimation of the site-response and to assess the sensitivity of the seismic wave-field to the different depths. It has to be noticed that these two parameters are derived separately from all the best S-wave velocity models obtained from the inversion, and the results is finally averaged to improve statistics.

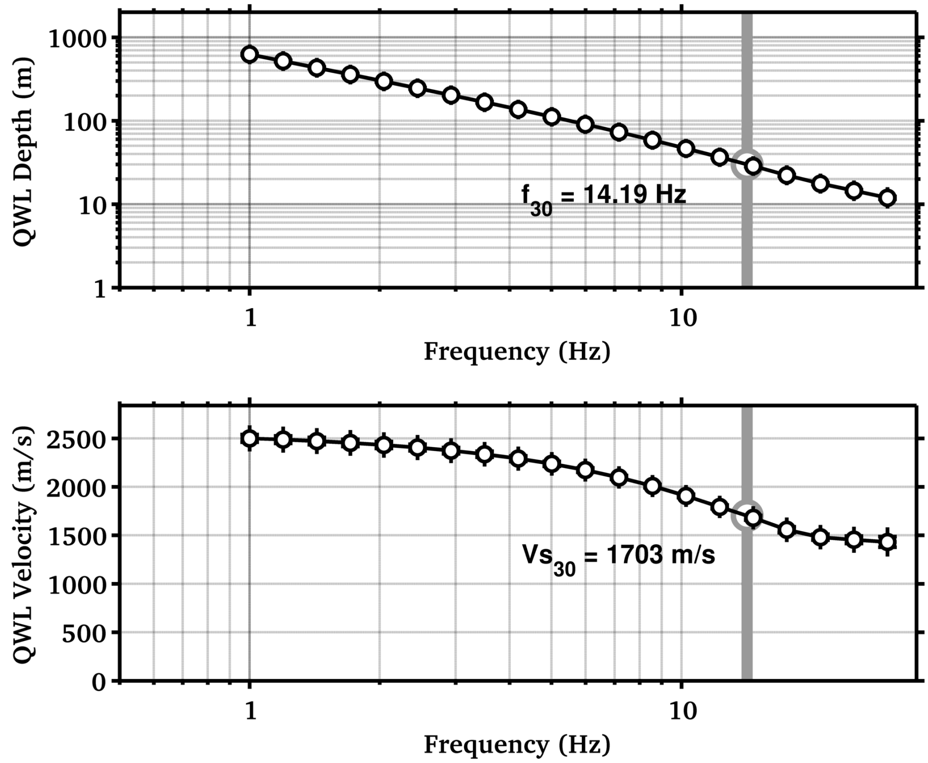

Figure 20 - *Quarter-wavelength representation of the inverted S-wave velocity profiles. Top: the depth-frequency dependency. Bottom: the QWL average velocity. The Vs30 value is indicated with its corresponding QWL frequency.*

12. Amplification models

Site amplification functions have been computed using two different approaches: the S-wave transfer function for vertical propagation and the quarter-wavelength amplification. In general the first method is used to evaluate the resonance characteristics of the site, while the second is more useful to assess the effect of the velocity contrasts between the lowermost rock layer (as reference) and the different QWL averaging depths. The two amplification functions are then corrected for the Swiss rock reference velocity profile as defined in Poggi et al. (2011), according to the procedure described in Edwards et al. (2013). Given the lower velocities in the uppermost part of the BERGE profile compared to the Swiss reference, the final corrected amplification function results in a general deamplification, with an average factor of about 0.3 at high frequencies (Figure 21).

Averaging depth	Vs-mean (m/s)	S.D.
5	1356.45	111.79
10	1416.48	61.66
15	1459.69	31.99
20	1514.80	22.54
25	1614.01	20.36
30	1703.22	15.88
40	1833.41	14.31
50	1939.84	12.86
75	2106.16	16.01
100	2204.53	20.20
150	2313.10	26.13
200	2371.50	29.69

Table 1 - *Average travel time velocities at different depths. Vs30 is highlighted.*

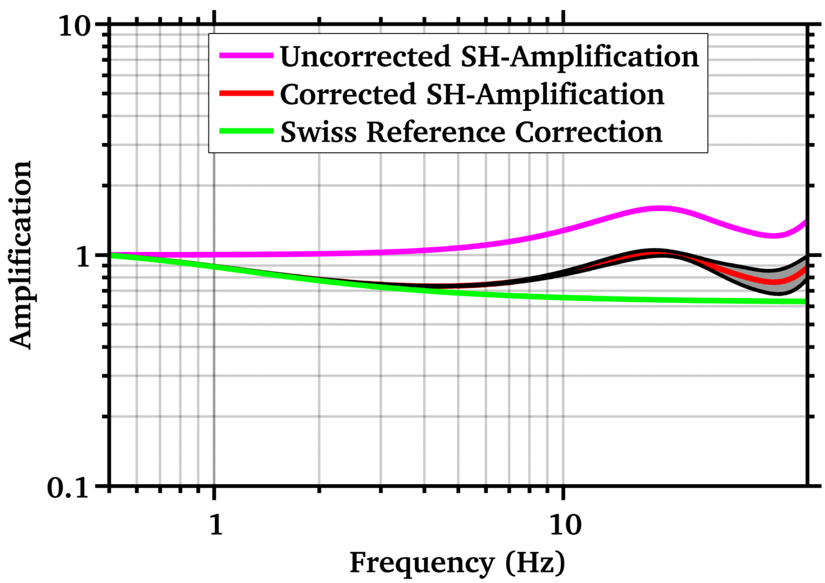

Figure 21 - *Correcting the SH-wave transfer function for the Swiss (rock) reference conditions (Poggi et al. 2011). The final corrected function shows a clear (average) deamplification of about 0.3 at high frequencies.*

Amplification functions using the transfer function and the quarter-wavelength approach are comparable (**Figure 22**), even if the transfer function provides a slightly larger amplification, because of the presence of some weak resonance peaks. At low frequencies both methods converge to the same amplification level. It has to be notice that the amplification functions do not include attenuation at this stage of the analysis, as the quality factors of the site are unknown.

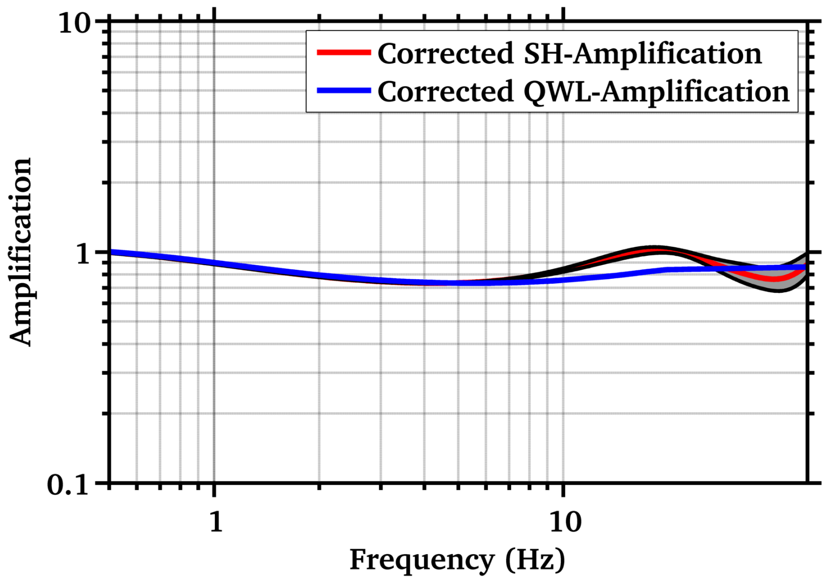

Figure 22 - *Comparison of amplification functions computed using the SH-wave transfer function and the quarter-wavelength formalism on the inverted velocity models. The functions are referenced to the Swiss rock reference model (Poggi et al. 2011).*

REFERENCES

Capon, J., 1969. High resolution frequency wavenumber spectrum analysis, Proc. IEEE, 57, 1408-1418.

Burjanek, J., G. Stamm, V. Poggi, J.R. Moore, and D. Fäh [2010], "Ambient vibration analysis of an unstable mountain slope", Geophys. J. Int., Vol. 180, pp. 820-828.

Edwards, B., C. Michel, V. Poggi and D. Fäh (2013). Determination of Site Amplification from Regional Seismicity: Application to the Swiss National Seismic Networks. Accepted for publication in Seismological Research Letters.

Joyner, W. B., R. E. Warrick and T. E. Fumal (1981). The Effect of Quaternary Alluvium on Strong Ground Motion in the Coyote Lake, California, Earthquake of 1979, Bulletin of the Seismological Society of America, 71, 1333-1349.

Poggi, V., B. Edwards and D. Fäh (2011). Derivation of a Reference Shear-Wave Velocity Model from Empirical Site Amplification, Bulletin of the Seismological Society of America, 101, 258-274.

Poggi, V. and Fäh D., 2010. Estimating Rayleigh wave particle motion from three-component array analysis of ambient vibrations. Geophys. J. Int., 180-1, 251-267.

Huguet. F. (2007). Cirques glaciaires et étagement des formes dans le massif du Feldberg, dans le sud de la Forêt Noire (Allemagne). Géomorphologie: relief, processus, environnement. 4, 309-318.

Eidgenössische Technische Hochschule Zürich
Swiss Federal Institute of Technology Zurich

SED
Schweizerischer Erdbebendienst
Swiss Seismological Service

Report on site characterization

Dagmarselle, Switzerland (DAGMA)

Poggi Valerio, Jan Burjanek, Donat Fäh

Last modified - 24 / 12 / 2014

1. Introduction

In the framework of the NAGRA seismic network project, an array measurement of the ambient vibration wave-field was performed at the location of the SED station DAGMA (Dagmarsellen, Switzerland). The scope of the survey is the seismic characterization of the area surrounding the installation (**Figure 1**), which consists in a broadband seismometer (Trillium Compact) with a high-resolution digitizer (Taurus 24Bit @200sps). Ambient vibration analysis has been used to infer the characteristics of the underground structure of the site, with special regard to the one-dimensional shear-wave velocity. Such profile was later used to assess the local seismic response of the station.

For the analysis, different spectral analysis techniques were implemented, consisting in both single and array methods, which are listed below:

- Time-frequency wavelet analysis
- Power-spectral density estimation
- Conventional horizontal to vertical spectral ratios
- Directional horizontal to vertical spectral ratios
- Wavelet polarization analysis
- Three-component high-resolution f-k analysis.

The results of all these analyses conformed to the definition of the final velocity model. In the following, the main results of these investigations are summarized and a final interpretation of the velocity profile is given. From this interpretation, engineering parameters are finally derived, e.g. the Qwl-Vs average velocity, VsZ (including Vs30) and the seismic amplification from the analytical SH-transfer function of the one-dimensional soil column.

2. Survey description

To characterize the seismic response of the site, an array measurement of ambient vibration was performed on 15/08/2013 (**Figure 1**). The array consists of a single measuring configuration of 14 sensors and about 160m in size. The decision of using a single geometry was taken on the base of the site accessibility. Deploying also a small array close to the SED seismic station was not practically possible, due to the presence of topographic obstacles (a steep slope and the nearby forest, **Figure 2**). A possibility could have been to move such configuration closer to the valley axes, where a flatter area is available, but in this case the result would not have been relevant for the characterization of the seismic station. High velocities were nevertheless expected for the underlying bedrock (Molasse), which is here shallow and in few cases outcropping. This justifies the use of a large geometry for the array to be successful. The maximum aperture of the array was again controlled by the available space in the valley (Lutertal), which was strongly limited toward North and South from dipping slopes. A precise prior estimation of the possible maximum penetration depth was not possible, due to the large uncertainty of the bedrock velocity, but resolution down to about 100m depth was expected.

During the survey, a total of about two hours of recordings has been acquired. However, not all the stations recorded properly (**Figure 3**). One station (5) did not record at all, probably due to GPS synchronization problems; the sensor of a second station (13) was accidentally badly coupled to the ground, providing too distorted recordings to be subsequently used. The quality of the remaining twelve stations was nevertheless satisfactory, in terms of signal and azimuthal coverage. As it will be better explained later, the sensors have been grouped in two concentric sub-configurations (**Figure 3**). The first configuration includes the most external stations, which are mostly located on rock, while the second (inner selection) samples only the shallow quaternary infill of the central part of the valley.

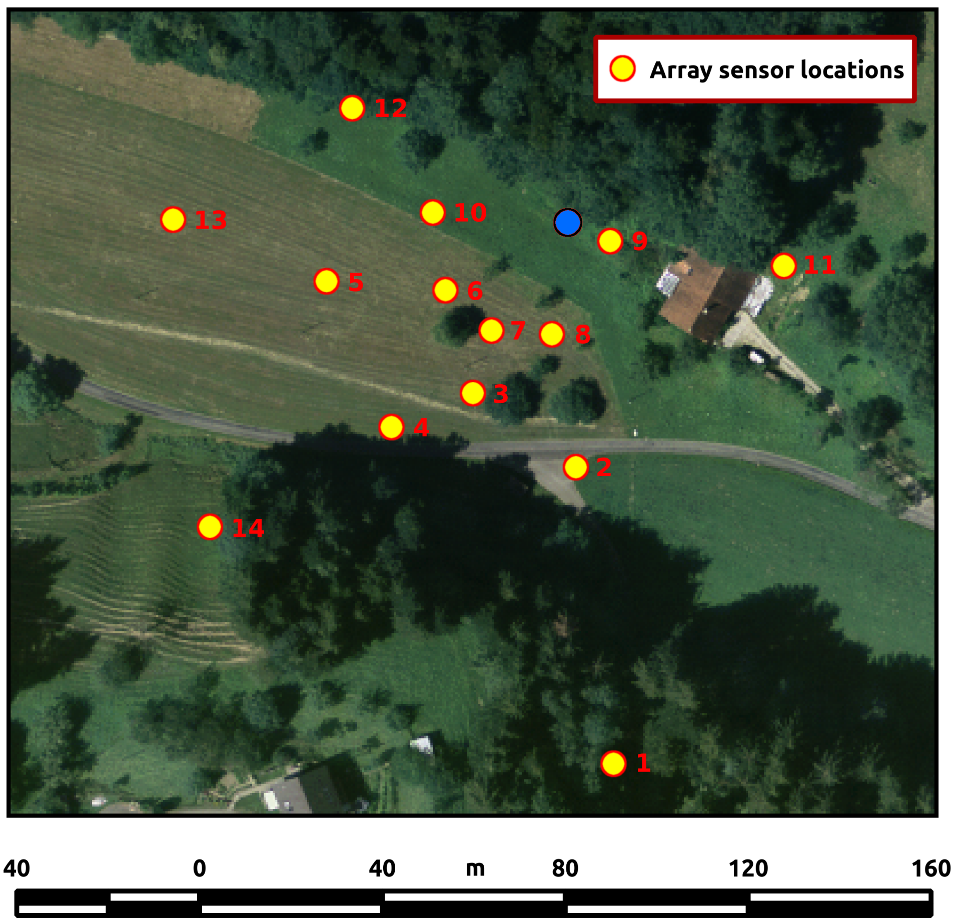

Figure 1 - *Location of the ambient vibration array survey performed in Dagmarsellen (SED station DAGMA) on 15/08/2013. Given the site characteristics, only one array configuration was performed, whose maximum diameter was limited by the available space. The approximate location of the seismic station is shown in blue.*

Figure 2 - *Overview of the measurement area. The array center is roughly located at the center of the picture, while the seismic station DAGMA is on the extreme right, positioned at the edge of the grass field, on a small terrace close to the forest border.*

3. Soil type, topography and geology

The array has been set in open field conditions, in a rural area (**Figure 1**, **Figure 2**). The influence of buildings and anthropogenic disturbances is virtually negligible. Array sensors have been deployed on free soil conditions. Good coupling with the ground was assured by means of digging small holes at the sensor's places, and by using a special support (*Trihedron*®) that facilitates the leveling of the device even for difficult soil conditions. The measurement area is located on a moderate slope dipping toward SSW. However, no topographic correction has been taken into account before processing.

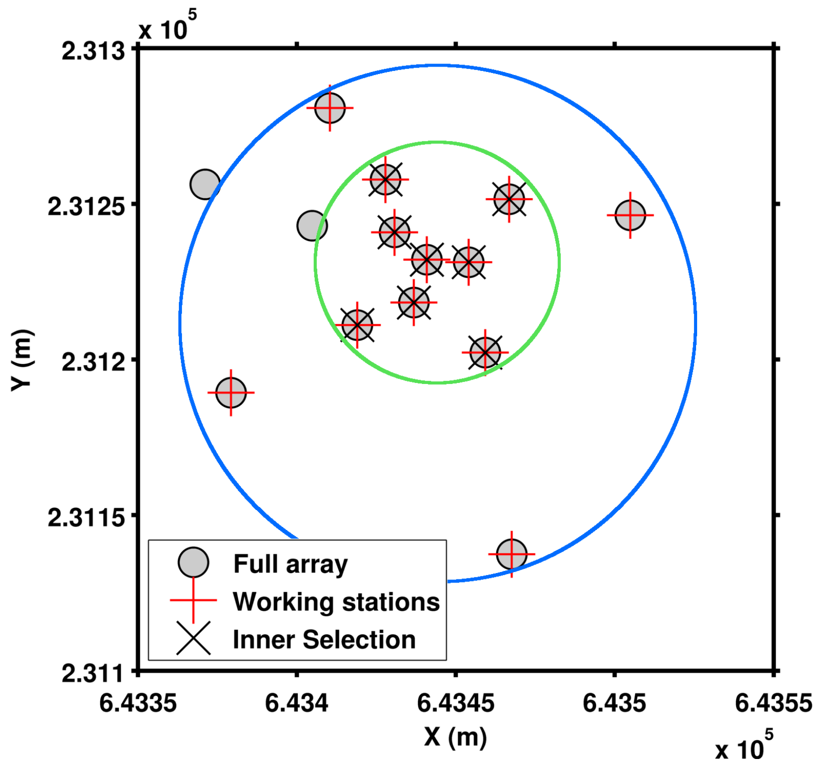

Figure 3 - *Geometry of the ambient vibration array deployed at the station DAGMA. With different symbols are indicated array stations actually used for the processing. The "inner selection" of 8 sensors on the quaternary sediment fill of the valley is also shown.*

From the geological points of view (**Figure 4**), the target area is a small lateral valley incised within the Molasse basin, surrounded by few moranic deposits, clearly identifiable from the surface topography and from the geological map of the area. The central part of such valley is filled by unconsolidated quaternary sediments. The bedrock is very shallow at the measuring location, but rarely exposed across the area (a thin cover of quaternary material is mostly present). The bedrock probably consists of consolidated sandstone with layers of different texture and granulometry, from marl and silt to conglomerate. The surface morphology is considerably smooth and modeled by the action of glaciers during the Pleistocene. Such site can be classified as of rock ground-type A.

4. Acquisition equipment

Each acquisition point within the array consisted of a three components seismometer (Lennartz 3C with 5s eigenperiod) and a 24 bit data logger (Quanterra Q330). Synchronization between stations was assured by standard GPS, while a more accurate differential GPS (Leica Viva system) was used to precisely locate the sensor's coordinates with a tolerance of less than 5cm.

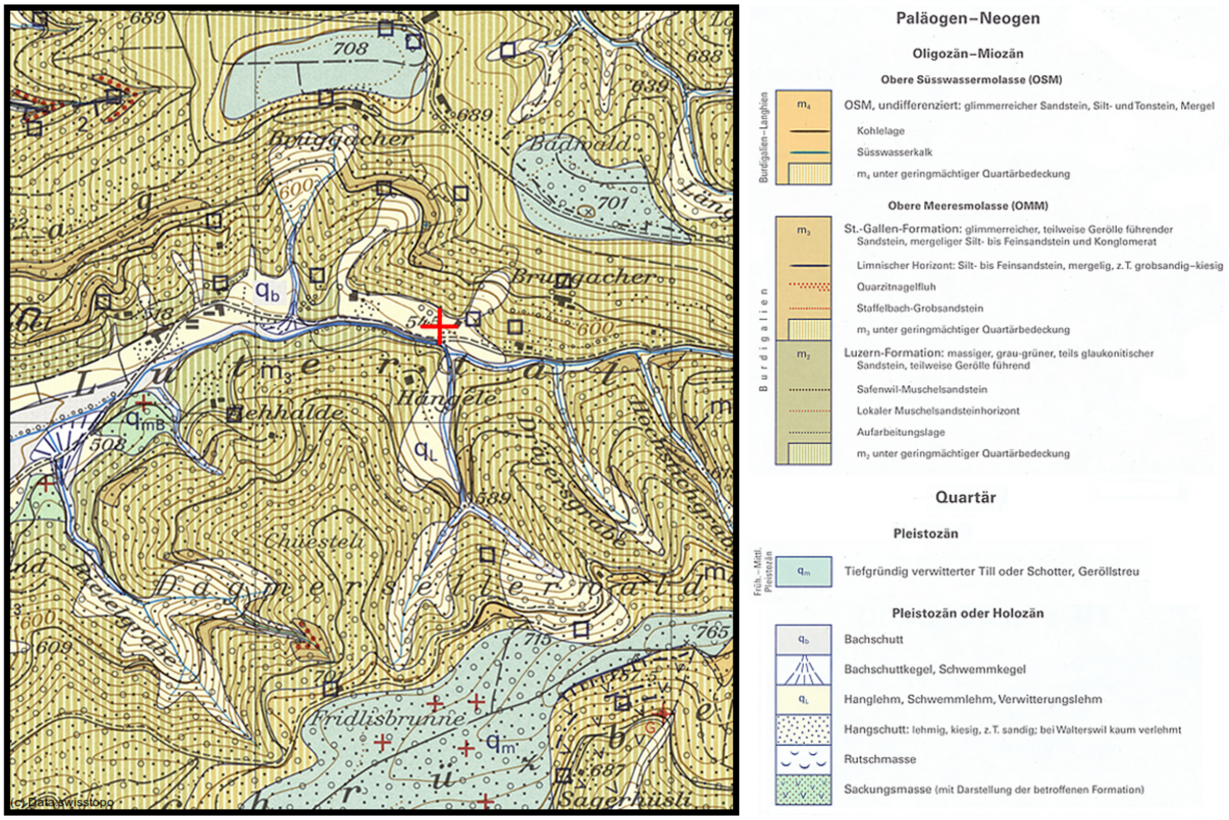

Figure 4 - *Geological map of the Lutertal, in the Dagmarsellen region (reproduced from Swisstopo, modified). In red the approximate location of the permanent station DAGMA.*

5. Weather conditions

The weather conditions were optimal and stable during the whole measurement, with no precipitations, no wind and an average (over the whole day) temperature of 18 degrees.

6. Pre-processing and preliminary data-quality control

The three-component recording has been filtered prior to analysis using a high-pass 6th order causal Butterworth filter with corner at 0.2Hz. Although it is not a strict requirement for spectral analysis techniques, such filtering was applied in order to facilitate the preliminary visual inspection of the noise traces and to evaluate the coherency of the wave-field (**Figure 5**). Such procedure gives essential information for the subsequent interpretation of the f-k analysis results.

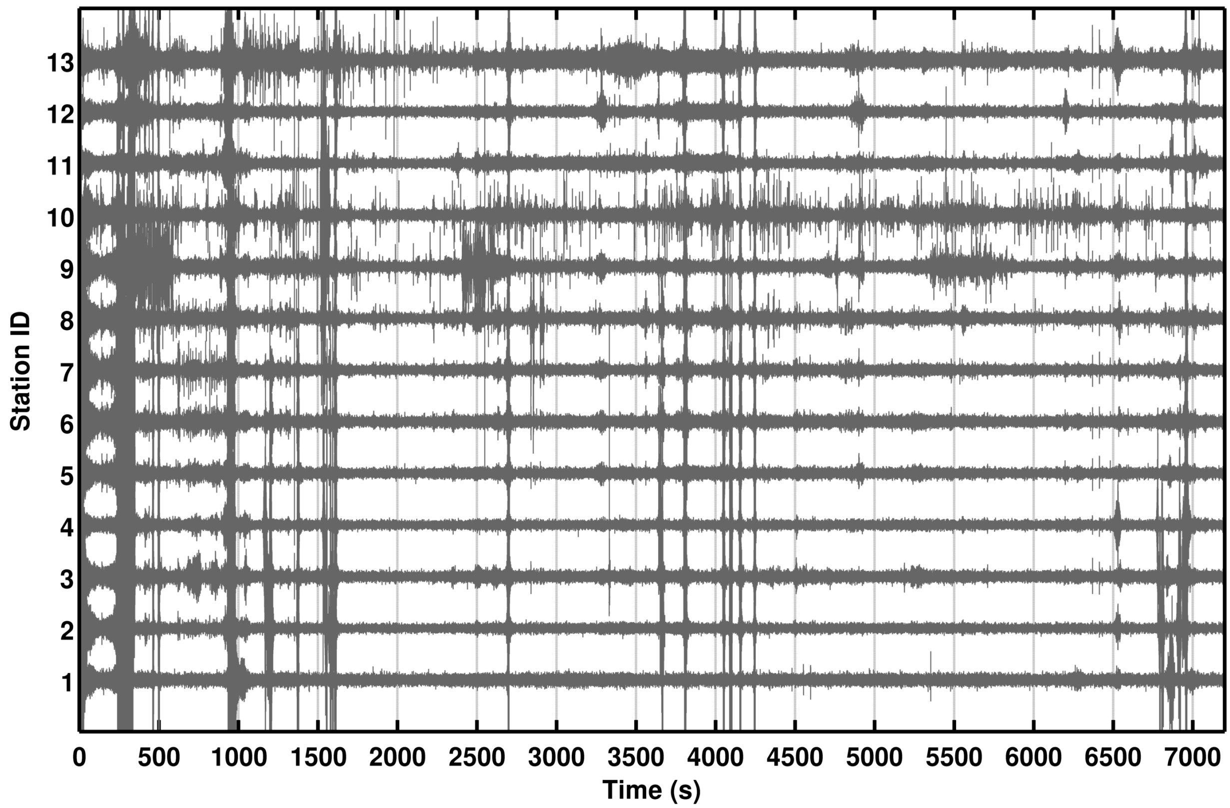

Figure 5 - *Inspection of the useful part of the ambient vibration recording of the array DAGMA. Several impulsive high-frequency transients of anthropogenic origin are visible. Excluding the first 500s of recordings the overall quality of the recording is good.*

To assess the quality of the ambient vibration recordings, spectral analysis was subsequently performed. Because of the stochastic nature of the ambient vibration wave-field, a statistical approach has to be used, such as the estimation of the power spectral density (*PSD*). This approach is useful to evaluate the average energy level of the recordings in the analyzed frequency range, and to access the presence of spurious spectral peaks, which might be related to human activity (machinery, pumps). By inspecting the PSD of the three-component recordings from the whole array in the range between 0.5 and 40Hz, a minor spurious peak is visible at about 14Hz. The peak is more pronounced at the center of the array (**Figure 6** bottom, station 7 - on the sedimentary part) than at the edges (**Figure 6** top, station 1 - on rock) probably because of a resonance. The peak - very narrow - is most likely of anthropogenic origin (from the nearby farm) and should be rejected from interpretation. The average energy level is nevertheless very low, within the minimum and maximum bounds of the USGS noise model.

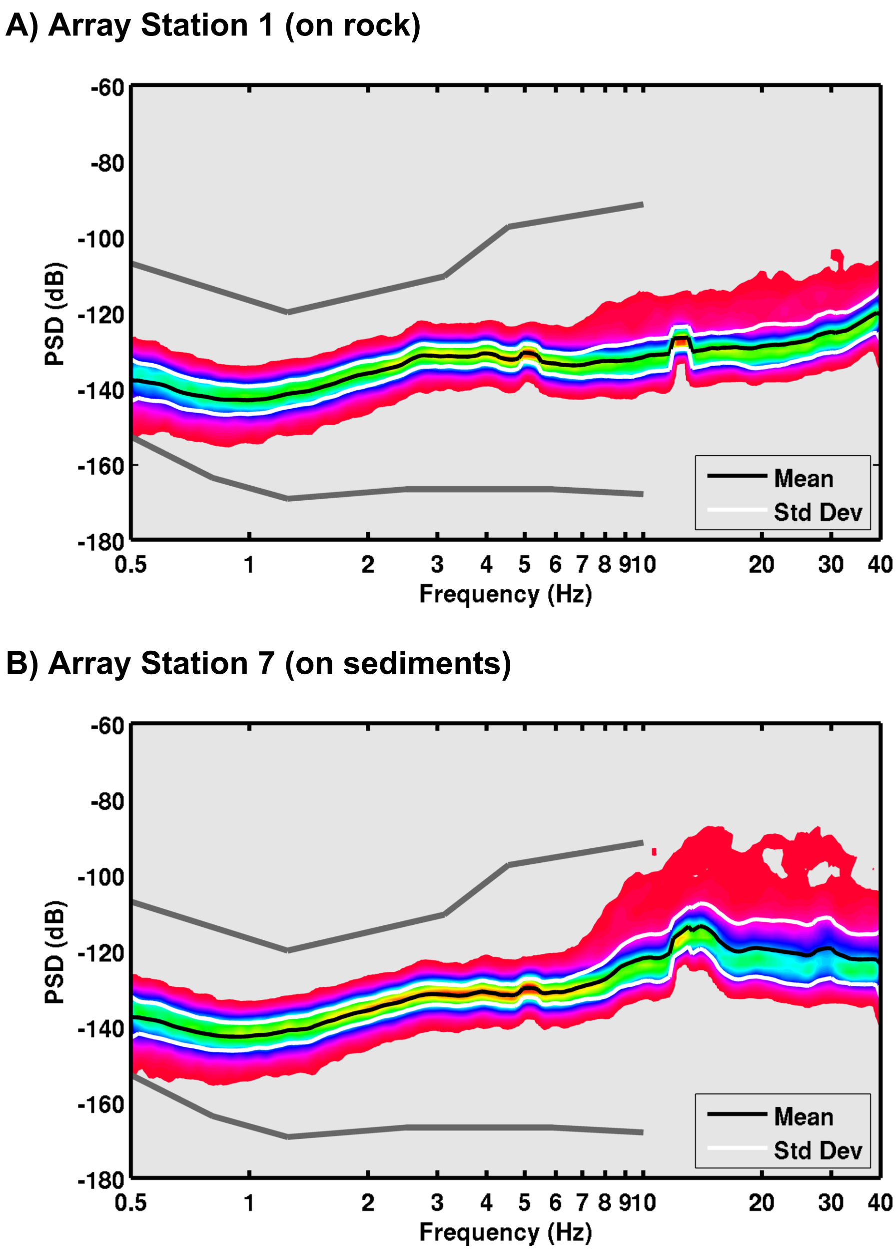

Figure 6 - *Power spectral density (PSD) computed for 2h recording at the central station of the array (station 7) and at the edge of the measuring area (station 1). Similar results were obtained from the other stations of the array. In gray lines are the minimum and the maximum bounds of the USGS noise model, for comparison.*

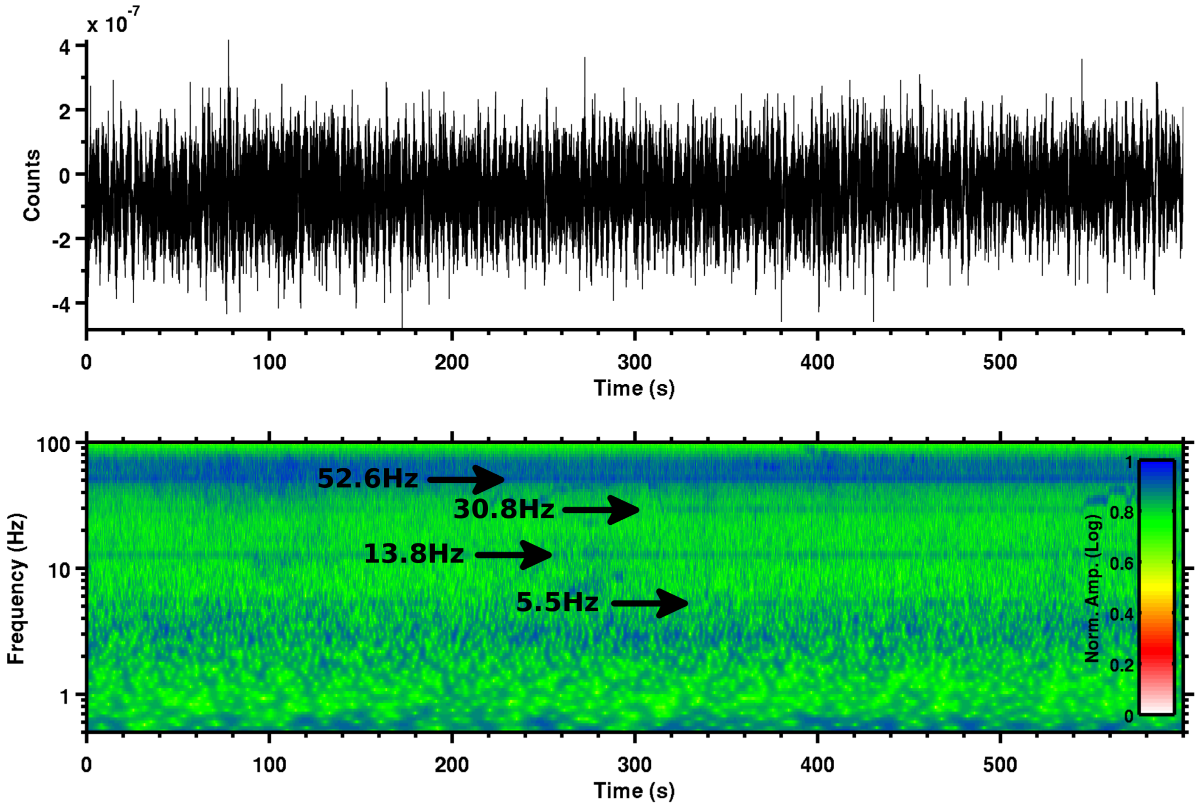

Figure 7 - *Example of spectrogram from 600s of recording of the station number 1 of the array (on rock, vertical component). For the analysis, the cosine wavelet is used (wavelet parameter = 12). Harmonic disturbances are visible on the whole spectrogram, but nevertheless not particularly energetic.*

Complementary to the aforementioned statistical methods, a spectral decomposition approach is more suitable to assess the stationarity of the ambient vibration wave-field over time. The wavelet time-frequency analysis was then performed over the whole recording time. From such analysis (**Figure 7**) an overall stability of the ambient-vibration wave-field over time is evident. The disturbance at about 14Hz is confirmed to be a nearly harmonic contribution, steady over the whole recording window. This provides a further confirmation of its possible anthropogenic origin. Additional harmonic contributions are evident, at 5.5Hz, 30.8Hz and 52.6Hz. These disturbances are nevertheless very weak and well localized in frequency; therefore they won't affect the following processing steps.

7. Conventional H/V spectral ratios

The horizontal-to-vertical (H/V) Fourier spectral ratio is a technique widely used in seismic site characterization because of its ability to provide an estimate of the SH wave fundamental frequency of resonance (f_0) of the site. Other than that, H/V ratios are useful to provide information on the Rayleigh wave ellipticity function, which can be used in the inversion procedure to constrain large velocity contrasts at depth. In this study, we use the H/V technique also to map the variability of the subsoil structure along the investigated area; this is necessary to verify the fulfillment of the 1D structure assumption, which is necessary for the f-k method applied later.

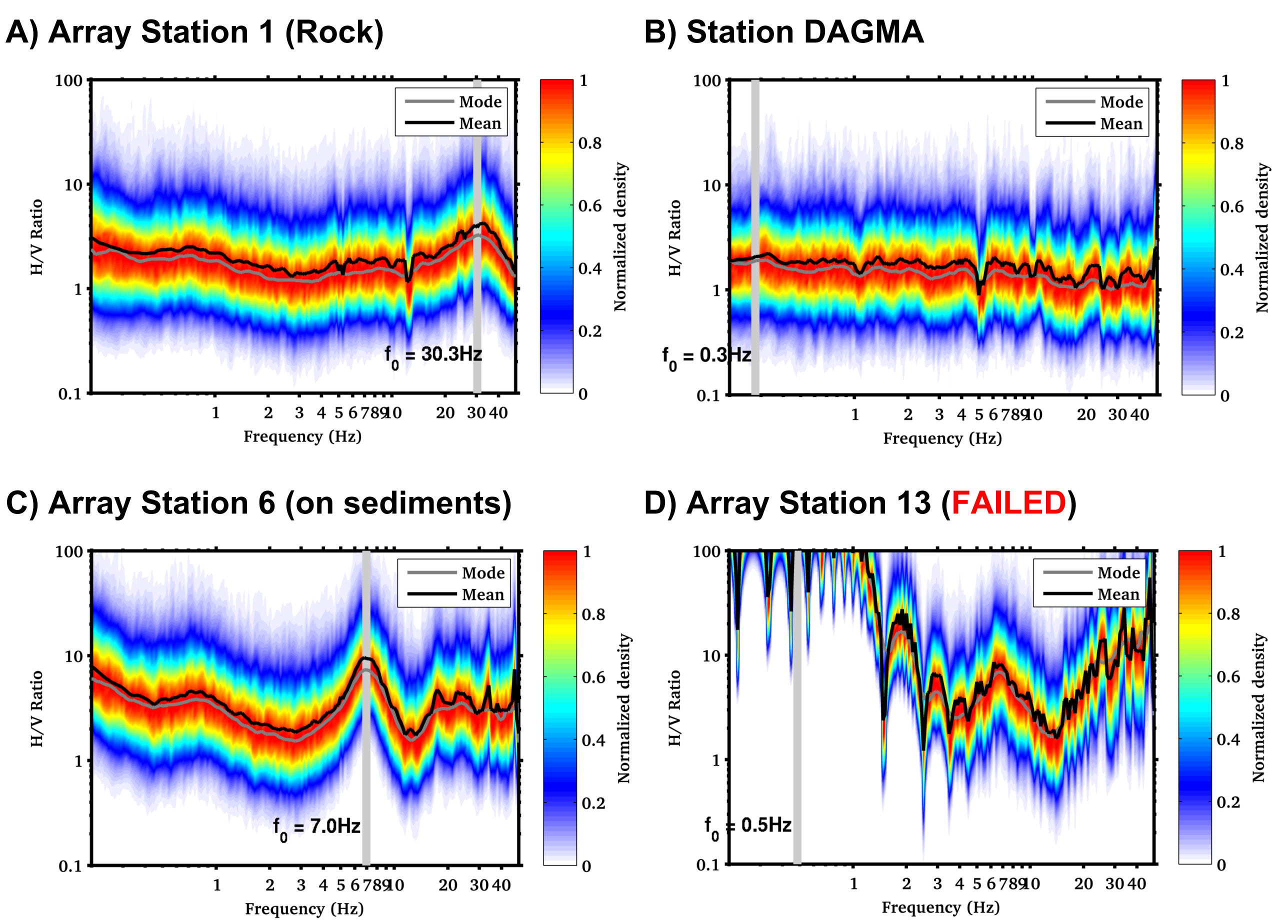

Figure 8 - *Example of H/V spectral ratios at three stations of the array and at the permanent station DAGMA. The bad coupling of the station 13 was evident by inspection of the H/V spectral ratios; this station has not been used for subsequent processing. The resonance frequency of the soil cover is indicated with a light gray line.*

H/V spectral ratios have been computed for the recordings at each station of the array and at the SED permanent station (e.g. **Figure 8**). The behavior of the noise wave-field at the different stations location reflects the characteristic of the valley morphology (**Figure 9**). A high frequency peak is evident over the whole array, however its frequency and amplitude increases moving accordingly from the valley axes, where the thickness of the quaternary deposits is larger, to the edges of the array, where the bedrock is shallower (**Figure 10**). This peak can definitely be used to map the variability of the quaternary fill over the measuring area (e.g. **Figure 11**). Therefore, a simple one-dimensional approximation is not sufficient to explain the high-frequency part of the wave-field (> 7Hz). Conversely, below 7Hz the wave-field is more stable, confirming the homogeneity of the underlying rock. A weak peak is also present at low frequency (< 1Hz), but the interpretation is of more difficult. Such maximum might be induced by a change in lithology within the profile at depth, which causes a modest contrast of seismic impedance. It is also interesting to compare the results of H/V analysis between a typical array station on rock (e.g. **Figure 8**,A) and the permanent station (**Figure 8**, B); the DAGMA station does not show evidence of any high frequency peak, as the sensor has been properly deployed removing the topmost part of the soil cover, which is however resonating in the array recordings.

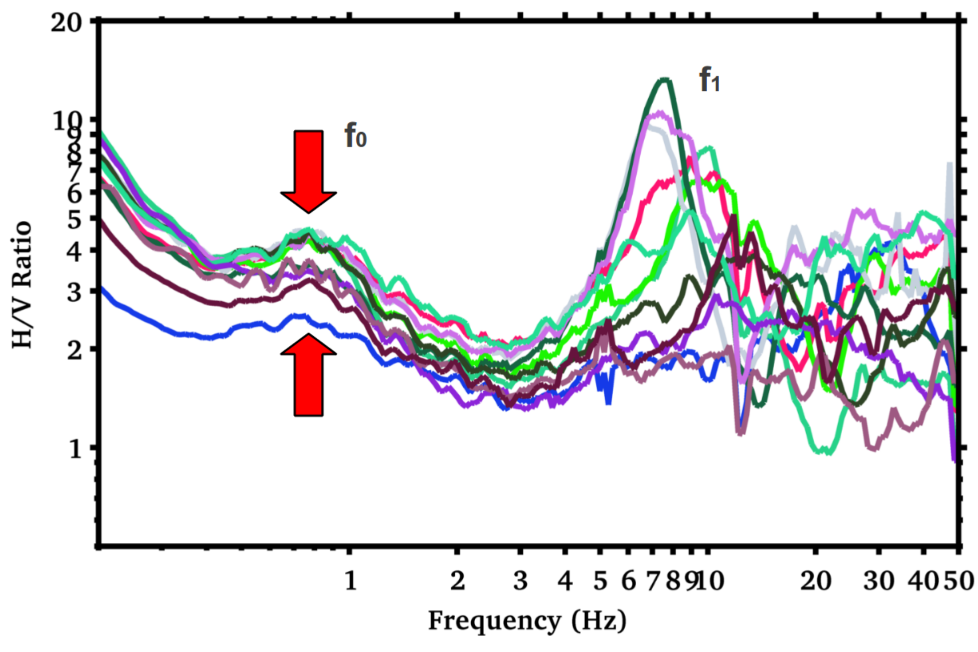

Figure 9 - *Comparison of the H/V spectral ratio curves of all the stations of the array. The curves are stable up to at least 7Hz, confirming the lateral homogeneity of the underlying bedrock velocity structure of the site. A low frequency peak is visible at about 0.8Hz. At high frequencies the spectral ratios are very variable across the array. This reflects the complex geometry of the quaternary sediments cover.*

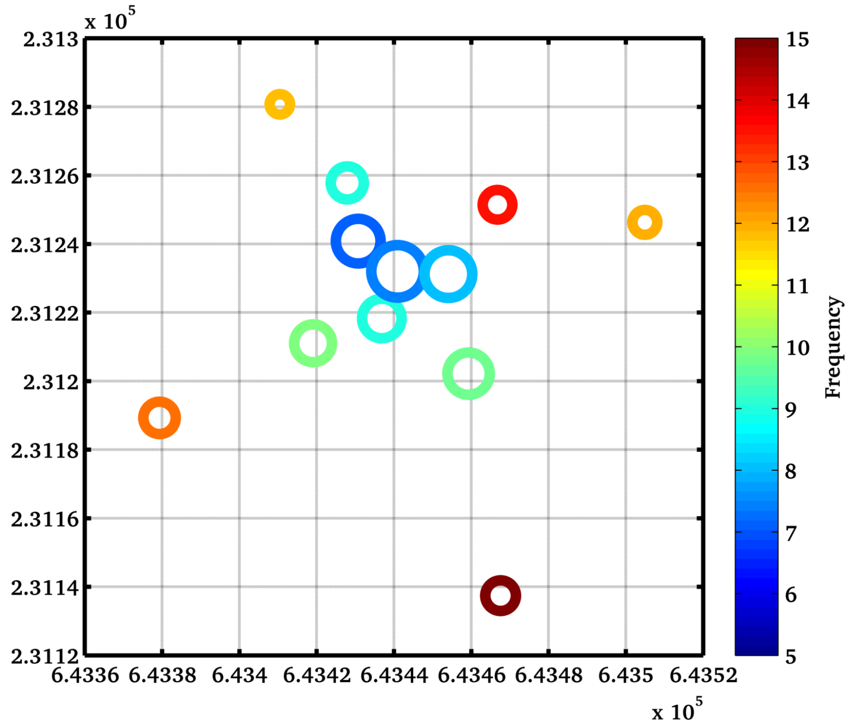

Figure 10 - *Mapping the variation in frequency (with different color) and amplitude (with circles of increasing size) of the high frequency peak (f_1) across the array. It is evident a clear trend from the center of the array to the edges, which reflects the complexity of the quaternary soil cover geometry.*

8. Directional H/V spectral ratios

The computation of directional H/V spectral ratio or polarization analysis is useful to reveal asymmetries in the ambient vibration wave-field. Different effects can induce such a behavior: 2D/3D structure, topographic effects or a non-homogeneous distribution of the noise sources. If a strong directionality is found by the analysis, it is generally recommended to carry out further investigations to properly address the origin of polarization.

By processing the directional H/Vs at all the recording stations of the array (e.g. **Figure 12**) it is possible to observe an isotropy of the wave-field in the low frequency range, roughly below 7Hz. At high frequencies, however, the variability of the H/V peak observed in **Figure 9** is noticeable also in their directionality. As already introduced, this can be explained by the variability of the uppermost soil cover layer over the study area, and should not be interpreted as an effect of non-homogenous distribution of the noise sources. This issue is later investigated through f-k analysis.

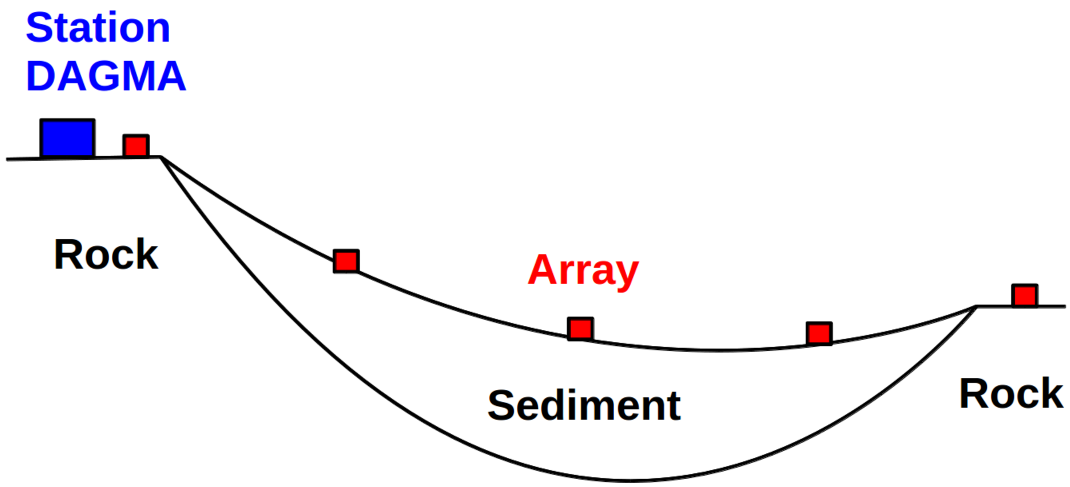

Figure 11 - *Schematic representation of the variability of the quaternary sediment fill over the measuring area. The sediment thickness appears to be maximum near the center of the array, while the bedrock is nearly outcropping at the edges.*

The valley morphology has probably some influence on the directionality of the ambient vibration wave-field at high frequency. This might be related to the geometrical elongation of the quaternary cover along the valley axes. An effect of the topographic slope seems to be unlikely in this case. All stations close to the center of the array are more affected by a certain directionality of the H/Vs at the resonance peak (f_1), which is aligned preferentially along the valley axes (e.g. **Figure 12**C, D). This is nevertheless not surprising, as this phenomenon is widely observed in sedimentary basins. Moving toward the edges of the measurement area, the directionality effect is confined to very high frequencies (e.g. about 30 Hz in **Figure 12**A), and it is therefore negligible for our purposes. At the permanent station, no evidence of directionality is present from the analysis of the H/V spectral ratios (**Figure 12**B).

The result of the directional analysis is also confirmed by applying the wavelet polarization analysis techniques as described in Burjanek et al. (2008) to permanent station DAGMA. Also in this case no sign of directionality (**Figure 13**A) and polarization (**Figure 13**B) of the wave-field are observable.

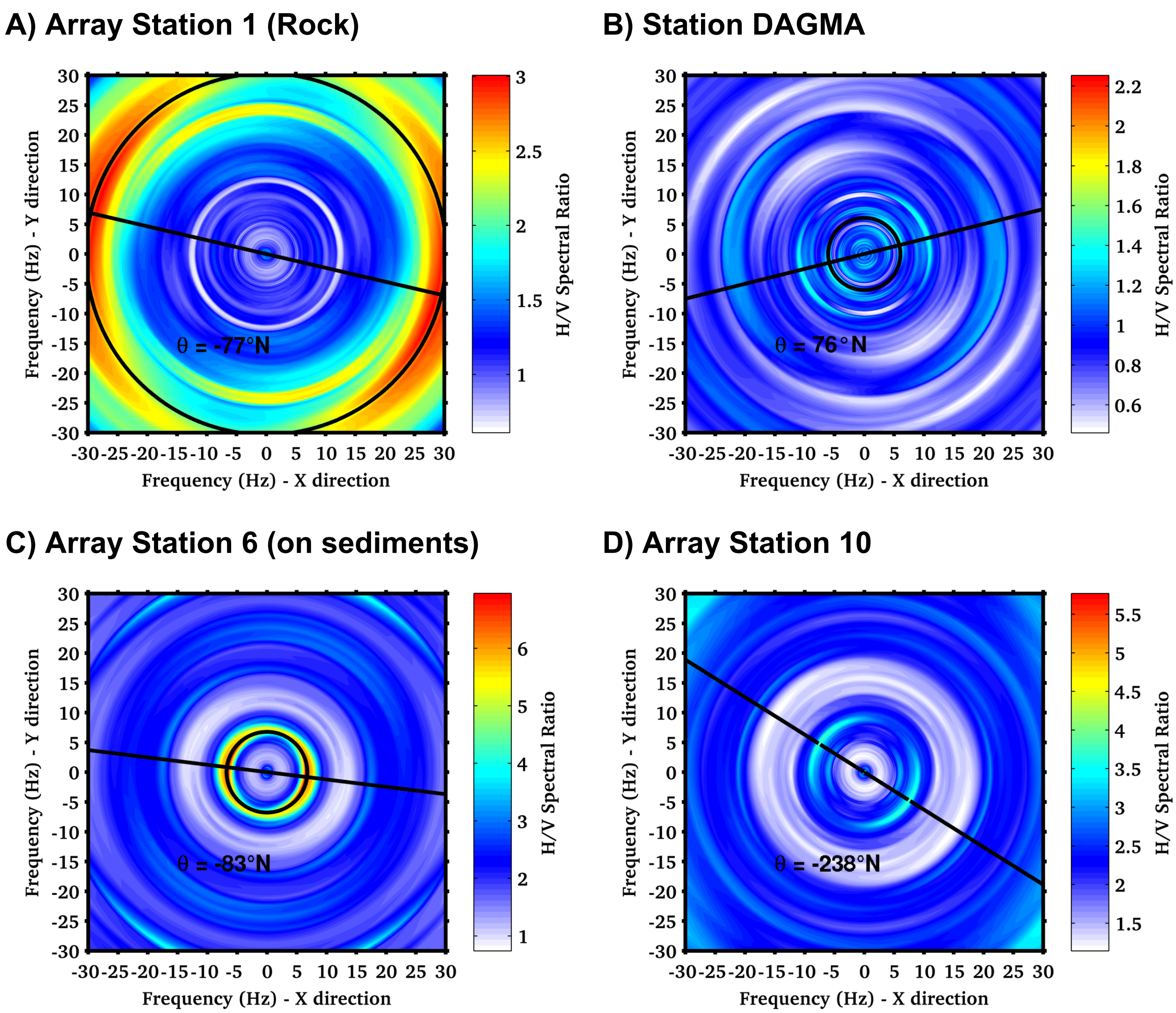

Figure 12 - *Example of directional H/V spectral ratios at three stations of the array and at the permanent station DAGMA. No consistent evidence of wave-field anisotropy is present at low frequency (below 7Hz), while the high frequency resonance peak (f_1, >7Hz) is preferentially aligned along the valley axes, and might be therefore influenced by the geometrical elongation of the quaternary cover.*

A)

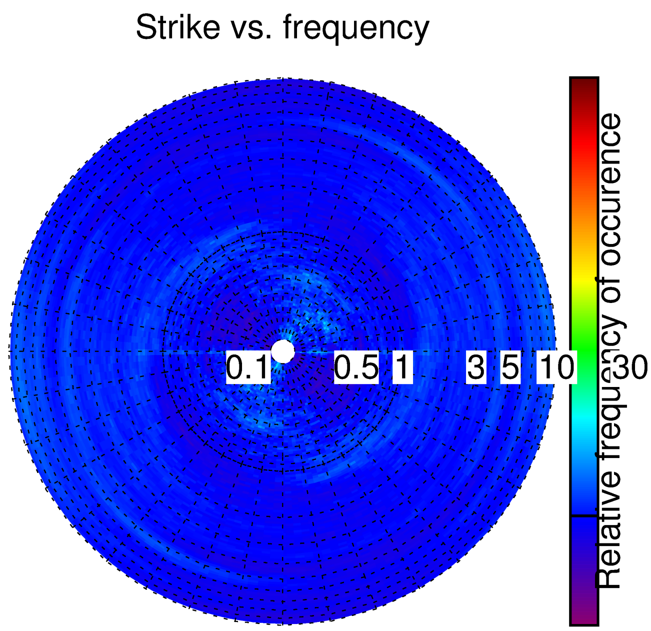

B)

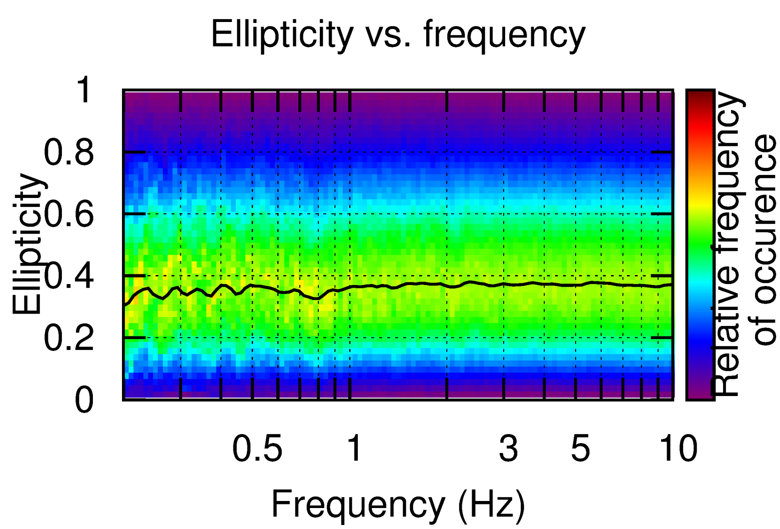

Figure 13 - *Wavelet-based polarization analysis at the permanent station DAGMA. By analyzing the polarization over strike (A) and the particle motion ellipticity plot (B), no directional effect is visible in the frequency range of interest.*

9. Three-component f-k analysis

The frequency-wavenumber analysis is a spectral technique based on seismic array recordings that allows retrieving the direction and the dispersion characteristics of the surface waves. We apply here this technique to three-component ambient vibration recordings using a modification of the high-resolution method of Capon (1969) as described in Poggi et al. (2010). Using all the three-components of motion gives the possibility to retrieve information about the propagation of the Rayleigh waves (vertical and radial processing direction) as well as of the Love waves (transversal direction).

As in the case of the previous methods, the ambient vibration recordings are treated statistically by subdividing the traces in sub-windows. For each consecutive window a separated f-k analysis is performed, and the results are then averaged over the whole recording, increasing the robustness of the final estimation.

As first step, from the f-k analysis it was possible to assess the noise source azimuthal distribution over a range of analyzed frequencies (e.g. **Figure 14**) for the vertical, the radial and the transversal component. A rather uniform (isotropic) distribution is observed for all the components, and particularly in the low frequency range (3-5Hz), confirming then the independency of the noise source distribution to the directional behavior observed in the H/V spectral ratio. Subsequently, the surface-wave dispersion curves are extracted from these distributions by visual inspection and manual picking of the f-k density plots (**Figure 15**).

3-5Hz

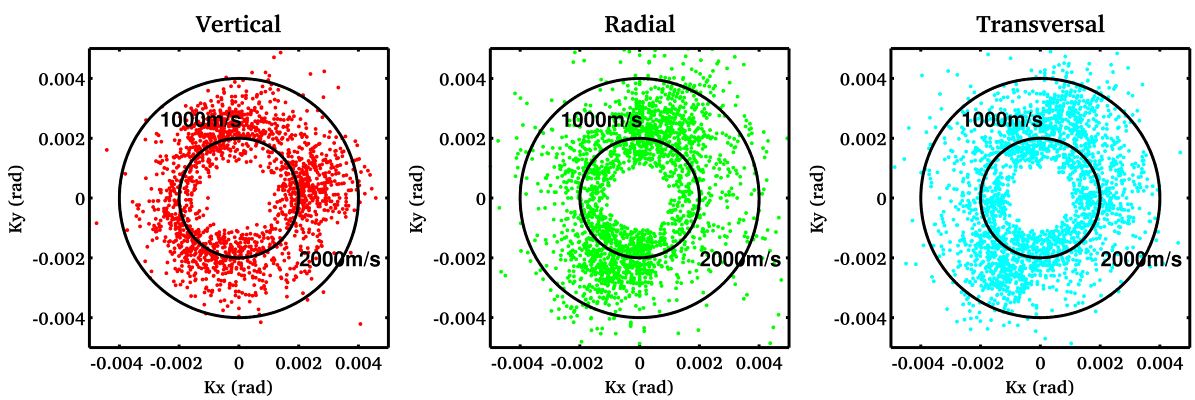

Figure 14 - *Example of distribution of noise sources in the low frequency range (3-5Hz) obtained from three-component f-k analysis. The source distribution is homogenous for all the components in the useful frequency band.*

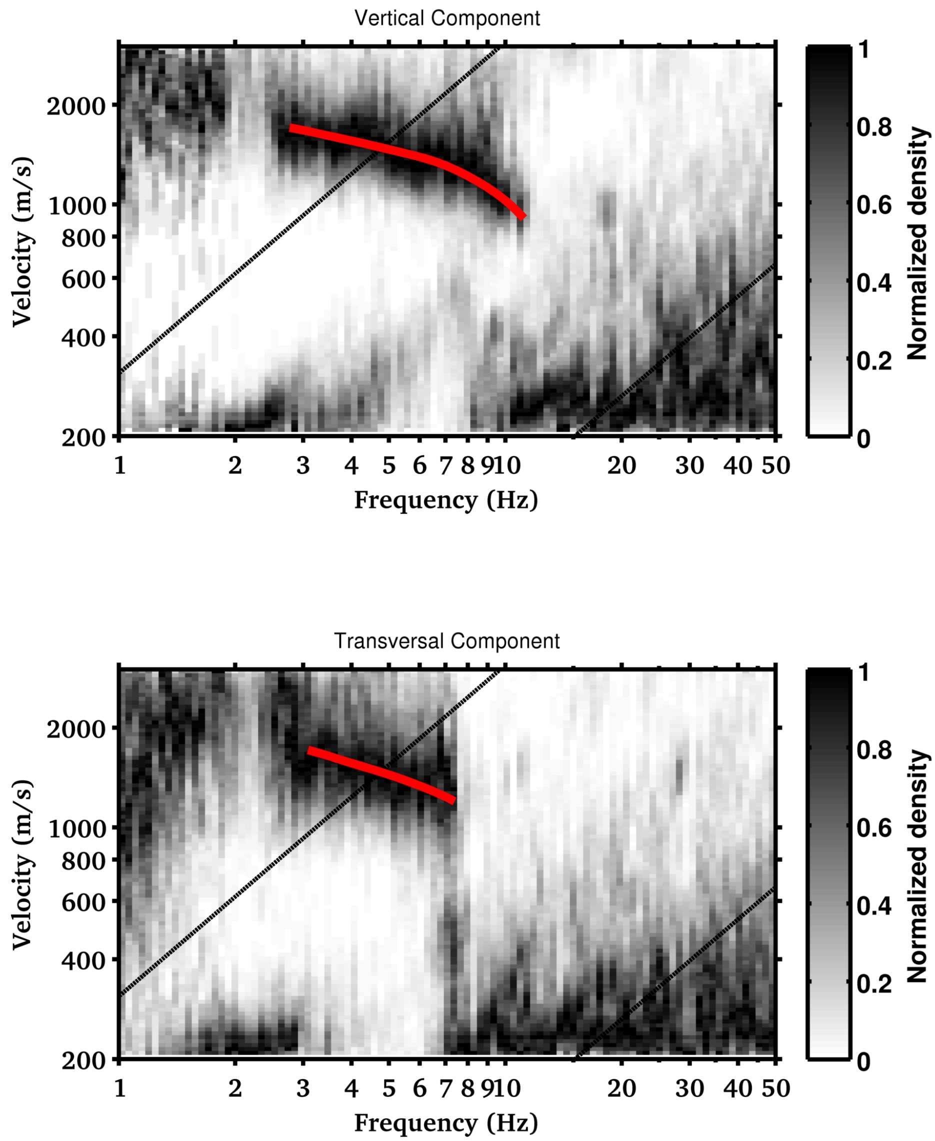

Figure 15 - *Density distribution of the surface wave signals obtained from the recording of the whole DAGMA array using three-component f-k analysis. Top: result from the analysis of the vertical component (Rayleigh waves); Bottom: result for the transverse component (Love waves). In red the interpreted dispersion curves are given (manually selected).*

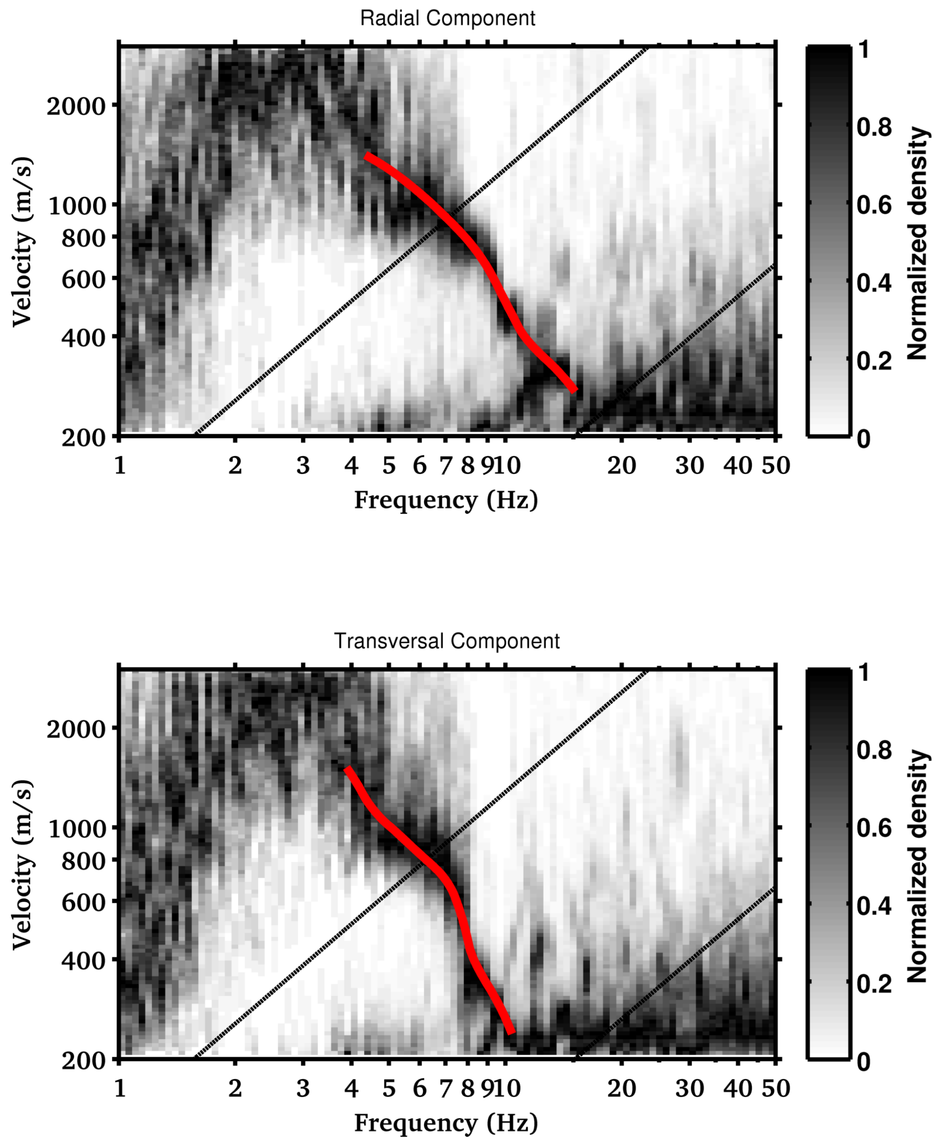

Figure 16 - *Density distribution of the surface wave signals obtained from the recording of the only "inner selection" of the DAGMA array using three-component f-k analysis. Top: result from the analysis of the vertical component (Rayleigh waves); Bottom: result for the transverse component (Love waves). In red the interpreted dispersion curves are given (manually selected).*

In a first attempt, all the receivers of the array have been used, with the only exception of station number 13, which was not properly coupled to the ground. In this case, due to the complex geometrical of the site, the dispersion patterns from soft sediment part and the rock part are interfering, leading to some difficulties in the modal interpretation. In order to isolate the contribution of the quaternary cover from the interpretation, a second test was performed by using the only “inner selection” configuration. This test confirmed the presence of shallow low velocity layers in the central part of the basin and subsequently gave the possibility to correctly isolate and address those portions of dispersion curves related to the bedrock.

We now focus on the rock part only, which is of interest for the characterization of the seismic response at the permanent station. From f-k analysis, the Rayleigh wave dispersion can clearly be tracked between about 3 and 8Hz, as well as the Love waves. The dispersion pattern is typical for a gradient velocity profile, with progressive decrease in velocity with frequency and no evident jump. The final interpretation of the modal dispersion pattern is then presented in **Figure 17** for both the Rayleigh and Love waves, also comparing the rock and the soft sediment model obtained from the inner array sub-selection.

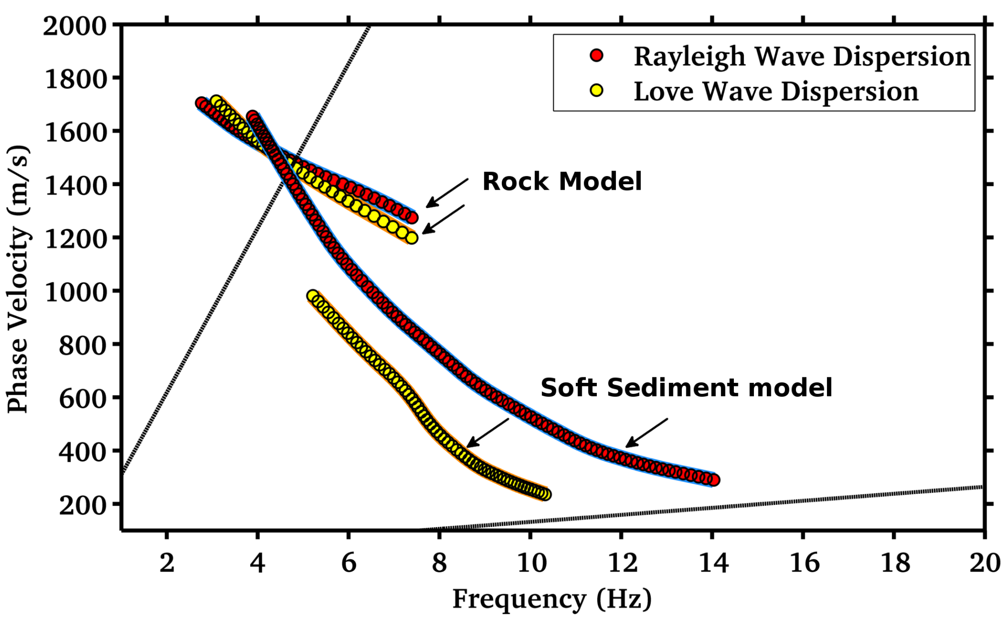

Figure 17 - *Final interpretation of the Rayleigh and Love dispersion curves from the different station selections of the DAGMA array. Minimum and maximum resolution bounds from the full array are indicated with black solid lines.*

10. Inversion of the dispersion curves

The surface wave dispersion curves (Rayleigh and Love) obtained from the three-component f-k analysis of the ambient vibrations were inverted to obtain an estimation of the velocity profile of the site (mainly S-wave velocity as function of depth, and to a lesser extend the P-wave velocity, due to the lower sensitivity). The analysis was performed using the software *Dinver* (www.geopsy.org), which implements a direct search approach (**Figure 18**) based on a conditional version of the neighborhood algorithm (Sambridge, 1999).

To parameterize the velocity model, two different approaches were implemented. The first one consisted in setting up an eight-layer model with free interface depths (**Figure 19**). In such a case the free inversion parameters are then the velocities (P and S) and layer thicknesses. In the second case, a fixed-thickness layer approach was used (**Figure 20**). The advantage of the former method stays in the possibility to better resolve sharp velocity interfaces, while the second is less unique and better constraints the seismic velocity. The two approaches have to be nevertheless considered complementary, and they should provide consistent results. Ten inversion tests (*runs*) have been performed for each of the two model schemes, in order to minimize the effect related to a possible unfavorable initial randomization of the parameter space. Additional ten runs were also performed with the above layering scheme, but using a Montecarlo search instead. This was done as supplementary consistency check, to evaluate the sensitivity of the inverted models, and to identify possible local minima in the parameter space. The best fitting models from of each run were then collected (**Figure 21**) and used later on for the computation of the derived soil parameters.

In more detail, the inverted velocity models (Vs and Vp) are gradient-like, with a faster increase in velocity in the first 20m, followed by a smoother part. This is generally expected for a rock velocity profile. The uppermost velocities of the profile, however, are not directly constrained by the data, because of the lack of information at high frequencies, and might be underestimating the true values for the topmost 10m. This was then confirmed by preliminary computing the SH-wave transfer function from these models, which showed considerable amplitude at high frequencies. It was then decide to introduce an a-priori constraint to the inversion result by homogenizing the top of each model to the velocity found at 10m. This expedient appropriately decreased the amplitude of the amplification function at high frequency, without significantly modifying the fit with observed dispersion curves (**Figure 22**). To have a better constraint on the shallower part of the profile, however, an active seismic experiment might be advisable (e.g. SASW).

Finally, by considering the minimum available frequency of the surface-wave dispersion curves, and by analyzing the scattering of the inverted models (**Figure 21**), it is realistic to assume the velocity profiles to be reliable down to a depth of about 140~160m. Below this value no direct constrain is available, and the velocity are obtained by pure extrapolation.

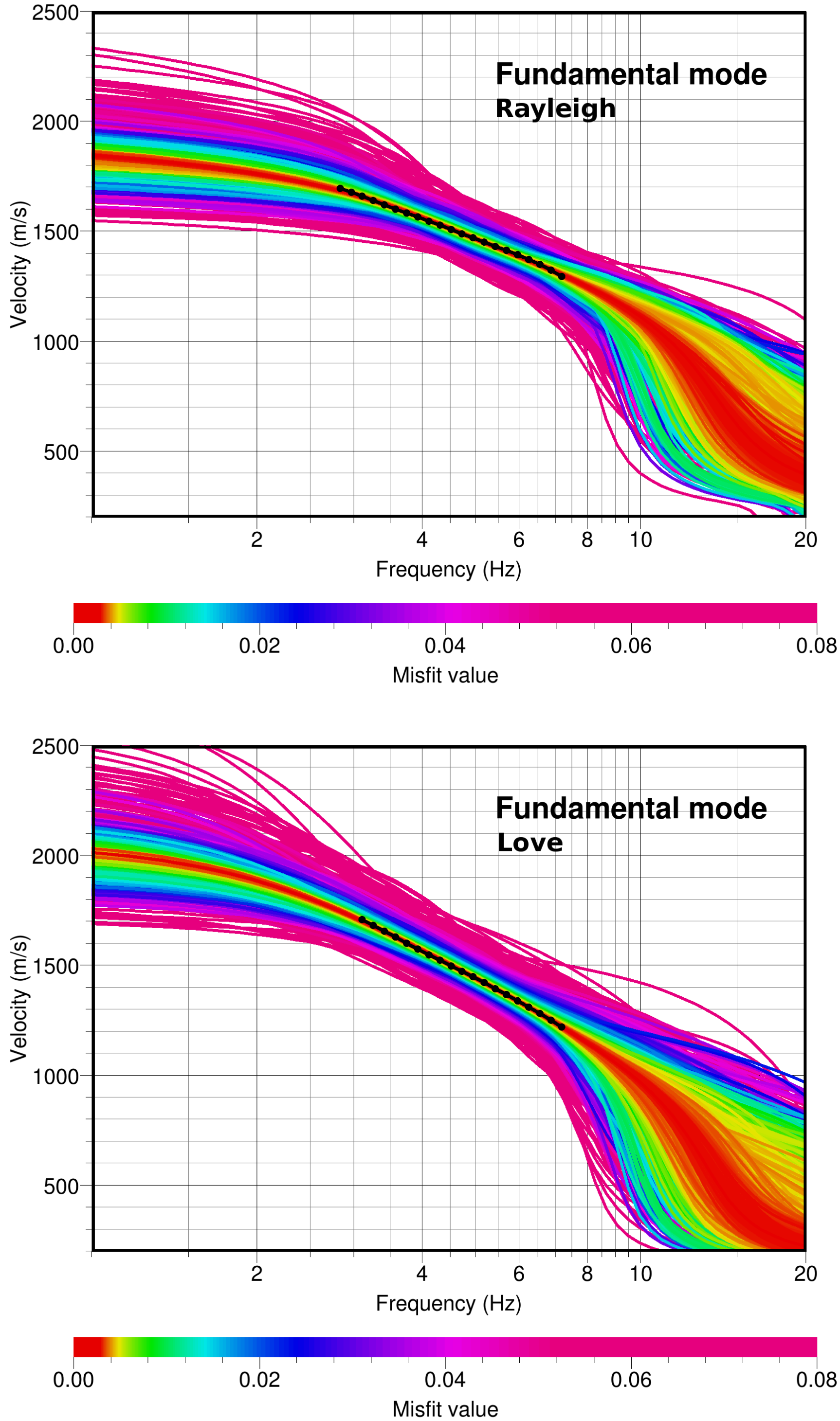

Figure 18 - *Fitting the surface dispersion data within the global optimization procedure. Different colors represent different misfit between the observed (in black) and the modeled dispersion curves during the search.*

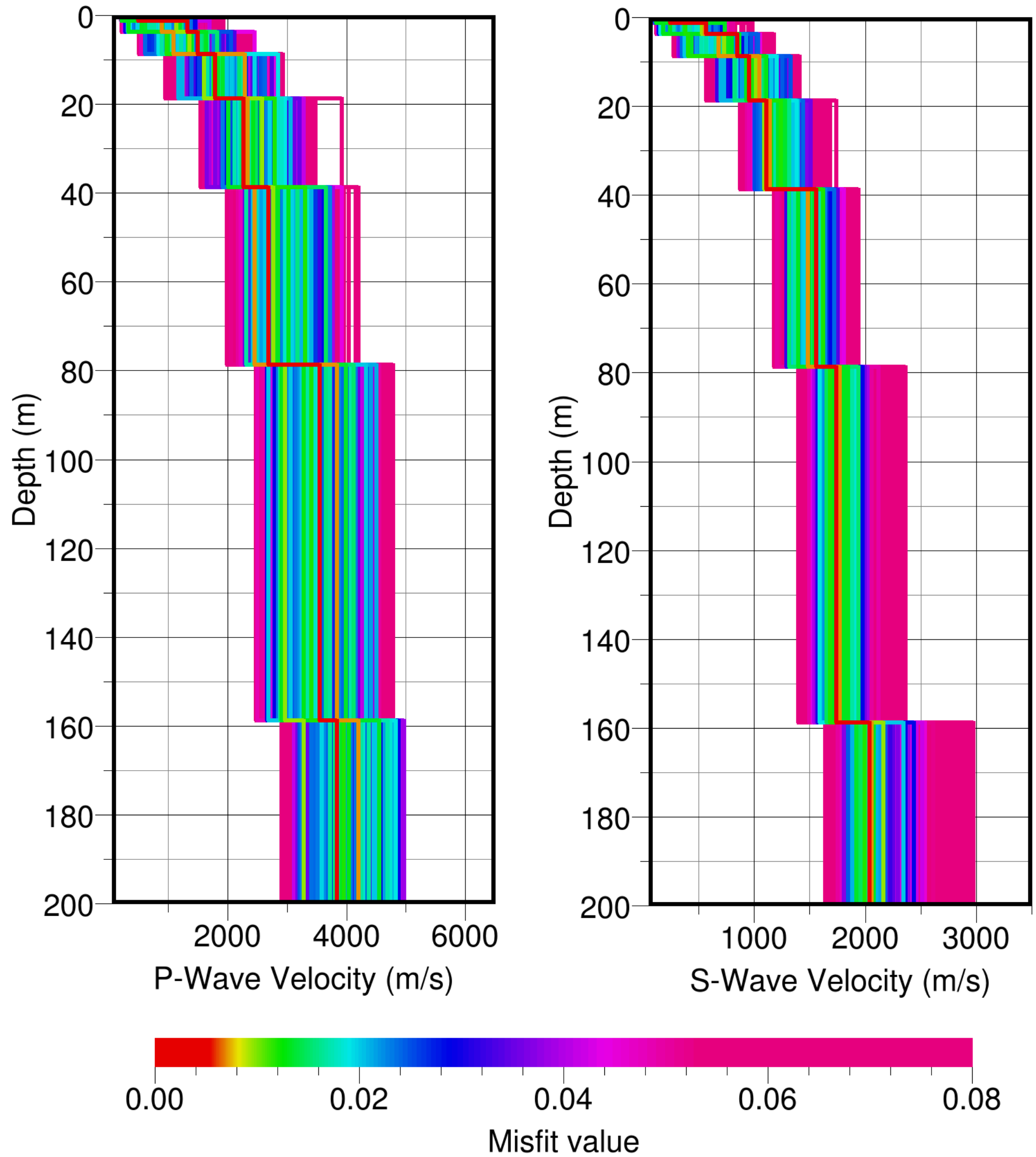

Figure 19 - *Distribution of the fix-layer velocity models generated during the inversion process and ordered by decreasing misfit, according to the color scheme of* **Figure 18***.*

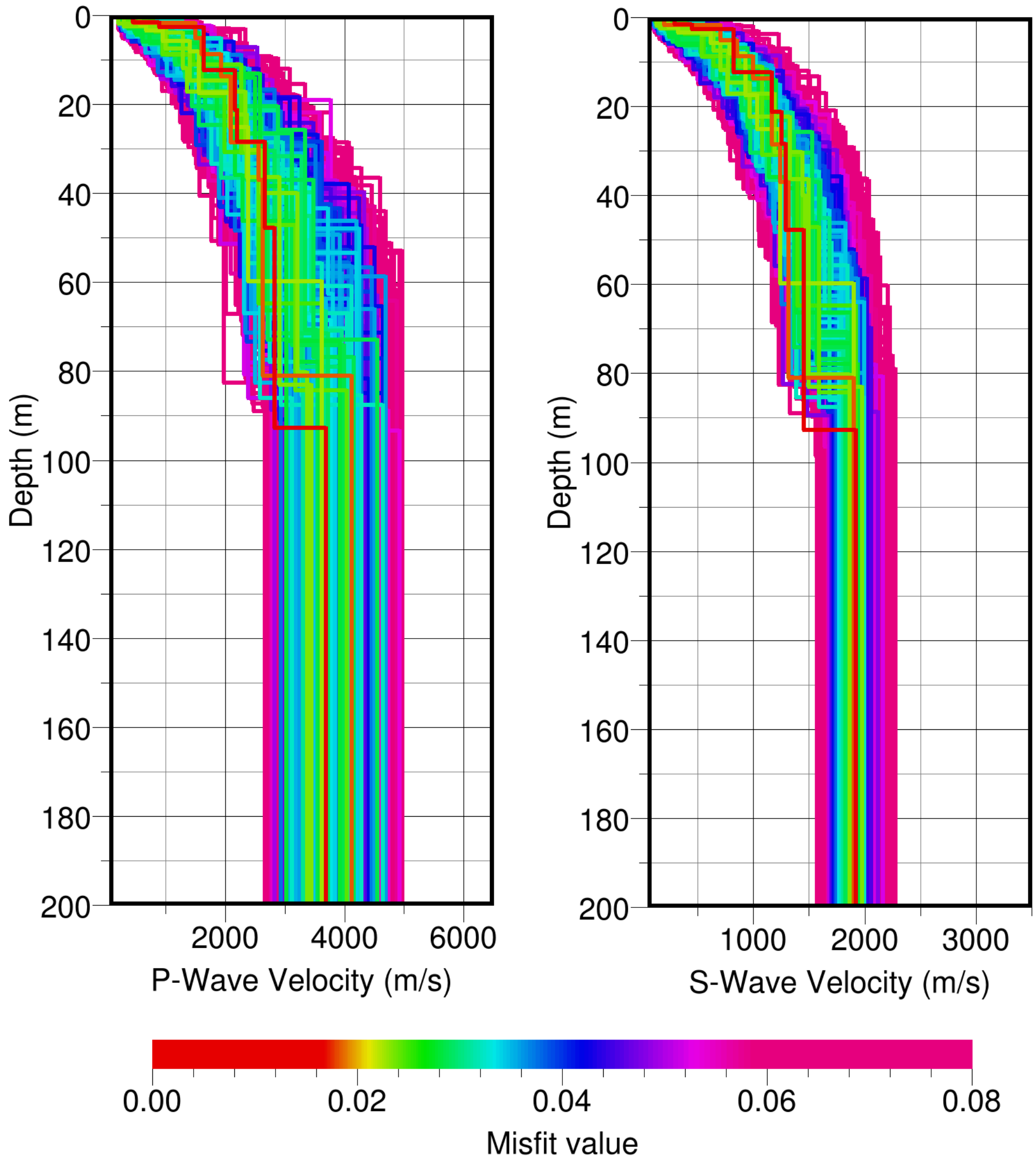

Figure 20 - *Distribution of the free-layer velocity models generated during the inversion process and ordered by decreasing misfit, according to the color scheme of* **Figure 18**.

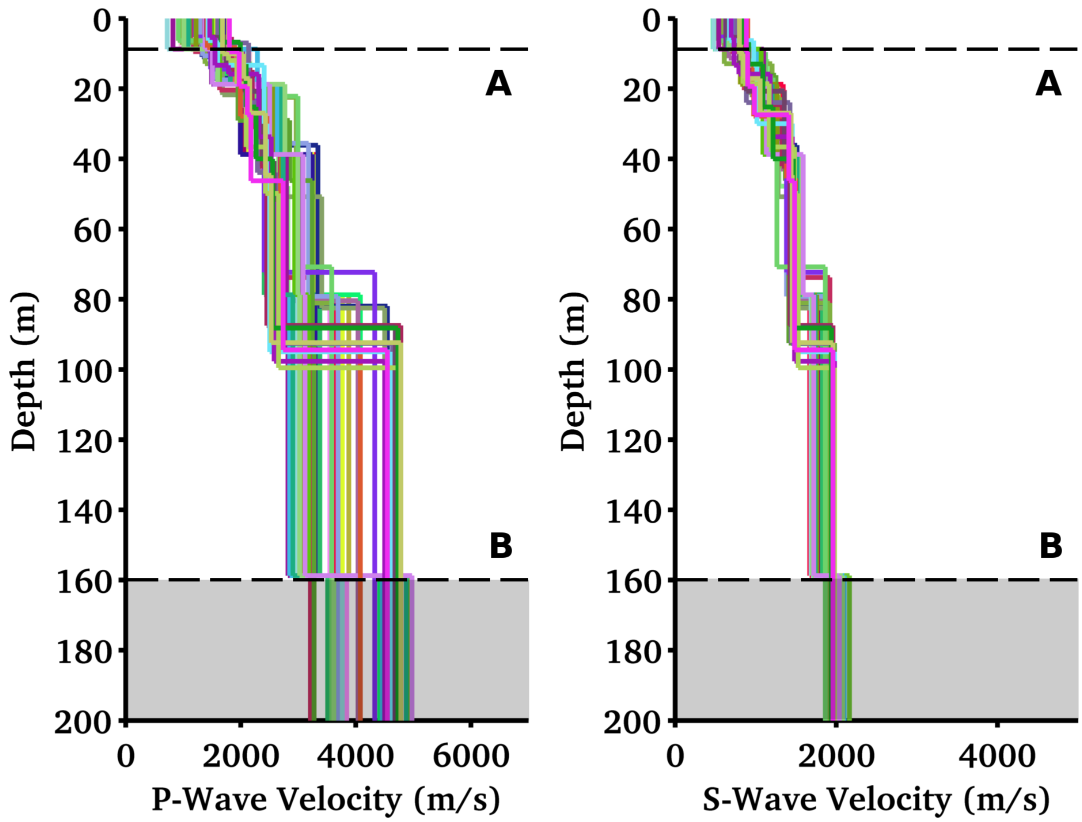

Figure 21 - *Comparison of all the best models from the two parameterization schemes (free and fixed layers). The two approaches are consistent down to a depth of about 140~160m, which can be considered the maximum resolved depth. The topmost layers of each model have also been homogenized at the a-priori depth of 10m.*

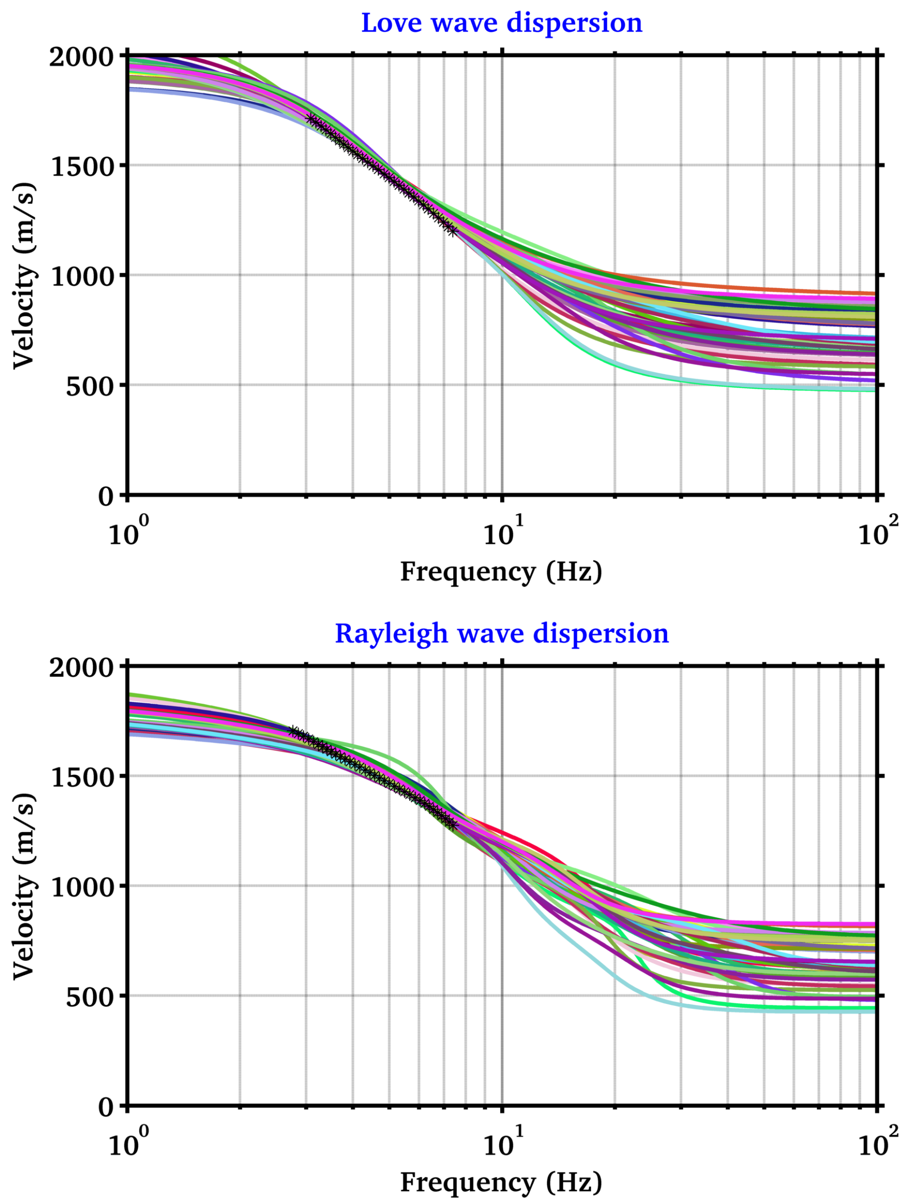

Figure 22 - *Comparison between observed and synthetic dispersion curves, these last computed from the adjusted velocity models of* **Figure 21***. The introduction of the a-priori selection of minimum and maximum resolved depth does not influence significantly the fitting with empirical data.*

11. Engineering soil parameters

The ensemble of all the best inverted velocity profiles is then used to derive average soil parameters like the VsZ (average travel-time S-wave velocity over the depth Z, including Vs30, Table 1) and the quarter-wavelength (QWL) average velocities (Joyner et al., 1984) for a range of frequencies between 0.6 and 30Hz (**Figure 23**). The former is a standard parameter for the classification of ground-types in most building codes and in ground motion prediction equations. The latter is a parameter useful for the empirical estimation of the site-response and to assess the sensitivity of the seismic wave-field to the different depths. It has to be noticed that these two parameters are derived separately from all the best S-wave velocity models obtained from the inversion, and the results is finally averaged to improve statistics.

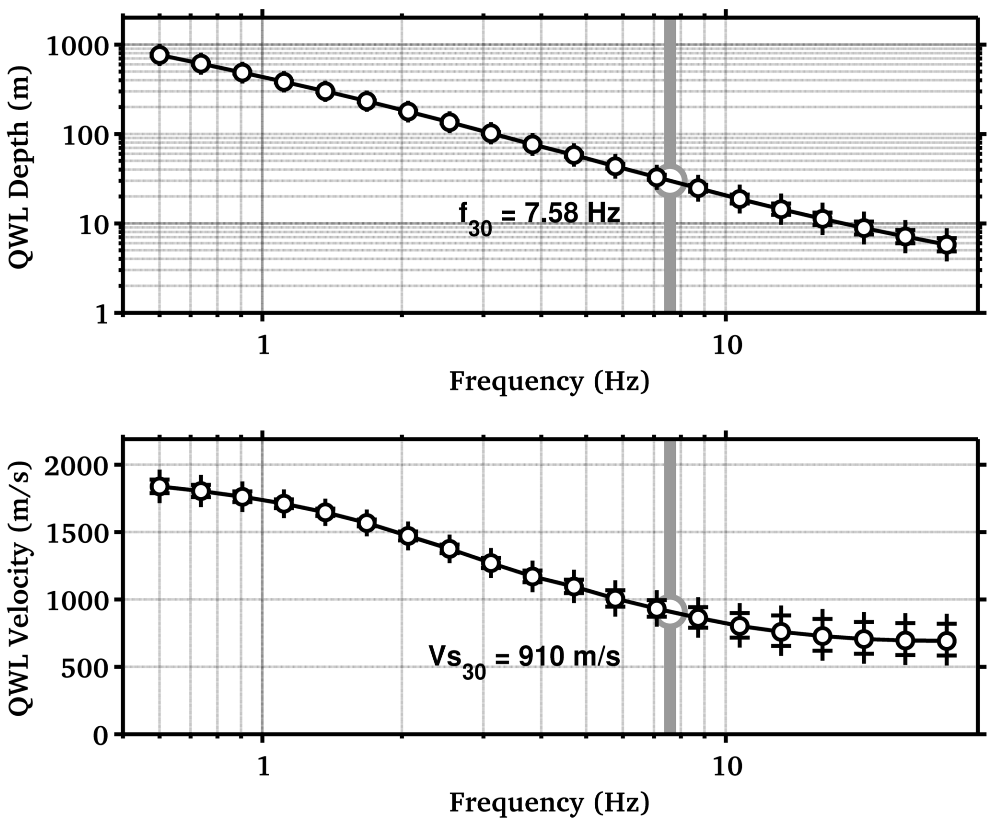

Figure 23 - *Quarter-wavelength representation of the inverted S-wave velocity profiles. Top: the depth-frequency dependency. Bottom: the QWL average velocity. The Vs30 value is indicated with its corresponding QWL frequency.*

Averaging depth	Vs-mean (m/s)	St.Dev.
5	701.25	114.27
10	729.08	98.97
15	779.38	76.98
20	823.92	63.31
25	872.30	52.97
30	**913.70**	**46.88**
40	982.23	42.70
50	1051.84	37.02
75	1167.08	32.34
100	1263.87	25.88
150	1408.94	26.00
200	1515.05	21.53

Table 1 - *Average travel time velocities at different depths. Vs30 is highlighted.*

12. Amplification models

Site amplification functions have been computed using two different approaches: the S-wave transfer function for vertical propagation and the quarter-wavelength amplification. In general the first method is used to evaluate the resonance characteristics of the site, while the second is more useful to assess the effect of the velocity contrasts between the lowermost rock layer (as reference) and the different QWL averaging depths. The two amplification functions are then corrected for the Swiss rock reference velocity profile as defined in Poggi et al. (2011), according to the procedure described in Edwards et al. (2013). Given the lower velocities in the uppermost part of the DAGMA profile compared to the Swiss reference, the final corrected amplification function shows a lower average amplification level at high frequencies than the uncorrected (**Figure 24**).

Amplification functions using the transfer function and the quarter-wavelength approach are comparable (**Figure 25**), even if the transfer function provides a slightly larger amplification, because of the presence of some weak resonance peaks. At low frequencies both methods converge to the same amplification level. It has to be notice that the amplification functions do not include attenuation at this stage of the analysis, as the quality factors of the site are unknown.

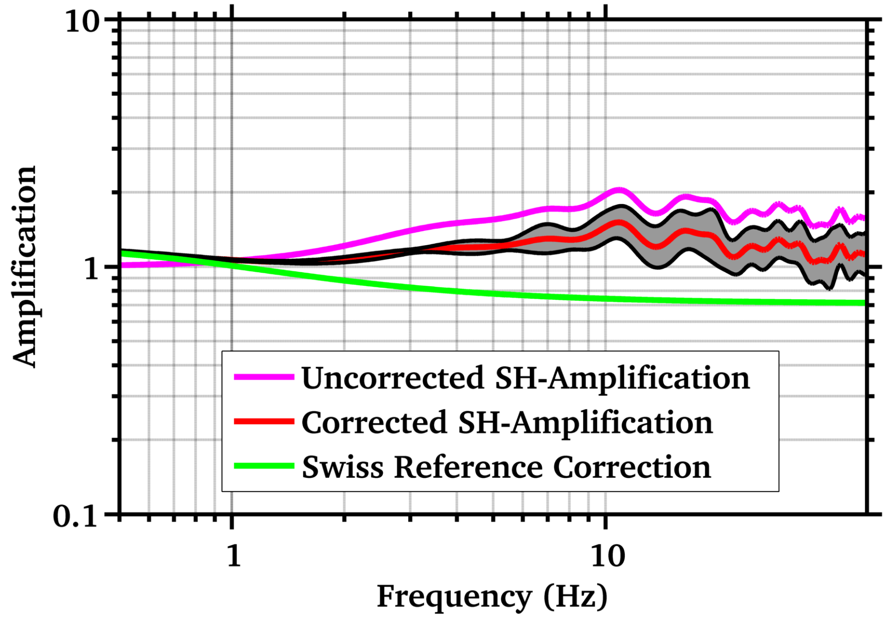

Figure 24 - *Correcting the SH-wave transfer function for the Swiss (rock) reference conditions (Poggi et al. 2011). The final corrected amplification function shows a lower (average) amplification at high frequencies than the uncorrected.*

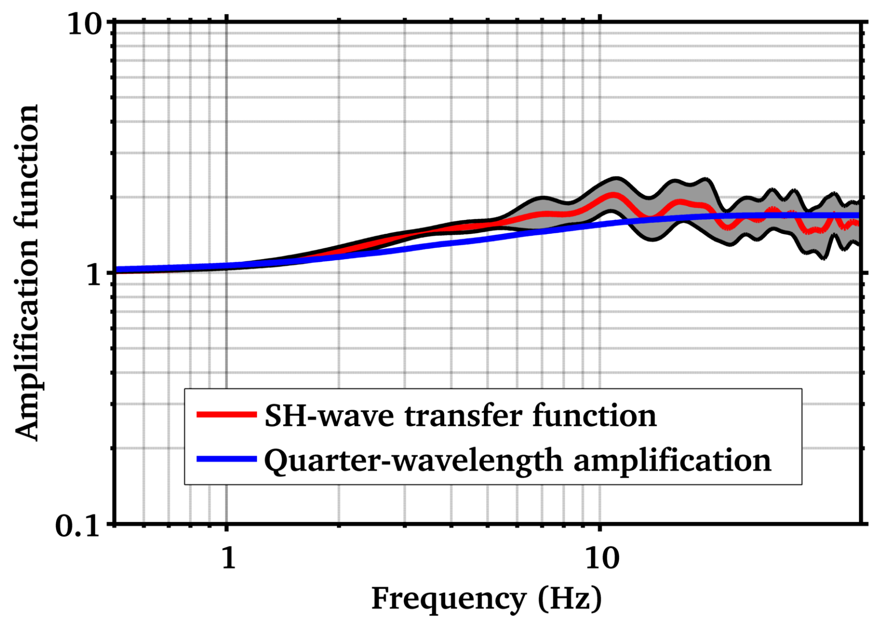

Figure 25 - *Comparison of amplification functions computed using the SH-wave transfer function and the quarter-wavelength formalism on the inverted velocity models. The functions are referenced to the Swiss rock reference model (Poggi et al. 2011).*

REFERENCES

Capon, J., 1969. High resolution frequency wavenumber spectrum analysis, Proc. IEEE, 57, 1408-1418.

Burjanek, J., G. Stamm, V. Poggi, J.R. Moore, and D. Fäh [2010], "Ambient vibration analysis of an unstable mountain slope", Geophys. J. Int., Vol. 180, pp. 820-828.

Edwards, B., C. Michel, V. Poggi and D. Fäh (2013). Determination of Site Amplification from Regional Seismicity: Application to the Swiss National Seismic Networks. Accepted for publication in Seismological Research Letters.

Joyner, W. B., R. E. Warrick and T. E. Fumal (1981). The Effect of Quaternary Alluvium on Strong Ground Motion in the Coyote Lake, California, Earthquake of 1979, Bulletin of the Seismological Society of America, 71, 1333-1349.

Poggi, V., B. Edwards and D. Fäh (2011). Derivation of a Reference Shear-Wave Velocity Model from Empirical Site Amplification, Bulletin of the Seismological Society of America, 101, 258-274.

Poggi, V. and Fäh D., 2010. Estimating Rayleigh wave particle motion from three-component array analysis of ambient vibrations. Geophys. J. Int., 180-1, 251-267.

Huguet. F. (2007). Cirques glaciaires et étagement des formes dans le massif du Feldberg, dans le sud de la Forêt Noire (Allemagne). Géomorphologie: relief, processus, environnement. 4, 309-318.

Eidgenössische Technische Hochschule Zürich
Swiss Federal Institute of Technology Zurich

SED
Schweizerischer Erdbebendienst
Swiss Seismological Service

Report on site characterization

Mettma, Germany
(METMA)

Poggi Valerio, Lorenz Keller

Last modified - 24 / 12 / 2014

1. Introduction

In the framework of the NAGRA seismic network project, an active seismic survey was performed by the company RoXplore at the location of the SED station METMA (Mettma, Germany). The station, installed in a tunnel at about 46m below the surface, consists in a broadband seismometer (Trillium Compact) with a high-resolution digitizer (Taurus 24Bit @200sps). The scope of the survey is the seismic characterization of the rock mass surrounding the installation. The primary target is the definition of an equivalent one-dimensional shear-wave velocity. Such profile is later used to assess the local seismic response of the station.

For the analysis, different active seismic techniques have been employed, which are listed below:

- Seismic refraction (Vp and Vs) tomography
- Cross-hole tomography
- Active surface wave analysis (MASW)

Results from all these analyses were collected, merged and interpreted by SED into two separated summary profiles; one starting the free surface and one representative of the tunnel conditions. In the following, the main results of these investigations are summarized and a final interpretation of the velocity profile is given. From this interpretation, engineering parameters are finally derived, e.g. the Qwl-Vs average velocity, VsZ (including Vs30) and the seismic amplification from the analytical SH-transfer function of the one-dimensional soil column.

2. Survey description

For the survey description and the processing results, we refer the reader to the RoXplore report in Appendix.

3. Soil type, topography and geology

From the geological points of view, the target area is characterized by an extended sandstone cover of Triassic age (unit 3 in **Figure 1**), on top of the Paleozoic granitic and high-grade metamorphic basement of the black forest (unit 1). Triassic shellbearing limestone (unit 2) is also occasionally present in the surroundings, however not visible at the measuring location. Topography is smooth and modeled by the action of glaciers during Pleistocene. Such site can be classified as of rock ground-type A.

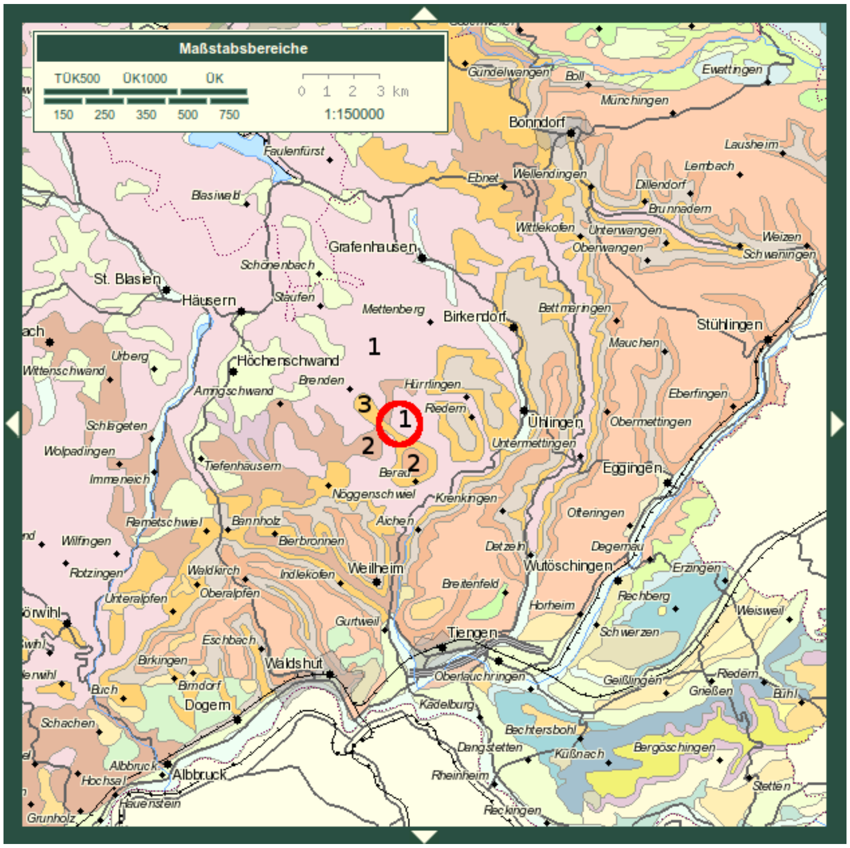

Figure 1 - *Geological map of the southern edge of the Black Forest (reproduced from Landesamt für Geologie, Rohstoffe und Bergbau (LGRB) Freiburg, modified). In red the approximate location of the permanent station EMMET.*

4. Profile selection

From the ensemble of all S-wave velocity profiles provided by RoXplore from the different applied seismic techniques (refraction tomography, cross-hole tomography and MASW analysis) a number of best models have been selected (**Figure 2**). These profiles are considered the most representative of the local geophysical conditions, spanning from the free-surface to about 35m below the station installation (in the tunnel). The selected profiles have however different resolution characteristics and depth extension (depending on the technique used for the analysis) and therefore they cannot easily be compared or simply averaged into a unique mean profile. We proceeded by generating a final Vs “summary” model by visual inspection and then manual interpretation of the available data at the different depths.

Calibration of a P-wave velocity model is a more complex task, because of the limited amount of usable information. Practically, Vp profiling is available only from refraction P-wave seismic surveying and active MASW analysis. In the former case, however, the maximum resolved depth is not sufficient to reach the depth of the station (in the tunnel). In case of MASW, conversely, the Vp values obtained by surface wave inversion are always quite uncertain, due to the scarce sensitivity of this parameters, and should therefore be used carefully. We then proceeded by calibrating an average Vp-Vs relation using log-linear regression on a sub-selection of the available data (**Figure 3**). The functional relation was then used to directly convert the previously obtained Vs model into a unique Vp profile (**Figure 4**). This procedure was applied to obtain two complementary models, one ranging from the surface to below the tunnel (**Figure 4**A) and a second profile more specific for the conditions below the station (**Figure 4**B).

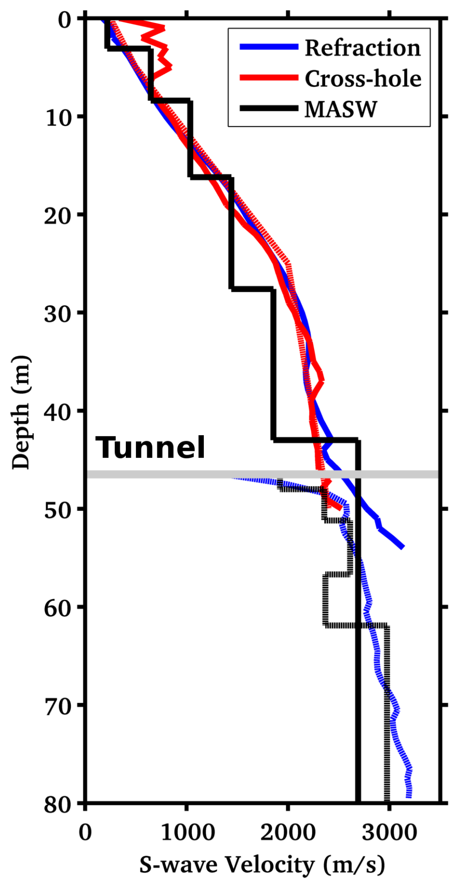

Figure 2 - *Ensemble of selected "best" Vs profiles from different techniques at the location of the seismic station METMA. Note that the refraction profile (in blue) is discontinuous because obtained from two independent surveys (at the surface and in the tunnel).*

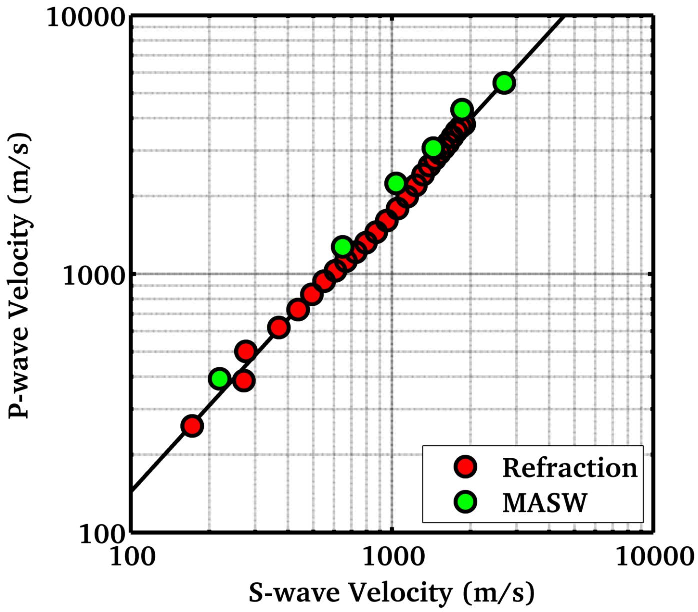

Figure 3 - *Calibration of log-linear regression relation between P and S seismic velocities. Calibration data are from a selection of refraction profiles and from the best MASW model (Rayleigh and Love wave join inversion).*

5. Engineering soil parameters

The obtained best velocity profile is then used to derive average soil parameters like the VsZ (average travel-time S-wave velocity over the depth Z, including Vs30, Table 1) and the quarter-wavelength (QWL) average velocities (Joyner et al., 1984) for a range of frequencies between 0.6 and 30Hz (**Figure 5** and **Figure 6**). The former is a standard parameter for the classification of ground-types in most building codes and in ground motion prediction equations. The latter is a parameter useful for the empirical estimation of the site-response and to assess the sensitivity of the seismic wave-field to the different depths.

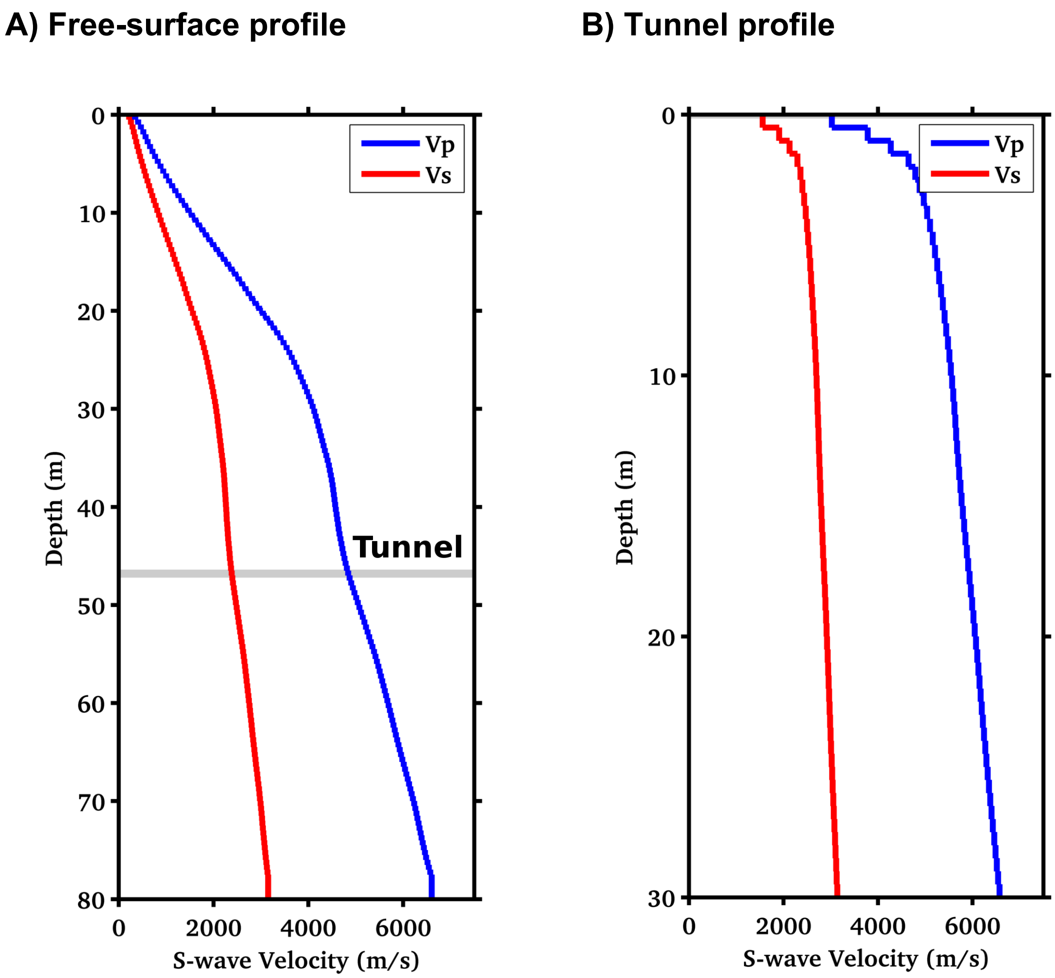

Figure 4 - *Final summary models (Vs and Vp) for the free surface and the tunnel. Vp profile is obtained converting Vs values using the log-linear relation in* **Figure 3***. It has to be noticed that in B the decrease in velocity in proximity of the gallery is realistically explainable by the stress release and fracturing induced by excavation.*

6. Amplification models

Site amplification functions have been computed using two different approaches: the S-wave transfer function for vertical propagation and the quarter-wavelength amplification. In general the first method is used to evaluate the resonance characteristics of the site, while the second is more useful to assess the effect of the velocity contrasts between the lowermost rock layer (as reference) and the different QWL averaging depths. The two amplification functions are then corrected for the Swiss rock reference velocity profile as defined in Poggi et al. (2011), according to the procedure described in Edwards et al. (2013). Given the lower velocities in the uppermost part of the EMMET profile compared to the Swiss reference, the final corrected amplification function shows a lower average amplification level at high frequencies than the uncorrected (**Figure 7**).

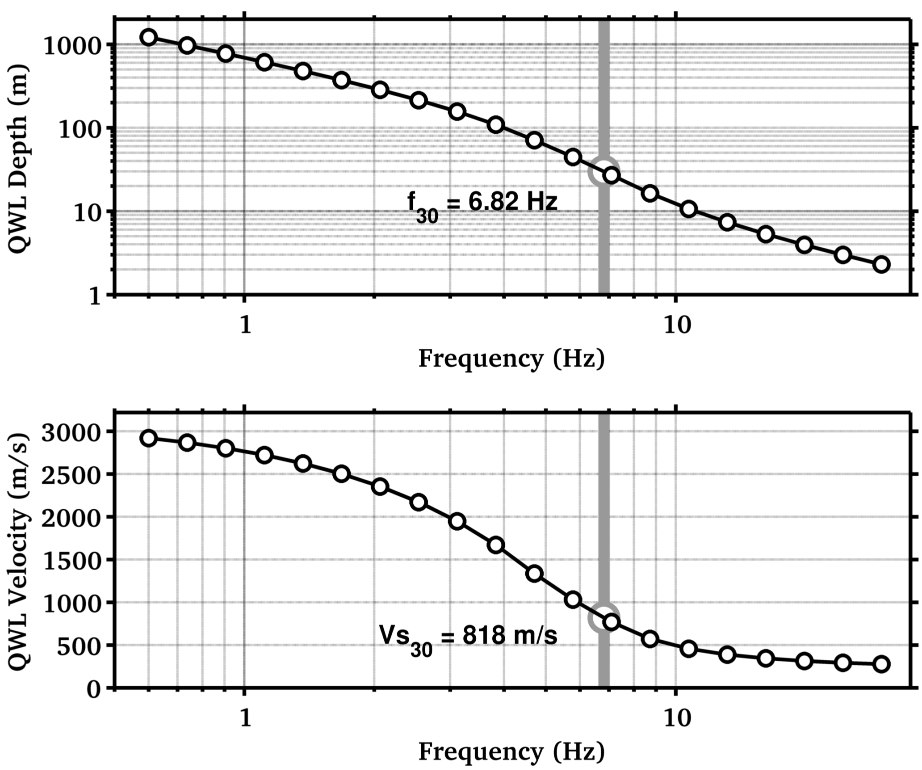

Figure 5 - *Quarter-wavelength representation of the summary S-wave velocity profile at the free-surface. Top: the depth-frequency dependency. Bottom: the QWL average velocity. The Vs30 value is indicated with its corresponding QWL frequency.*

Amplification functions using the transfer function and the quarter-wavelength approach are comparable (**Figure 8**), even if the transfer function provides a slightly larger amplification, because of the presence of some weak resonance peaks. At low frequencies both methods converge to the same amplification level. It has to be notice that the amplification functions do not include attenuation at this stage of the analysis, as the quality factors of the site are unknown.

Amplification function has also been computed at the depth of the tunnel from the extended velocity profile (free surface plus tunnel model, **Figure 9**) using the SH transfer function formalism. With respect to the amplification computed assuming free-surface conditions (Figure 7), the ground motion model obtained when accounting for the full-wave propagation along the extended profile presents the typical troughs due to negative interference of up-going and down-going reflected waves.

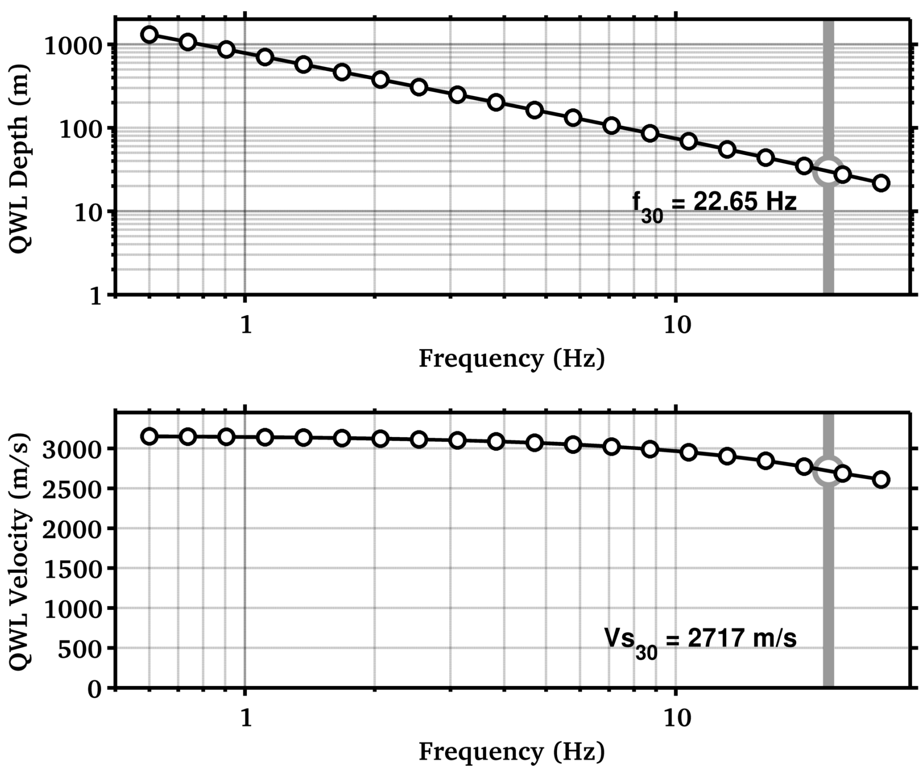

Figure 6 - *Quarter-wavelength representation of the summary S-wave velocity profile within the tunnel. Top: the depth-frequency dependency. Bottom: the QWL average velocity. The Vs30 value is indicated with its corresponding QWL frequency.*

Averaging depth (m)	Vs-mean (m/s)	St.Dev.
5	336.6193	--
10	442.717	--
15	544.2156	--
20	640.811	--
25	732.5255	--
30	**817.9385**	**--**
40	969.0425	--
50	1098.196	--
75	1376.764	--
100	1602.18	--
150	1916.331	--
200	2124.626	--

Table 1 - *Average travel-time velocities at different depths of the free-surface velocity model. Vs30 is highlighted.*

Averaging depth (m)	Vs-mean (m/s)	St.Dev.
5	2211.929	--
10	2399.862	--
15	2505.403	--
20	2585.154	--
25	2654.243	--
30	**2717.461**	**--**
40	2816.634	--
50	2879.79	--
75	2968.541	--
100	3014.999	--
150	3062.935	--
200	3087.479	--

Table 2 - *Average travel-time velocities at different depths of the tunnel velocity model. Vs30 is highlighted.*

A) Free-surface profile

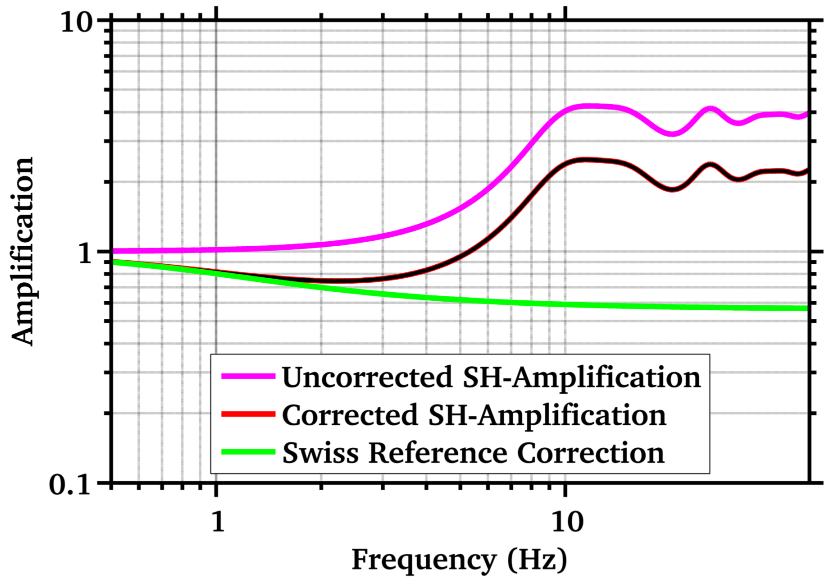

A) Tunnel profile

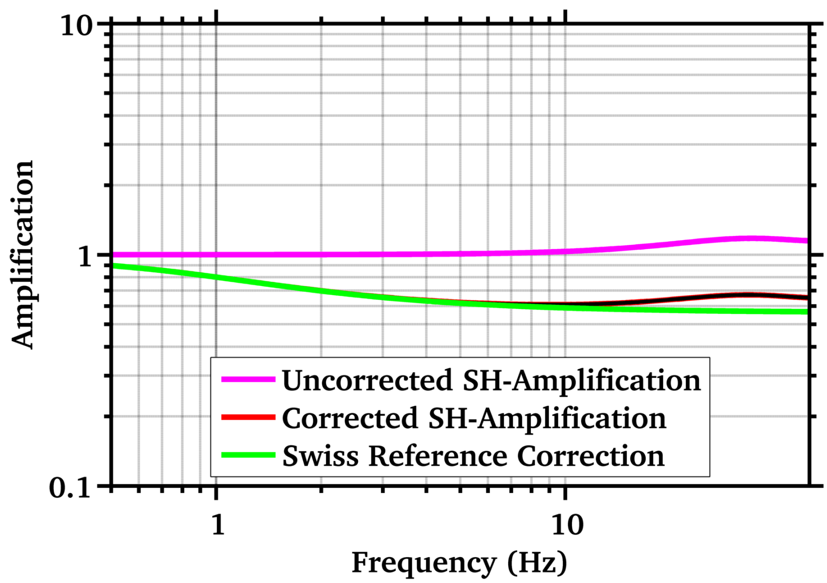

Figure 7 - *Correcting the SH-wave transfer function for the Swiss (rock) reference conditions (Poggi et al. 2011). The final corrected amplification function shows a lower (average) amplification at high frequencies than the uncorrected.*

A) Free-surface profile

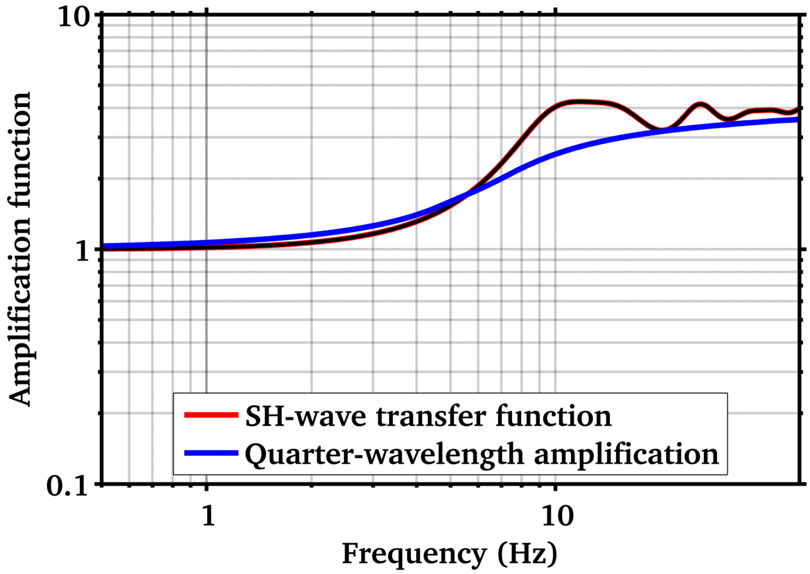

A) Tunnel profile

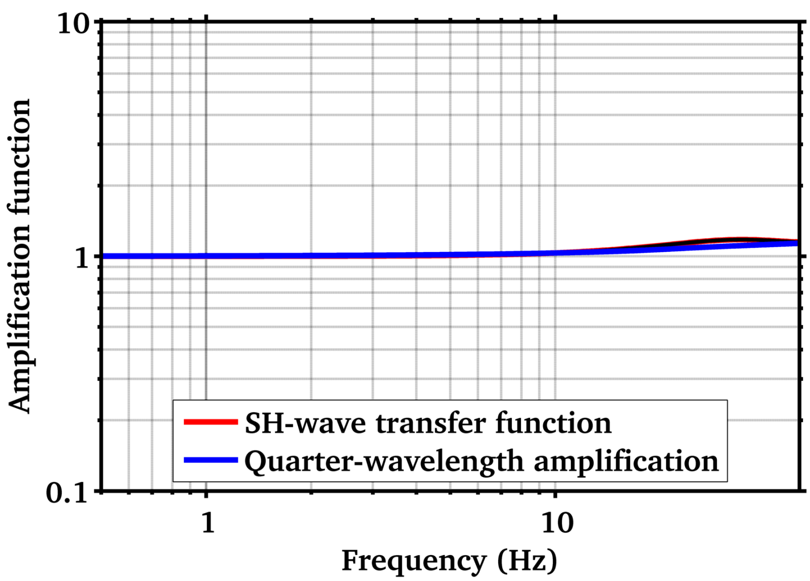

Figure 8 - *Comparison of amplification functions computed using the SH-wave transfer function and the quarter-wavelength formalism on the inverted velocity models (in this case functions are not corrected for the Swiss reference conditions).*

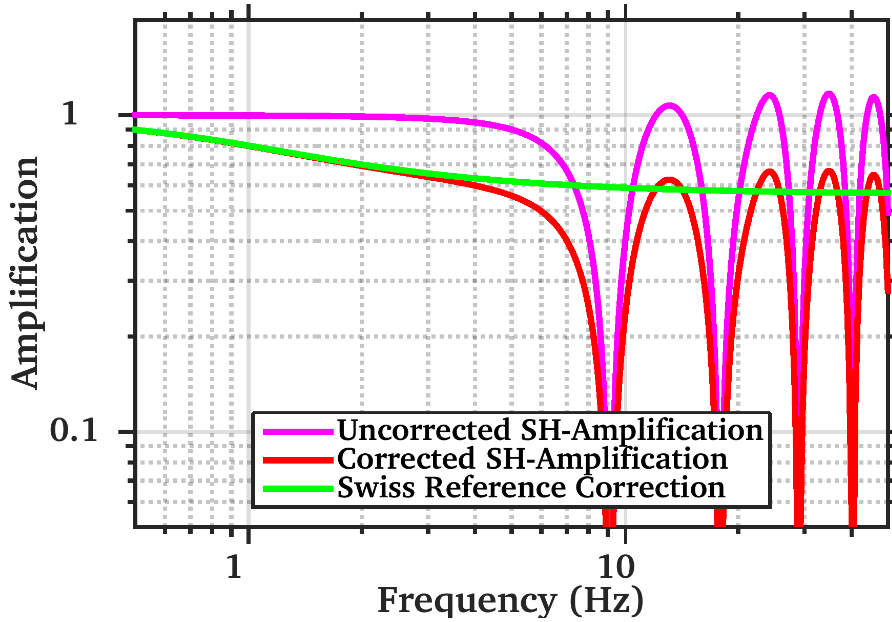

Figure 9 - *Amplification functions computed at the depth of the tunnel using the extended profile (free surface plus tunnel). Negative peaks induced by destructive interferences of reflected phases from the surfaces are clearly visible.*

REFERENCES

Edwards, B., C. Michel, V. Poggi and D. Fäh (2013). Determination of Site Amplification from Regional Seismicity: Application to the Swiss National Seismic Networks. Accepted for publication in Seismological Research Letters.

Joyner, W. B., R. E. Warrick and T. E. Fumal (1981). The Effect of Quaternary Alluvium on Strong Ground Motion in the Coyote Lake, California, Earthquake of 1979, Bulletin of the Seismological Society of America, 71, 1333-1349.

Poggi, V., B. Edwards and D. Fäh (2011). Derivation of a Reference Shear-Wave Velocity Model from Empirical Site Amplification, Bulletin of the Seismological Society of America, 101, 258-274.

APPENDIX A

Active Seismic report

Eidgenössische Technische Hochschule Zürich
Swiss Federal Institute of Technology Zurich

SED
Schweizerischer Erdbebendienst
Swiss Seismological Service

Report on site characterization

Rothenfluh, Switzerland (ROTHE)

Poggi Valerio, Manel Hobiger, Donat Fäh

Last modified - 24 / 12 / 2014

1. Introduction

In the framework of the NAGRA seismic network project, an array measurement of the ambient vibration wave-field was performed at the location of the SED station ROTHE (Rothenfluh, Switzerland). The scope of the survey is the seismic characterization of the area surrounding the installation (**Figure 1**), which consists in a broadband seismometer (Trillium Compact) with a high-resolution digitizer (Taurus 24Bit @200sps). Ambient vibration analysis has been used to infer the characteristics of the underground structure of the site, with special regard to the one-dimensional shear-wave velocity. Such profile was later used to assess the local seismic response of the station.

For the analysis, different spectral analysis techniques were implemented, consisting in both single and array methods, which are listed below:

- Time-frequency wavelet analysis
- Power-spectral density estimation
- Conventional horizontal to vertical spectral ratios
- Directional horizontal to vertical spectral ratios
- Wavelet polarization analysis
- Three-component high-resolution f-k analysis.

The results of all these analyses conformed to the definition of the final velocity model. In the following, the main results of these investigations are summarized and a final interpretation of the velocity profile is given. From this interpretation, engineering parameters are finally derived, e.g. the Qwl-Vs average velocity, VsZ (including Vs30) and the seismic amplification from the analytical SH-transfer function of the one-dimensional soil column.

2. Survey description

To characterize the seismic response of the site, two array measurements of ambient vibration were performed on 30/01/2014 and on 02/02/2014 (**Figure 1**). Each array consists of a single measuring configuration, of 14 and 11 sensors respectively. The first array (A1) has circular geometry and a diameter of about 120m, while the second (A2), more irregular, has a total aperture of nearly 760m. Performing two separate surveys was imposed by the difficult measuring conditions, mostly related to the dense vegetation of the forest. This dramatically affected the GPS performance for station synchronization and differential localization, which required hours to be completed. In particular, geometry of array A2 was implemented to follow an existing road though the forest. In spite of the dissimilarities in geometry, the two configurations have nevertheless overlapping f-k resolution bands, which assure a continuous mapping of the surface wave phase velocity dispersion curves over frequency. Configuration A1 recorded for a total of 1h00m, while configuration A2 for 2h00m. The differences in the recording length are due to the different resolution characteristics of the two geometries.

As a general rule, larger arrays require longer recording time to produce a reasonable statistics of the ambient vibration processing results. In this case, however, due to an unfortunate presence of strong disturbances induced by human activity (wood log cutting) during acquisition, the usable signal length for configuration A1 was reduced to about 20m only (**Figure 3**). Satisfactory results were nevertheless obtained from the analysis of the two geometries.

High velocities and relatively shallow geophysical bedrock (Hauptrogenstein formation, tabular Jura) were expected for the site. This justifies the use of a large geometry for the array to be successful. However, the maximum aperture of the arrays was again controlled by accessibility through the forest. A precise prior estimation of the possible maximum resolved depth was not possible, due to the large uncertainty of the bedrock velocity and the irregularity of the larger configuration (A2).

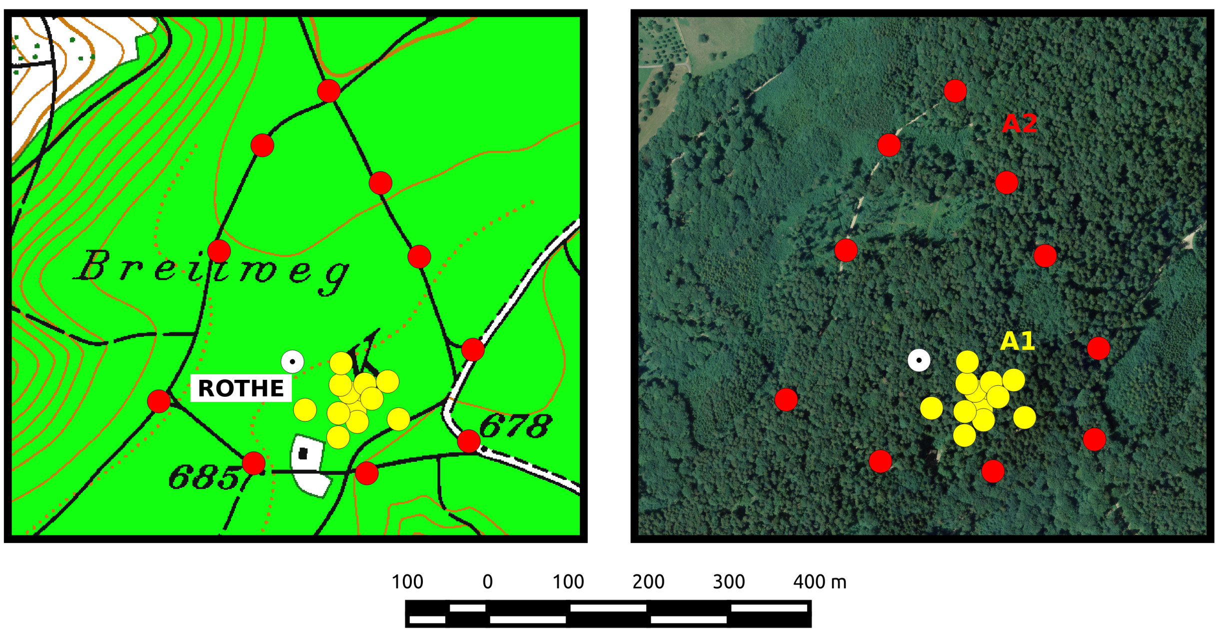

Figure 1 - *Location of the two ambient vibration array surveys performed in Rothenfluh, (SED station ROTHE) on 30/01/2014 and on 02/02/2014. Two concentric configurations of increasing aperture were set up (named A1 in yellow and A2 in red). Location of the permanent station is shown with a white mark.*

3. Soil type, topography and geology

The array has been set in open field conditions, in a protected forest reserve area (**Figure 1**). The influence of buildings and anthropogenic disturbances is virtually negligible, even though some monochromatic harmonic signals affected the second half of the survey (while recording with array configuration A2). Array sensors have been deployed on free soil. Good coupling with the ground was assured by means of digging small holes at the sensor's places, and by using a special support (*Trihedron*®) that facilitates the leveling of the device even for difficult soil conditions. The measurement area was located on top of a small ridge, locally quite flat. However, no topographic correction has been taken into account before processing.

Figure 2 - *Geological map of the region surrounding the measuring area in Rothenfluh (reproduced from Swisstopo, Geologische Generalkarte der Schweiz 1:200000, modified). In red the approximate location of the permanent station ROTHE.*

From the geological points of view (**Figure 2**), the target area is located on a small hill in the South-East portion of the Tabular Jura, within the Hauptrogenstein formation, a marine carbonate formation of Jurassic age (Spatkalk, oolitic limestone). The surface morphology is considerably smooth and modeled by the action of glaciers during the Pleistocene. The calcareous bedrock is likely very shallow at the measuring location, but never exposed across the area (a variable-thick cover of quaternary material is generally present). Such site can be classified as of rock ground-type A.

4. Acquisition equipment

Each acquisition point within the array consisted of a three components seismometer (Lennartz 3C with 5s eigenperiod) and a 24 bit data logger (Quanterra Q330). Synchronization between stations was assured by standard GPS, while a more accurate differential GPS (Leica Viva system) was used to precisely locate the sensor's coordinates with a tolerance of less than 5cm.

5. Weather conditions

The weather conditions were optimal and stable during the whole measurements, with no precipitations, no wind and an average (over the two days) temperature of 7 degrees.

6. Pre-processing and preliminary data-quality control

The three-component recordings have been filtered prior to analysis using a band-pass 6^{th} order causal Butterworth filter with corners at 0.2Hz and 50Hz. Although it is not a strict requirement for spectral analysis techniques, such filtering was applied in order to facilitate the preliminary visual inspection of the noise traces and to evaluate the coherency of the wave-field (**Figure 3**). Such procedure gives essential information for the subsequent interpretation of the f-k analysis results.

By visual inspection of the ambient vibration recordings of array configuration A1, it was evident the presence of about 15m of large amplitude transients, unfortunately induced by the activity of some workers cutting wood logs in the vicinity of the stations. The low quality and not usability of this portion of the signal was later confirmed by preliminary f-k processing. The maximum continuous usable recording length for A1 was then reduced to only 20m (light blue window). The quality was nevertheless sufficient to ensure reliable results. No significant disturbances were apparent on the recordings of array configuration A2.

To assess the quality of the ambient vibration recordings, spectral analysis was subsequently performed. Because of the stochastic nature of the ambient vibration wave-field, a statistical approach has to be used, such as the estimation of the power spectral density (*PSD*). This approach is useful to evaluate the average energy level of the recordings in the analyzed frequency range, and to access the presence of spurious spectral peaks, which might be related to human activity (machinery, pumps). By inspecting the PSD of all the three-component recordings of the array in the range between 0.5 and 40Hz, is found that the average energy level of the spectrum is overall very low, well within the minimum and maximum bounds of the USGS noise model (**Figure 4**). A negligible presence of two harmonic signals of anthropogenic origin is visible on configuration A2 between about 5 and 6Hz. These disturbances however do not affect the quality of the processing.

A) Array 1 - 30/01/2014, 1h00m

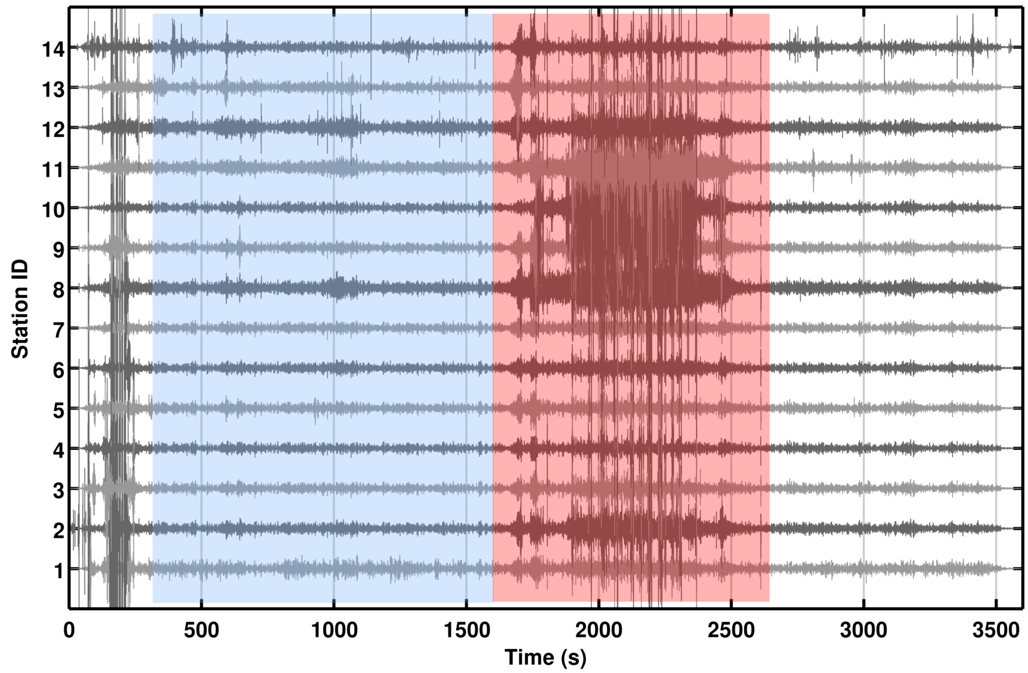

B) Array 2 - 02/02/2014, 2h00m

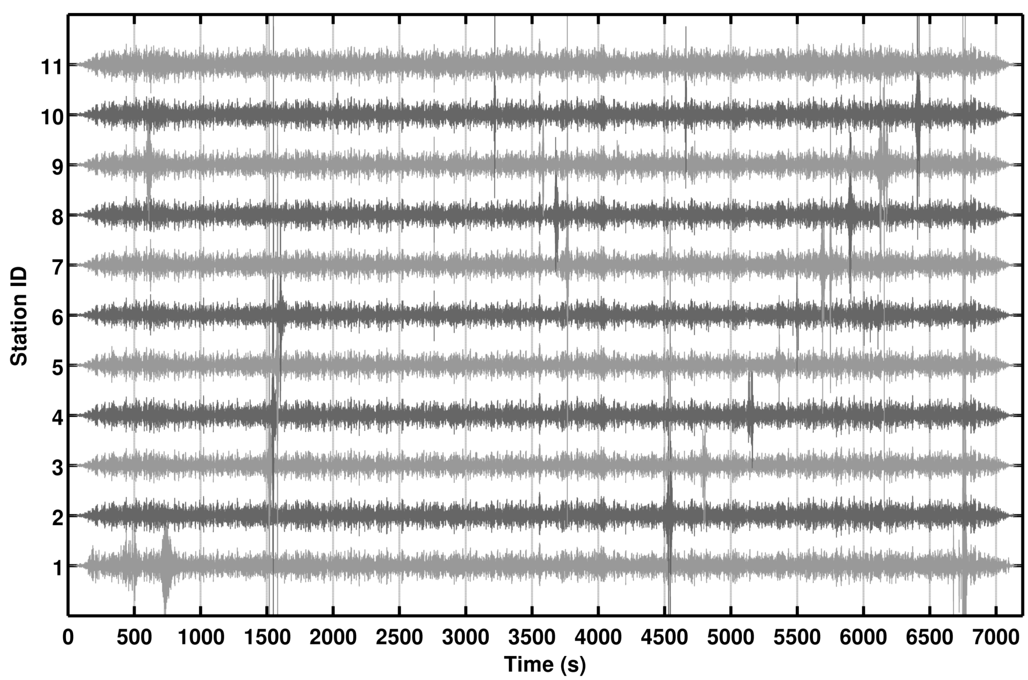

Figure 3 - *Inspection of the quality the ambient vibration recordings of the Rothenfluh arrays (configurations A1 and A2). For array A1, disturbances induced by human activity (red window) limited the usable recording length to about 20m (in light blue).*

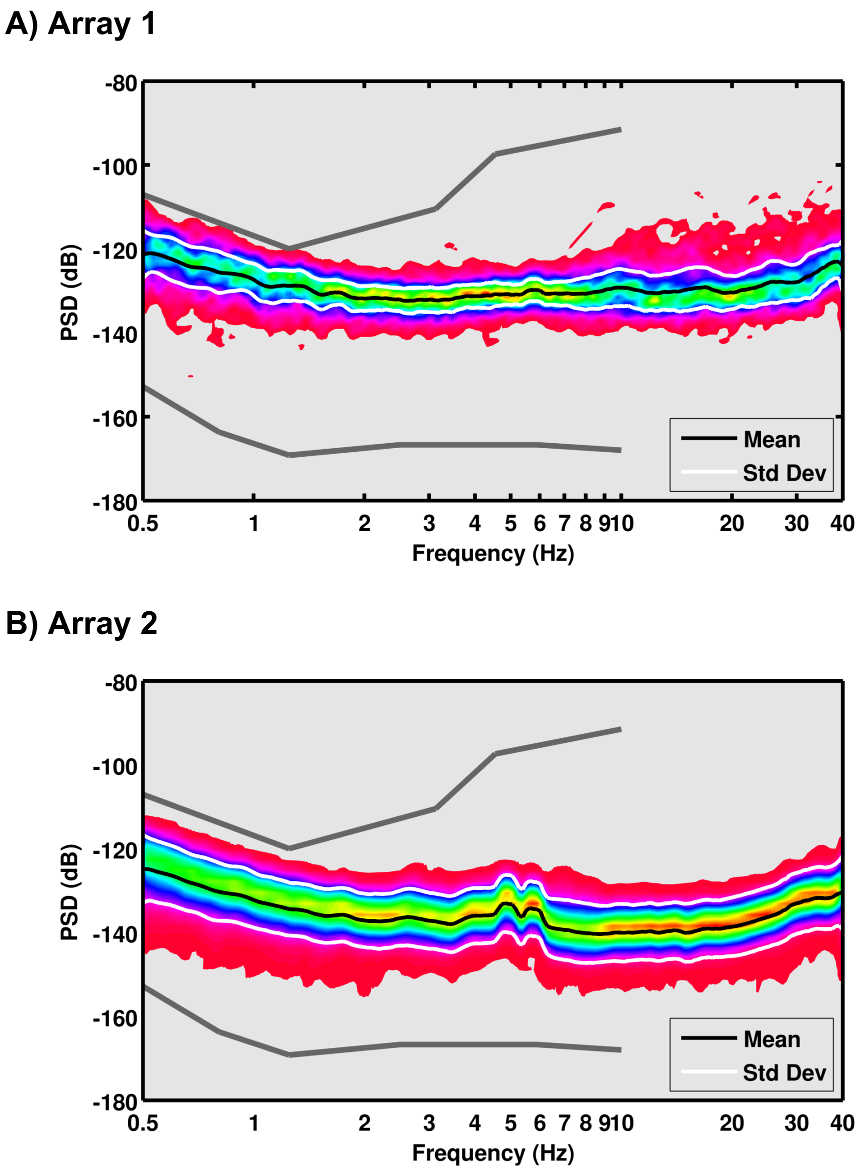

Figure 4 - *Power spectral density (PSD) computed at the central station the array configuration A1 (top) and A2 (bottom), NS component. Similar results were obtained from the other stations and components of the array. In gray lines are the minimum and the maximum bounds of the USGS noise model, for comparison.*

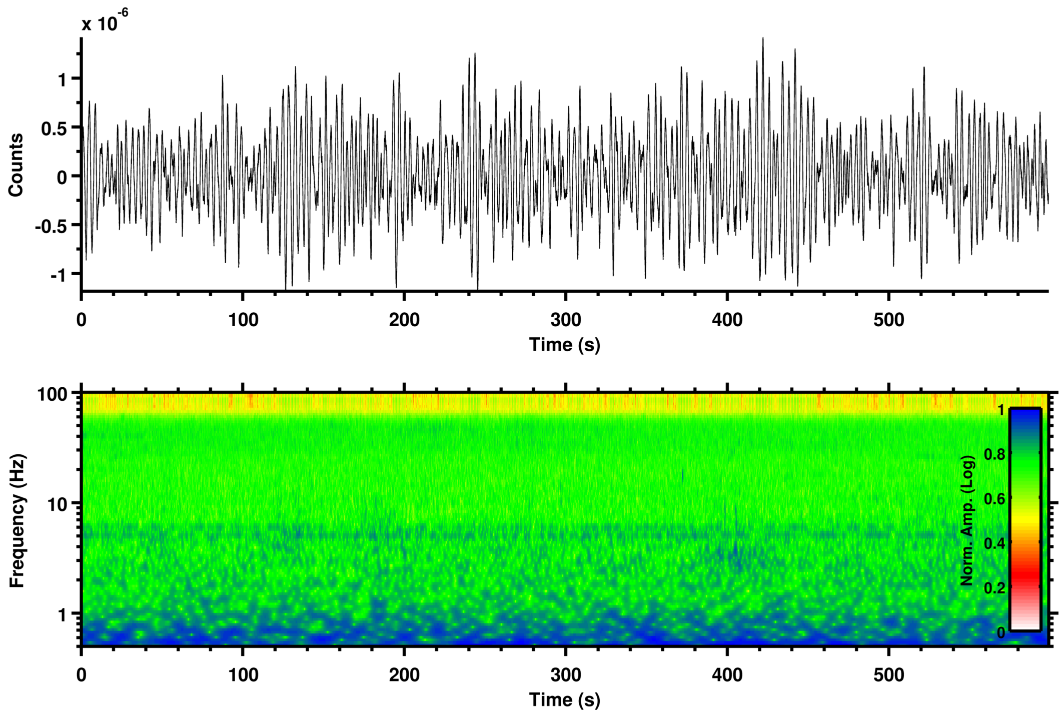

Figure 5 - *Example of spectrogram from 600s of recording of the central station of the array configuration A2. Two negligible harmonic disturbances are visible on the spectrogram, between 5 and 6Hz. These signals were not present during the recordings of configuration A1. For the analysis, the cosine wavelet is used (wavelet parameter = 12).*

Complementary to the aforementioned statistical methods, a spectral decomposition approach is more suitable to assess the stationarity of the ambient vibration wave-field over time. The wavelet time-frequency analysis was then performed over the whole recording time. From such analysis (**Figure 5**) an overall stability of the ambient-vibration wave-field over time is evident. The aforementioned disturbances in A2 at about 5~6Hz are confirmed to be nearly harmonic contributions, more pronounced at the end of the recordings window. This provides a further confirmation of their anthropogenic origin. These disturbances are nevertheless very weak and well localized in frequency; therefore they won't affect the subsequent processing steps.

7. Conventional H/V spectral ratios

The horizontal-to-vertical (H/V) Fourier spectral ratio is a technique widely used in seismic site characterization because of its ability to provide an estimate of the SH wave fundamental frequency of resonance (f_0) of the site. Other than that, H/V ratios are useful to provide information on the Rayleigh wave ellipticity function, which can be used in surface wave dispersion inversion procedures to constrain large velocity contrasts at depth. In this study, we use the H/V technique also to map the variability of the subsoil structure along the investigated area; this is necessary to verify the fulfillment of the 1D structure assumption, which is necessary for the f-k method applied later.

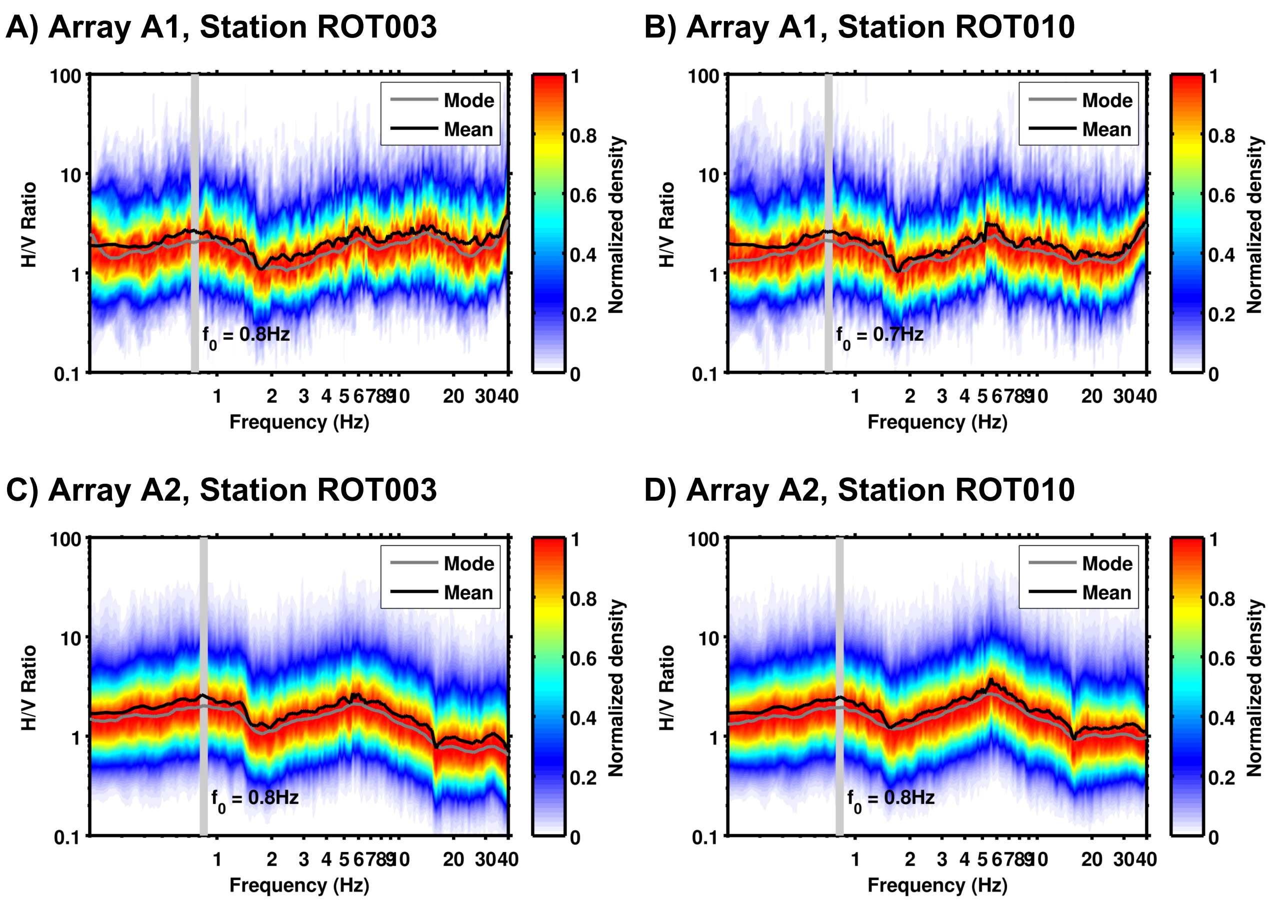

Figure 6 - *Example of H/V spectral ratios for the two concentric configurations A1 and A2. With the exception of the very high frequency range, H/V curves are stable on all stations and between array geometries. The resonance frequency is indicated with a light gray line. An additional peak is also present at about 6Hz, but with more variability.*

H/V spectral ratios have been computed for all the recordings at each station of the array and separately for configurations A1 and A2 (e.g. **Figure 6**). H/V curves have relatively low amplitudes and their shape is compatible with typical of stiff-soil/rock velocity profiles. The behavior of the noise wave-field at the different stations location is very comparable (**Figure 7**). A relatively small peak is always visible at low frequency (around 0.7~0.8Hz), quite stable over the whole measuring area. Such maximum is likely induced by a change in lithology at large depth, which causes a moderate contrast of seismic impedance. The peak should be regarded as the fundamental resonance frequency of the site. A second peak at about 6Hz is also present, with slightly larger amplitude (between 2 and 3). This second peak is of more difficult interpretation, as it could be addressable to a further velocity contrast or to a secondary maximum in the Rayleigh wave ellipticity function. This aspect will be clarified later in the analysis. Finally, the high frequency region (> 8~10Hz) is more variable within and between the two array configurations. In this range, H/V curves are however more diverse in A1 than A2. This can be explained by the difference in soil cover between the geometries, which was unconsolidated detritus in A1, and compacted ground in A2 (along the road).

8. Directional analysis

The computation of directional H/V spectral ratio or polarization analysis is useful to reveal asymmetries in the ambient vibration wave-field. Different effects can induce such a behavior: 2D/3D structure, topographic effects or a non-homogeneous distribution of the noise sources. If a strong directionality is found by the analysis, it is generally recommended to carry out further investigations to properly address the origin of polarization.

By processing the directional H/V ratios at all the recording stations of the two arrays (e.g. **Figure 8**) it is possible to observe an overall isotropy of the wave-field in the low to intermediate frequency range, roughly below 6Hz. The fundamental frequency peak at about 0.8Hz does not show any preferential directionality pattern between the different station locations. Conversely, the secondary peak reveals in several stations of the array A2 a moderate directionality towards E-W. Such behavior is also present - but nevertheless far less evident - in some stations of array A1.

The results of the H/V directional analysis are partially confirmed by applying the wavelet polarization analysis techniques as described in Burjanek et al. (2008). Also in this case no sign of significant directionality (**Figure 9**A) and polarization (**Figure 9**B) of the wave-field is observable in the low frequency band. Here, however, no preferential polarization direction is observed for the secondary maximum.

A) Array 1, H/V summary

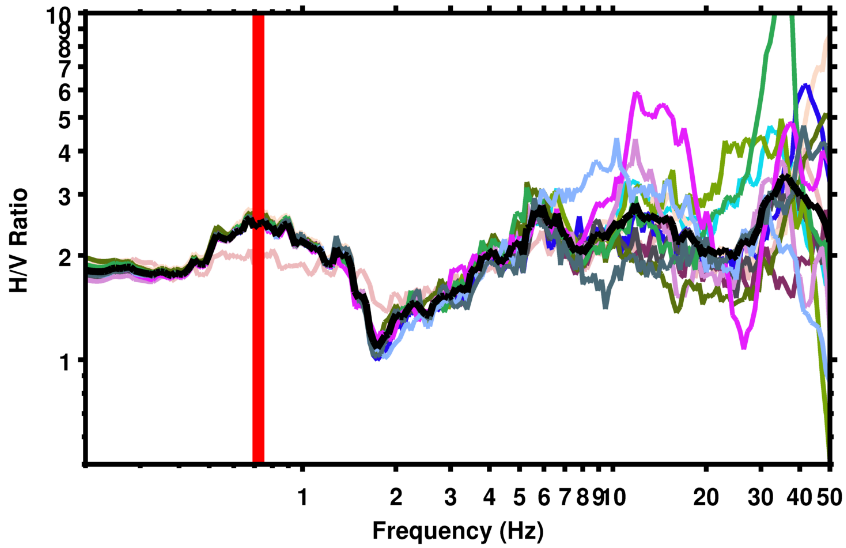

B) Array 2, H/V summary

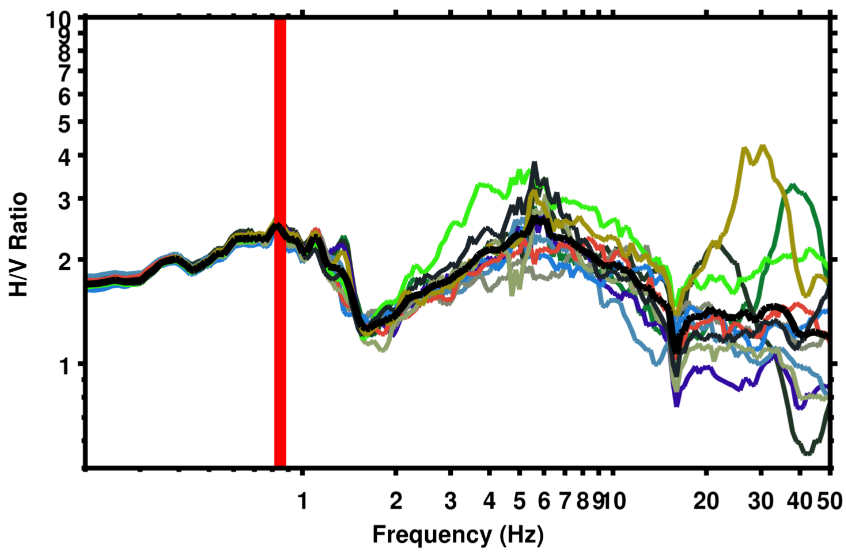

Figure 7 - *Comparison of H/V spectral ratio curves for all the stations of the array A1 and A2. The fundamental frequency can be identified at about 0.7~0.8Hz. The curves are stable and comparable up to the secondary maximum at about 6Hz, confirming the lateral homogeneity of the underlying deep velocity structure of the site. At high frequencies spectral ratios are more variable across the arrays. This reflects the heterogeneity of the soil cover.*

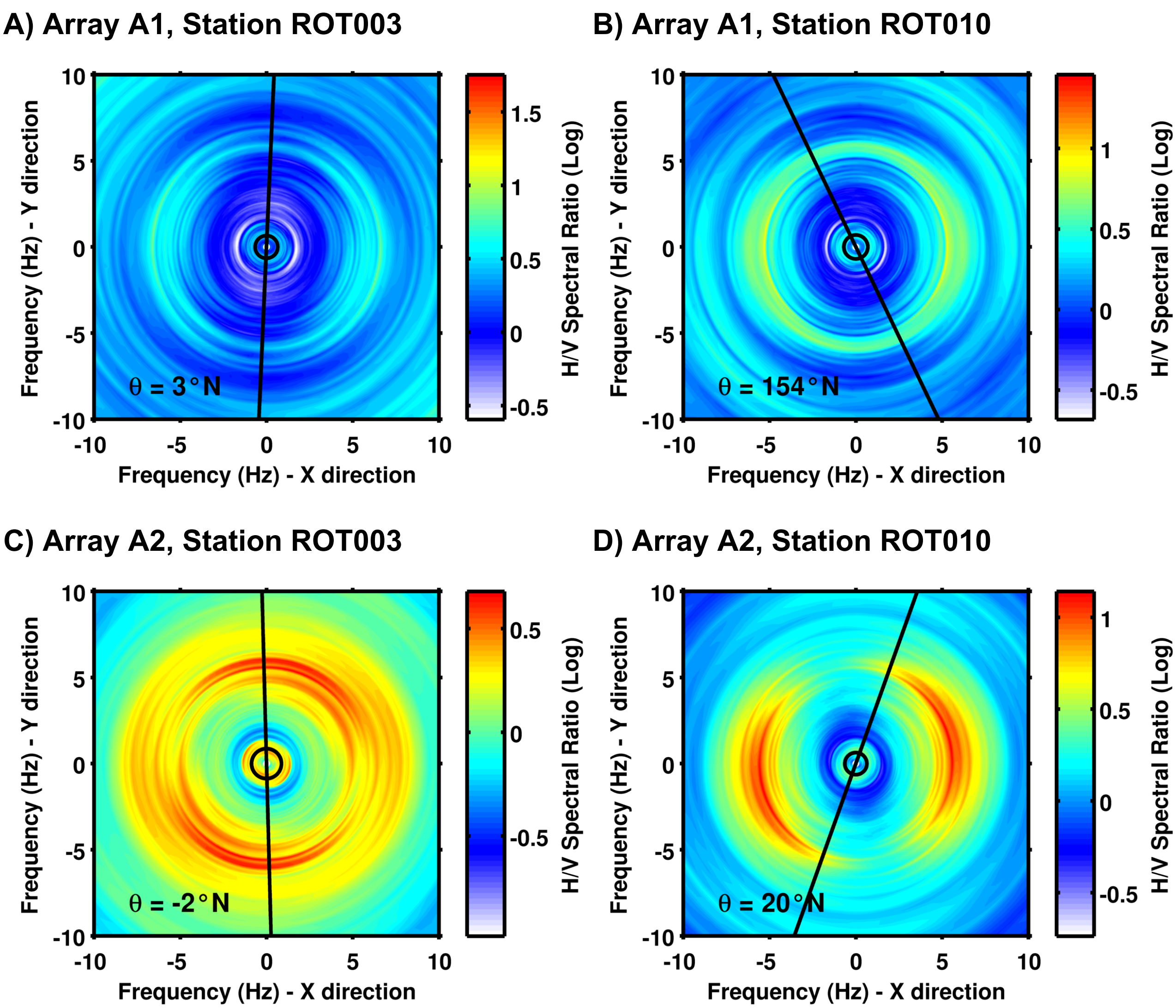

Figure 8 - *Example of directional H/V spectral ratios for the two array configurations A1 and A2. No evidence of wave-field anisotropy is present in the low frequency range (up to about 6Hz), while the secondary H/V peak is preferentially aligned toward E-W in many stations of array configuration A2. This behavior is nevertheless less evident within the stations of configuration A1.*

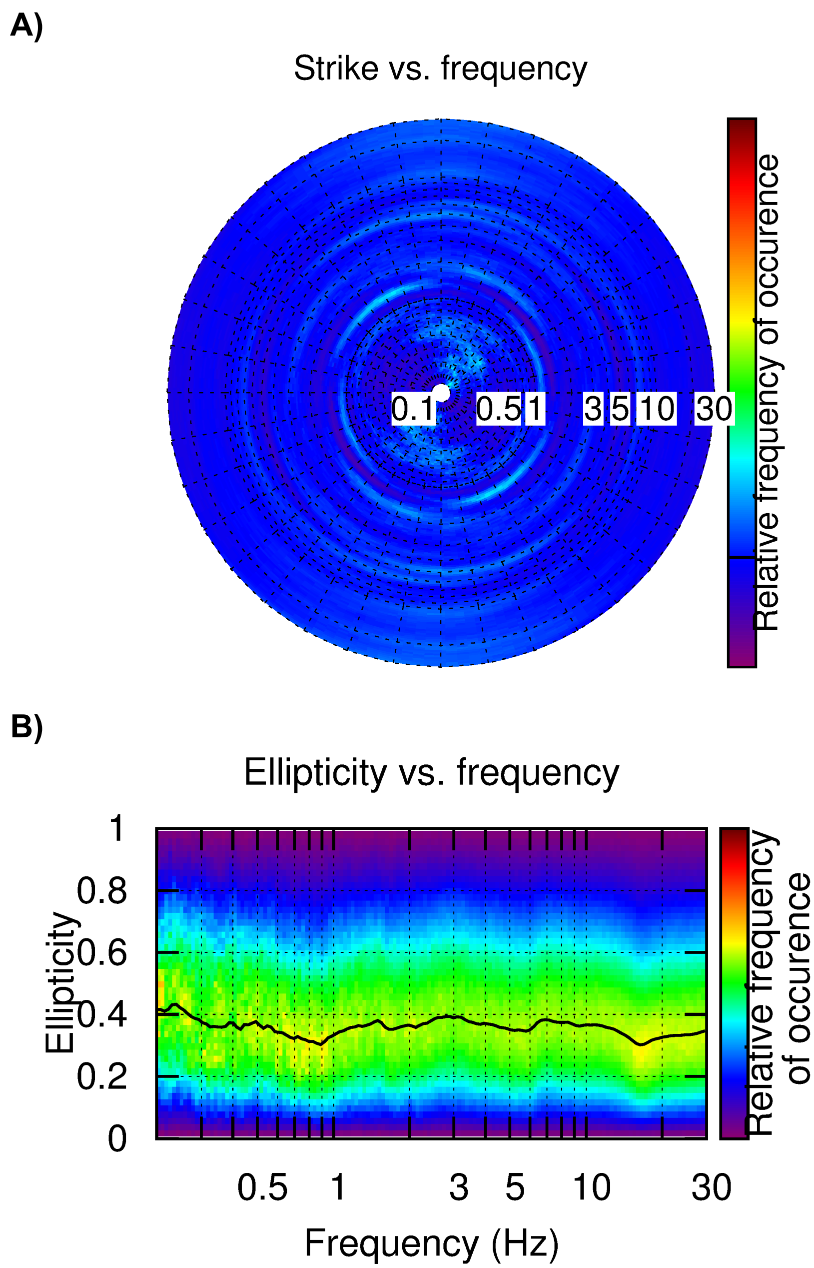

Figure 9 – *Example of wavelet-based polarization analysis at the station ROT003 of the array configuration A1. By analyzing the polarization over strike (A) and the particle motion ellipticity plot (B), no directional effect is visible in the frequency range of interest.*

9. Three-component f-k analysis

The frequency-wavenumber analysis is a spectral technique based on seismic array recordings that allows retrieving direction and dispersion characteristics of the surface waves. We apply this technique to three-component ambient vibration recordings using a modification of the high-resolution method of Capon (1969) as described in Poggi et al. (2010). Using all the three-components of motion gives the possibility to retrieve information about the propagation of the Rayleigh waves (vertical and radial processing direction) as well as of the Love waves (transversal direction).

As in the case of the previous methods, the ambient vibration recordings are treated statistically by subdividing the traces in sub-windows. For each consecutive window a separated f-k analysis is performed, and the results are then averaged over the whole recording, increasing the robustness of the final estimation.

A) 2-4Hz

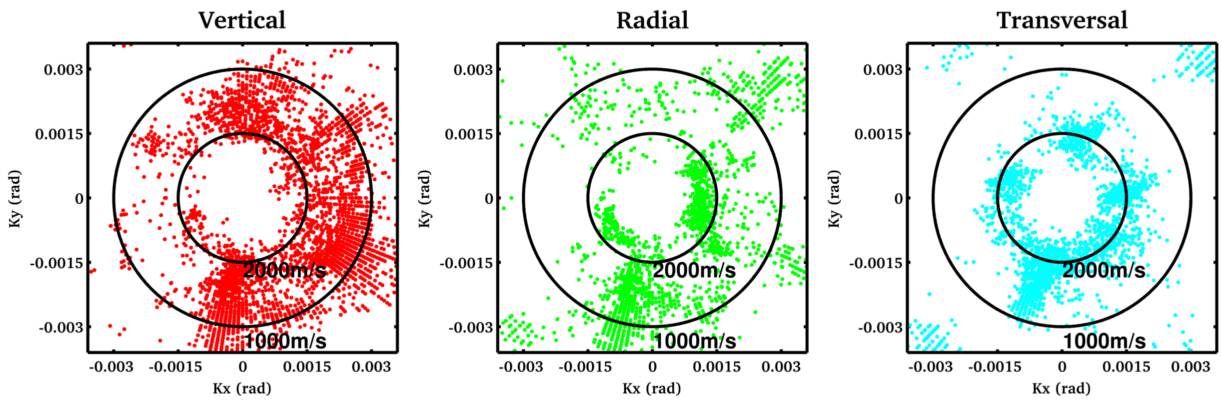

B) 4-8Hz

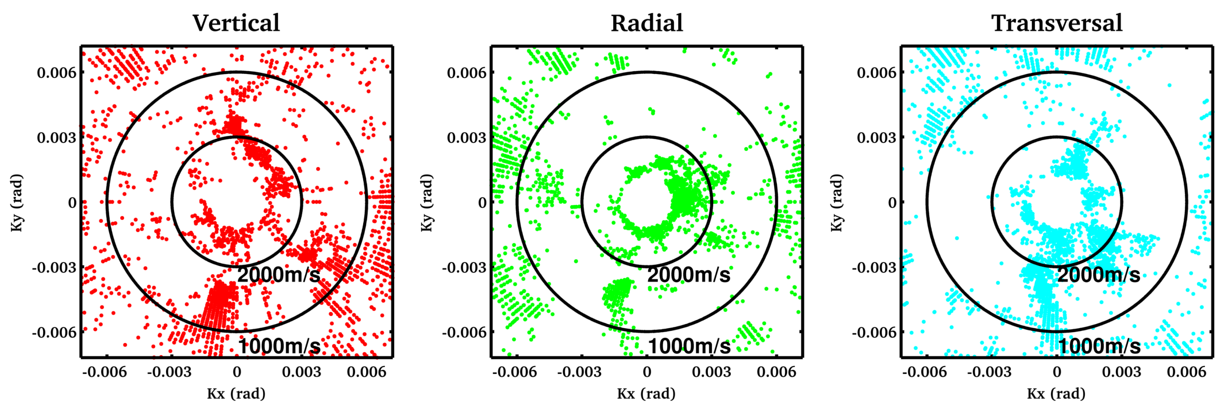

Figure 10 - *Example of distribution of noise sources in the low (2-4Hz) and intermediate frequency range (4-8Hz) obtained from three-component f-k analysis of A2. The source distribution is irregular but not strictly directional on all the propagation components.*

As first step, from the f-k analysis it is possible to assess the noise source azimuthal distribution for different frequency ranges (e.g. **Figure 10**) separately for the vertical, the radial and the transversal direction of polarization. From the analysis of the two geometries A1 and A2, source distribution appears to be quite inhomogeneous in all the components, without nevertheless displaying a clear directional pattern.

As a second step, the surface-wave dispersion curves are extracted by visual inspection and manual picking of the f-k density plots (**Figure 11** and **Figure 12**), separately for the three polarization direction. Complementary results have been obtained for the two array configurations A1 and A2, whose resolution limits partially overlap.

Rayleigh wave dispersion can be well tracked for A1 on both the vertical and the radial components (**Figure 11**). Here, a single mode with nearly constant velocity can be well identified on a broad frequency range. Only at very high frequency the mode seems to be bending to lower velocities (of doubtful interpretation, given the frequency). Results from A1 are complemented at low frequencies by the f-k processing of A2 (**Figure 12**), which extends the resolution on the mode down to about 1.6Hz. As well, Love wave dispersion is also resolved in array configuration 1, but nearly invisible in the processing from configuration 2. The results from the two arrays are also not perfectly matching in velocity. A summary of all the preliminary identified modes from vertical, radial and transversal direction of propagation is presented in **Figure 13**.

For the modal interpretation we proposed two alternative models. In the first model we assume the Rayleigh and Love dispersion described by a single fundamental mode (**Figure 14**A). Such pattern is common in rock sites without strong variations of velocity with depth. Alternatively, for the second model we propose a more complex interpretation, based on the possibility of existence of several consecutive higher modes close to osculation (**Figure 14**B). In such a case, the modal energy may transfer from a mode to the subsequent, giving rise to an observed modal pattern with apparent nearly-constant phase velocity (similar cases are well documented in literature related to active surface wave analysis). According to this hypothesis, the identified Rayleigh mode is then split into three independent modes (one fundamental and two higher) at those frequencies where the dispersion curve shows large irregularities (~5Hz and ~10Hz). Same approach is therefore applied to Love dispersion too, as a single mode was found not compatible with multimodal Rayleigh dispersion (as we later tested).

10. Inversion of the dispersion curves

The surface wave dispersion curves (Rayleigh and Love) obtained from the three-component f-k analysis of the ambient vibrations are inverted to obtain an estimation of the velocity profile of the site (mainly S-wave velocity as function of depth, and to a lesser extend the P-wave velocity, due to the lower sensitivity). The analysis is performed using the software *Dinver* (www.geopsy.org), which implements a direct search approach (e.g. **Figure 15** and **Figure 16**) based on a conditional version of the neighborhood algorithm (Sambridge, 1999).

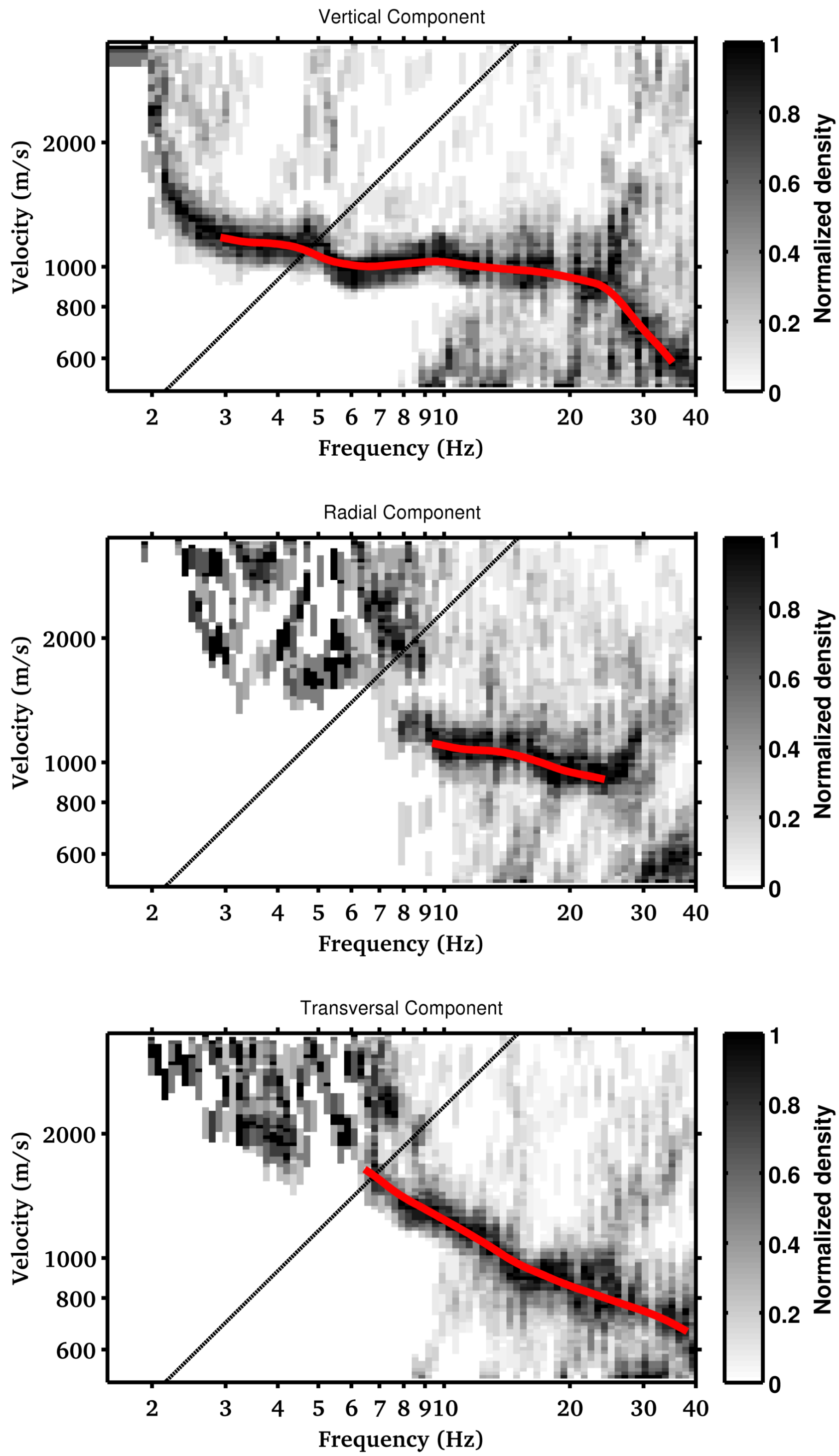

Figure 11 - *Density distribution of the surface wave signals obtained from the recording of the array configuration A1 using three-component f-k analysis. From top to bottom: Rayleigh vertical, Rayleigh radial and Love wave dispersion. In red the preliminary interpreted dispersion curves are given (manually selected).*

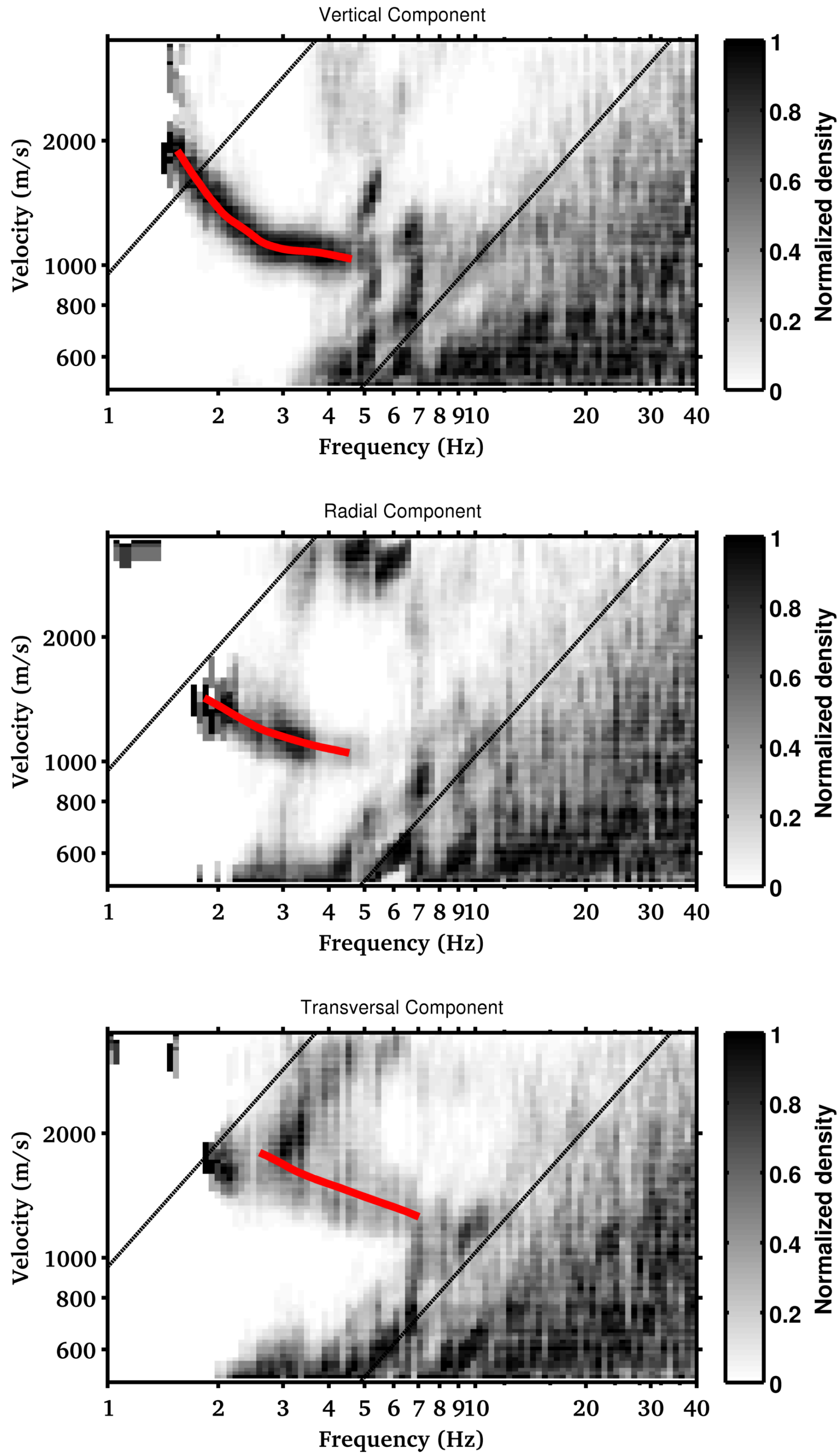

Figure 12 - *Density distribution of the surface wave signals obtained from the recording of the array configuration A2 using three-component f-k analysis. From top to bottom: Rayleigh vertical, Rayleigh radial and Love wave dispersion. In red the preliminary interpreted dispersion curves are given (manually selected).*

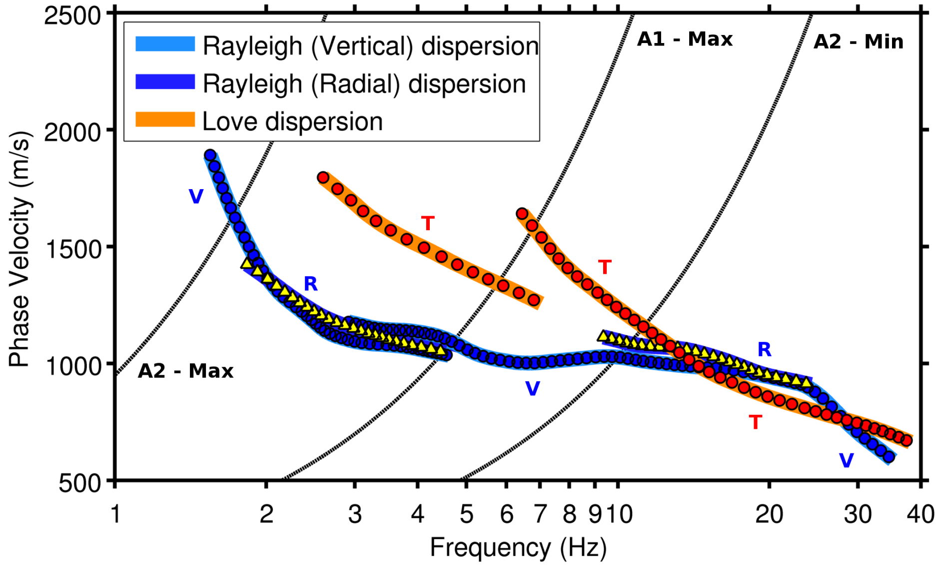

Figure 13 - *Summary of all picked dispersion curves obtained from three-component f-k analysis of the two array configurations A1 and A2. Minimum and maximum resolution bounds of the two array geometries are indicated with black solid lines.*

To parameterize the velocity model, two different approaches were implemented. The first one consisted in setting up an eight-layer model with fix interface depths (**Figure 17** A and C). In such a case the free inversion parameters are then the velocities (P and S) and layer thicknesses. In the second case, a free-thickness layer approach was used (**Figure 17** B and D). The advantage of the former method stays in the possibility to better resolve sharp velocity interfaces, while the second is less unique and better constraints the seismic velocity. The two approaches have to be nevertheless considered complementary, and they should provide consistent results. Ten inversion tests (*runs*) were performed for each of the two interpretation schemes (single mode and multimode), in order to minimize the effect related to a possible unfavorable initial randomization of the parameter space. The best fitting model from of each run was then collected, evaluated and used for the computation of the derived soil parameters.

A) Single mode model

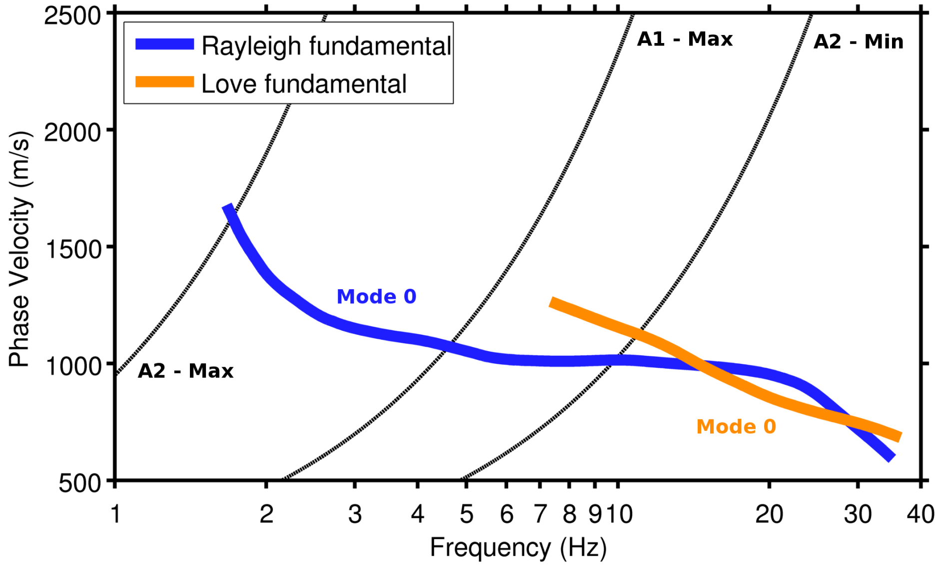

B) Multimode model

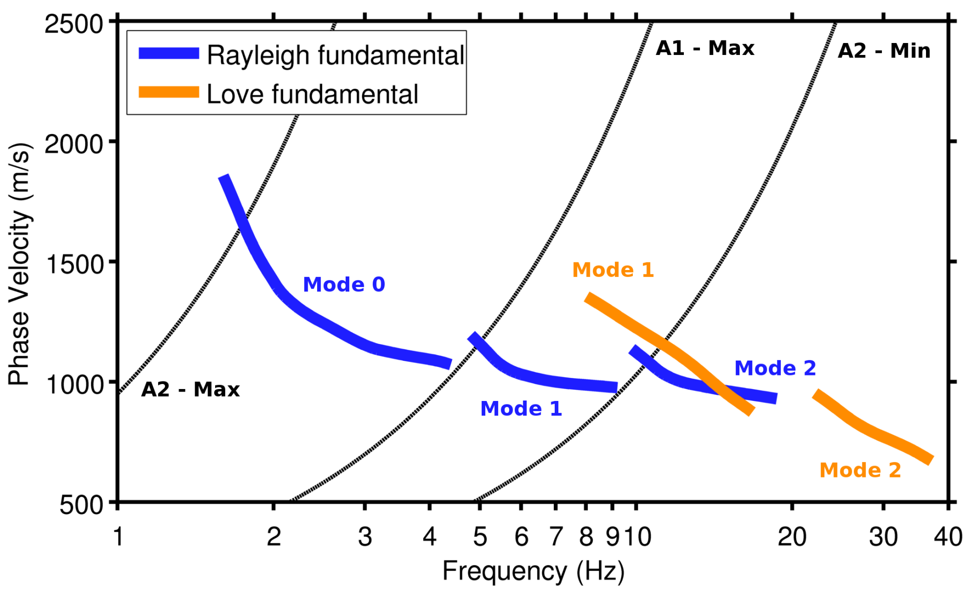

Figure 14 - *Final interpretation of the Rayleigh and Love dispersion curves for ROTHE. Two independent models are presented for comparison (named "single mode" and "multimode"). Minimum and maximum resolution bounds of the two array geometries are indicated with black solid lines.*

A) Single mode model, Love waves

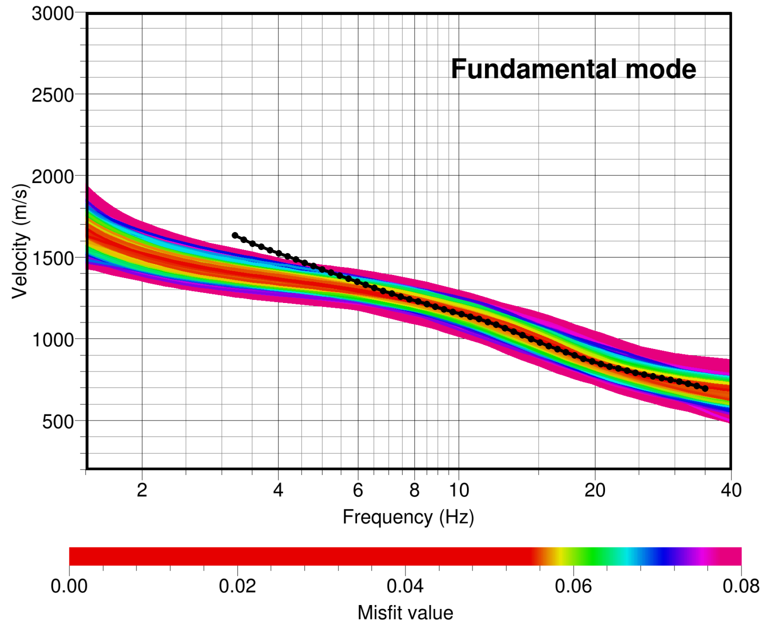

B) Single mode model, Rayleigh waves

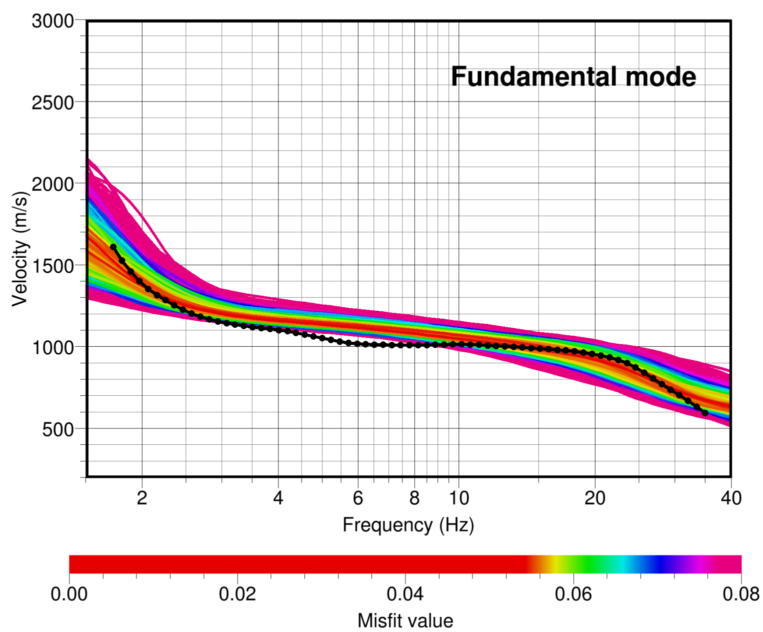

Figure 15 - *Fitting of the surface dispersion data within the global optimization inversion of the "single mode" interpretation. Different colors represent different misfit between the observed (in black) and the modeled dispersion curves during the search.*

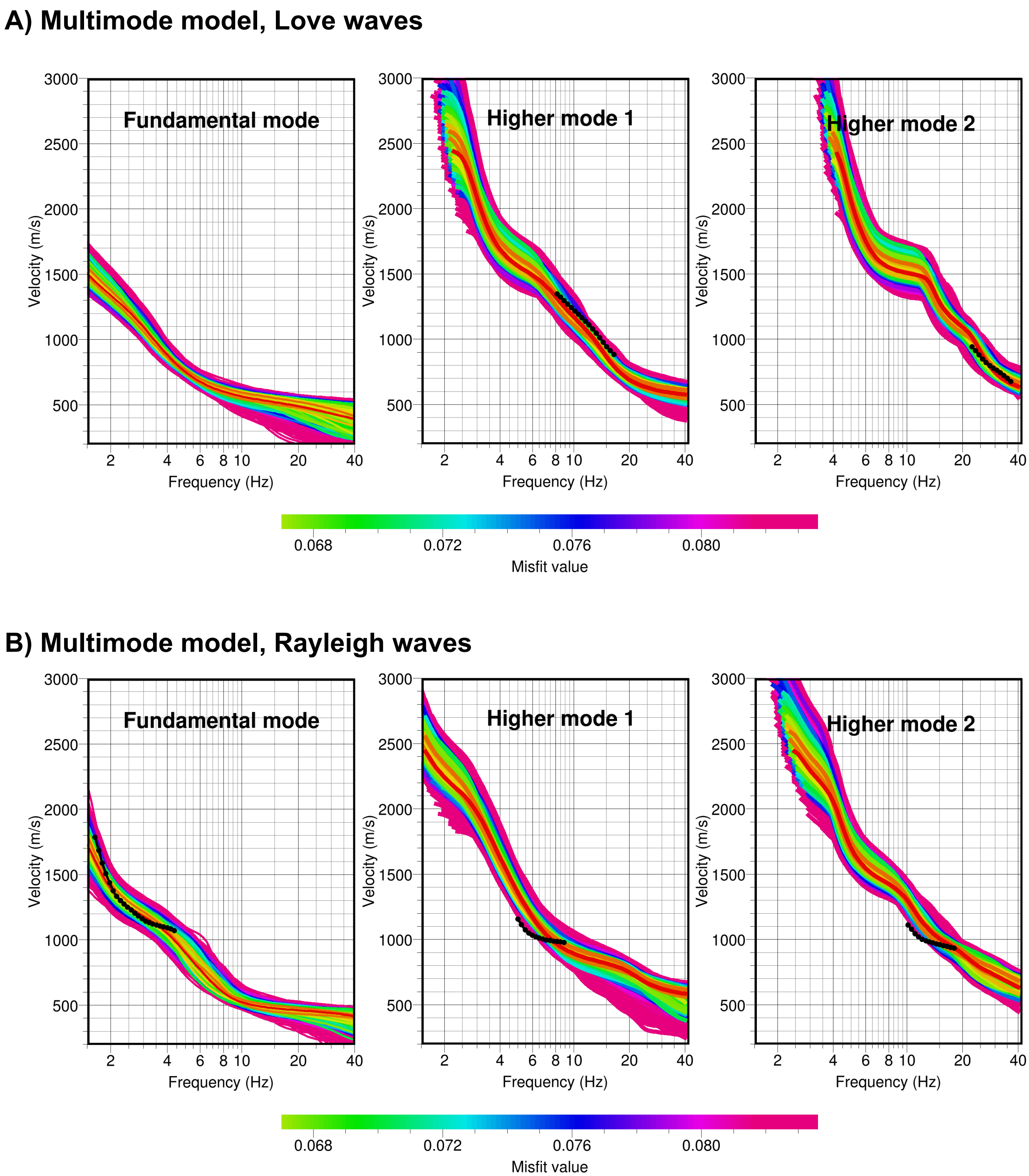

Figure 16 - *Fitting of the surface dispersion data within the global optimization inversion of the "multimode" interpretation. Different colors represent different misfit between the observed (in black) and the modeled dispersion curves during the search.*

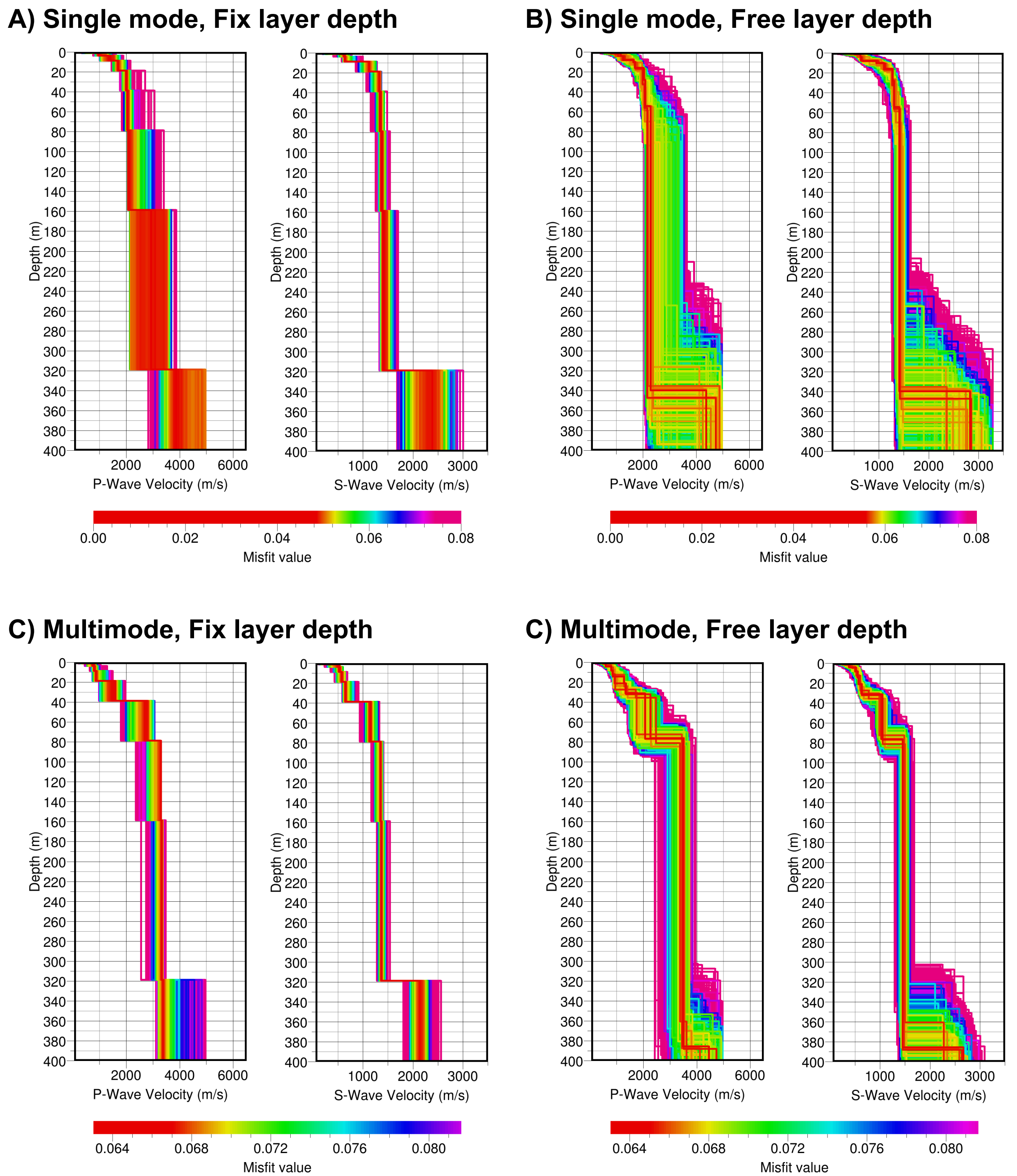

Figure 17 - *Distribution of the free- and fix-layer velocity models generated during the inversion process, ordered by decreasing misfit, according to the color scheme of* **Figure 15** *and* **Figure 16**.

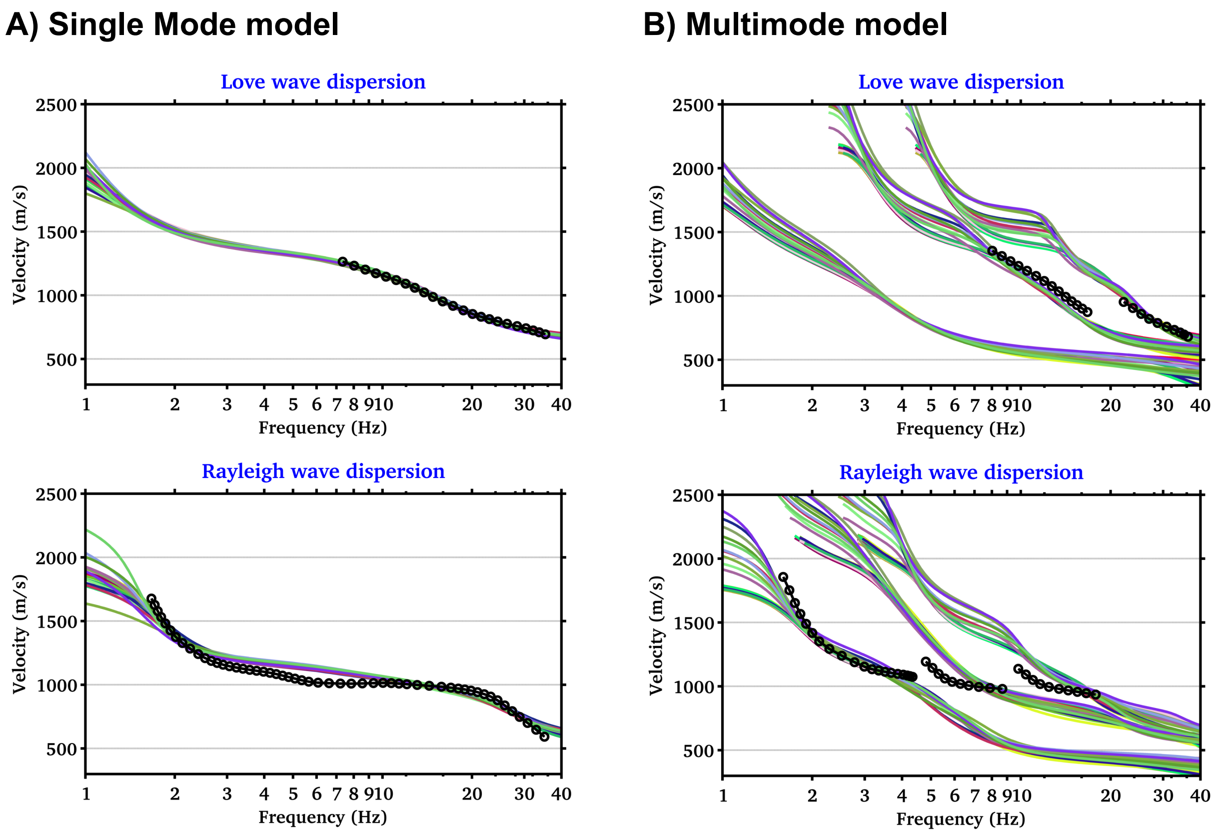

Figure 18 - *Dispersion curves computed from the best fitting models of the two proposed interpretation schemes; pictures include all inversion runs performed using both the free-layers and fixed-layers parameterization schemes.*

In more detail, the inverted velocity models (Vs and Vp) for the two proposed interpretations are quite dissimilar, particularly in the shallower part of the profile. Results from “single mode” interpretation are gradient-like, with a faster increase in velocity in the first 20m, followed by a smoother and nearly-constant velocity part. This is realistically expected for a rock site. Results from “multimode” model have a more complex structure, with two evident velocity jumps at about 25m and 80m and of relatively high impedance contrast. At larger depth, S-wave velocities are comparable for both the schemes, while Vp is considerably different. The deeper interface at about 350~450m is solely constrained by inverting the Rayleigh wave ellipticity peak obtained from H/V analysis. Below this value no direct constrain is available from f-k analysis, and the velocity values are defined by pure extrapolation.

A) Single Mode model

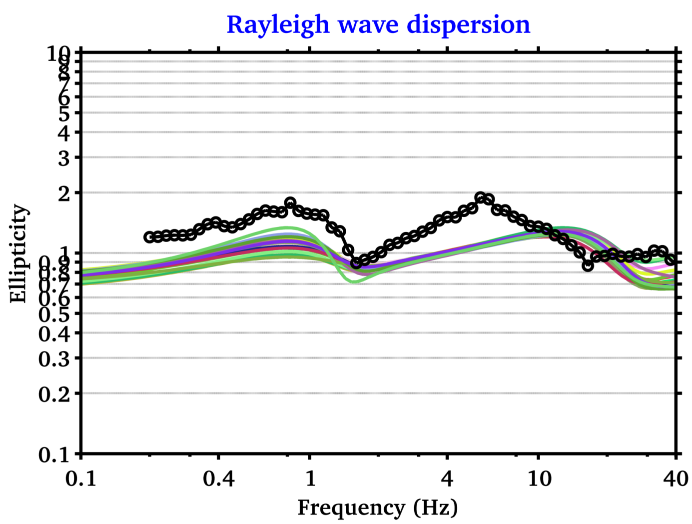

B) Multimode model

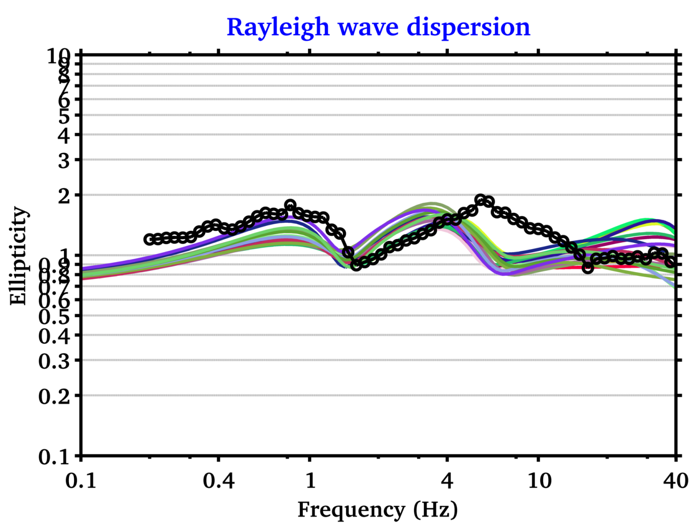

Figure 19 – *Rayleigh ellipticity curves computed from the best fitting models of the two proposed interpretation schemes; pictures include all inversion runs performed using both the free-layers and fixed-layers parameterization schemes. Only the first ellipticity peak was used as constraint for the inversion.*

A) Single mode model

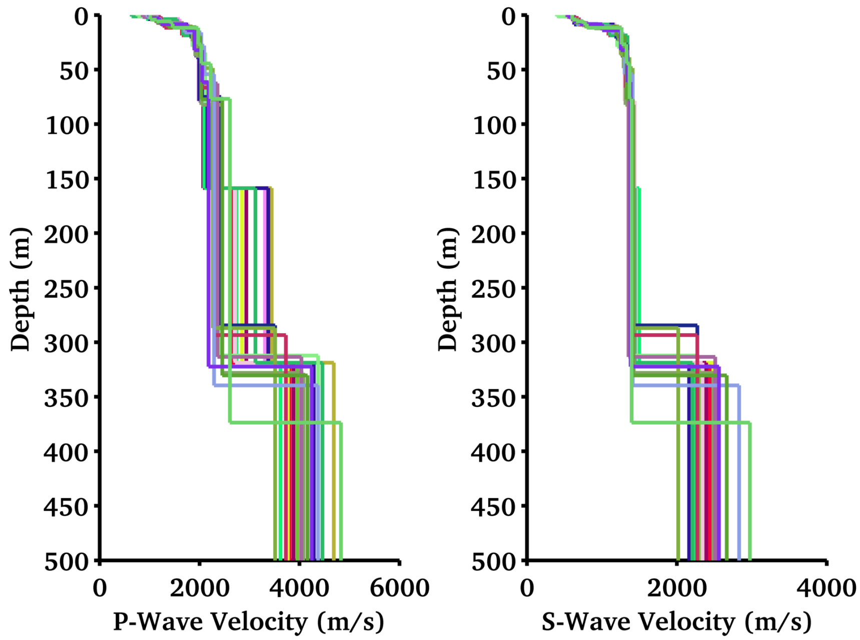

B) Multimode model

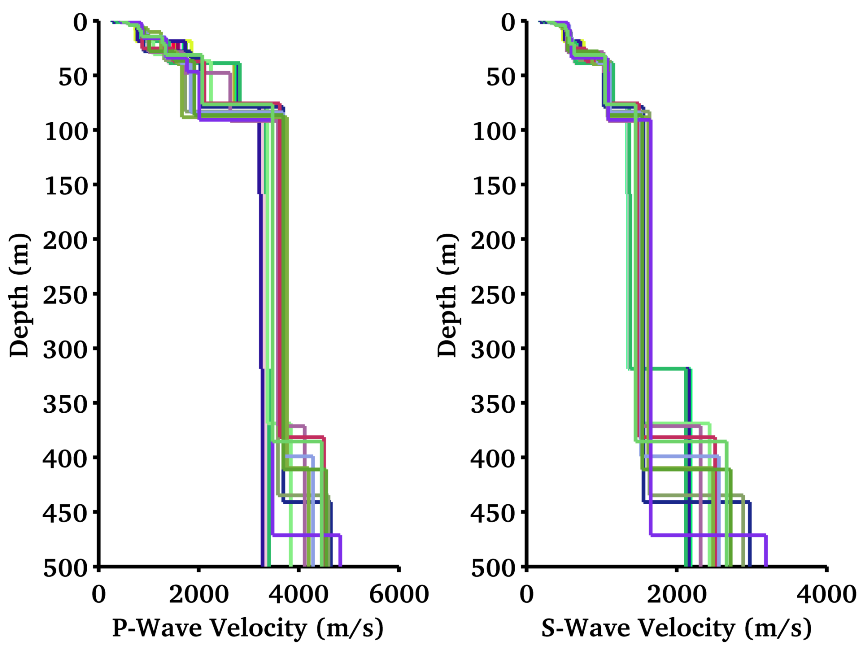

Figure 20 - *Best fitting models of the two proposed interpretation schemes; pictures include all inversion runs performed using both the free-layers and fixed-layers parameterization schemes.*

11. Amplification models

Synthetic site amplification is computed using two different approaches: the S-wave transfer function for vertical propagation and the quarter-wavelength approach. In general the first method is used to evaluate the resonance characteristics of the site, while the second is more useful to assess the effect of the velocity contrasts between the lowermost rock layer (as reference) and the different QWL averaging depths. The two amplification functions are then corrected for the Swiss rock reference velocity profile as defined in Poggi et al. (2011), according to the procedure described in Edwards et al. (2013). Given the lower velocities in the uppermost part of the ROTHE profile compared to the Swiss reference, the final corrected amplification function shows a lower average amplification level at high frequencies than the uncorrected (e.g. **Figure 21**). It has to be notice that the amplification functions do not include attenuation at this stage of the analysis, as the quality factors of the site are unknown.

Amplification computed from the two sets of inverted models (**Figure 22**) is then compared with empirical amplification from spectral modeling of low magnate events (Edwards and Fäh, 2013). Results obtained from the "single mode" models show to be more consistent with observations than those from the "multimode" approach. This last, in more detail, shows higher amplification in the intermediate frequency range (2-10Hz) not supported by data. Such amplification is related to the impedance contrasts at 25m and 80m. For this reason, the "single mode" model is finally selected as representative for the site.

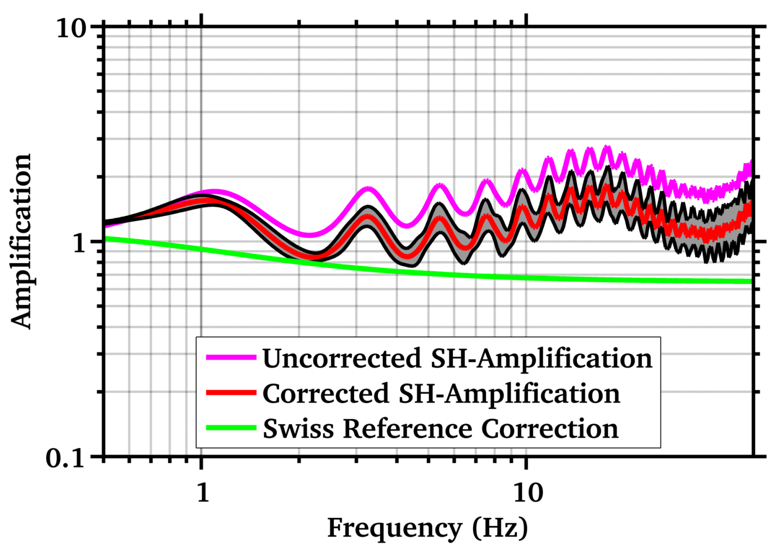

Figure 21 - *Example of correcting the SH-wave transfer function for the Swiss (rock) reference conditions (Poggi et al. 2011). The final corrected amplification function shows a lower (average) amplification at high frequencies than the uncorrected. In this example, amplification is computed from the single mode inversion model.*

A) Single mode model

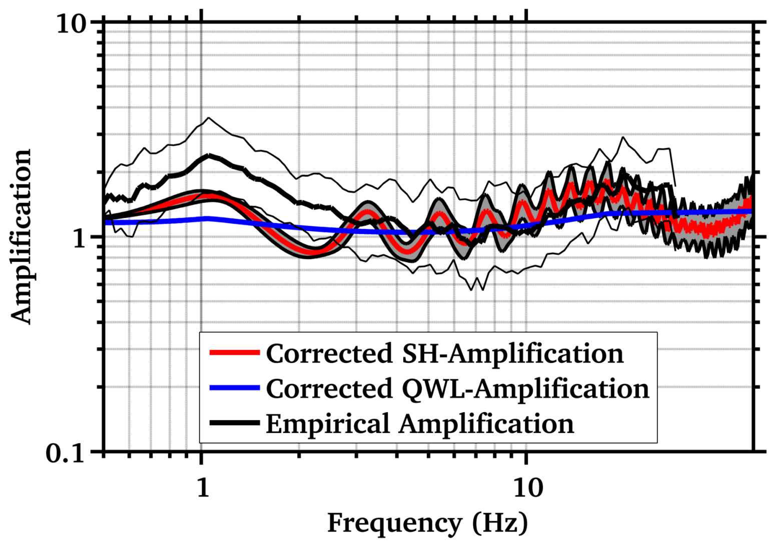

B) Multimode model

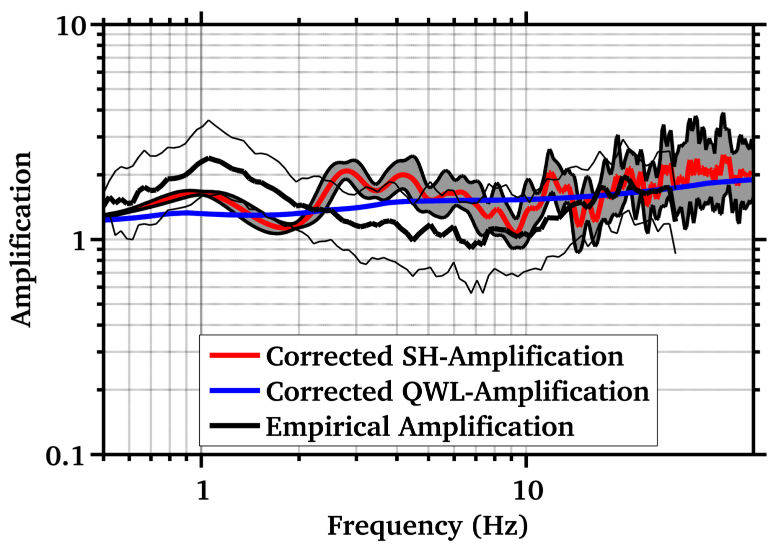

Figure 22 - *Comparison between modeled amplification functions computed using the SH-wave transfer function and the quarter-wavelength formalism with observed empirical amplification from Earthquake spectral fitting (Edwards and Fäh, 2013). All the functions are referenced to the Swiss rock reference model (Poggi et al. 2011).*

12. Engineering soil parameters

The ensemble of all the best inverted velocity profiles is then used to derive average soil parameters like the VsZ (average travel-time S-wave velocity over the depth Z, including Vs30, **Table 1**) and the quarter-wavelength (QWL) average velocities (Joyner et al., 1984) for a range of frequencies between 0.6 and 30Hz (**Figure 23**). The former is a standard parameter for the classification of ground-types in most building codes and in ground motion prediction equations. The latter is a parameter useful for the empirical estimation of the site-response and to assess the sensitivity of the seismic wave-field to the different depths. It has to be noticed that these two parameters are derived separately from all the best S-wave velocity models obtained from the inversion, and the results is finally averaged to improve statistics.

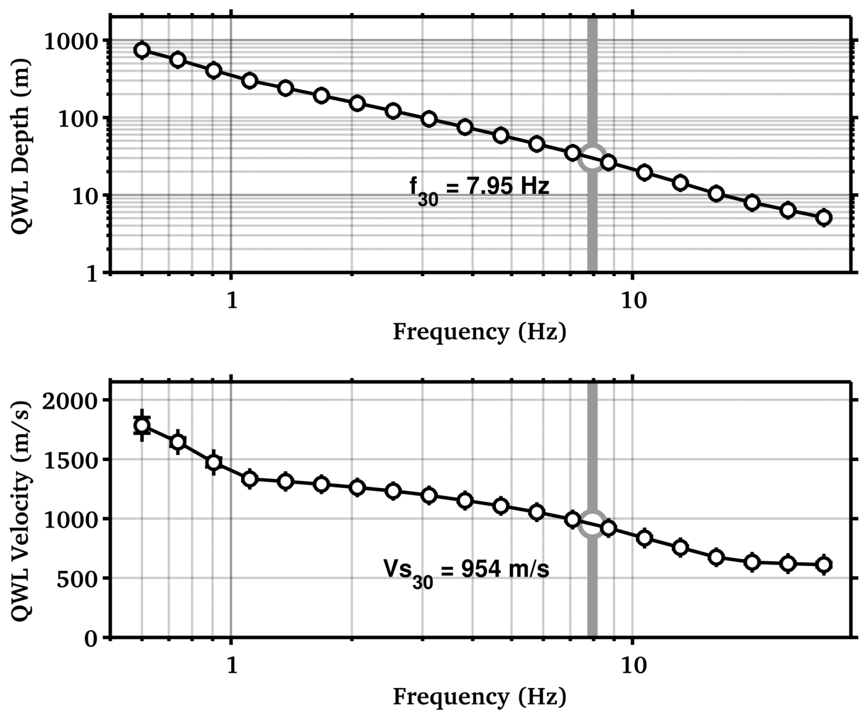

Figure 23 - *Quarter-wavelength representation of the inverted S-wave velocity profiles from the "single mode" model. Top: the depth-frequency dependency. Bottom: the QWL average velocity. The Vs30 value is indicated with its corresponding QWL frequency.*

Averaging depth (m)	Vs-mean (m/s)	St.Dev.
5	611.916	17.02094
10	665.9669	8.102553
15	768.0926	7.986122
20	843.8919	9.470917
25	906.2958	7.852841
30	954.3979	8.363619
40	1024.602	8.108233
50	1074.296	8.152109
75	1151.914	9.642955
100	1202.775	8.382917
150	1260.223	8.431377
200	1294.471	9.926153

Table 1 - *Average travel-time velocities at different depths. Vs30 is highlighted.*

REFERENCES

Capon, J., 1969. High resolution frequency wavenumber spectrum analysis, Proc. IEEE, 57, 1408-1418.

Burjanek, J., G. Stamm, V. Poggi, J.R. Moore, and D. Fäh [2010], "Ambient vibration analysis of an unstable mountain slope", Geophys. J. Int., Vol. 180, pp. 820-828.

Edwards, B., C. Michel, V. Poggi and D. Fäh (2013). Determination of Site Amplification from Regional Seismicity: Application to the Swiss National Seismic Networks. Accepted for publication in Seismological Research Letters.

Edwards, B. and D. Fäh (2013). A Stochastic Ground-Motion Model for Switzerland, Bulletin of the Seismological Society of America, 103 (1), 78-98.

Joyner, W. B., R. E. Warrick and T. E. Fumal (1981). The Effect of Quaternary Alluvium on Strong Ground Motion in the Coyote Lake, California, Earthquake of 1979, Bulletin of the Seismological Society of America, 71, 1333-1349.

Poggi, V., B. Edwards and D. Fäh (2011). Derivation of a Reference Shear-Wave Velocity Model from Empirical Site Amplification, Bulletin of the Seismological Society of America, 101, 258-274.

Poggi, V. and Fäh D., 2010. Estimating Rayleigh wave particle motion from three-component array analysis of ambient vibrations. Geophys. J. Int., 180-1, 251-267.

Eidgenössische Technische Hochschule Zürich
Swiss Federal Institute of Technology Zurich

SED
Schweizerischer Erdbebendienst
Swiss Seismological Service

Report on site characterization

Hämikon, Switzerland (HAMIK)

Poggi Valerio, Ulrike Kleinbrod, Donat Fäh

Last modified - 23 / 12 / 2014

1. Introduction

In the framework of the NAGRA seismic network project, an array measurement of the ambient vibration wave-field was performed at the location of the SED borehole station HAMIK (Hämikon, Switzerland). The scope of the survey is the seismic characterization of the area surrounding the installation (**Figure 1**), which consists in a short period borehole sensor at about 100m, and a collocated strong motion seismometer at the surface, with a high-resolution digitizer (Taurus 24Bit @200sps). Ambient vibration analysis has been used to infer the characteristics of the underground structure of the site, with special regard to the one-dimensional shear-wave velocity. Such profile was later compared with the results from active seismic measurements and used to assess the local seismic response of the station.

For the analysis, different spectral analysis techniques were implemented, consisting in both single and array methods, which are listed below:

- Time-frequency wavelet analysis
- Power-spectral density estimation
- Conventional horizontal to vertical spectral ratios
- Directional horizontal to vertical spectral ratios
- Wavelet polarization analysis
- Three-component high-resolution f-k analysis.

The results of all these analyses conformed to the definition of the final velocity model. In the following, the main results of these investigations are summarized and a final interpretation of the velocity profile is given. From this interpretation, engineering parameters are finally derived, e.g. the Qwl-Vs average velocity, VsZ (including Vs30) and the seismic amplification from the analytical SH-transfer function of the one-dimensional soil column.

2. Survey description

To characterize the seismic response of the site, an array measurement of ambient vibration was performed on 25/02/2014 (**Figure 1**). The array consists of three concentric measuring configurations (called “rings”, R1, R2 and R3) of 14 sensors each and increasing diameter (about 40m, 120m and 200m respectively). The three configurations were planned to partially overlap, with the aim of providing a continuous frequency resolution between the geometries. Configuration R1 recorded for a total of 35m, while configuration R2 for 45m and R2 for 1h15m. The differences in the recording length are due to the different resolution characteristics of the three geometries. As a general rule, larger arrays require longer recording time to produce a reasonable statistics of the ambient vibration processing results. Satisfactory results were obtained from the analysis of all the geometries. For the larger configuration, a penetration depth of 100~150m was initially expected.

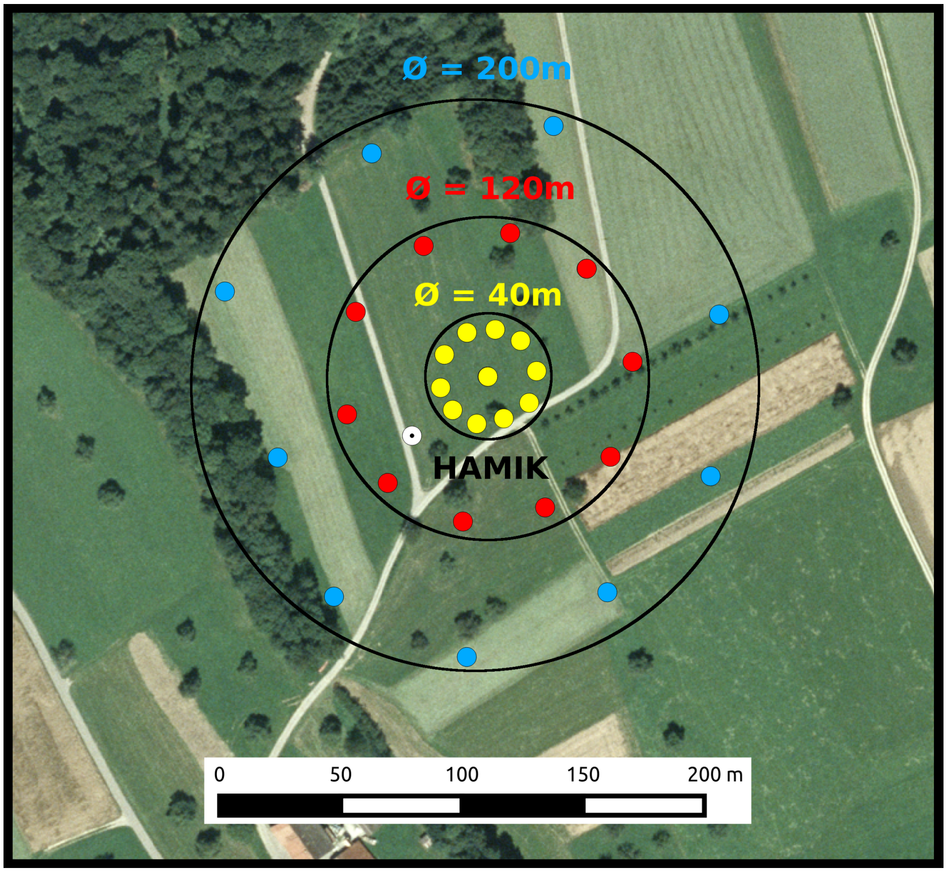

Figure 1 - *Location of the ambient vibration array survey performed in Hämikon, (SED station HAMIK) on 25/02/2014. Three concentric configurations of increasing diameter were implemented (named R1, R2 and R3). Location of the permanent station is shown with a white dot, between configurations R1 an R2.*

3. Soil type, topography and geology

The array has been set in open field conditions, in a rural area (**Figure 1**, **Figure 3**). The influence of buildings and anthropogenic disturbances is virtually negligible. Array sensors have been deployed on free soil. Good coupling with the ground was assured by means of digging small holes at the sensor's places, and by using a special support (*Trihedron*®) that facilitates the leveling of the device even for difficult soil conditions. The measurement area was located on a small ridge, roughly aligned N-S. However, maximum elevation difference between sensor locations was less than 5m, and therefore no topographic correction was necessary before processing.

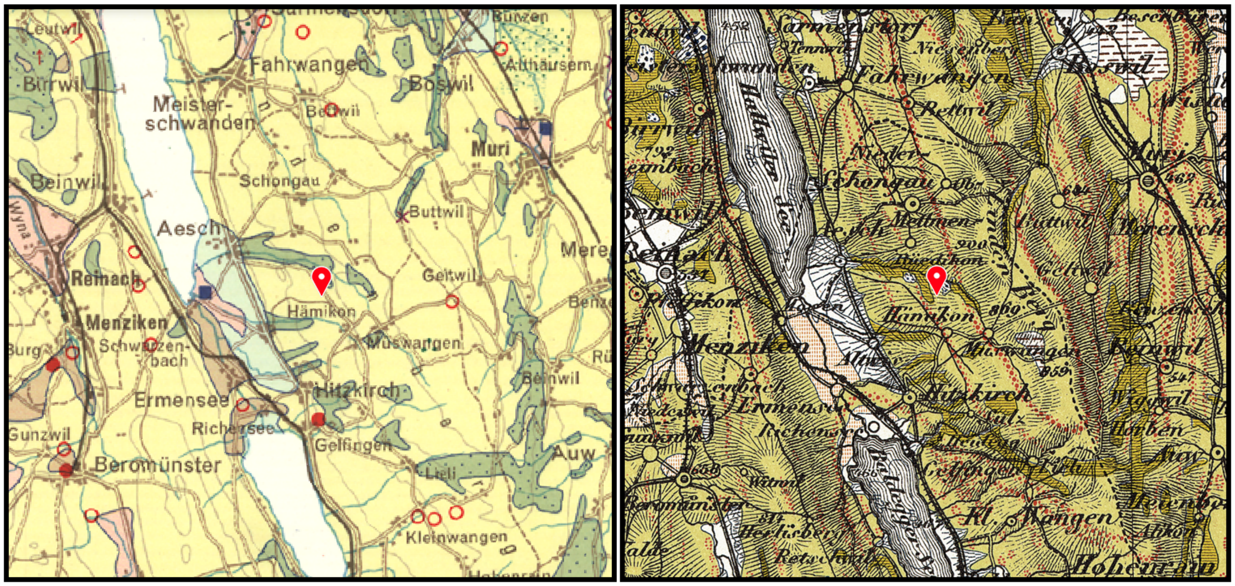

Figure 2 - *Geological map of the measuring area, in the surroundings of Hämikon (reproduced from Swisstopo, "Geologische Generalkarte der Schweiz" to the right, "Geotechnics and rocks" to the left, modified). In red the approximate location of the permanent station HAMIK.*

From the geological points of view (**Figure 2**) the target area is located on a small hill on the Molasse basin. The surface morphology is considerably smooth and modeled by the action of glaciers during the Pleistocene. The measuring area is visibly surrounded by moranic deposits, clearly identifiable from the surface morphology and confirmed by the geological map of the area. The Molassic bedrock is never exposed across the area (a variable-thick cover of quaternary soil material is generally present). The bedrock probably consists of marl and consolidated sandstone with layers of different texture and granulometry, from very fine sand and silt to occasionally conglomerate. Such site can be classified as of rock ground-type A.

4. Weather conditions

The weather conditions were optimal and stable during the whole measurement, with no precipitations, no wind and an average temperature of 5 degrees.

Figure 3 - *Overview of the measurement area at the location of the array central station.*

5. Acquisition equipment

Each acquisition point within the array consisted of a three components seismometer (Lennartz 3C with 5s eigenperiod) and a 24 bit data logger (Quanterra Q330). Synchronization between stations was assured by standard GPS, while a more accurate differential GPS (Leica Viva system) was used to precisely locate the sensor's coordinates with a tolerance of less than 5cm.

6. Pre-processing and preliminary data-quality control

The three-component recording has been filtered prior to analysis using a band-pass 6^{th} order causal Butterworth filter with corners at 0.2Hz and 50Hz. Although it is not a strict requirement for spectral analysis techniques, such filtering was applied in order to facilitate the preliminary visual inspection of the noise traces and to evaluate the coherency of the wave-field (**Figure 4**). Such procedure gives essential information for the subsequent interpretation of the f-k analysis results.

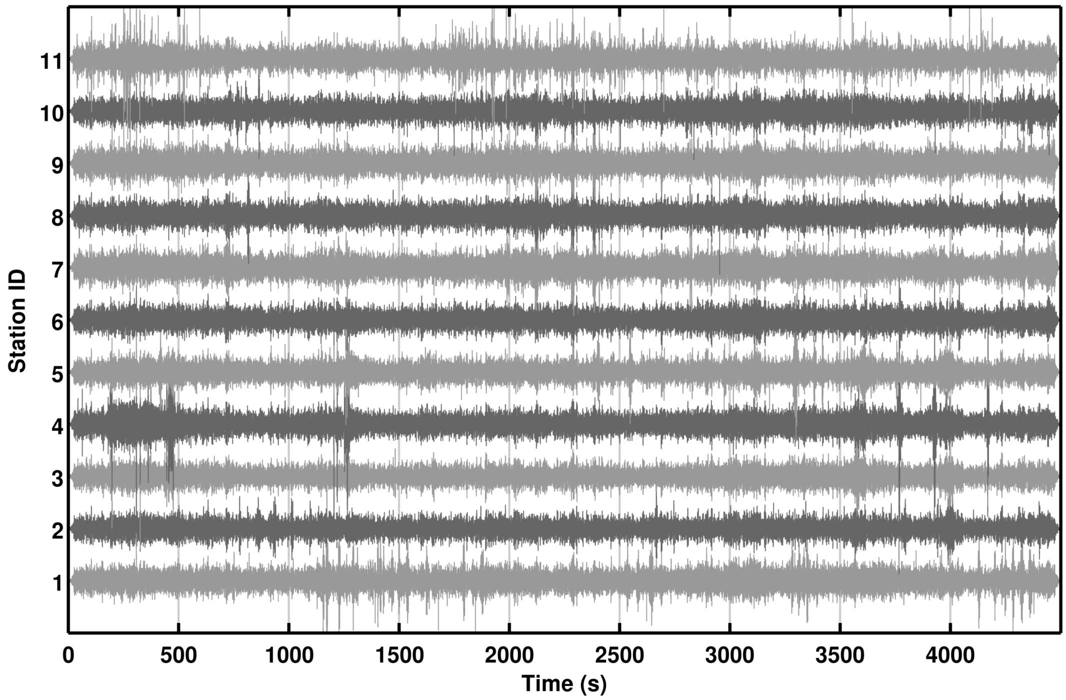

Figure 4 - *Inspection of the useful part of the ambient vibration recording of the Hämikon array (here ring configuration R3). No strong transients were present during the acquisition, which resulted in an overall good quality of the recordings.*

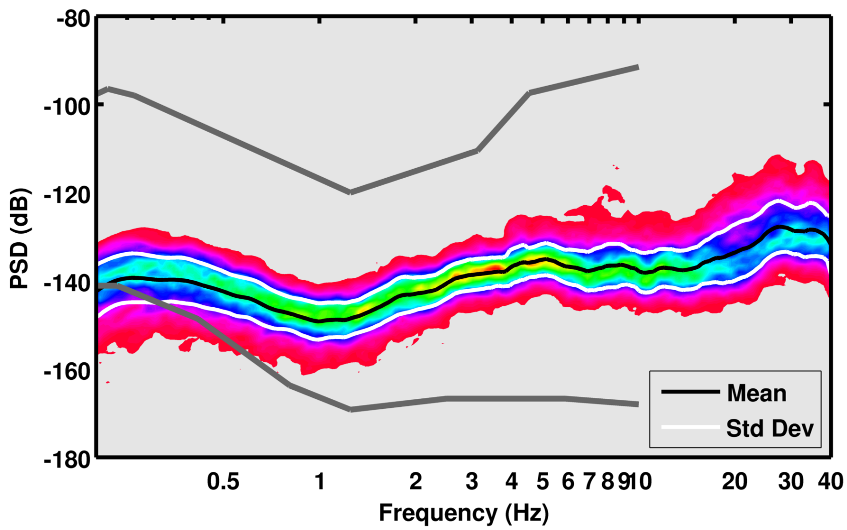

Figure 5 - *Power spectral density (PSD) computed for 1h15m recording at the central station of the array configuration R3, horizontal direction N-S. Similar results were obtained for the other stations of the array. In gray lines are the minimum and the maximum bounds of the USGS noise model, for comparison.*

To assess the quality of the ambient vibration recordings, spectral analysis was subsequently performed. Because of the stochastic nature of the ambient vibration wave-field, a statistical approach has to be used, such as the estimation of the power spectral density (*PSD*). This approach is useful to evaluate the average energy level of the recordings in the analyzed frequency range, and to access the presence of spurious spectral peaks, which might be related to human activity (machinery, pumps).

By inspecting the PSD of all the three-component recordings of the array in the range between 0.5 and 40Hz, is found that the average energy level of the spectrum is overall very low, well within the minimum and maximum bounds of the USGS noise model (**Figure 5**). No relevant peaks of anthropogenic origin, which might affect the processing, are identified.

Complementary to the aforementioned statistical methods, a spectral decomposition approach is more suitable to assess the stationarity of the ambient vibration wave-field over time. The wavelet time-frequency analysis was then performed over the whole recording time. From such analysis (**Figure 6**) an overall stability of the ambient-vibration wave-field over time is evident.

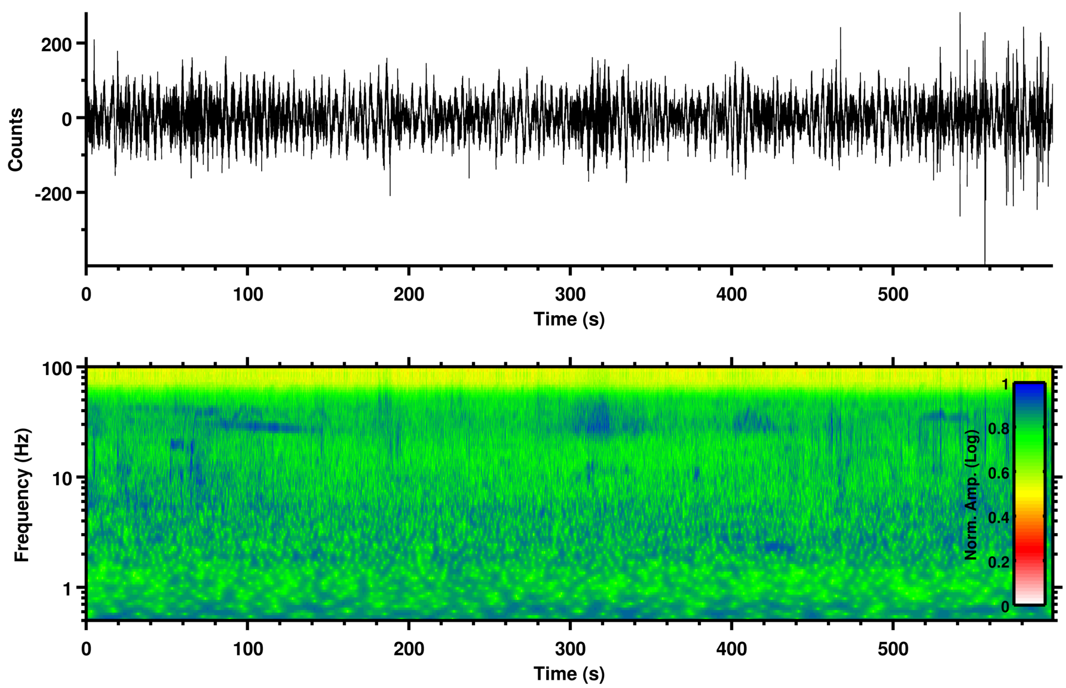

Figure 6 - *Example of spectrogram from 600s of recording of the central station (HMK11) of the array configuration A2. A part from few very localized transients, no sign of persistent disturbances are visible on the whole spectrogram. For the analysis, the cosine wavelet is used (wavelet parameter = 12).*

7. Conventional H/V spectral ratios

The horizontal-to-vertical (H/V) Fourier spectral ratio is a technique widely used in seismic site characterization because of its ability to provide an estimate of the SH wave fundamental frequency of resonance (f_0) of the site. Other than that, H/V ratios are useful to provide information on the Rayleigh wave ellipticity function, which can be used in surface wave dispersion inversion procedures to constrain large velocity contrasts at depth. In this study, we use the H/V technique also to map the variability of the subsoil structure along the investigated area; this is necessary to verify the fulfillment of the 1D structure assumption, which is necessary for the f-k method applied later.

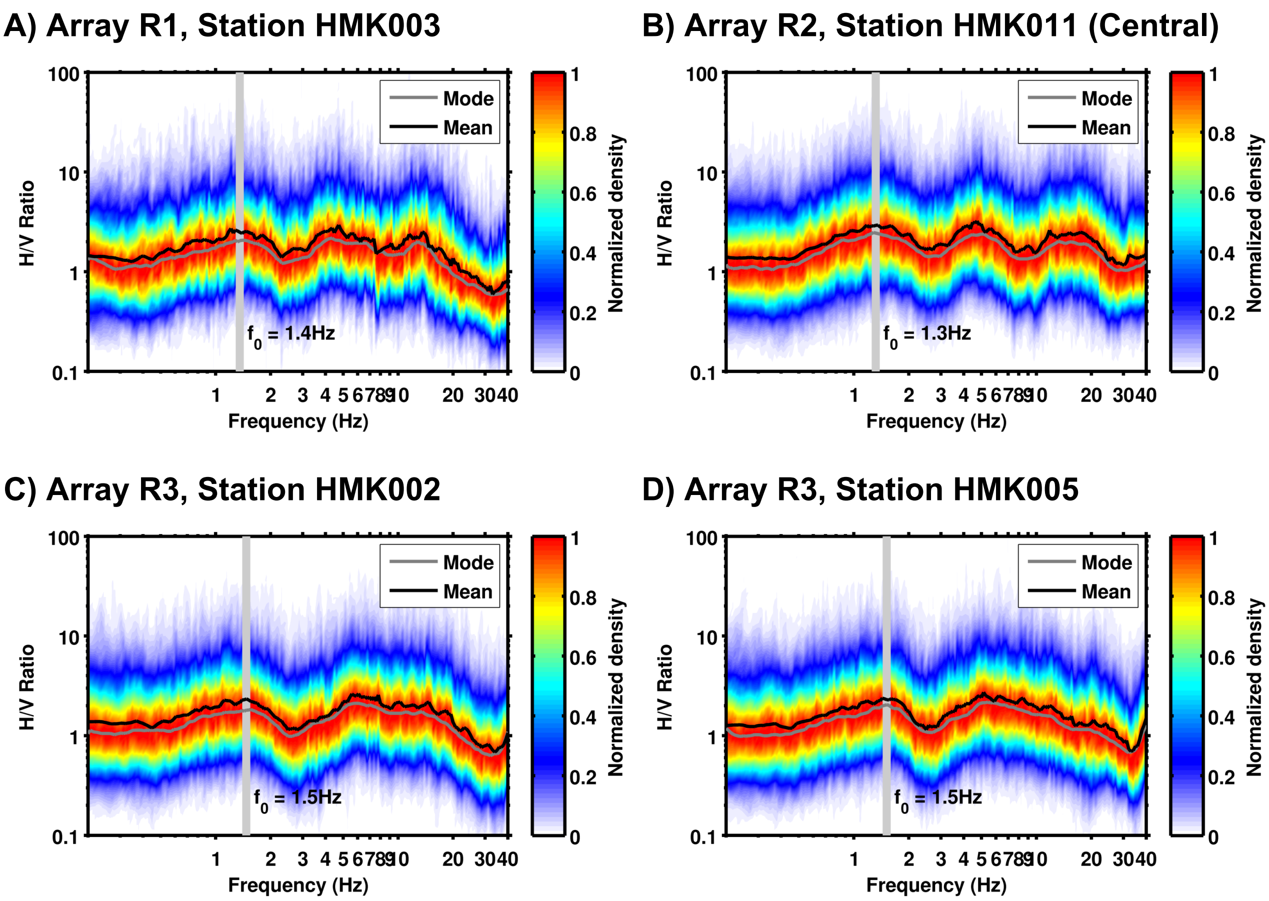

Figure 7 - *Example of H/V spectral ratios for the three concentric configurations R1, R2 and R3. The resonance frequency is indicated with a light gray line (~1.4Hz). An additional peak is visible at about 5~6Hz, more pronounced on those stations close to the center (in R1 and R2) and located on top of the small ridge.*

H/V spectral ratios have been computed for all the recordings at each station of the array and separately for configurations R1, R2 and R3 (e.g. **Figure 7**). The behavior of the noise wave-field at the different stations location is comparable at low frequency (roughly < 6-8Hz), while the high frequency region shows more variability, within and between arrays. In average (**Figure 8**) spectral curves show a relatively stable low frequency peak (around 1.4Hz). Such maximum is likely induced by a change in lithology at depth, which causes a modest contrast of seismic impedance. The peak should be regarded as the fundamental resonance frequency of the site (f_0). A second peak is also present at about 5~6Hz, but not stable over all stations. Such peak, in particular, is more persistent on the inner configurations (R1 and R2), which are located on top of the ridge (the flat part). On stations close to the array center, an additional third peak is identified (~14Hz). The peak is however less visible on stations from the larger configuration (R3); such maximum is likely induced by the Quaternary soil cover, which can be very heterogeneous over the measuring area. The behavior of the site can be considered laterally homogeneous for the f-k analysis.

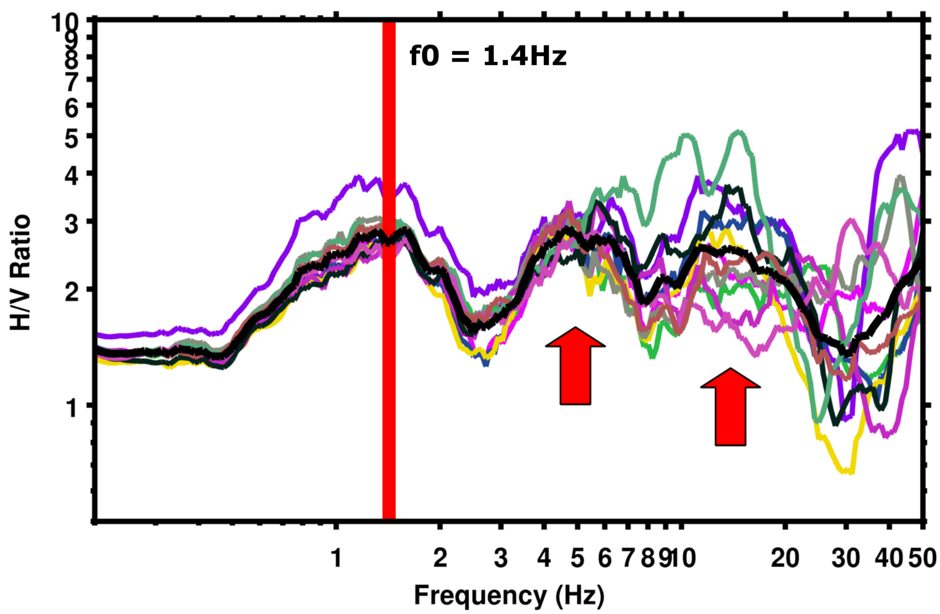

Figure 8 - *Comparison of the H/V spectral ratio curves of all the stations of the array (in this example for the array configuration R3). The curves are stable up to at least 8Hz, confirming the lateral homogeneity of the underlying bedrock velocity structure of the site. A low frequency peak is visible at about 1.4Hz. Two additional peaks can be identified at 5-6Hz and ~14Hz.*

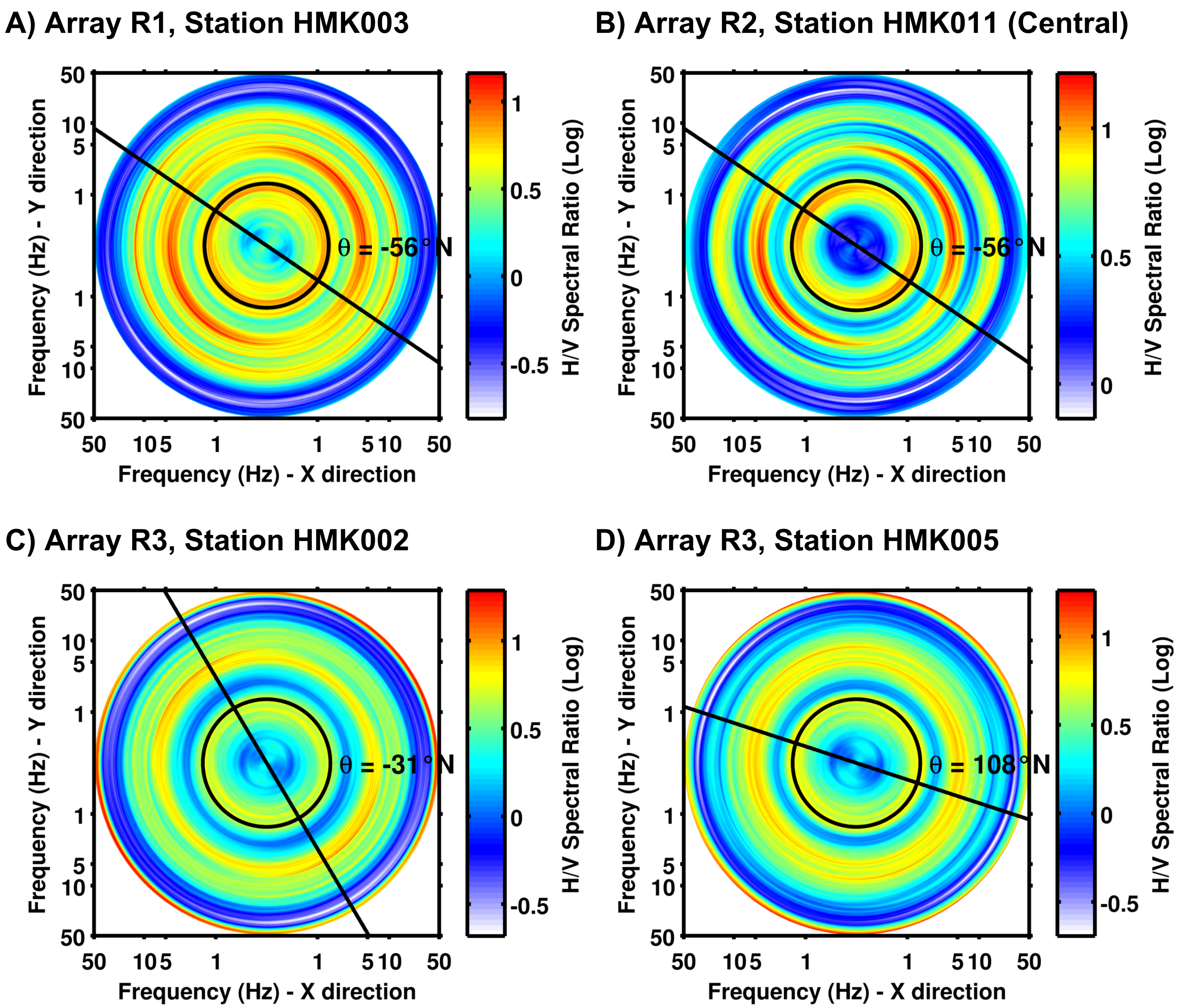

Figure 9 - *Example of directional H/V spectral ratios for the three concentric configurations R1, R2 and R3. The low frequency resonance peak (f_0) is preferentially (but not always) aligned roughly NW-SE (along the ridge axis). Also the second peak (5~6Hz) shows a nearly constant polarization direction (approx. ~60°N), but only for those stations close to the array center (R1 and R2, on top of the ridge).*

8. Directional analysis

The computation of directional H/V spectral ratio or polarization analysis is useful to reveal asymmetries in the ambient vibration wave-field. Different effects can induce such a behavior: 2D/3D structure, topographic effects or a non-homogeneous distribution of the noise sources. If a strong directionality is found by the analysis, it is generally recommended to carry out further investigations to properly address the origin of polarization. By processing the directional H/V ratios at all the recording stations of the array (e.g. **Figure 9**) it is possible to observe a moderate directionality of the identified resonance peaks. The fundamental frequency shows a preferential (but not strict) alignment along direction NW-SE, visible on most but not all the stations of the three geometries. Such direction is consistent with the approximate direction of the topographic ridge. Conversely, the second peak shows evidences of strong directionality toward NE-SW (~60°N), but only on those stations close to the array center (on the hilltop, e.g. **Figure 9**A, B); at the edges (stations of configuration R3) such directionality is lost (e.g. **Figure 9**C, D). This behavior is likely induced by the local geology.

The results of the H/V directional analysis are only partially confirmed by applying the wavelet polarization analysis technique (Burjanek et al., 2008). Here, the particle motion shows to be mostly elliptical, with just a weak polarization at the resonance frequencies (**Figure 10**). The frequency corresponding to f_0 shows nearly no (or very weak) directionality on azimuth (**Figure 11**A), but a strong directionality on the dip (**Figure 11**B). The second peak has weak directionality, but consistent with H/V spectral ratio.

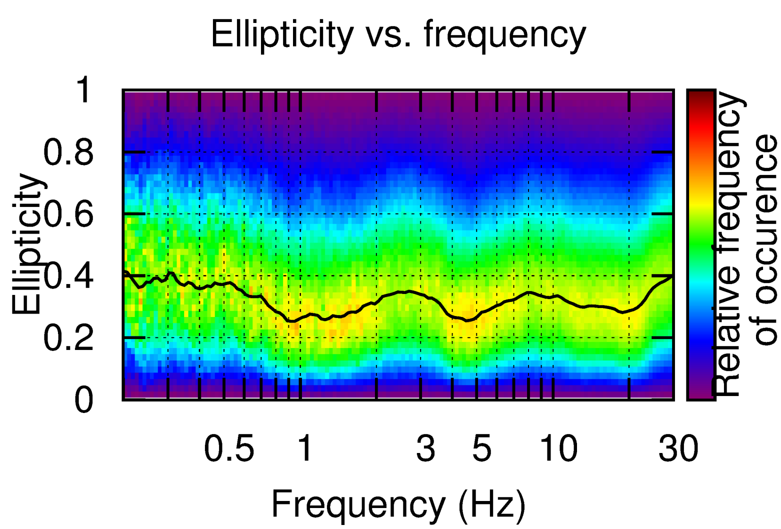

Figure 10 - *Ellipticity of the particle motion from wavelet-based polarization analysis at the central station of the array (HMK11).*

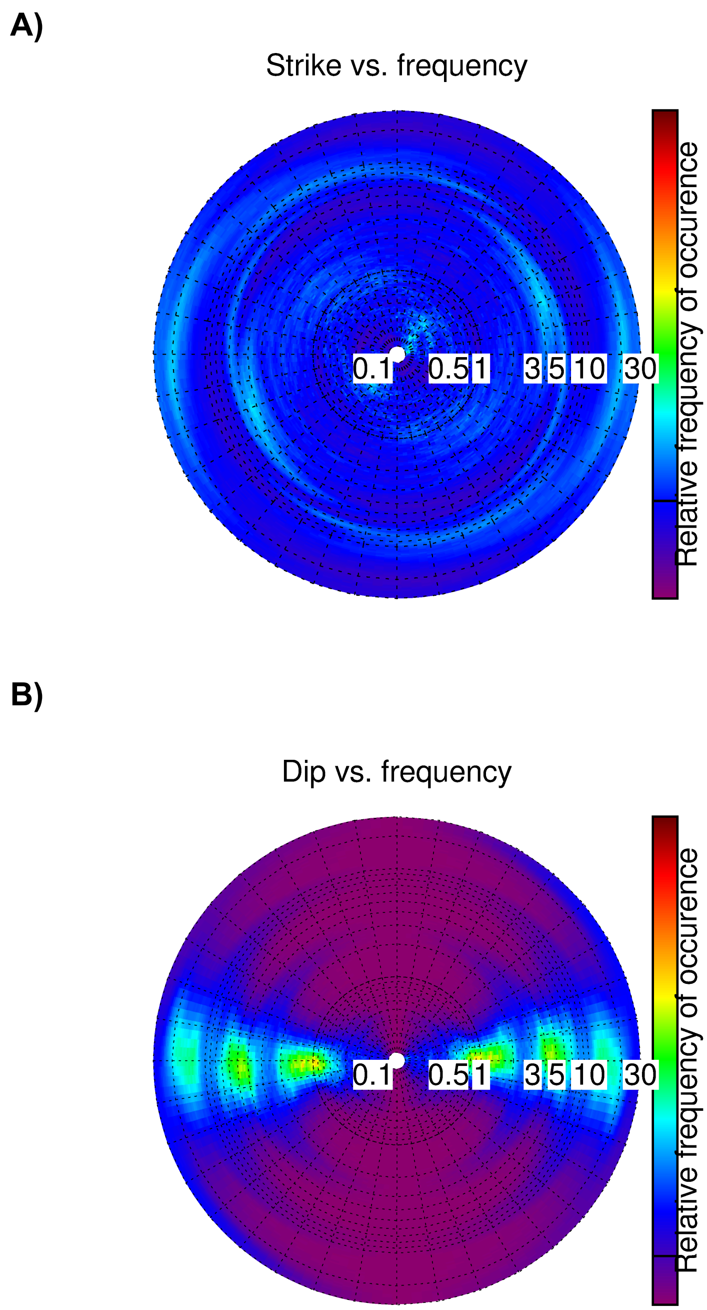

Figure 11 - *Directionality of the particle motion from wavelet-based polarization analysis (dip direction in B, strike in A) at the central station of the array (HMK11).*

9. Three-component f-k analysis

The frequency-wavenumber analysis is a spectral technique based on seismic array recordings that allows retrieving direction and dispersion characteristics of the surface waves. We apply this technique to three-component ambient vibration recordings using a modification of the high-resolution method of Capon (1969) as described in Poggi et al. (2010). Using all the three-components of motion gives the possibility to retrieve information about the propagation of the Rayleigh waves (vertical and radial processing direction) as well as of the Love waves (transversal direction).

As in the case of the previous methods, the ambient vibration recordings are treated statistically by subdividing the traces in sub-windows. For each consecutive window a separated f-k analysis is performed, and the results are then averaged over the whole recording, increasing the robustness of the final estimation.

A) Ring 2, 2-5Hz

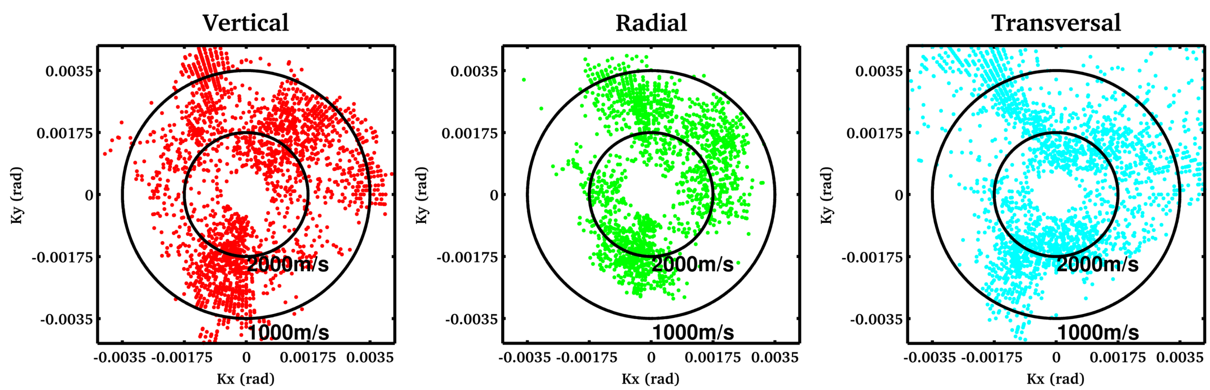

B) Ring2, 5-10Hz

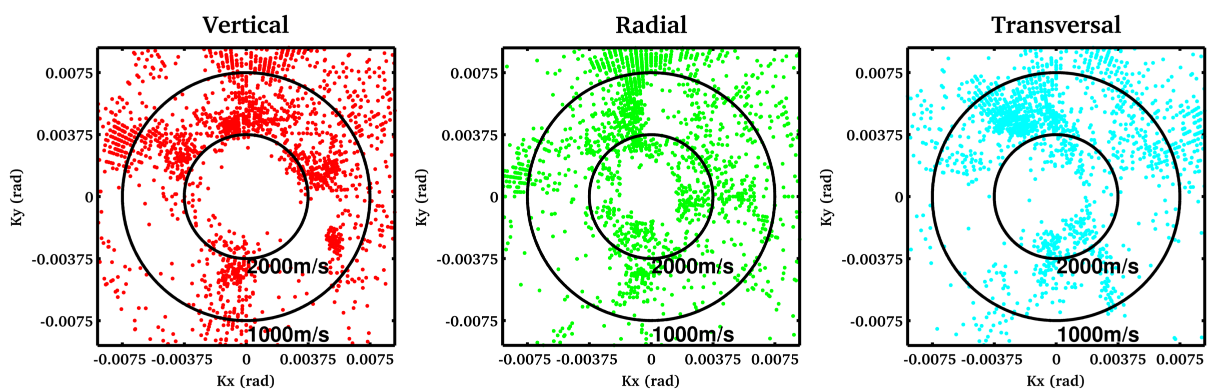

Figure 12 - *Example of distribution of noise sources in the low (2-6Hz) and intermediate frequency range (5-10Hz) obtained from three-component f-k analysis. The source distribution is irregular but not strictly directional on all the propagation components.*

As first step, from the f-k analysis it is possible to assess the noise source azimuthal distribution over different ranges of frequencies (e.g. **Figure 12**) separately for the vertical, the radial and the transversal direction of polarization. From the analysis of the two geometries A1 and A2, source distribution appears to be quite inhomogeneous in all the components, without nevertheless displaying a clear directional pattern.

As a second step, the surface-wave dispersion curves are extracted by visual inspection and manual picking of the f-k density plots (**Figure 13**, **Figure 14** and **Figure 15**), separately for the three polarization directions. Complementary results have been obtained for the three array configurations. In particular, Love wave dispersion can be well tracked in a broad frequency range (from 1.6Hz to about 18Hz) from R1 to R3; velocity estimates are also consistent between the different geometries. Rayleigh wave dispersion is of more difficult interpretation. Vertical and radial components from configurations R2 and R3 show a considerable discontinuity at about 4-5Hz. Dispersion function can then be interpreted in two ways. As first attempt, the discontinuity can be considered as the effect of a modal jump, leading to a two-mode interpretation (fundamental plus first higher). Alternatively, the whole dispersion can be addressed to a single mode (fundamental) with a minimum energy content at 4-5Hz due to velocity osculation with a higher mode. The first interpretation is not supported by inversion, showing clear incompatibility with Love wave dispersion. Conversely, the second interpretation results in good fitting of all available data (see next section). We therefore consider the single mode hypothesis as the more reliable.

A summary of all the identified modes from vertical, radial and transversal direction of propagation is presented in **Figure 16**, while the final interpretation of Rayleigh and Love wave dispersion pattern is in **Figure 17**, together with the results from an active seismic survey performed on the same location by the company *RoXplore*. Active surface wave analysis results (MASW) are compatible with our interpretation, extending the resolution at high frequencies and adding a Rayleigh wave higher mode to the interpretation model.

10. Inversion of the dispersion curves

The surface wave dispersion curves (Rayleigh and Love) obtained from the three-component f-k analysis of the ambient vibrations and the fundamental frequency of resonance (f_0) from average H/V spectral ratios are inverted to obtain an estimation of the velocity profile of the site (mainly S-wave velocity as function of depth, and to a lesser extend the P-wave velocity, due to the lower sensitivity). The analysis is performed using the software *Dinver* (www.geopsy.org), which implements a direct search approach (**Figure 18**) based on a conditional version of the neighborhood algorithm (Sambridge, 1999).

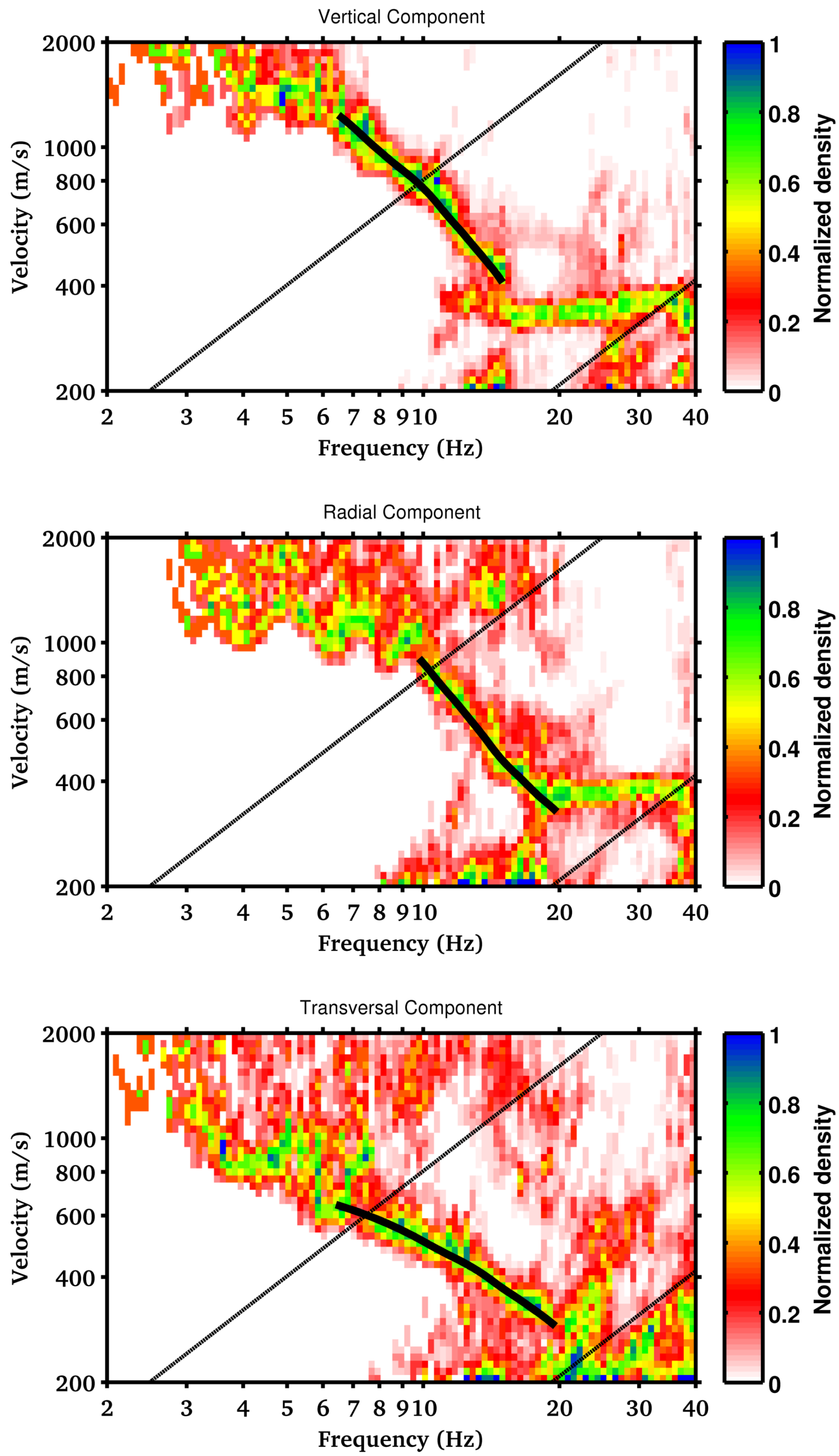

Figure 13 - *Density distribution of the surface wave signals obtained from the recording of the array configuration R1 using three-component f-k analysis. From top to bottom: Rayleigh vertical, Rayleigh radial and Love wave dispersion. In black the interpreted dispersion curves are given (manually selected).*

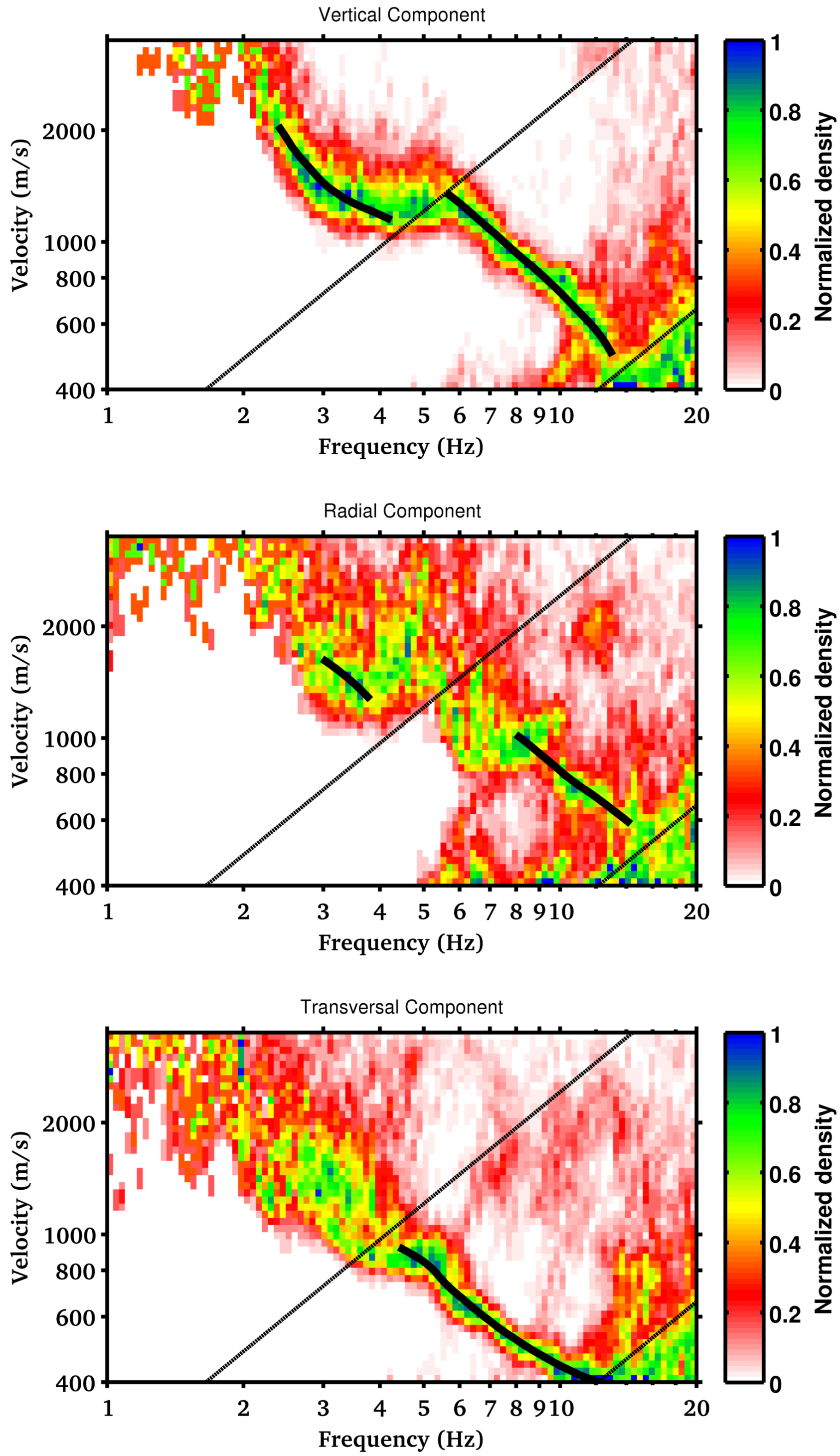

Figure 14 - *Density distribution of the surface wave signals obtained from the recording of the array configuration R2 using three-component f-k analysis. From top to bottom: Rayleigh vertical, Rayleigh radial and Love wave dispersion. In black the interpreted dispersion curves are given (manually selected).*

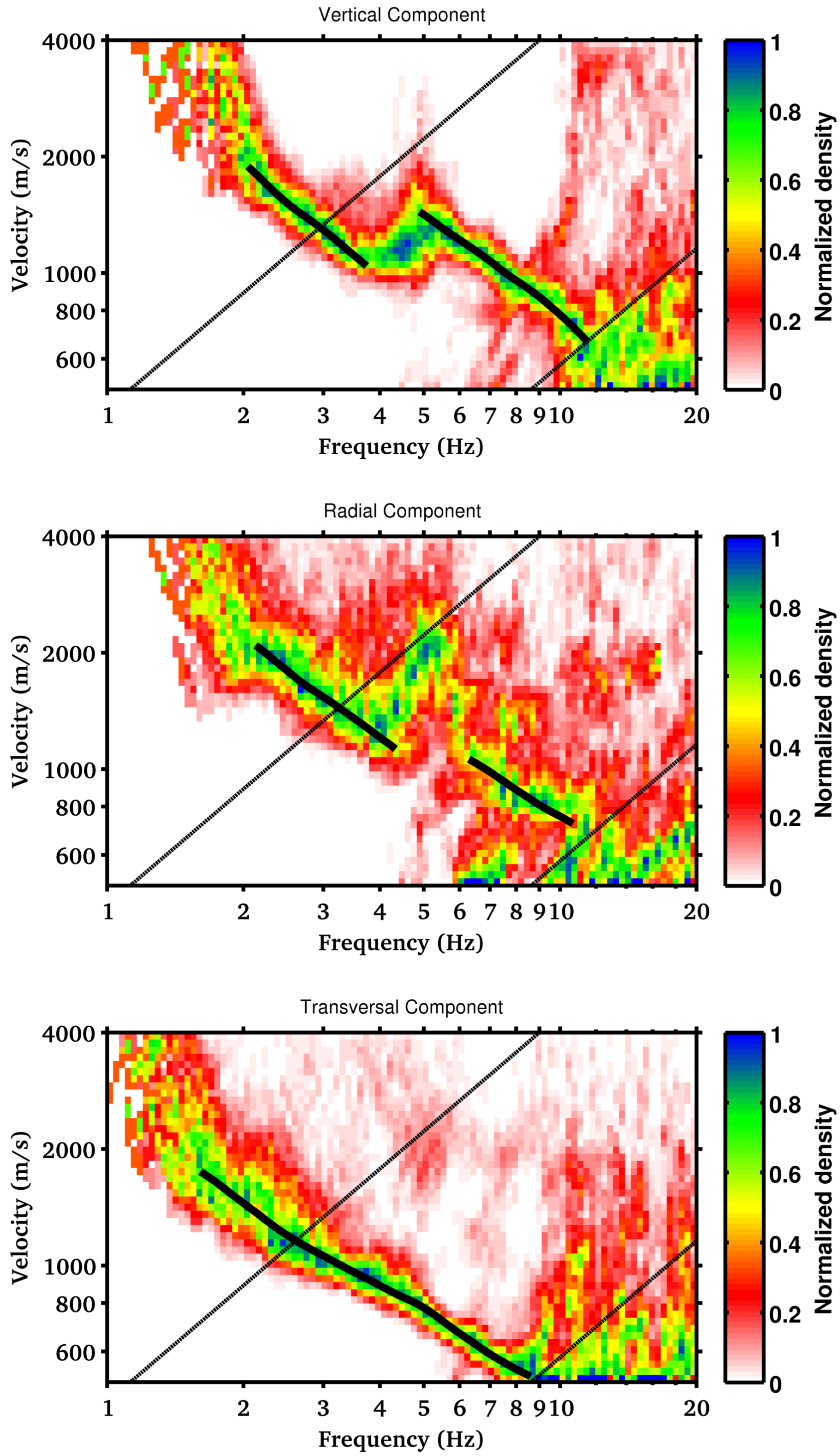

Figure 15 - *Density distribution of the surface wave signals obtained from the recording of the array configuration R3 using three-component f-k analysis. From top to bottom: Rayleigh vertical, Rayleigh radial and Love wave dispersion. In red the interpreted dispersion curves are given (manually selected).*

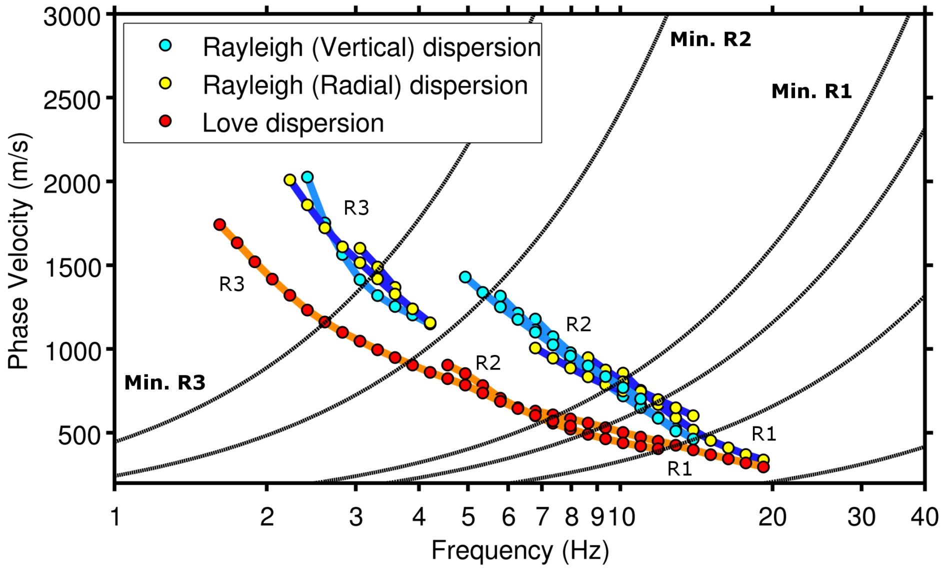

Figure 16 - *Summary of all dispersion curves obtained from three-component f-k analysis of the three array configurations R1, R2 and R3. Minimum and maximum resolution bounds from the two geometries are indicated with black solid lines.*

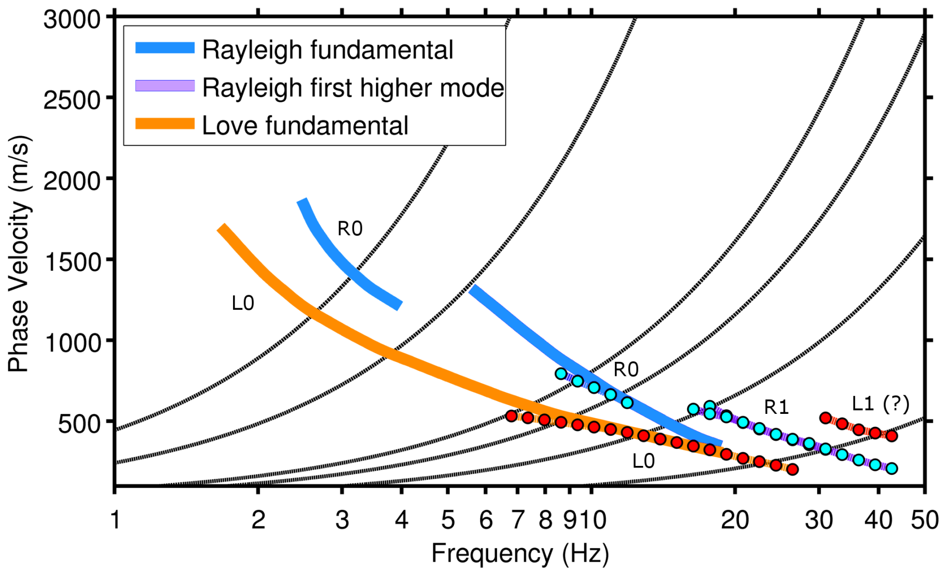

Figure 17 - *Final interpretation of the Rayleigh and Love dispersion curves for HAMIK, including the results from active surface wave analysis (MASW, with dots). Minimum and maximum resolution bounds from the full array are indicated with black solid lines.*

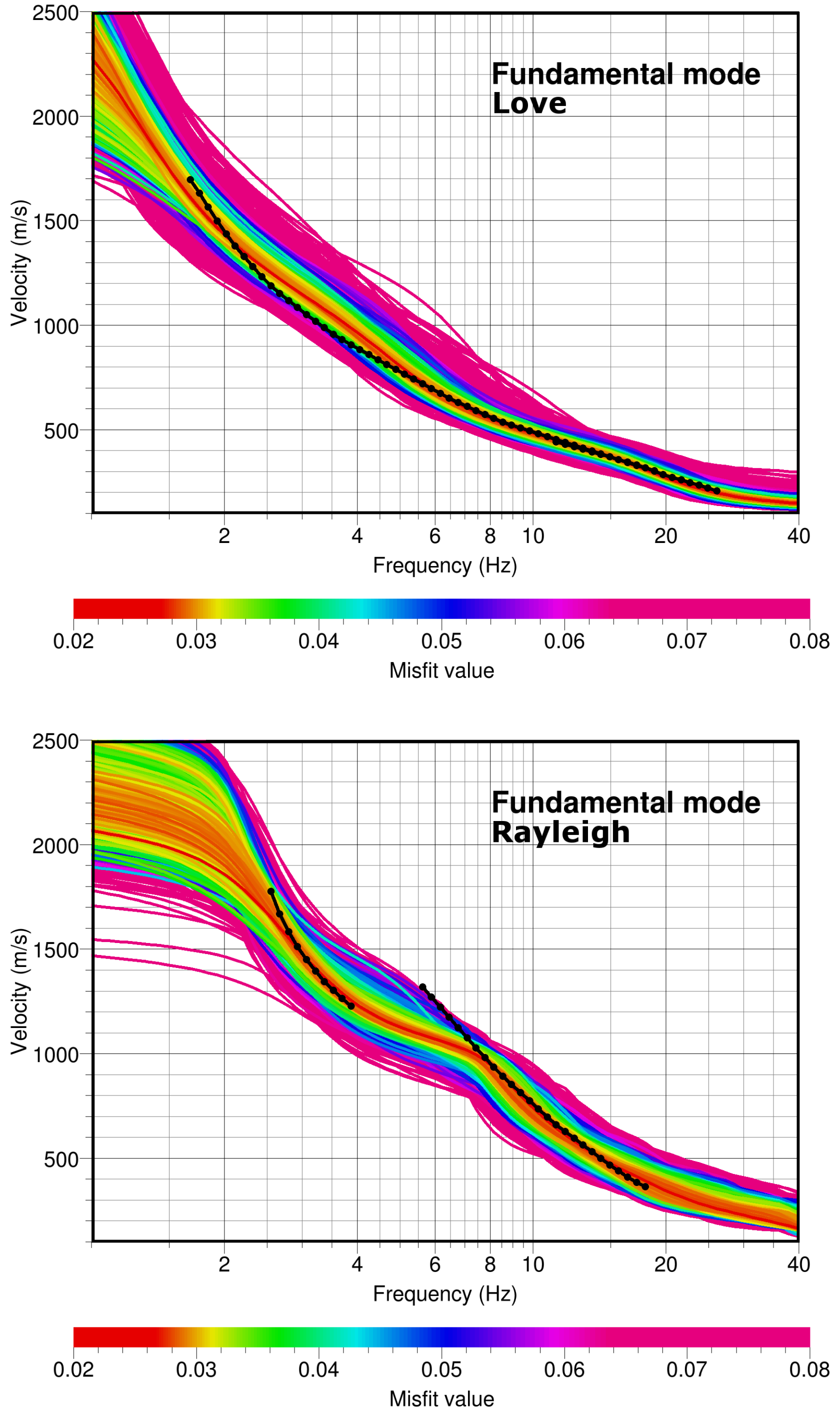

Figure 18 - *Example of fitting the surface dispersion data within the global optimization procedure. Different colors represent different misfit between the observed (in black) and the modeled dispersion curves during the search.*

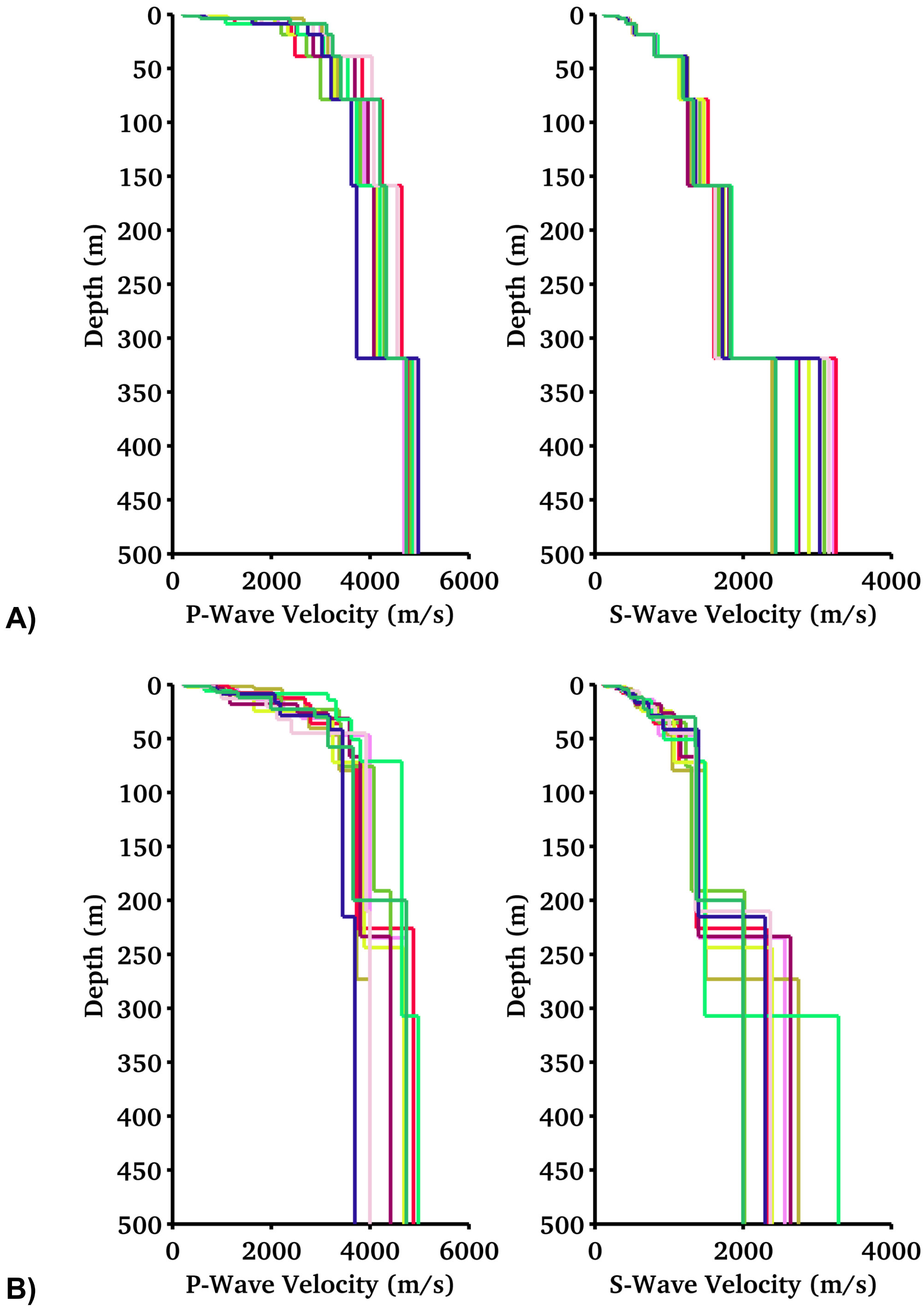

Figure 19 - *Collecting the best fitting models from the ten separated inversion runs using the free-layers (A, top) and fixed-layers (B, bottom) parameterization schemes.*

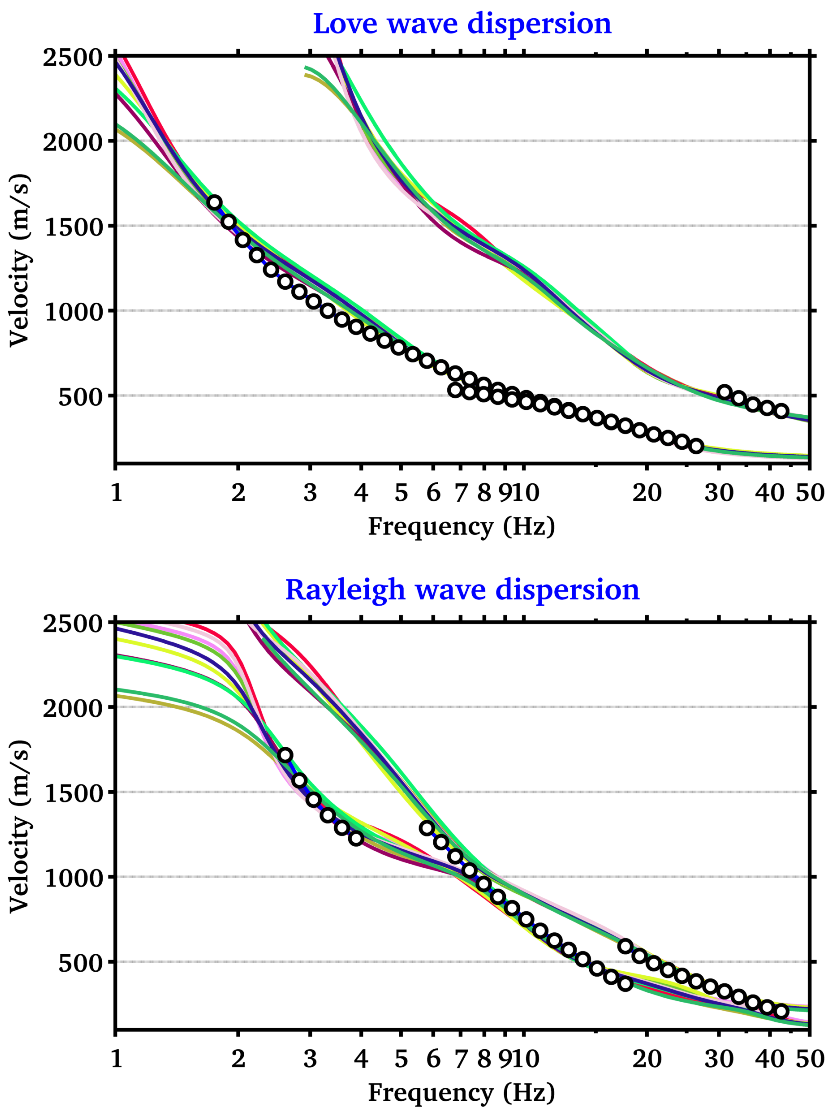

Figure 20 - *Dispersion curves computed from the best fitting models of the two proposed interpretation schemes (free and fix layers), compared with picked dispersion from active and passive seismic experiments.*

To parameterize the velocity model, two different approaches were implemented. The first one consisted in setting up an eight-layer model with fix interface depths. In such a case the free inversion parameters are then the velocities (P and S) and layer thicknesses. In the second case, a free-thickness layer approach was used. The advantage of the former method stays in the possibility to better resolve sharp velocity interfaces, while the second is less unique and better constraints the seismic velocity. The two approaches have to be nevertheless considered complementary, and they should provide consistent results.

Ten inversion tests (*runs*) were performed for each of the two model schemes, in order to minimize the effect related to a possible unfavorable initial randomization of the parameter space. The best fitting model from of each run was then collected (**Figure 19** and **Figure 22**) and used later on for the computation of the derived soil parameters.

In mode detail, the inverted velocity profiles (Vs and Vp) are gradient-like, but with at least two major interfaces, at about 40m and 200~300m. The first interface is actually constrained by high frequency part of the Rayleigh and Love dispersion curves (including higher modes from active surface wave analysis, **Figure 20**), which also gives good resolution on the uppermost portion of the velocity profile. The second boundary (less resolved) is solely controlled by the use of f_0 form H/V spectral ratios (**Figure 21**), and shows a considerable scatter. By considering the minimum available frequency of the surface-wave analysis, and by analyzing the scattering of the inverted models (**Figure 22**), it is realistic to assume the velocity profiles to be reliable down to a depth of about 200~350m. Below this value no direct constrain is available from data, and the velocity values are obtained by pure extrapolation.

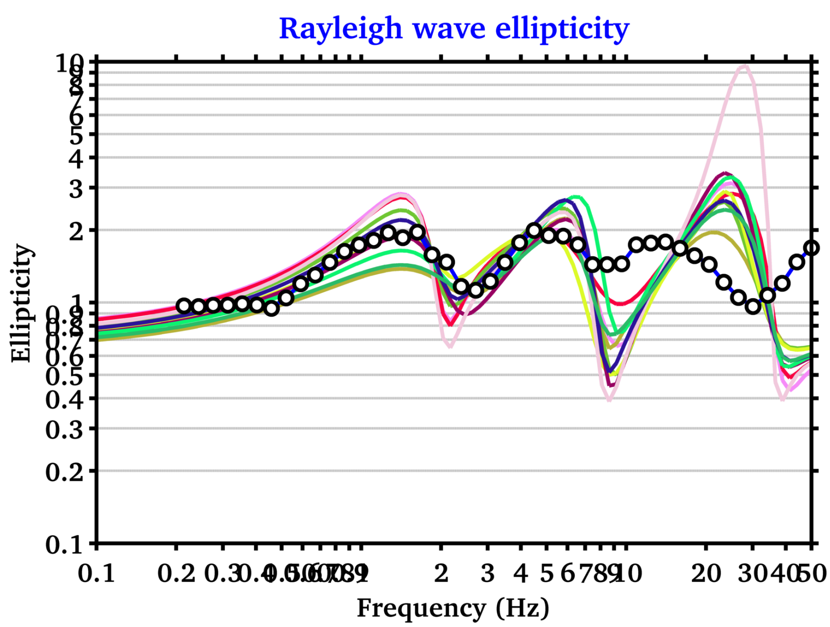

Figure 21 - *Rayleigh wave ellipticity curves computed from the best fitting models of the two proposed interpretation schemes (free and fixed layers), compared with average H/V spectral ratio from configuration R2 (scaled by sqrt(2)). The first two peaks are clearly reproducible, even though the H/V curve was not used during the inversion.*

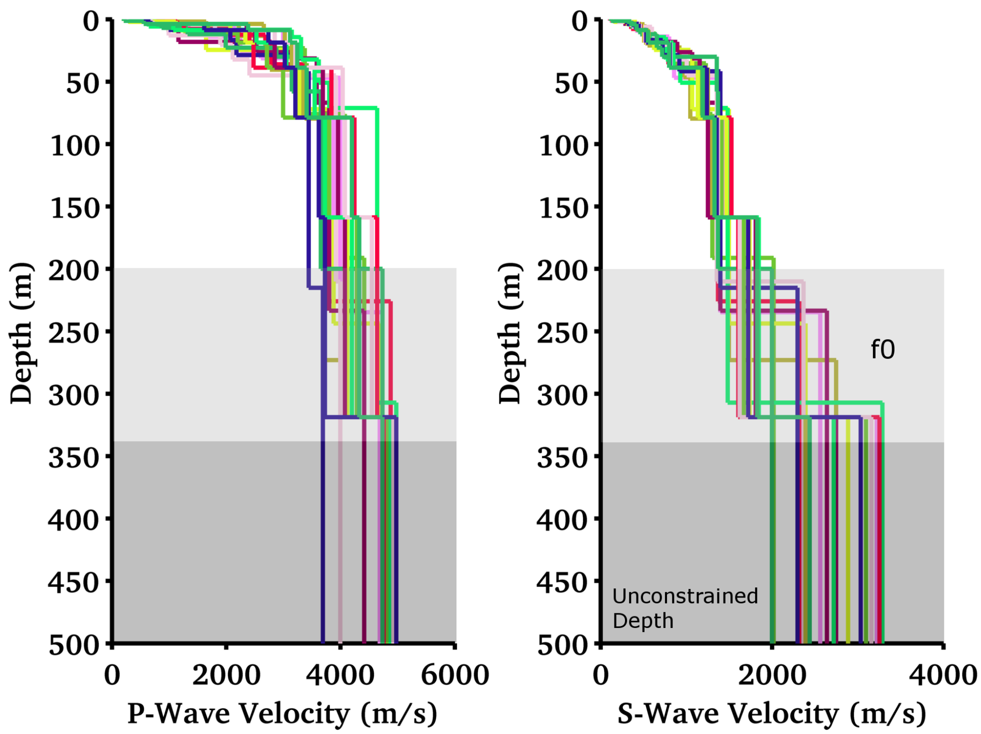

Figure 22 - *Comparison of all the best models from the two parameterization schemes (free and fixed layers). The two approaches produce consistent results. Depth range between about 200m and 350m is solely constrained by f_0 and should be considered approximately the maximum resolved depth.*

11. Engineering soil parameters

The ensemble of all the best inverted velocity profiles is then used to derive average soil parameters like the VsZ (average travel-time S-wave velocity over the depth Z, including Vs30, Table 1) and the quarter-wavelength (QWL) average velocities (Joyner et al., 1984) for a range of frequencies between 0.6 and 30Hz (**Figure 23**). The former is a standard parameter for the classification of ground-types in most building codes and in ground motion prediction equations. The latter is a parameter useful for the empirical estimation of the site-response and to assess the sensitivity of the seismic wave-field to the different depths. It has to be noticed that these two parameters are derived separately from all the best S-wave velocity models obtained from the inversion, and the results is finally averaged to improve statistics.

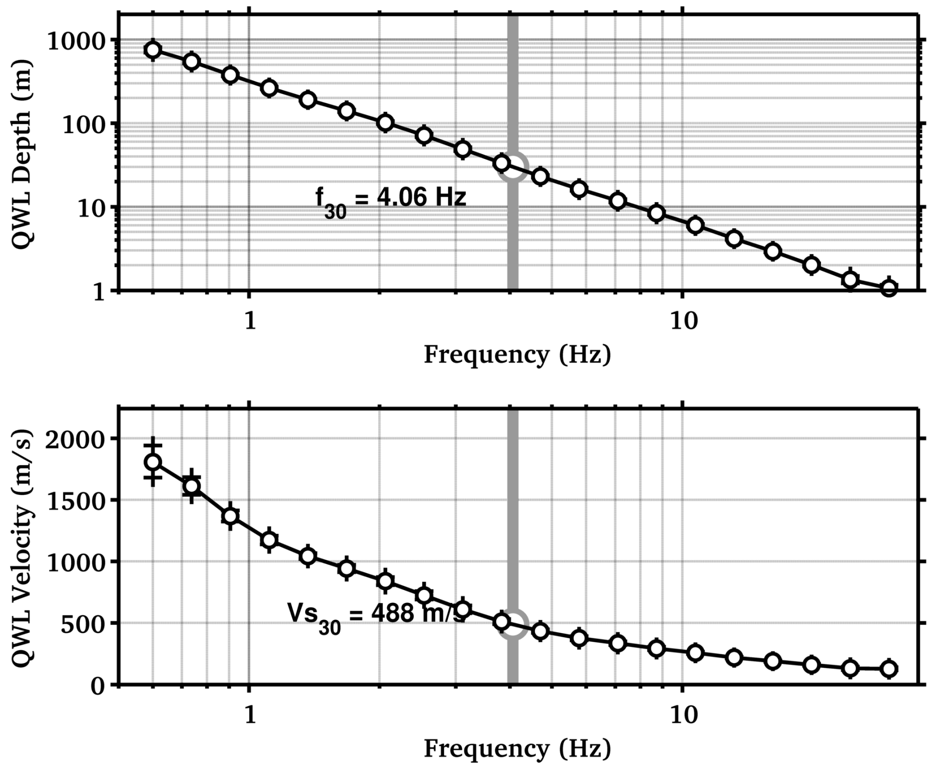

Figure 23 - *Quarter-wavelength representation of the inverted S-wave velocity profiles. Top: the depth-frequency dependency. Bottom: the QWL average velocity. The Vs30 value is indicated with its corresponding QWL frequency.*

12. Amplification models

Site amplification functions have been computed using two different approaches: the S-wave transfer function for vertical propagation and the quarter-wavelength amplification. In general the first method is used to evaluate the resonance characteristics of the site, while the second is more useful to assess the effect of the velocity contrasts between the lowermost rock layer (as reference) and the different QWL averaging depths. The two amplification functions are then corrected for the Swiss rock reference velocity profile as defined in Poggi et al. (2011), according to the procedure described in Edwards et al. (2013). Given the lower velocities in the uppermost part of the HAMIK profile compared to the Swiss reference, the final corrected amplification function shows a lower average amplification level at high frequencies than the uncorrected (**Figure 24**).

Averaging depth (m)	Vs-mean (m/s)	St.Dev.
5	238.32	3.71
10	314.41	8.61
15	365.85	9.92
20	407.07	9.40
25	450.41	7.92
30	**487.57**	**9.52**
40	552.09	15.62
50	616.39	16.86
75	738.90	21.16
100	834.85	20.56
150	962.88	21.21
200	1060.16	15.69

Table 1 - *Average travel-time velocities at different depths. Vs30 is highlighted.*

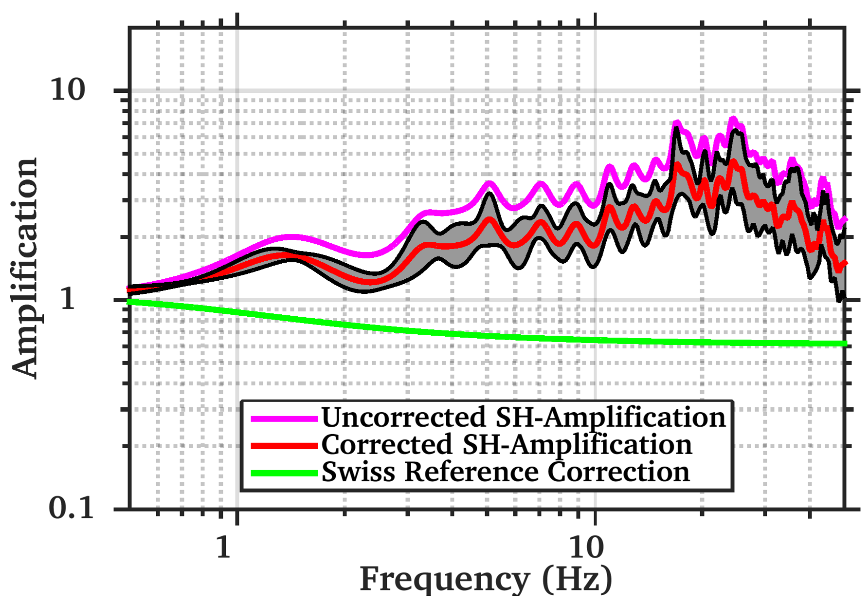

Figure 24 - *Correcting the SH-wave transfer function for the Swiss (rock) reference conditions (Poggi et al. 2011). The final corrected amplification function shows a lower (average) amplification at high frequencies than the uncorrected.*

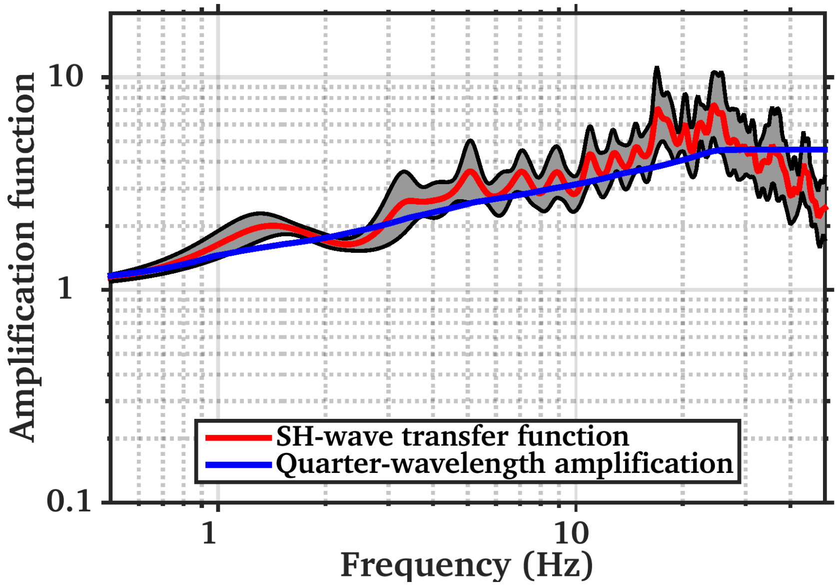

Figure 25 - *Comparison of amplification functions computed using the SH-wave transfer function and the quarter-wavelength formalism on the inverted velocity models.*

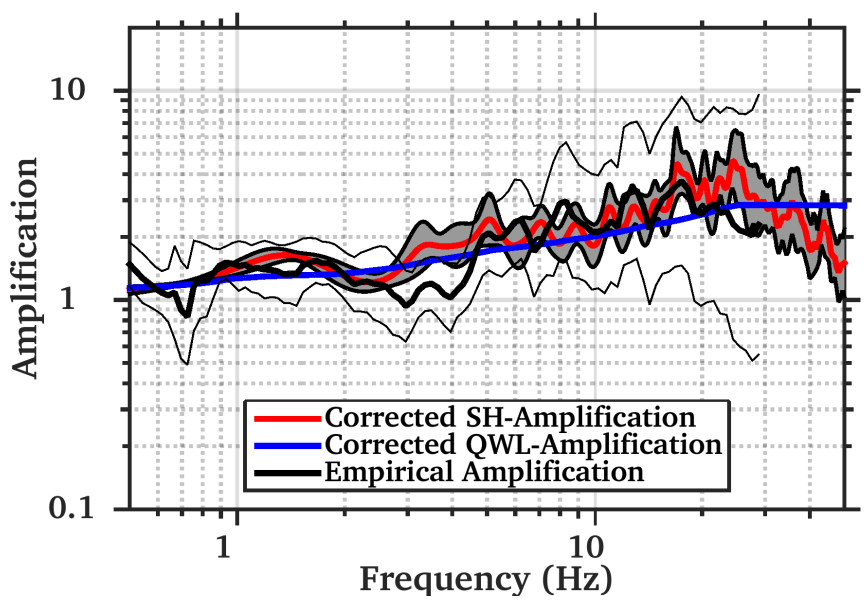

Figure 26 - *Comparison of amplification functions computed using the SH-wave transfer function and the quarter-wavelength approach with empirical observation from spectral modeling of low-magnitude earthquakes (here the anelastic spectrum). All functions are referenced to the Swiss rock reference model (Poggi et al. 2011).*

Amplification functions using the transfer function and the quarter-wavelength approach are comparable (**Figure 25**), even if the transfer function provides a slightly larger amplification, because of the presence of some weak resonance peaks. At low frequencies both methods converge to the same amplification level. It has to be notice that the amplification functions do not include attenuation at this stage of the analysis, as the quality factors of the site are too uncertain.

A good matching is obtained by comparison between the one-dimensional transfer function and the empirical amplification from spectral modeling of low-magnitude earthquakes as described in Edwards et al., 2013. However, the general trend is well reproduced by the analytical solution only when compared to the anelastic empirical amplification (**Figure 26**). The corresponding elastic function has low amplitude than the anelastic at high frequencies. This is likely due to a hill-constrained estimation of the attenuation operator *kappa* in presence of strong resonance peaks at high frequencies, which bias the fit of the attenuation decay function to be removed.

REFERENCES

Capon, J., 1969. High resolution frequency wavenumber spectrum analysis, Proc. IEEE, 57, 1408-1418.

Burjanek, J., G. Stamm, V. Poggi, J.R. Moore, and D. Fäh [2010], "Ambient vibration analysis of an unstable mountain slope", Geophys. J. Int., Vol. 180, pp. 820-828.

Edwards, B., C. Michel, V. Poggi and D. Fäh (2013). Determination of Site Amplification from Regional Seismicity: Application to the Swiss National Seismic Networks. Accepted for publication in Seismological Research Letters.

Joyner, W. B., R. E. Warrick and T. E. Fumal (1981). The Effect of Quaternary Alluvium on Strong Ground Motion in the Coyote Lake, California, Earthquake of 1979, Bulletin of the Seismological Society of America, 71, 1333-1349.

Poggi, V., B. Edwards and D. Fäh (2011). Derivation of a Reference Shear-Wave Velocity Model from Empirical Site Amplification, Bulletin of the Seismological Society of America, 101, 258-274.

Poggi, V. and Fäh D., 2010. Estimating Rayleigh wave particle motion from three-component array analysis of ambient vibrations. Geophys. J. Int., 180-1, 251-267.

Eidgenössische Technische Hochschule Zürich
Swiss Federal Institute of Technology Zurich

SED
Schweizerischer Erdbebendienst
Swiss Seismological Service

Report on site characterization

Böbikon, Switzerland (BOBI)

Poggi Valerio, Donat Fäh

Last modified - 22 / 12 / 2014

1. Introduction

In the framework of the NAGRA seismic network project, an array measurement of the ambient vibration wave-field was performed at the location of the SED borehole station BOBI (Böbikon, Switzerland). The scope of the survey is the seismic characterization of the area surrounding the installation (**Figure 1**), which consists in a short period borehole sensor at about 100m, and a collocated strong motion seismometer at the surface, with a high-resolution digitizer (Taurus 24Bit @200sps). Ambient vibration analysis has been used to infer the characteristics of the underground structure of the site, with special regard to the one-dimensional shear-wave velocity. Such profile was later compared with the results from active seismic measurements and used to assess the local seismic response of the station.

For the analysis, different spectral analysis techniques were implemented, consisting in both single and array methods, which are listed below:

- Time-frequency wavelet analysis
- Power-spectral density estimation
- Conventional horizontal to vertical spectral ratios
- Directional horizontal to vertical spectral ratios
- Wavelet polarization analysis
- Three-component high-resolution f-k analysis.

The results of all these analyses conformed to the definition of the final velocity model. In the following, the main results of these investigations are summarized and a final interpretation of the velocity profile is given. From this interpretation, engineering parameters are finally derived, e.g. the Qwl-Vs average velocity, VsZ (including Vs30) and the seismic amplification from the analytical SH-transfer function of the one-dimensional soil column.

2. Survey description

To characterize the seismic response of the site, an array measurement of ambient vibration was performed on 19/03/2014 (**Figure 1**). The array consists of two measuring configurations (A1 and A2) of 14 sensors each and increasing diameter of about 120m and 300m respectively. The two configurations were planned to partially overlap, by sharing 9 common sensors, with the aim of providing a continuous frequency resolution between the two geometries. Second configuration was initially planned to be smaller, but unforeseen circumstances (a farmed field) forced the geometry to cross the nearby forest. Configuration A1 recorded for a total of 1h30m, while configuration A2 for 1h only. As a general rule, larger arrays would require longer recording time to produce a reasonable statistics of the ambient vibration processing results. In this case, however, due to the difficulties in the setup of the second configuration, the available time for recording was limited. Satisfactory results were nevertheless obtained. For the larger configuration, a penetration depth of about 200~250m was initially expected.

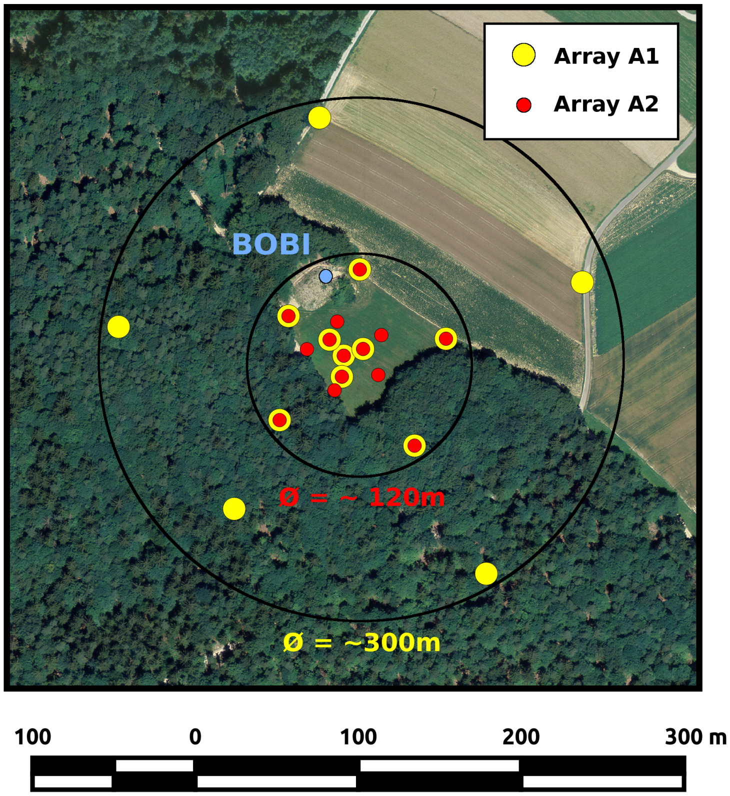

Figure 1 - *Location of the ambient vibration array survey performed in Böbikon, (SED station BOBI) on 19/03/2014. Two concentric configurations of increasing diameter were implemented (named A1 and A2). Location of the permanent station is shown in blue.*

3. Soil type, topography and geology

The array has been set in open field conditions, in a rural area (**Figure 1**, **Figure 3**). The influence of buildings and anthropogenic disturbances is virtually negligible. However, recordings have been affected by harmonic contributions (see section 6) in relatively narrow frequency bands. Array sensors have been deployed on free soil. Good coupling with the ground was assured by means of digging small holes at the sensor's places, and by using a special support (*Trihedron*®) that facilitates the leveling of the device even for difficult soil conditions. The measurement area was located on a nearly flat area; therefore no topographic correction was necessary before processing.

4. Weather conditions

The weather conditions were optimal and stable during the whole measurement, with no precipitations, no wind and an average temperature of 15 degrees.

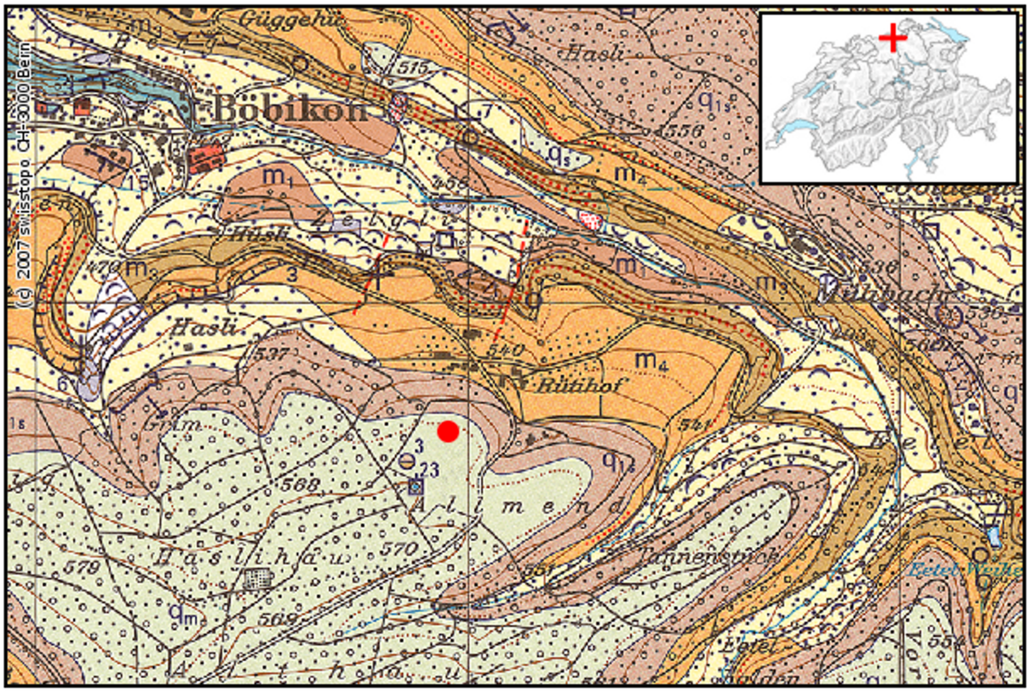

Figure 2 - *Geological map of the measuring area, in the surroundings of Böbikon (reproduced from Swisstopo, "Geologische Generalkarte der Schweiz", modified). In red the approximate location of the permanent station BOBI.*

From the geological points of view (**Figure 2**) the target area is located on the western edge of the Tabular Jura. The surface morphology is considerably smooth and modeled by the action of glaciers during the Pleistocene. The station is likely located on top of a large moranic deposit, clearly identifiable from the surface morphology and confirmed by the geological map of the area (unit Q_m and Q_{1s}). Geophysical bedrock is never exposed (supposedly deep at the measuring location) and is likely composed of consolidated sandstones and conglomerates of the Molassic basin (unit m_4) of Miocenic age. A variable-thick cover of quaternary soil material is generally present. Such site can be classified as of rock ground-type A.

5. Acquisition equipment

Each acquisition point within the array consisted of a three components seismometer (Lennartz 3C with 5s eigenperiod) and a 24 bit data logger (Quanterra Q330). Synchronization between stations was assured by standard GPS, while a more accurate differential GPS (Leica Viva system) was used to precisely locate the sensor's coordinates with a tolerance of less than 5cm.

Figure 3 - *Overview of the measurement area. Location of the SED station BOBI is indicated by the red arrow.*

6. Pre-processing and preliminary data-quality control

The three-component recording has been filtered prior to analysis using a band-pass 6th order causal Butterworth filter with corners at 0.2Hz and 50Hz. Although it is not a strict requirement for spectral analysis techniques, such filtering was applied in order to facilitate the preliminary visual inspection of the noise traces and to evaluate the coherency of the wave-field (**Figure 4**). Such procedure gives essential information for the subsequent interpretation of the f-k analysis results.

Contrary to expectation (given the rural location), the recordings have been affected by a certain amount of high-frequency transients. Additionally, two stations did not properly work; station BOB10 had a cable failure, while station BOB08 did not register the N-S component for unknown reasons (**Figure 4**). These stations were discarded from the analysis. To assess the quality of the ambient vibration recordings, spectral analysis was subsequently performed. Because of the stochastic nature of the ambient vibration wave-field, a statistical approach has to be used, such as the estimation of the power spectral density (*PSD*). This approach is useful to evaluate the average energy level of the recordings in the analyzed frequency range, and to access the presence of spurious spectral peaks, which might be related to human activity (machinery, pumps).

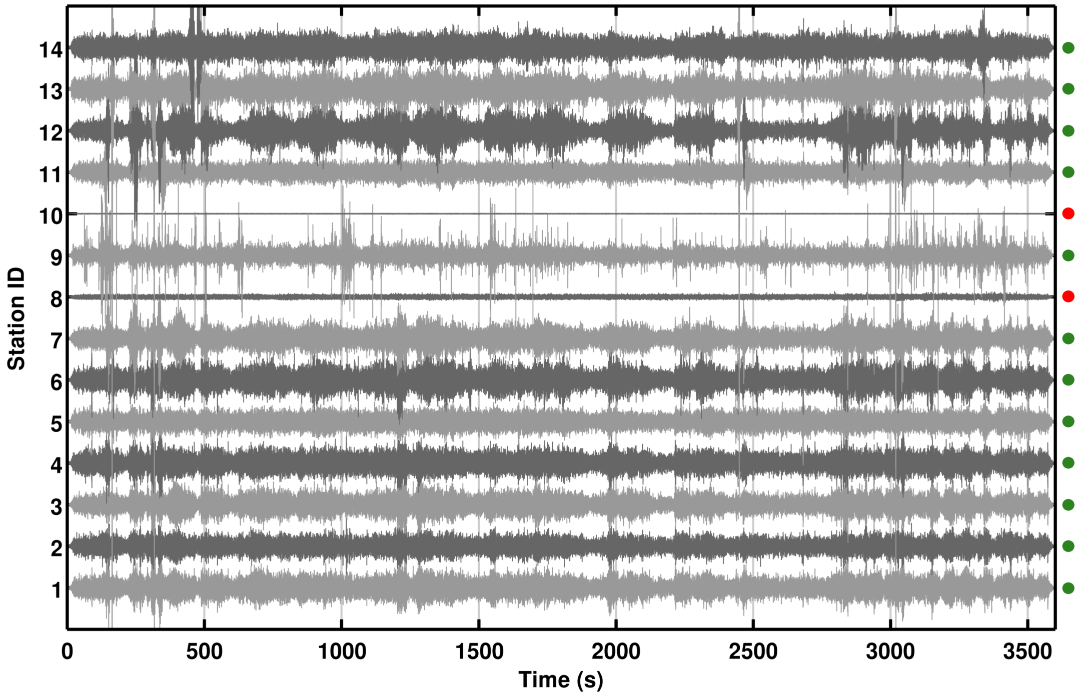

Figure 4 - *Inspection of the useful part of the ambient vibration recording of the Böbikon array (here configuration A2). A certain amount of short high-frequency transients were present during the acquisition, which nevertheless did not bias the subsequent f-k processing results.*

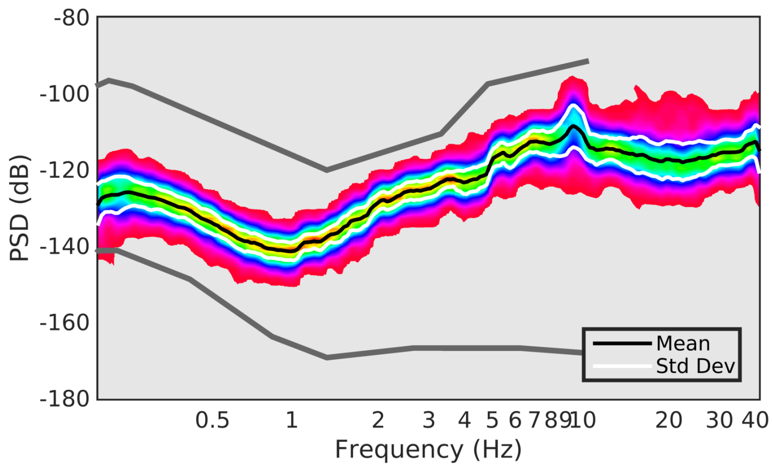

Figure 5 - *Power spectral density (PSD) computed for 1h30m recording at the central station of the array configuration A2, horizontal direction N-S. Similar results were obtained for the other stations of the array. In gray lines are the minimum and the maximum bounds of the USGS noise model, for comparison.*

By inspecting the PSD of all the three-component recordings of the array in the range between 0.5 and 40Hz, is found that the average energy level of the spectrum is overall very low at low frequencies (roughly < 1Hz), while it tends to progressively increase at increasing frequencies, nevertheless well within the minimum and maximum bounds of the USGS noise model (**Figure 5**) Two peaks of possibly anthropogenic origin are clearly visible, at about 5 and 9 Hz. These bands should be properly rejected from interpretation and processing.

Complementary to the aforementioned statistical methods, a spectral decomposition approach is more suitable to assess the stationarity of the ambient vibration wave-field over time. The wavelet time-frequency analysis was then performed over the whole recording time. From such analysis (**Figure 6**) an overall stability of the ambient-vibration wave-field over time is evident. The two disturbances at about 5Hz and 9Hz are confirmed to be nearly harmonic contributions, steady over the whole recording window. This provides a further confirmation of their possible anthropogenic origin. A strong additional harmonic signal is evident, at 6.5Hz, but not always present on the recordings. All these disturbances are nevertheless well localized in frequency; therefore they won't likely affect the following processing steps.

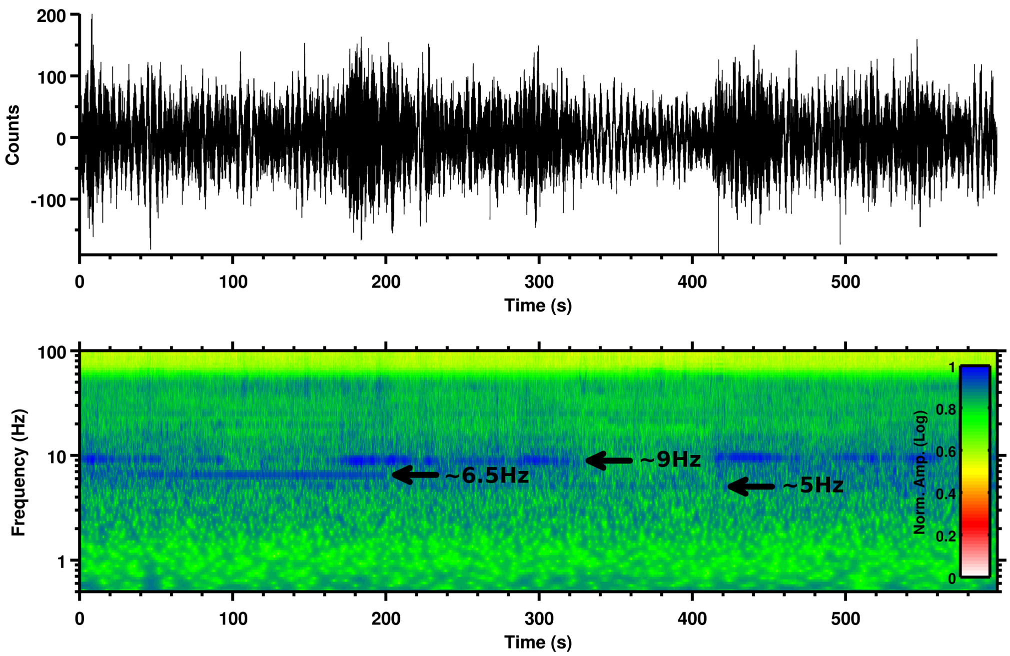

Figure 6 - *Example of spectrogram from 600s of recording of the central station (BOB01) of the array configuration A2. Harmonic disturbances are visible on the whole spectrogram, at about 5Hz, 6.5Hz and 9Hz. These signals were also present during the recordings of configuration A1. For the analysis, the cosine wavelet is used (wavelet parameter = 12).*

7. Conventional H/V spectral ratios

The horizontal-to-vertical (H/V) Fourier spectral ratio is a technique widely used in seismic site characterization because of its ability to provide an estimate of the SH wave fundamental frequency of resonance (f_0) of the site. Other than that, H/V ratios are useful to provide information on the Rayleigh wave ellipticity function, which can be used in surface wave dispersion inversion procedures to constrain large velocity contrasts at depth. In this study, we use the H/V technique also to map the variability of the subsoil structure along the investigated area; this is necessary to verify the fulfillment of the 1D structure assumption, which is necessary for the f-k method applied later.

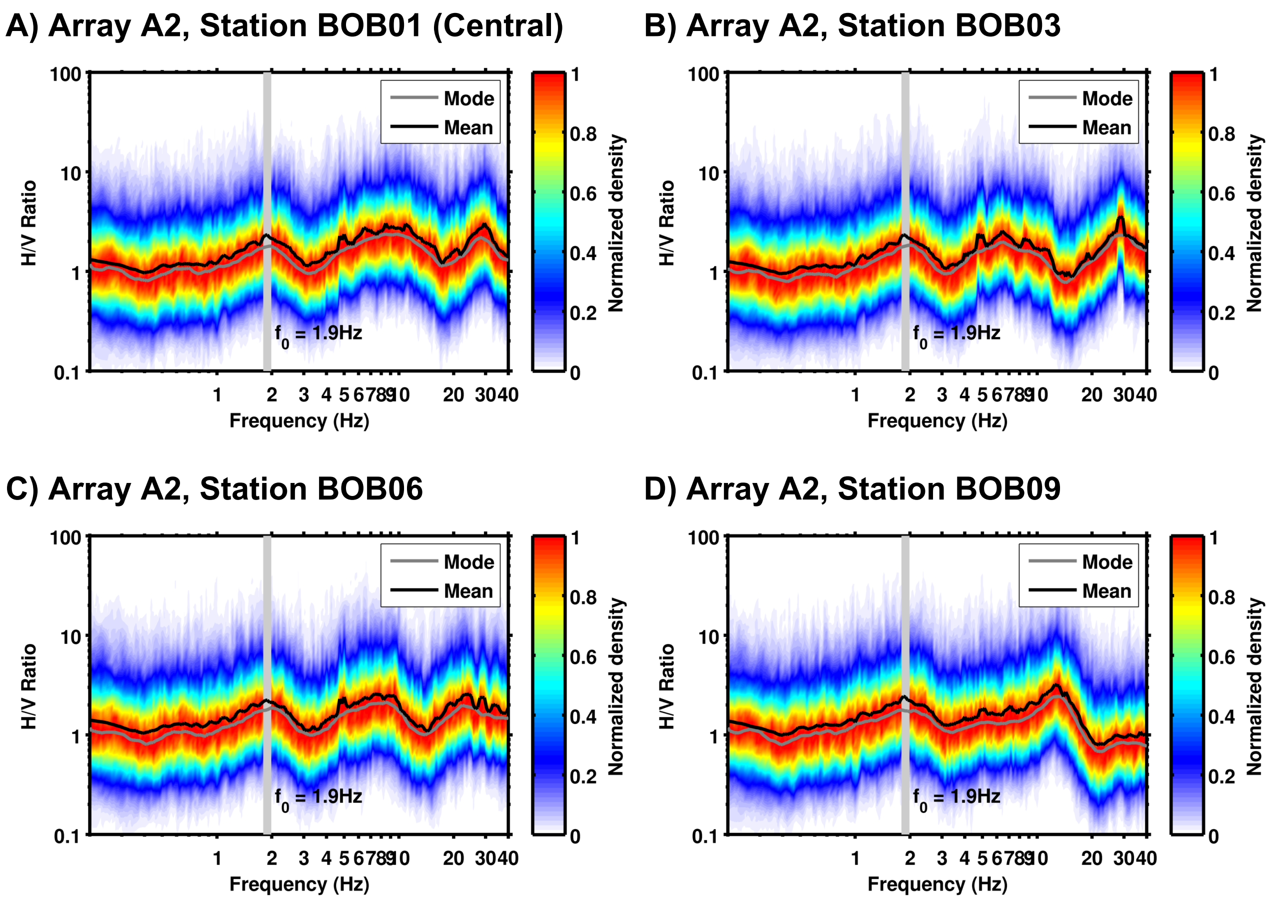

Figure 7 - *Example of H/V spectral ratios for the configurations A2. The resonance frequency of the soil cover is indicated with a light gray line (~1.9Hz). An additional peak is visible in a range between 7 to 15Hz. A third peak is also occasionally visible at rather high frequencies.*

H/V spectral ratios have been computed for all the recordings at each station of the array and separately for configurations A1 and A2 (e.g. **Figure 7**). The behavior of the noise wave-field at the different stations location is comparable at low frequencies (roughly < 9Hz), while the high frequency region shows more variability, within and between arrays. In average (**Figure 8**) spectral curves show a relatively stable low frequency peak (around 1.8~1.9Hz). Such maximum is likely induced by a change in lithology at depth, which causes a modest contrast of seismic impedance. The peak should be regarded as the fundamental resonance frequency of the site (f_0). A second broad peak is also present between about 7Hz and 10Hz, stable on nearly all stations. Interpretation of this second peak is however not straightforward; it might be related to a secondary velocity interface at intermediate depth or – more likely - to the some maximum in the Rayleigh ellipticity function. This will be clarified after the inversion phase. A third peak is finally also present at very high frequency in most (but not all) of the stations. Such maximum is of more difficult interpretation; but probably induced by the Quaternary soil cover, which can be very heterogeneous over the measuring area. The behavior of the site can be considered laterally homogeneous for the f-k analysis.

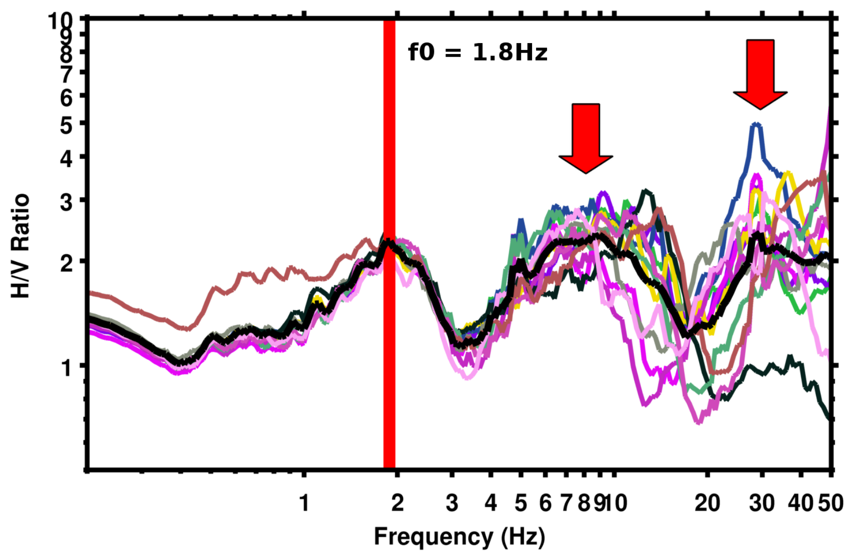

Figure 8 - *Comparison of the H/V spectral ratio curves of all the stations of the array (in this example for the array configuration A2). The curves are stable up to at least 10Hz, confirming the lateral homogeneity of the underlying bedrock velocity structure of the site. A low frequency peak (f_0) is visible at about 1.8~1.9Hz. Two additional peaks can be identified at 7-10Hz and ~30Hz.*

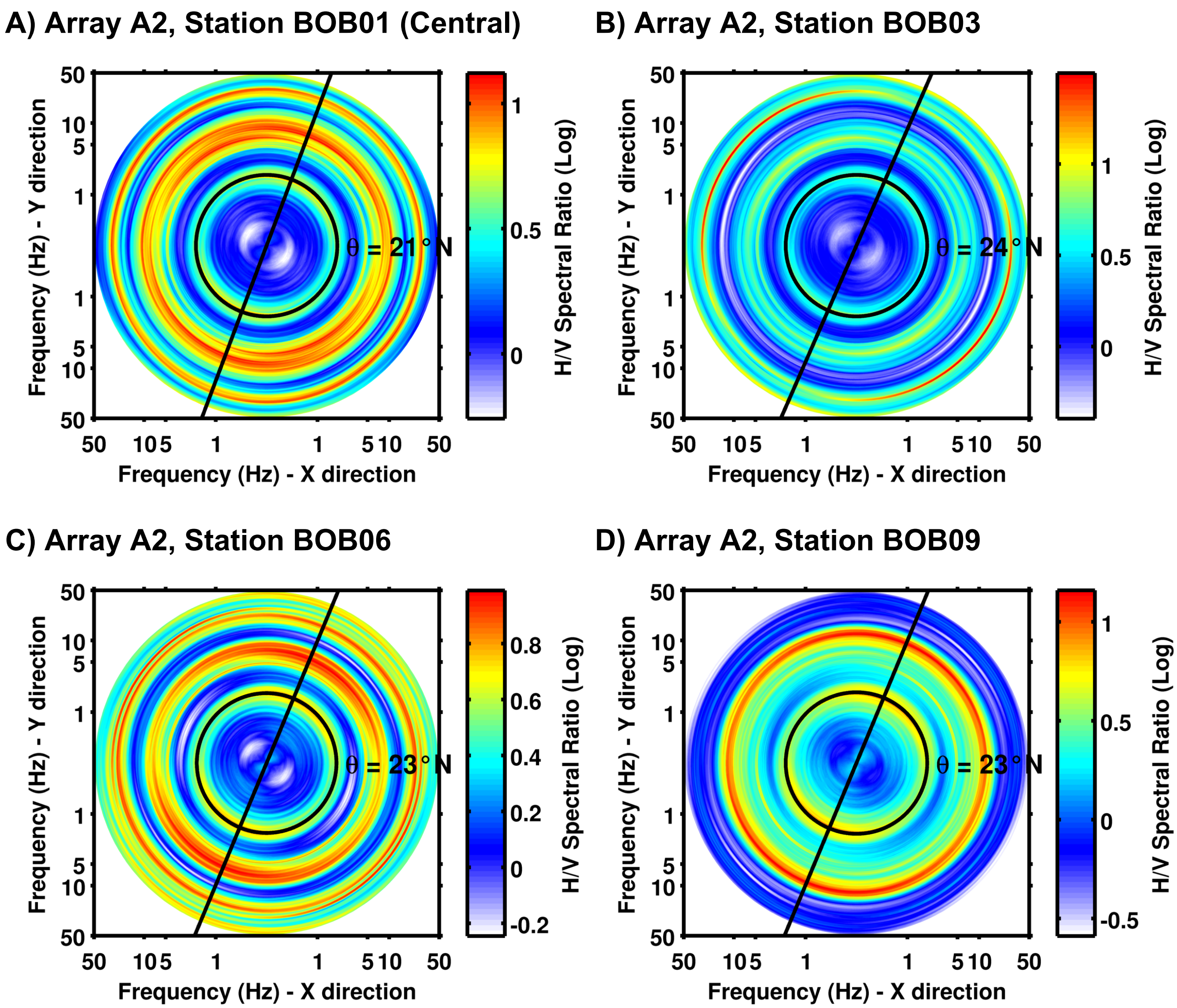

Figure 9 - *Example of directional H/V spectral ratios for configuration A2. The low frequency resonance peak (f_0) is preferentially and consistently aligned roughly NW-SE (~22-23°). No common pattern can be defined for the second and the third peak.*

8. Directional analysis

The computation of directional H/V spectral ratio or polarization analysis is useful to reveal asymmetries in the ambient vibration wave-field. Different effects can induce such a behavior: 2D/3D structure, topographic effects or a non-homogeneous distribution of the noise sources. If a strong directionality is found by the analysis, it is generally recommended to carry out further investigations to properly address the origin of polarization. By processing the directional H/V ratios at all the recording stations of the array (e.g. **Figure 9**) it is possible to describe some directionality in the ground motion. The fundamental frequency shows a preferential (very stable) alignment along direction NW-SE, roughly 22~23°, visible on most of stations of the two geometries. Such direction has however no direct relation with none of the topographic features of the area, and might be therefore induced by some preferential distribution of noise source or to some irregularity of the bedrock geometry at depth (dipping?). Second option seems to be more plausible, since noise source directionality would also (partially) affected the higher frequencies. No preferential direction pattern can be observed for the second or the third peak.

The results of the H/V directional analysis are partially confirmed by applying the wavelet polarization analysis technique (Burjanek et al., 2008). Here, the particle motion shows to be mostly elliptical, with just a weak polarization at the resonance frequencies (**Figure 10**). The second peak is also weakly polarized, which supports its relation to ground structure. A very weak directionality on azimuth is visible at f_0 (**Figure 11**A), nevertheless consistent with H/V results.

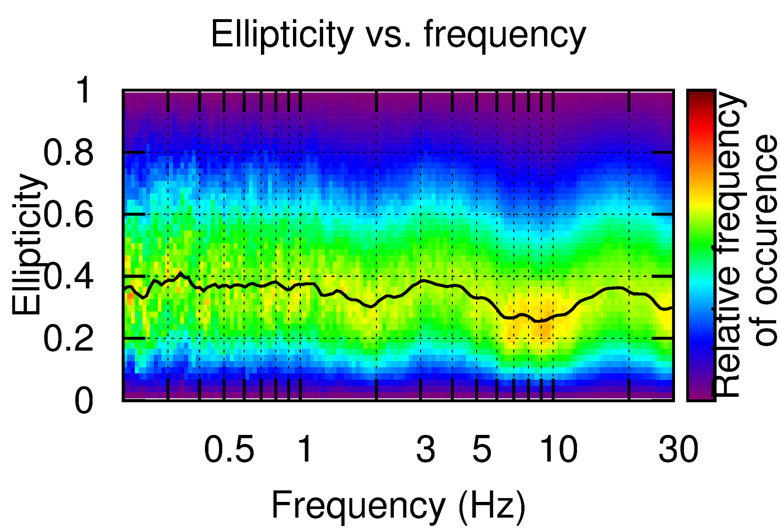

Figure 10 - *Ellipticity of the particle motion from wavelet-based polarization analysis at the central station of the array (BOB01). Similar results can be obtained for other stations of the arrays.*

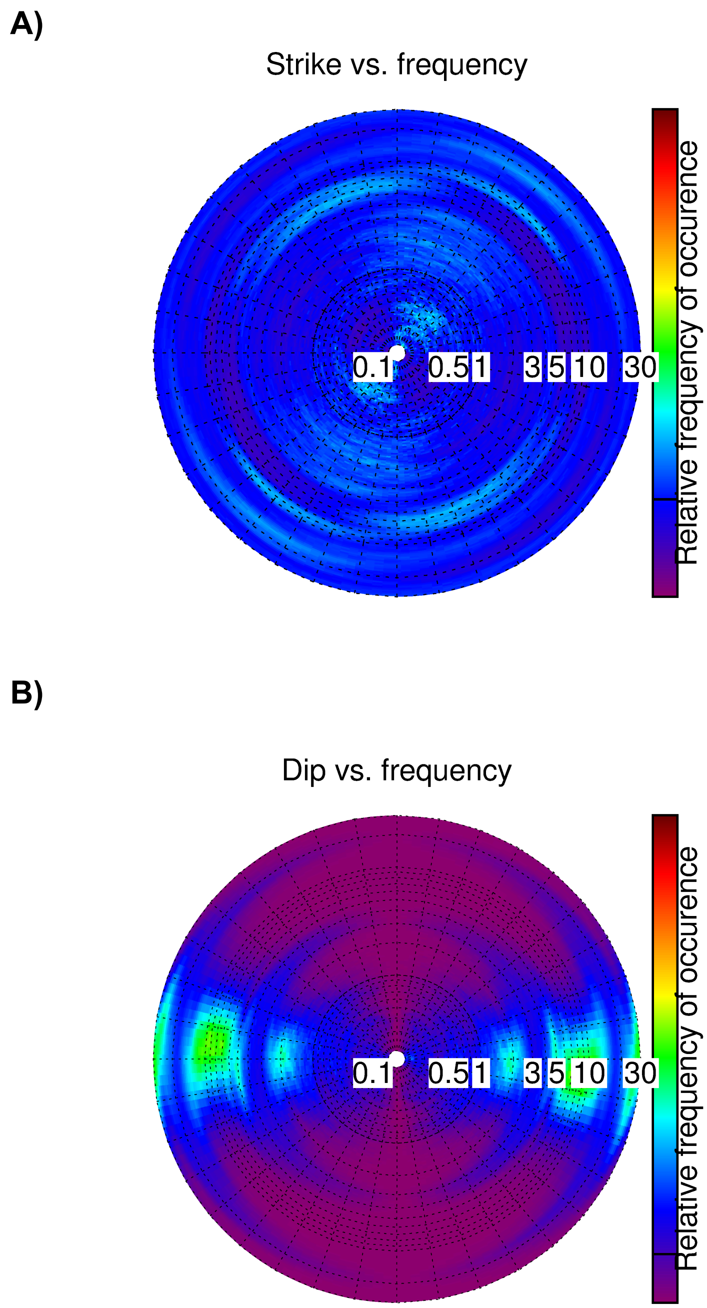

Figure 11 - *Directionality of the particle motion from wavelet-based polarization analysis (dip direction in A, strike in B) at the central station of the array (BOB01). Similar results can be obtained for other stations of the arrays.*

9. Three-component f-k analysis

The frequency-wavenumber analysis is a spectral technique based on seismic array recordings that allows retrieving direction and dispersion characteristics of the surface waves. We apply this technique to three-component ambient vibration recordings using a modification of the high-resolution method of Capon (1969) as described in Poggi et al. (2010). Using all the three-components of motion gives the possibility to retrieve information about the propagation of the Rayleigh waves (vertical and radial processing direction) as well as of the Love waves (transversal direction).

As in the case of the previous methods, the ambient vibration recordings are treated statistically by subdividing the traces in sub-windows. For each consecutive window a separated f-k analysis is performed, and the results are then averaged over the whole recording, increasing the robustness of the final estimation.

A) Ring 2, 3-5Hz

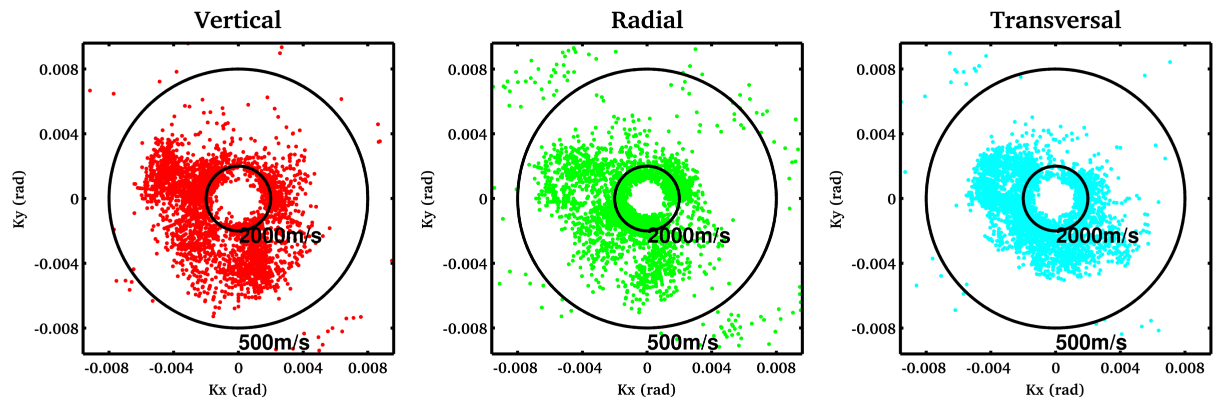

B) Ring2, 5-10Hz

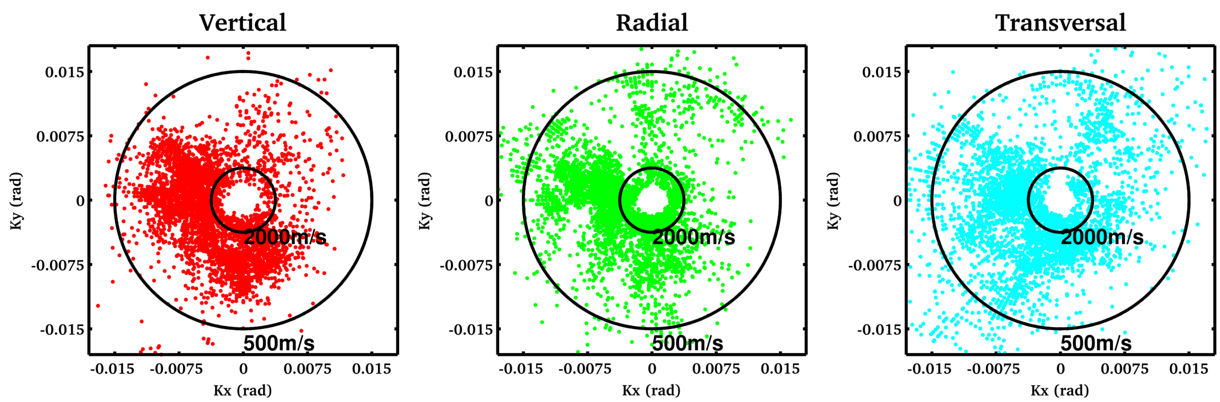

Figure 12 - *Example of distribution of noise sources in the low (3-5Hz) and intermediate frequency range (5-10Hz) obtained from three-component f-k analysis. The source distribution is irregular but not strictly directional on all the propagation components.*

As first step, from the f-k analysis it is possible to assess the azimuthal distribution of noise sources over different frequency ranges (e.g. **Figure 12**) separately for the vertical, the radial and the transversal direction of polarization. From the analysis of the two geometries A1 and A2, source distribution appears to be slight inhomogeneous in all the components, with a preferential clustering of sources in the SW quadrant.

As a second step, the surface-wave dispersion curves are extracted by visual inspection and manual picking of the f-k density plots (**Figure 13** and **Figure 14**), separately for the three polarization directions. Complementary results have been obtained for the three array configurations. In particular, Love wave's fundamental mode dispersion can be well tracked in a broad frequency range (from 2.5Hz to about 30Hz) on both A1 to A2; velocity estimates are also consistent and well overlapping between the two geometries. Rayleigh wave's fundamental mode can be well tracked from about 3Hz to 10Hz on the vertical direction and for both array configurations, while radial direction provides reliable results only for configuration A2. A second higher mode is occasionally visible, but well consistent between vertical and radial directions and between configurations.

A summary of all the identified modes from vertical, radial and transversal direction of propagation is presented in **Figure 15**, while the final interpretation of Rayleigh and Love wave dispersion pattern is in **Figure 16**, together with the results from an active seismic survey performed on the same location by the company *RoXplore*. Active surface wave analysis results (MASW) are compatible with our interpretation, extending the resolution at high frequencies and adding a Rayleigh wave higher mode to the interpretation model.

10. Inversion of the dispersion curves

The surface wave dispersion curves (Rayleigh and Love) obtained from the three-component f-k analysis of the ambient vibrations and the fundamental frequency of resonance (f_0) from average H/V spectral ratios are inverted to obtain an estimation of the velocity profile of the site (mainly S-wave velocity as function of depth, and to a lesser extend the P-wave velocity, due to the lower sensitivity). The analysis is performed using the software *Dinver* (www.geopsy.org), which implements a direct search approach (**Figure 17**) based on a conditional version of the neighborhood algorithm (Sambridge, 1999).

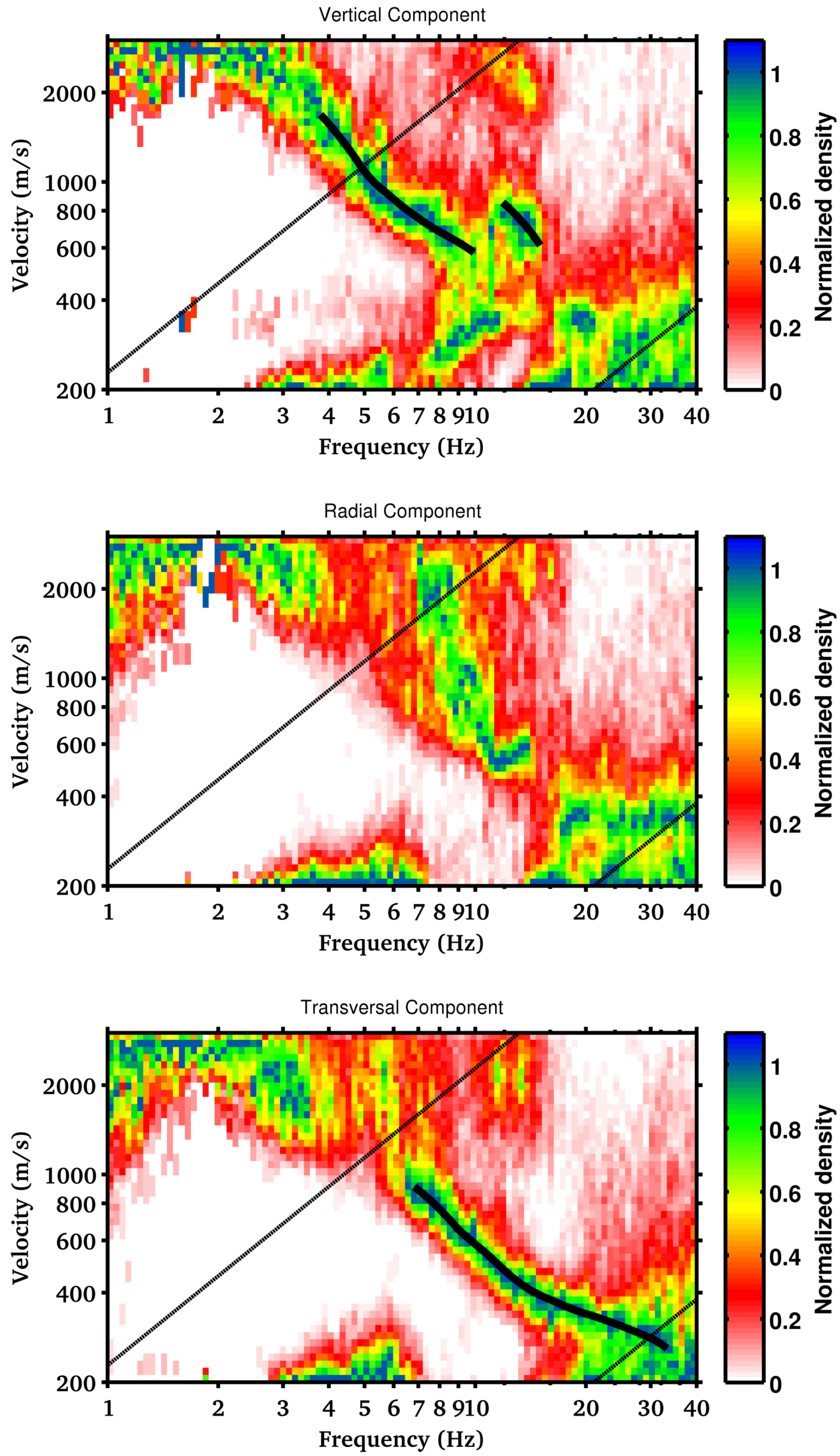

Figure 13 - *Density distribution of the surface wave signals obtained from the recording of the array configuration A1 using three-component f-k analysis. From top to bottom: Rayleigh vertical, Rayleigh radial and Love wave dispersion. In red the interpreted dispersion curves are given (manually selected).*

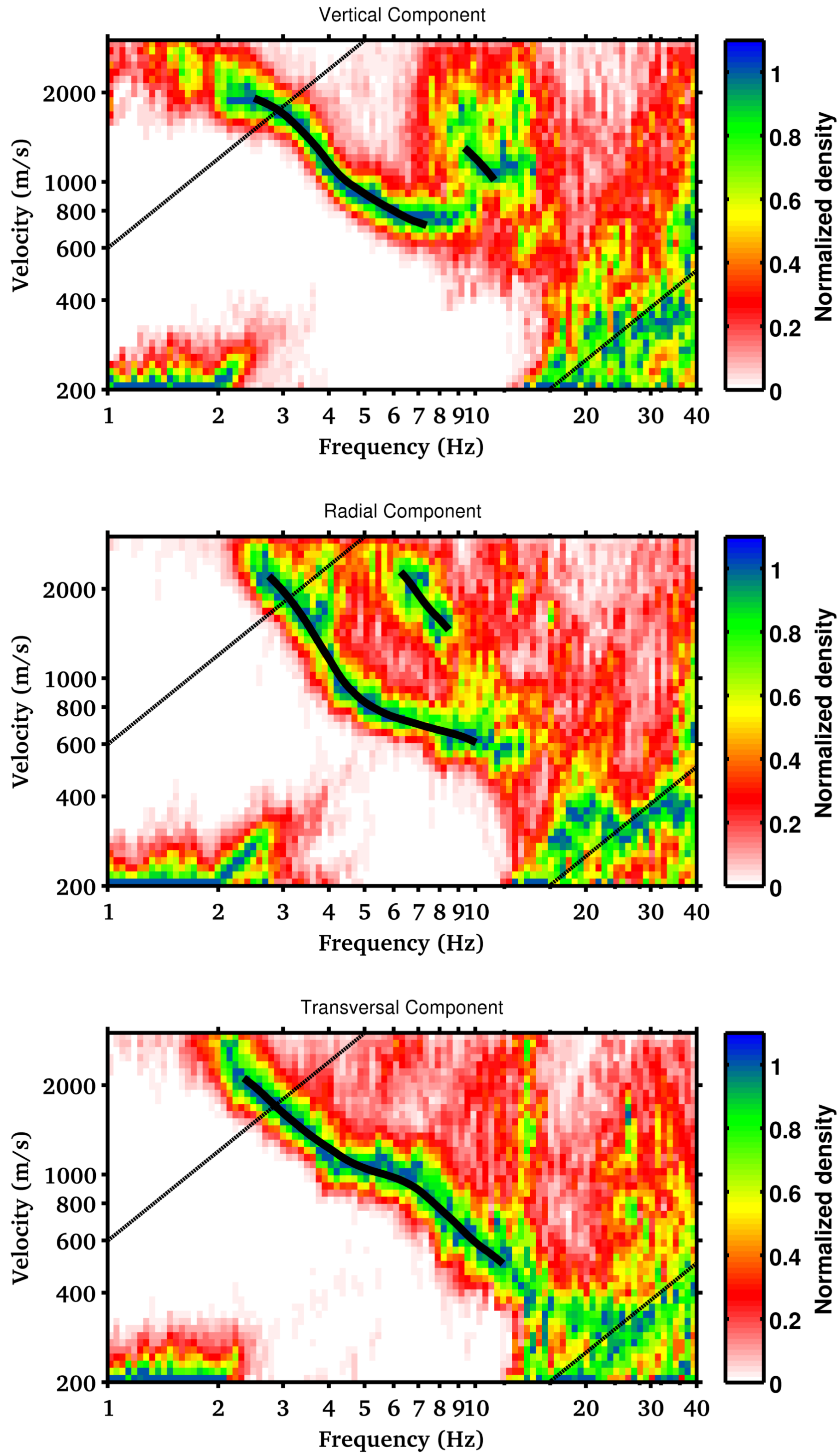

Figure 14 - *Density distribution of the surface wave signals obtained from the recording of the array configuration A2 using three-component f-k analysis. From top to bottom: Rayleigh vertical, Rayleigh radial and Love wave dispersion. In red the interpreted dispersion curves are given (manually selected).*

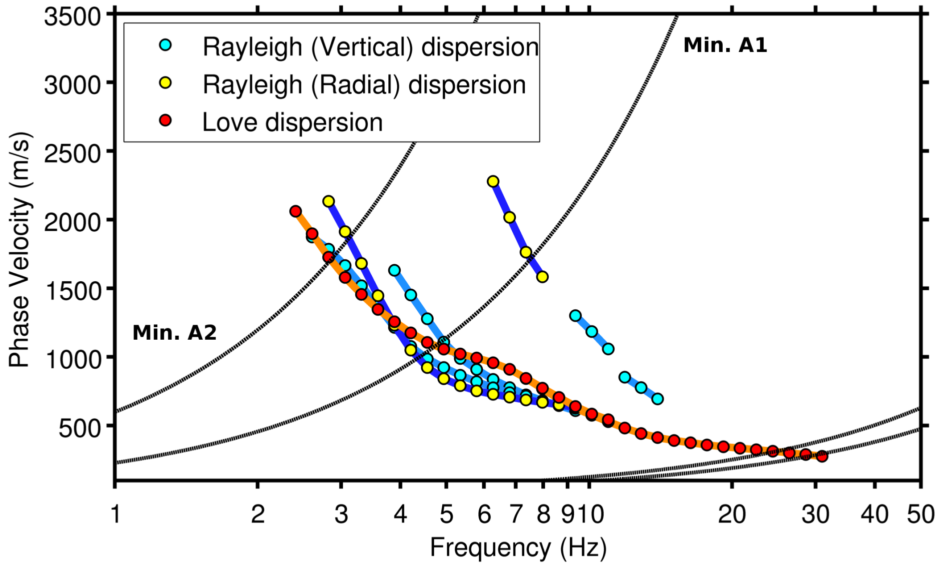

Figure 15 - *Summary of all dispersion curves obtained from three-component f-k analysis of the three array configurations A1 and A2. Minimum and maximum resolution bounds from the two geometries are indicated with black solid lines.*

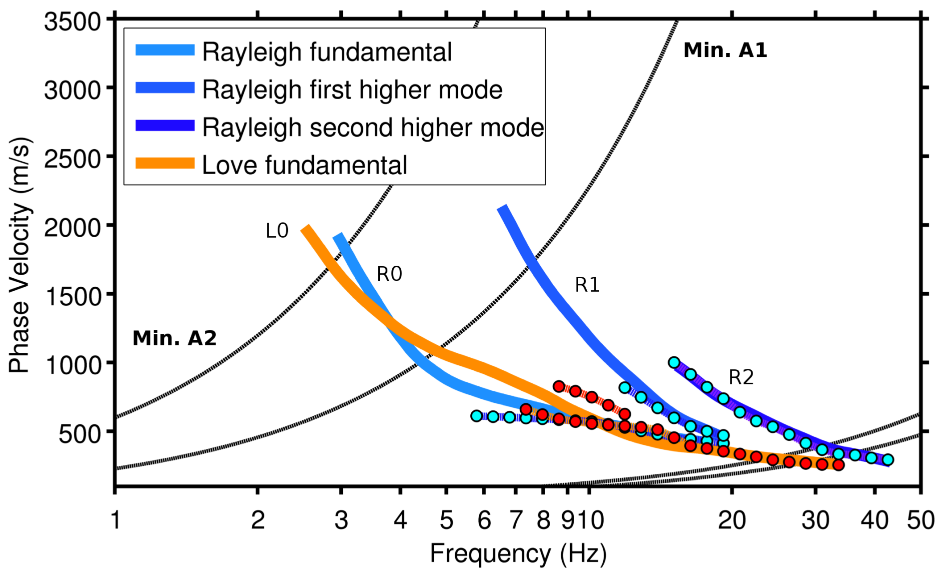

Figure 16 - *Final interpretation of the Rayleigh and Love dispersion curves for BOBI, including the results from active surface wave analysis (MASW, with dots). Minimum and maximum resolution bounds from the full array are indicated with black solid lines.*

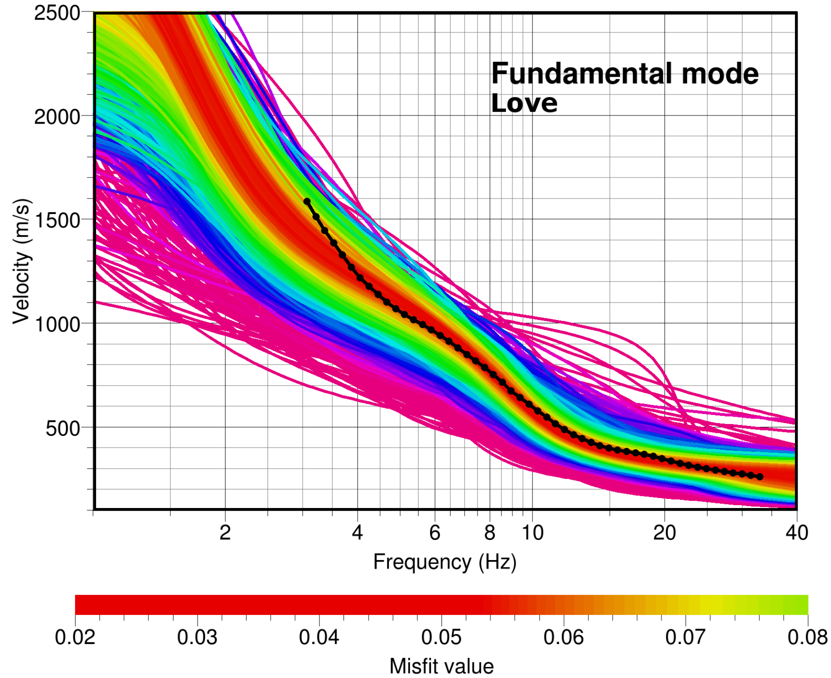

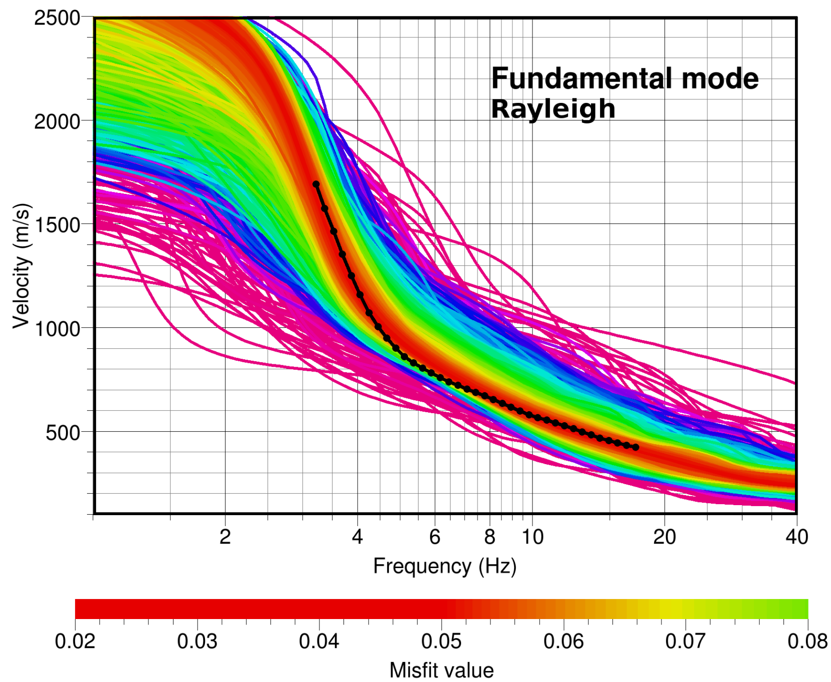

Figure 17 - *Example of fitting the surface dispersion data within the global optimization procedure. Different colors represent different misfit between the observed (in black) and the modeled dispersion curves during the search.*

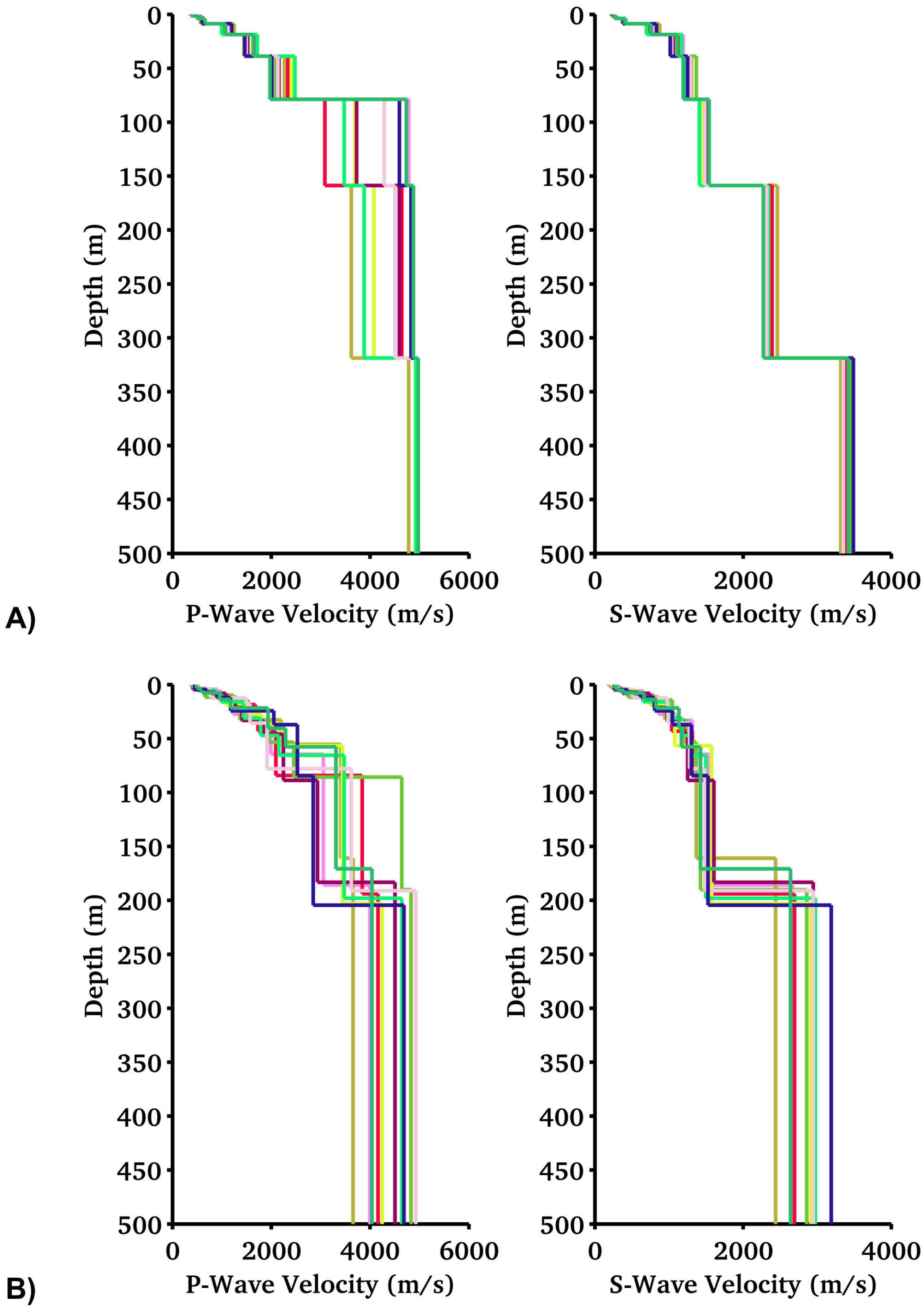

Figure 18 - *Collecting the best fitting models from the ten separated inversion runs using the free-layers (A, top) and fixed-layers (B, bottom) parameterization schemes.*

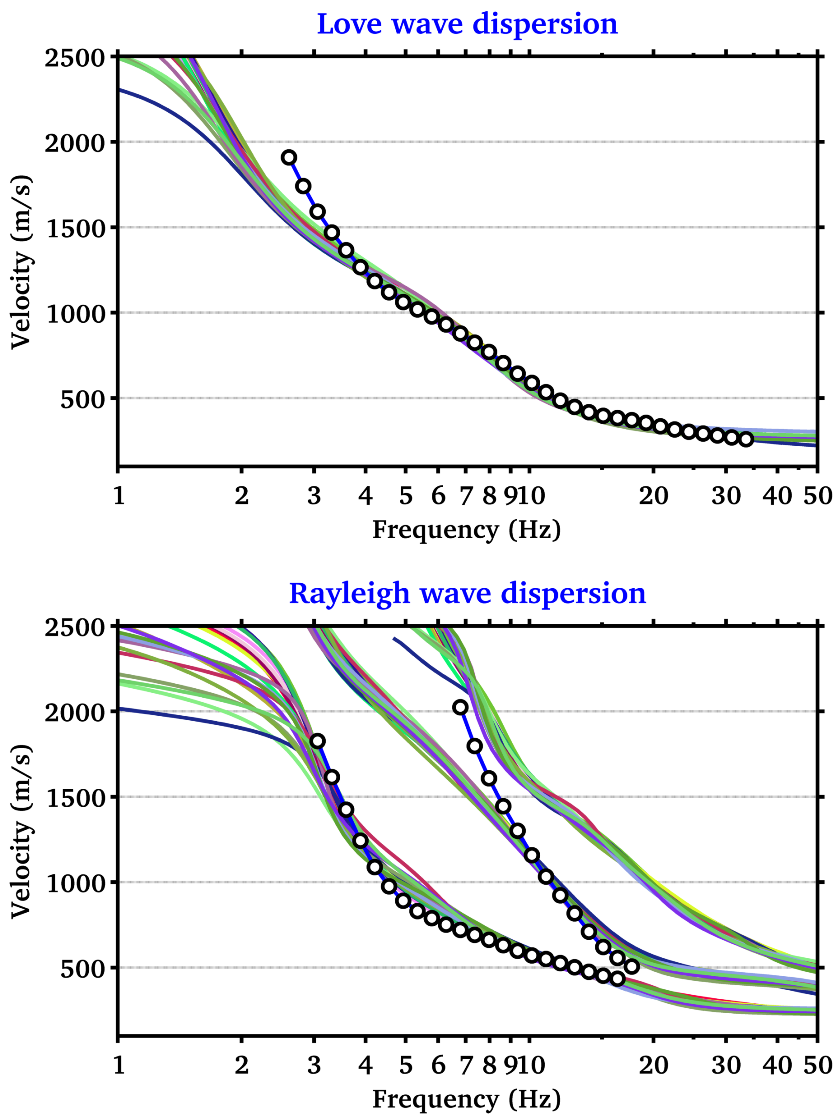

Figure 19 - *Dispersion curves computed from the best fitting models of the two proposed interpretation schemes (free and fix layers), compared with picked dispersion from active and passive seismic experiments.*

To parameterize the velocity model, two different approaches were implemented. The first one consisted in setting up an eight-layer model with fix interface depths. In such a case the free inversion parameters are then the velocities (P and S) and layer thicknesses. In the second case, a free-thickness layer approach was used. The advantage of the former method stays in the possibility to better resolve sharp velocity interfaces, while the second is less unique and better constraints the seismic velocity. The two approaches have to be nevertheless considered complementary, and they should provide consistent results.

Ten inversion tests (*runs*) were performed for each of the two model schemes, in order to minimize the effect related to a possible unfavorable initial randomization of the parameter space. The best fitting model from of each run was then collected (**Figure 18** and **Figure 21**) and used later on for the computation of the derived soil parameters.

In more detail, the inverted velocity profiles (Vs and Vp) are gradient-like in the top part, with a major interface between about 150m and 250m. While top part is actually constrained by high frequency part of the Rayleigh and Love dispersion curves (including results from active surface wave analysis, **Figure 19**), the interface is solely controlled by the use of f_0 form H/V spectral ratios (**Figure 20**). By subsequent comparison, the theoretical ellipticity is nevertheless matching the shape of great part of the whole average H/V curve, including the second peak (which can then be addressed to Rayleigh wave), but not the third peak (then probably an effect of the soil cover).

By considering the minimum available frequency of the surface-wave analysis, and by analyzing the scattering of the inverted models (**Figure 21**), it is realistic to assume the velocity profiles to be reliable down to a depth of about 150~250m. Below this value no direct constrain is available from data, and the velocity values are obtained by pure extrapolation.

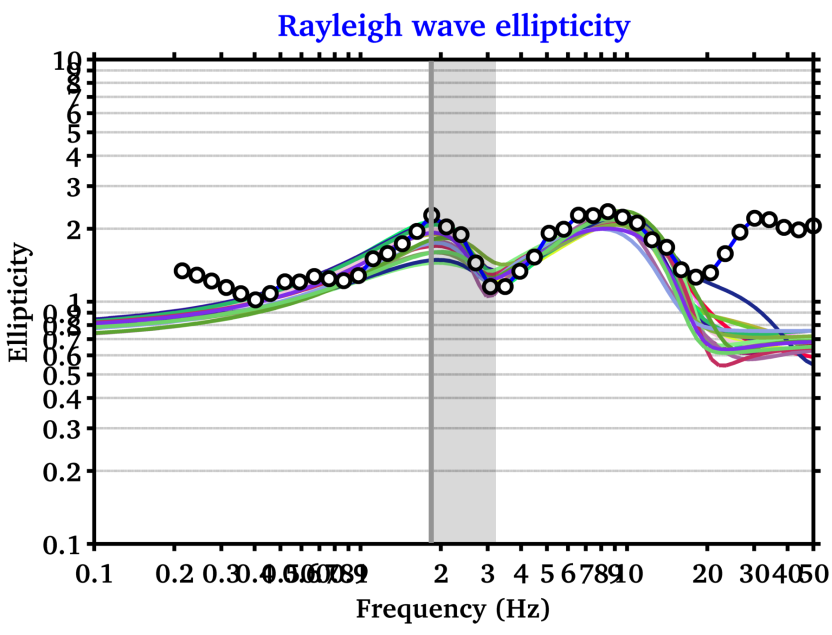

Figure 20 - *Rayleigh wave ellipticity curves computed from the best fitting models of the two proposed interpretation schemes (free and fixed layers), compared with average H/V spectral ratio from configuration A2 (scaled by sqrt(2)). The first two peaks are clearly reproducible, even though the whole H/V curve was not used during the inversion.*

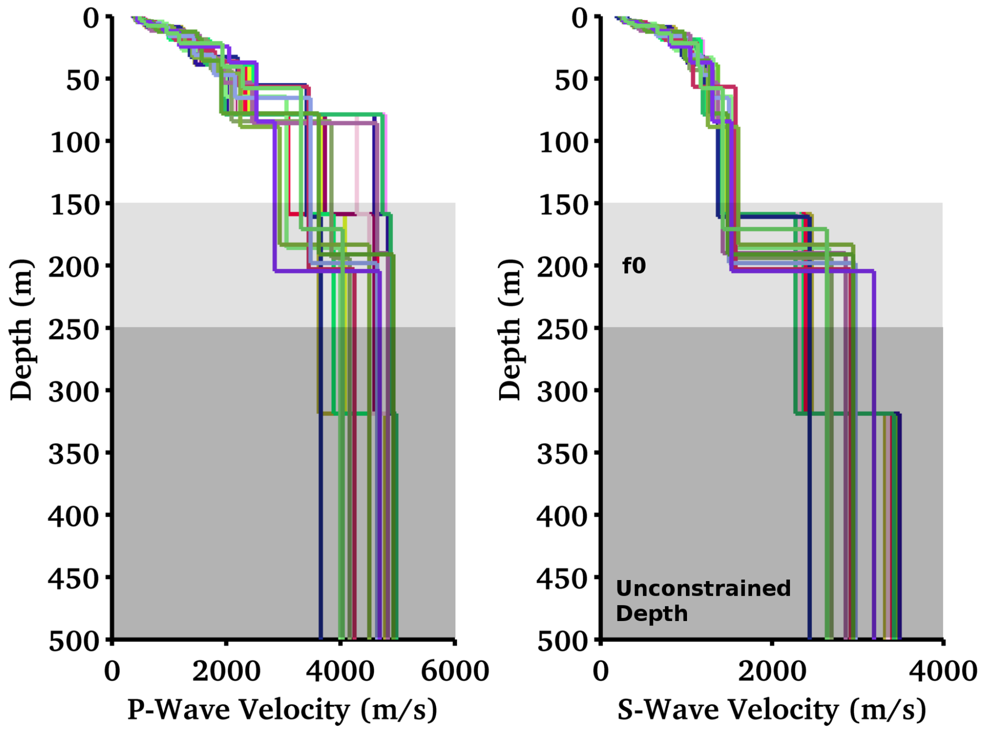

Figure 21 - *Comparison of all the best models from the two parameterization schemes (free and fixed layers). The two approaches produce consistent results. Depth range between about 150m and 250m is solely constrained by f_0 and should be considered approximately the maximum resolved depth.*

11. Engineering soil parameters

The ensemble of all the best inverted velocity profiles is then used to derive average soil parameters like the VsZ (average travel-time S-wave velocity over the depth Z, including Vs30, Table 1) and the quarter-wavelength (QWL) average velocities (Joyner et al., 1984) for a range of frequencies between 0.6 and 30Hz (**Figure 22**). The former is a standard parameter for the classification of ground-types in most building codes and in ground motion prediction equations. The latter is a parameter useful for the empirical estimation of the site-response and to assess the sensitivity of the seismic wave-field to the different depths. It has to be noticed that these two parameters are derived separately from all the best S-wave velocity models obtained from the inversion, and the results is finally averaged to improve statistics.

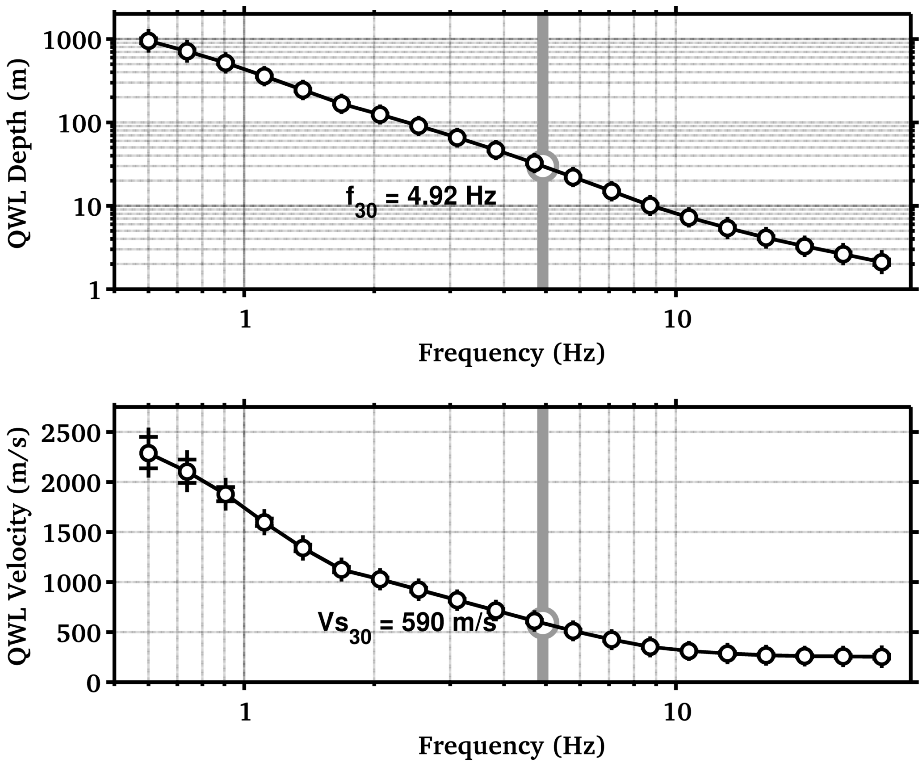

Figure 22 - *Quarter-wavelength representation of the inverted S-wave velocity profiles. Top: the depth-frequency dependency. Bottom: the QWL average velocity. The Vs30 value is indicated with its corresponding QWL frequency.*

12. Amplification models

Site amplification functions have been computed using two different approaches: the S-wave transfer function for vertical propagation and the quarter-wavelength amplification. In general the first method is used to evaluate the resonance characteristics of the site, while the second is more useful to assess the effect of the velocity contrasts between the lowermost rock layer (as reference) and the different QWL averaging depths. The two amplification functions are then corrected for the Swiss rock reference velocity profile as defined in Poggi et al. (2011), according to the procedure described in Edwards et al. (2013). Given the lower velocities in the uppermost part of the BOBI profile compared to the Swiss reference, the final corrected amplification function shows a lower average amplification level at high frequencies than the uncorrected (**Figure 23**).

Averaging depth (m)	Vs-mean (m/s)	St.Dev.
5	279.95	10.38
10	350.94	6.34
15	425.41	5.16
20	486.22	5.58
25	542.75	6.45
30	**590.02**	**7.46**
40	668.27	7.93
50	736.00	8.73
75	859.28	10.16
100	955.85	11.90
150	1084.30	15.41
200	1212.99	24.30

Table 1 - *Average travel-time velocities at different depths. Vs30 is highlighted.*

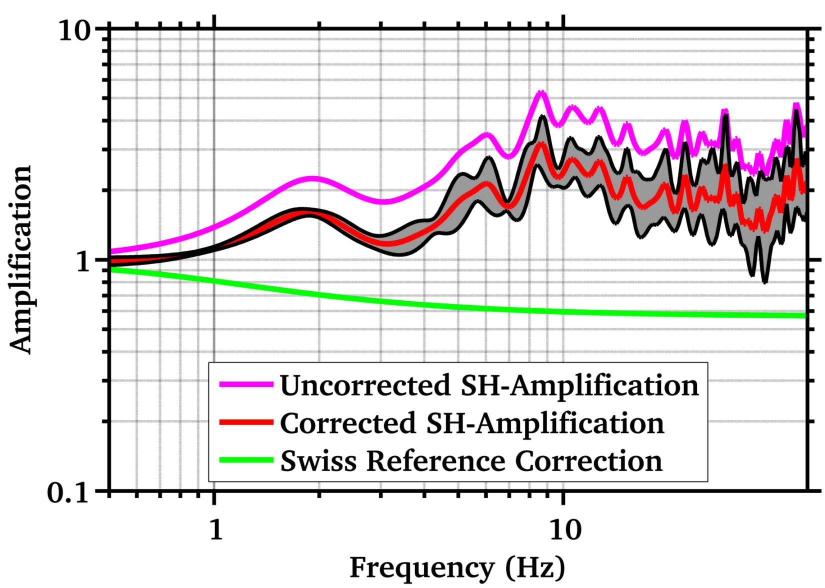

Figure 23 - *Correcting the SH-wave transfer function for the Swiss (rock) reference conditions (Poggi et al. 2011). The final corrected amplification function shows a lower (average) amplification at high frequencies than the uncorrected.*

Amplification functions using the transfer function and the quarter-wavelength approach are comparable (**Figure 24**), even if the transfer function provides a slightly larger amplification, because of the presence of some weak resonance peaks. At low frequencies both methods converge to the same amplification level. It has to be notice that the amplification functions do not include attenuation at this stage of the analysis, as the quality factors of the site are too uncertain.

A good matching is obtained by comparison between the one-dimensional transfer function and the empirical amplification from spectral modeling of low-magnitude earthquakes as described in Edwards et al., 2013 (**Figure 25**). This confirms the reliability of the inverted velocity profile in light of the current assumptions of one-dimensionality.

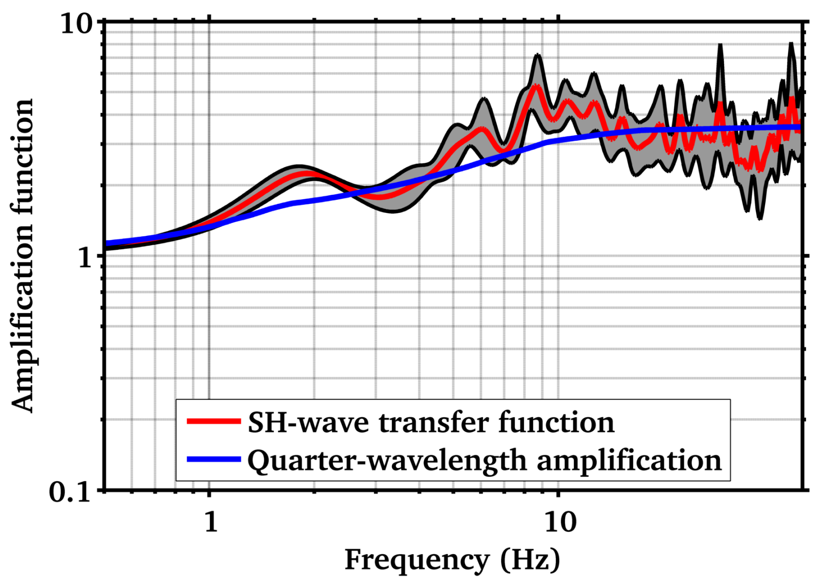

Figure 24 - *Comparison of amplification functions computed using the SH-wave transfer function and the quarter-wavelength formalism on the inverted velocity models. The functions are referenced to the Swiss rock reference model (Poggi et al. 2011).*

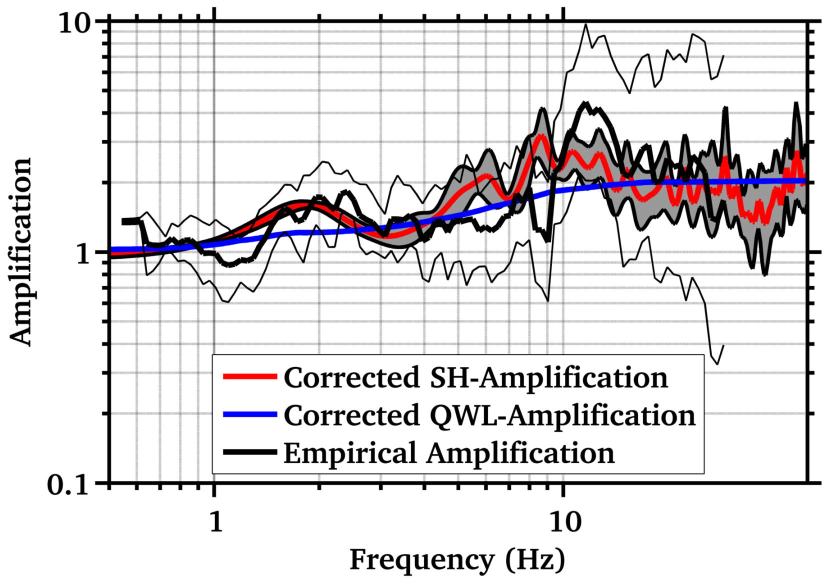

Figure 25 - *Comparison of amplification functions computed using the SH-wave transfer function and the quarter-wavelength approach with empirical observation from spectral modeling of low-magnitude earthquakes. All functions are referenced to the Swiss rock reference model (Poggi et al. 2011).*

REFERENCES

Capon, J., 1969. High resolution frequency wavenumber spectrum analysis, Proc. IEEE, 57, 1408-1418.

Burjanek, J., G. Stamm, V. Poggi, J.R. Moore, and D. Fäh [2010], “Ambient vibration analysis of an unstable mountain slope”, Geophys. J. Int., Vol. 180, pp. 820-828.

Edwards, B., C. Michel, V. Poggi and D. Fäh (2013). Determination of Site Amplification from Regional Seismicity: Application to the Swiss National Seismic Networks. Accepted for publication in Seismological Research Letters.

Joyner, W. B., R. E. Warrick and T. E. Fumal (1981). The Effect of Quaternary Alluvium on Strong Ground Motion in the Coyote Lake, California, Earthquake of 1979, Bulletin of the Seismological Society of America, 71, 1333-1349.

Poggi, V., B. Edwards and D. Fäh (2011). Derivation of a Reference Shear-Wave Velocity Model from Empirical Site Amplification, Bulletin of the Seismological Society of America, 101, 258-274.

Poggi, V. and Fäh D., 2010. Estimating Rayleigh wave particle motion from three-component array analysis of ambient vibrations. Geophys. J. Int., 180-1, 251-267.

Eidgenössische Technische Hochschule Zürich
Swiss Federal Institute of Technology Zurich

SED
Schweizerischer Erdbebendienst
Swiss Seismological Service

Report on site characterization

Wallhausen, Germany (WALHA)

Poggi Valerio, Manel Hobiger, Donat Fäh

Last modified - 23 / 12 / 2014

1. Introduction

In the framework of the NAGRA seismic network project, an array measurement of the ambient vibration wave-field was performed at the location of the SED station WALHA (Wallhausen, Germany). The scope of the survey is the seismic characterization of the area surrounding the installation (**Figure 1**), which consists in a broadband seismometer (Trillium Compact) with a high-resolution digitizer (Taurus 24Bit @200sps). Ambient vibration analysis has been used to infer the characteristics of the underground structure of the site, with special regard to the one-dimensional shear-wave velocity. Such profile was later used to assess the local seismic response of the station.

For the analysis, different spectral analysis techniques were implemented, consisting in both single and array methods, which are listed below:

- Time-frequency wavelet analysis
- Power-spectral density estimation
- Conventional horizontal to vertical spectral ratios
- Directional horizontal to vertical spectral ratios
- Wavelet polarization analysis
- Three-component high-resolution f-k analysis.

The results of all these analyses conformed to the definition of the final velocity model. In the following, the main results of these investigations are summarized and a final interpretation of the velocity profile is given. From this interpretation, engineering parameters are finally derived, e.g. the Qwl-Vs average velocity, VsZ (including Vs30) and the seismic amplification from the analytical SH-transfer function of the one-dimensional soil column.

2. Survey description

To characterize the seismic response of the site, an array measurement of ambient vibration was performed on 24/06/2014 (**Figure 1**). The array consists of two measuring configurations (A1 and A2) of 14 sensors each and increasing diameter of about 100m and 200m respectively. The two configurations were planned to partially overlap, by sharing 9 common sensors, with the aim of providing a continuous frequency resolution between the two geometries. Configuration A1 recorded for a total of 1h10m, while configuration A2 for 1h40m. The differences in the recording length are due to the different resolution characteristics of the two geometries. As a general rule, larger arrays require longer recording time to produce a reasonable statistics of the ambient vibration processing results. In this case, however, due to an unfortunate presence of transient disturbances, the usable signal length for configuration A2 was reduced to about 1h only. Satisfactory results were nevertheless obtained from the analysis of the two geometries.

High velocities and relatively shallow geophysical bedrock (undeep marine Molasse) were expected for the site. This justifies the use of a large geometry for the array to be successful. The maximum aperture of the array was again controlled by the available space on the hilltop, which was quite flat over the measuring area, but limited toward North-East and South-West from dipping slopes and forests. A precise prior estimation of the possible maximum resolved depth was not possible, due to the large uncertainty of the bedrock velocity, but resolution down to about 110~150m depth was expected.

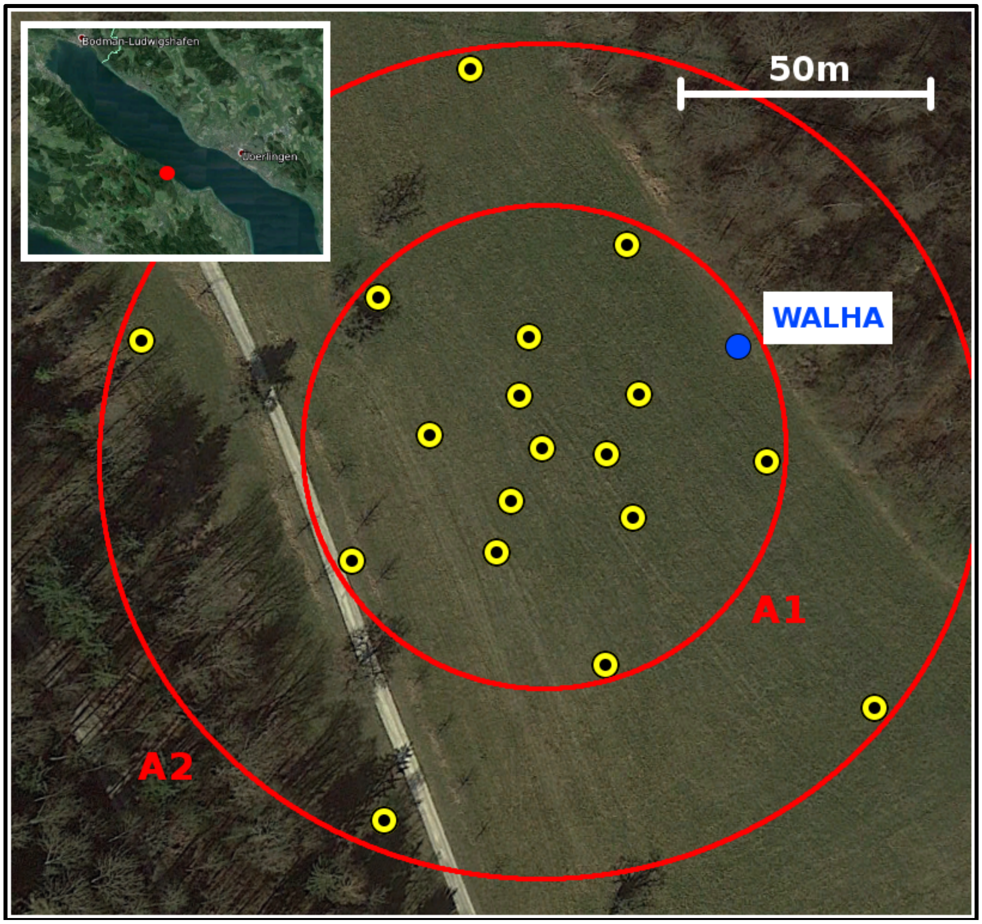

Figure 1 - *Location of the ambient vibration array survey performed in Wallhausen, (SED station WALHA) on 24/06/2014. Two concentric configurations of increasing diameter were implemented (name A1 and A2). Location of the permanent station is shown in blue.*

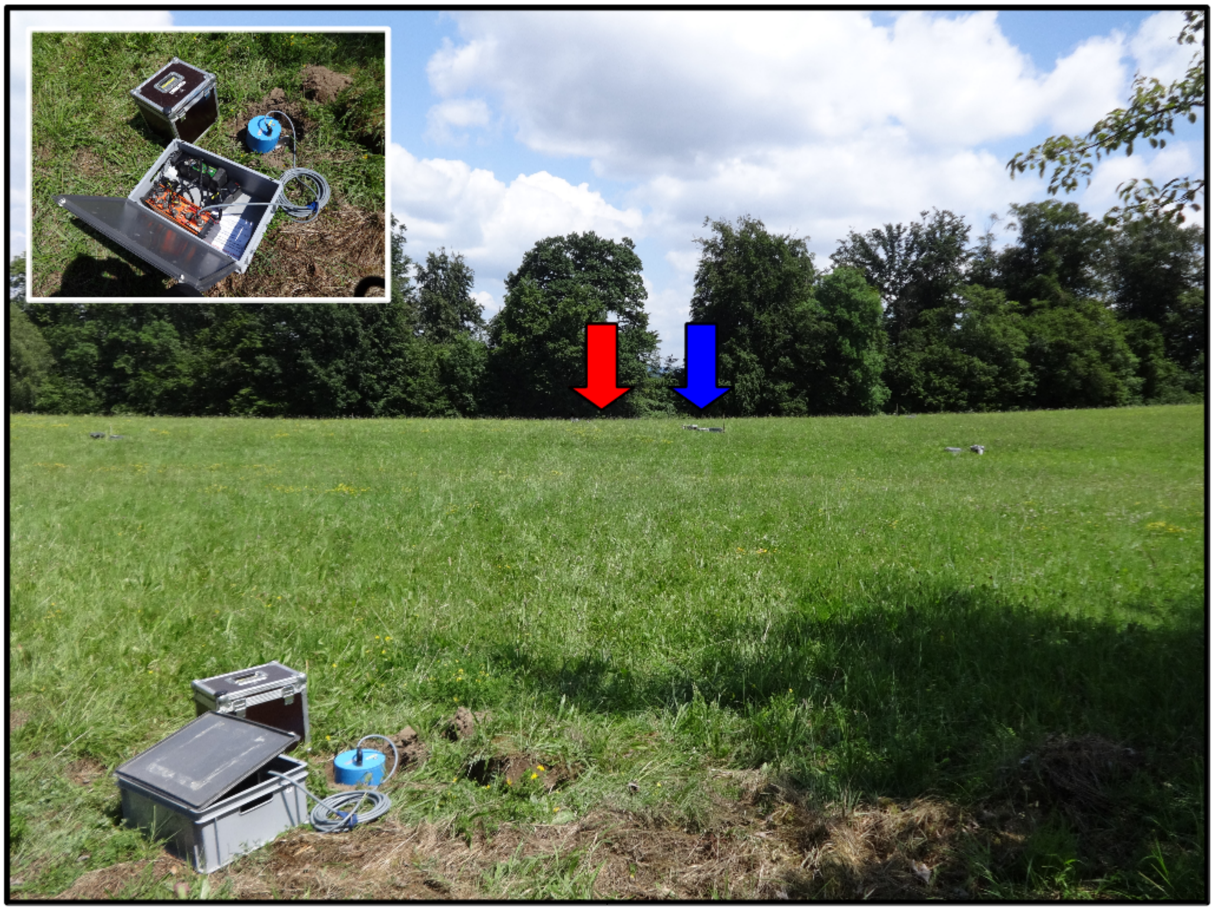

Figure 2 - *Overview of the measurement area. Location of the array central station and of the permanent station WALHA (at the edge of the grass field, close to the forest border) are indicated with blue and red arrows respectively.*

3. Soil type, topography and geology

The array has been set in open field conditions, in a rural area (**Figure 1**, **Figure 2**). The influence of buildings and anthropogenic disturbances is virtually negligible, even though some monochromatic harmonic signals affected the second half of the survey (while recording with array configuration A2). Array sensors have been deployed on free soil. Good coupling with the ground was assured by means of digging small holes at the sensor's places, and by using a special support (*Trihedron*®) that facilitates the leveling of the device even for difficult soil conditions. The measurement area was located on a nearly flat area, just little dipping toward NE. However, no topographic correction has been taken into account before processing.

From the geological points of view (**Figure 3**), the target area is located on a small hill on the Molasse basin (precisely undeep marine Molasse). The surface morphology is considerably smooth and modeled by the action of glaciers during the Pleistocene. The measuring area is visibly surrounded by moranic deposits, clearly identifiable from the surface morphology and confirmed by the geological map of the area. The Molassic bedrock is likely very shallow at the measuring location, but never exposed across the area (a variable-thick cover of quaternary material is generally present). The bedrock probably consists of marl and consolidated sandstone with layers of different texture and granulometry, from very fine sand and silt to occasionally conglomerate. Such site can be classified as of rock ground-type A.

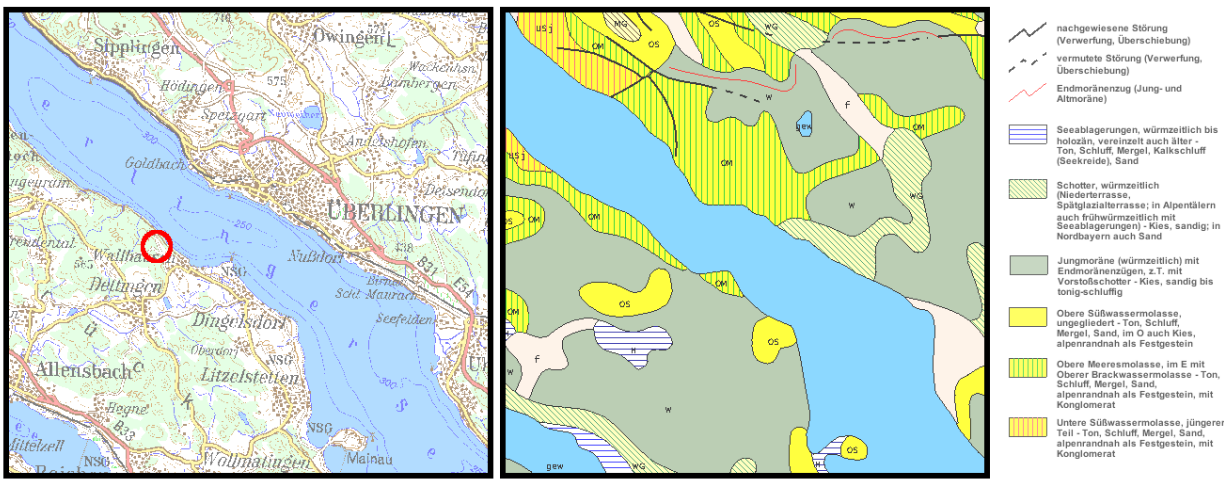

Figure 3 - *Geological map of the lake Constance, in the surroundings of Wallhausen (reproduced from GeoFachdatenAtlas, Bodeninformationssystem Bayern, modified). In red the approximate location of the permanent station WALHA.*

4. Acquisition equipment

Each acquisition point within the array consisted of a three components seismometer (Lennartz 3C with 5s eigenperiod) and a 24 bit data logger (Quanterra Q330). Synchronization between stations was assured by standard GPS, while a more accurate differential GPS (Leica Viva system) was used to precisely locate the sensor's coordinates with a tolerance of less than 5cm.

5. Weather conditions

The weather conditions were optimal and stable during the whole measurement, with no precipitations, no wind and an average (over the whole day) temperature of 16 degrees. Soil was nevertheless most likely saturated from precipitations occurred during the days preceding the survey.

6. Pre-processing and preliminary data-quality control

The three-component recording has been filtered prior to analysis using a band-pass 6th order causal Butterworth filter with corners at 0.2Hz and 50Hz. Although it is not a strict requirement for spectral analysis techniques, such filtering was applied in order to facilitate the preliminary visual inspection of the noise traces and to evaluate the coherency of the wave-field (**Figure 4**). Such procedure gives essential information for the subsequent interpretation of the f-k analysis results.

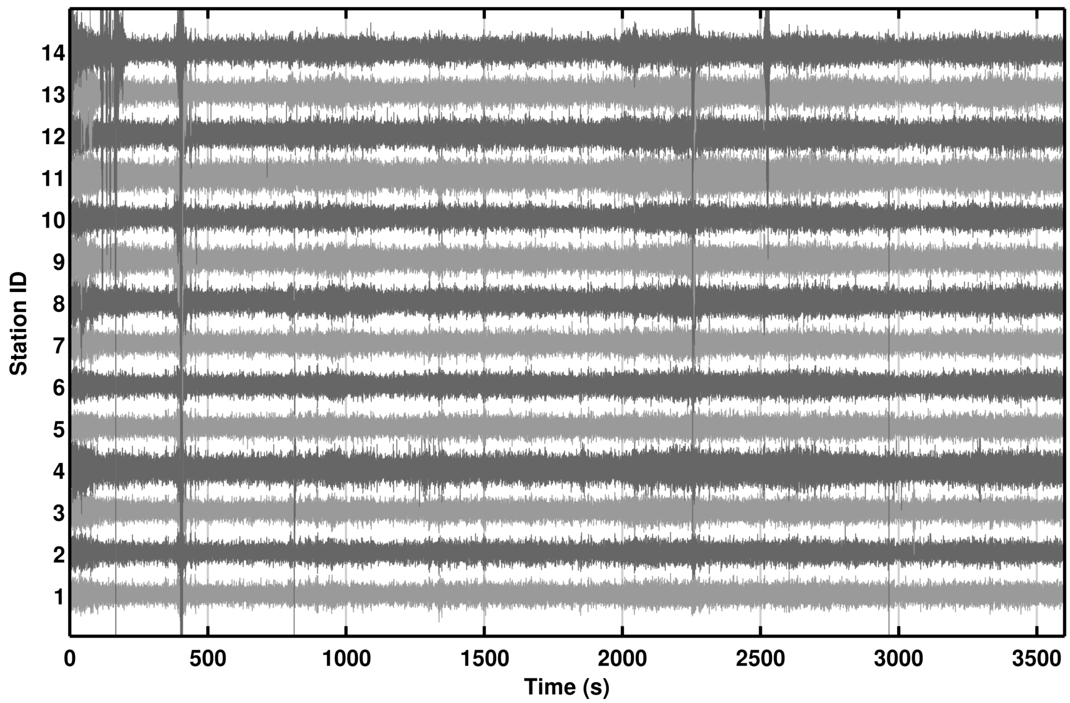

Figure 4 - *Inspection of the useful part of the ambient vibration recording of the Wallhausen array (in this example configuration A1). No strong transients were present during the acquisition, which resulted in an overall good quality of the recordings.*

To assess the quality of the ambient vibration recordings, spectral analysis was subsequently performed. Because of the stochastic nature of the ambient vibration wave-field, a statistical approach has to be used, such as the estimation of the power spectral density (*PSD*). This approach is useful to evaluate the average energy level of the recordings in the analyzed frequency range, and to access the presence of spurious spectral peaks, which might be related to human activity (machinery, pumps). By inspecting the PSD of all the three-component recordings of the array in the range between 0.5 and 40Hz, it is found that the average energy level of the spectrum is overall very low, well within the minimum and maximum bounds of the USGS noise model.

Two spurious peaks have been identified at about 5Hz and 7Hz. Such peaks - very narrow - were nevertheless present only for configuration A2, and did not affect the recordings of configuration A1 (**Figure 5**). This gives a confirmation of their anthropogenic origin (likely a nearby farm). Such harmonic contributions are therefore rejected from any subsequent interpretation.

A1)

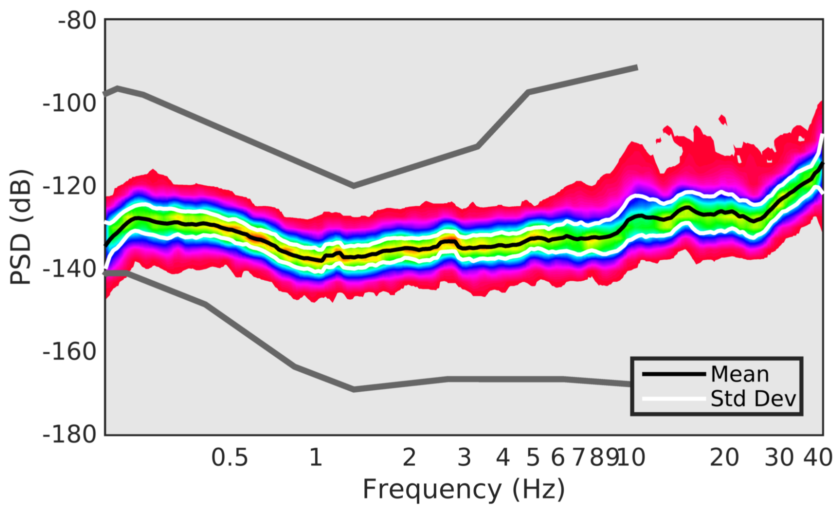

A2)

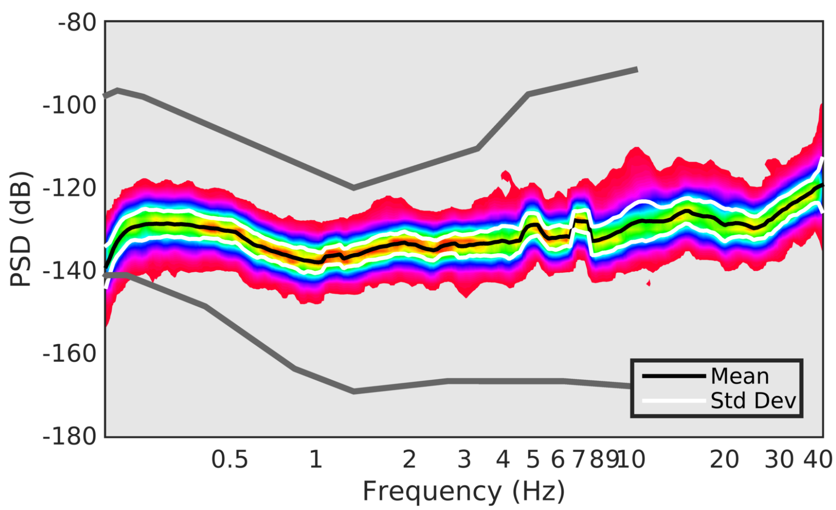

Figure 5 - *Power spectral density (PSD) computed for 1h recording at the central station (WAL002) of the array configuration A1 (top) and A2 (bottom). Similar results were obtained from the other stations of the array. In gray lines are the minimum and the maximum bounds of the USGS noise model, for comparison.*

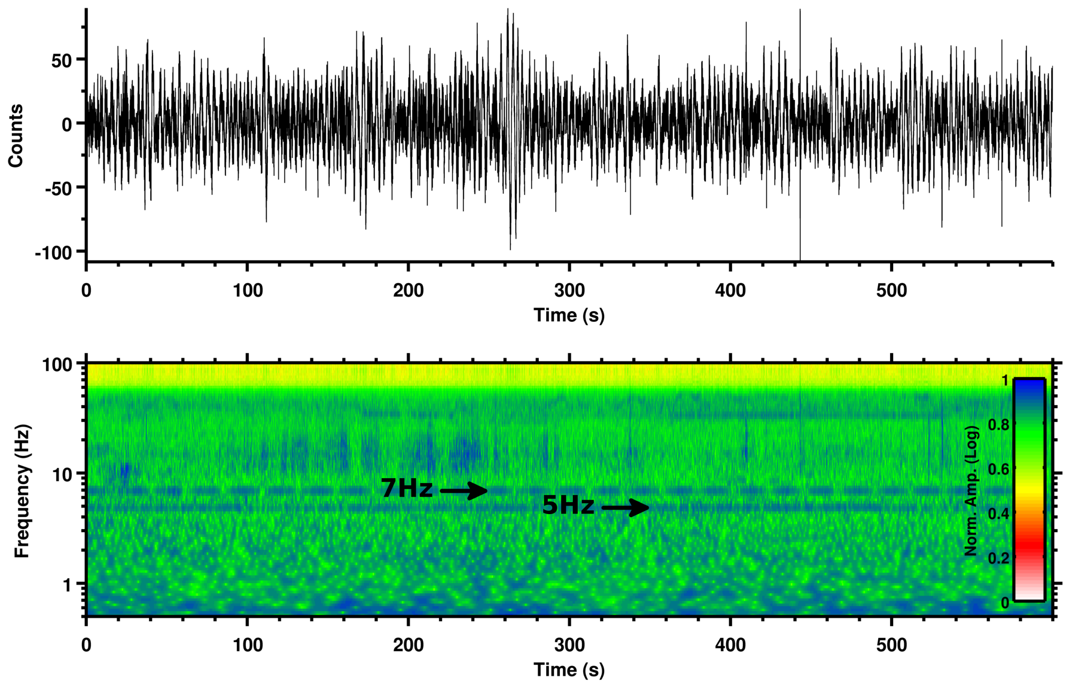

Figure 6 - *Example of spectrogram from 600s of recording of the central station (WAL002) of the array configuration A2. Two harmonic disturbances are visible on the whole spectrogram, at about 5 and 7Hz. These signals were not present during the recordings of configuration A1. For the analysis, the cosine wavelet is used (wavelet parameter = 12).*

Complementary to the aforementioned statistical methods, a spectral decomposition approach is more suitable to assess the stationarity of the ambient vibration wave-field over time. The wavelet time-frequency analysis was then performed over the whole recording time. From such analysis (**Figure 6**) an overall stability of the ambient-vibration wave-field over time is evident. The disturbances at about 5Hz and 7Hz are confirmed to be a nearly harmonic contribution, steady over the whole recording window. This provides a further confirmation of their anthropogenic origin. These disturbances are nevertheless very weak and well localized in frequency; therefore they won't affect the subsequent processing steps.

7. Conventional H/V spectral ratios

The horizontal-to-vertical (H/V) Fourier spectral ratio is a technique widely used in seismic site characterization because of its ability to provide an estimate of the SH wave fundamental frequency of resonance (f_0) of the site. Other than that, H/V ratios are useful to provide information on the Rayleigh wave ellipticity function, which can be used in surface wave dispersion inversion procedures to constrain large velocity contrasts at depth. In this study, we use the H/V technique also to map the variability of the subsoil structure along the investigated area; this is necessary to verify the fulfillment of the 1D structure assumption, which is necessary for the f-k method applied later.

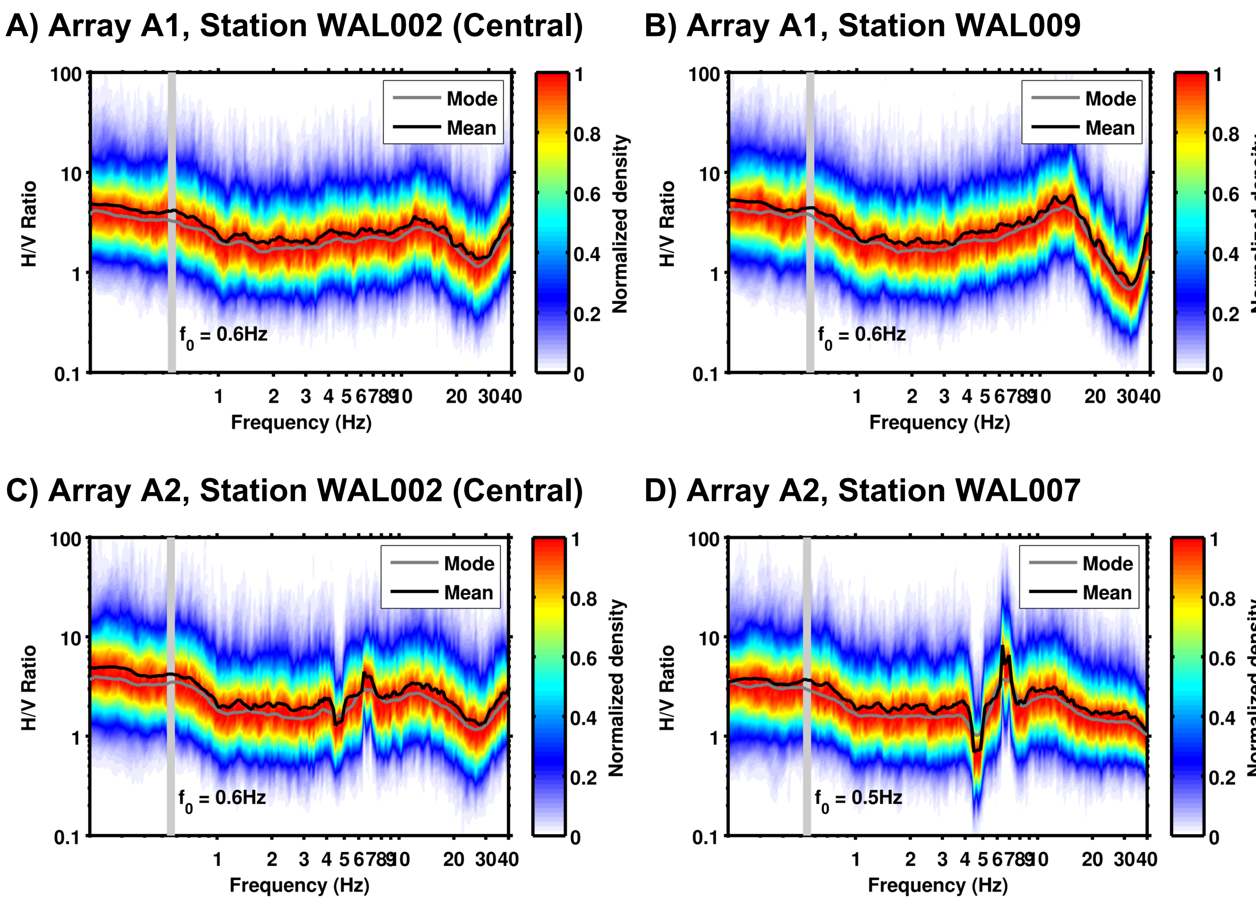

Figure 7 - *Example of H/V spectral ratios for the two concentric configurations A1 and A2. The presence of anthropogenic signals is quite evident in all stations of A2. The resonance frequency of the soil cover, indicated with a light gray line, is due to a lithology change within rock. The additional resonance peak at about 14Hz is likely due to a velocity contrast between topmost soil and underlying rock.*

H/V spectral ratios have been computed for all the recordings at each station of the array and separately for configurations A1 and A2 (e.g. **Figure 7**). The shape of the computed H/V curves is typical of stiff-soil/rock velocity profiles whereas the soil thickness is rather small. The behavior of the noise wave-field at the different stations location is very comparable (**Figure 8**). A relatively small peak is visible at low frequency (around 0.56Hz), quite stable over the whole measuring area. Such maximum is likely induced by a change in lithology at depth, which causes a modest contrast of seismic impedance. The peak should be regarded as the fundamental resonance frequency of the site. Above this frequency, H/V curves are quite flat till about 10~12Hz, with a stable amplitude slightly above 2. At higher frequencies the variability of H/V curves reflects the variability of the topmost part of the ground structure. A second maximum can be observed between about 12Hz and 25Hz. This peak is likely induced by the Quaternary soil cover, which can be very heterogeneous over the measuring area. Interesting to notice how the two previously identified anthropogenic disturbances show a different behavior on H/V ratios (e.g. **Figure 7**C and D). This means, the harmonic signal at 5Hz is mostly vertically polarized, while that one at 7Hz is more pronounced on the horizontal components.

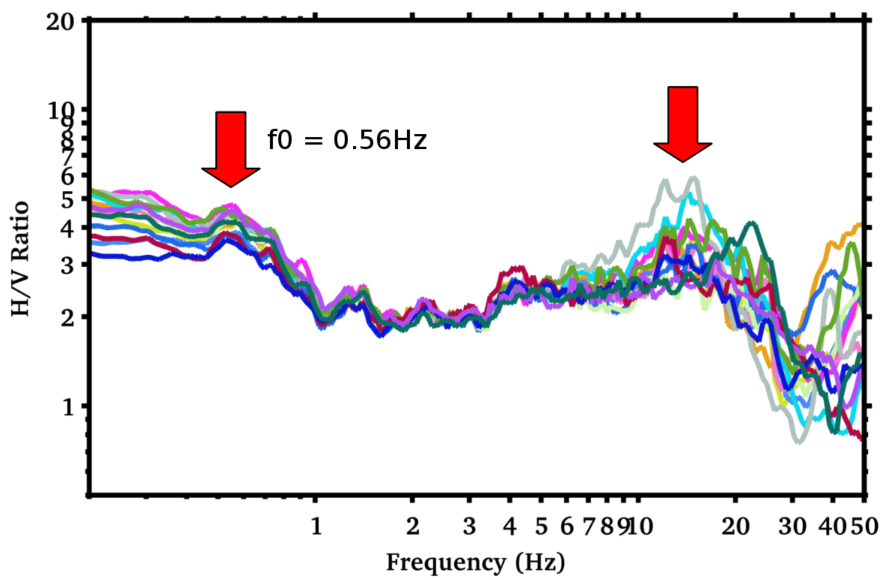

Figure 8 - *Comparison of the H/V spectral ratio curves of all the stations of the array (in this example for the array configuration A1). The curves are stable up to at least 10Hz, confirming the lateral homogeneity of the underlying bedrock velocity structure of the site. A low frequency peak is visible at about 0.56Hz. At high frequencies the spectral ratios are variable across the array. This reflects the complex geometry of the quaternary sediments cover.*

8. Directional analysis

The computation of directional H/V spectral ratio or polarization analysis is useful to reveal asymmetries in the ambient vibration wave-field. Different effects can induce such a behavior: 2D/3D structure, topographic effects or a non-homogeneous distribution of the noise sources. If a strong directionality is found by the analysis, it is generally recommended to carry out further investigations to properly address the origin of polarization.

By processing the directional H/V ratios at all the recording stations of the array (e.g. **Figure 9**) it is possible to observe an overall isotropy of the wave-field in the intermediate frequency range, roughly between 1 and 10Hz. However, the resonance peak at about 0.56Hz has surprisingly a stable directionality of nearly 50°N. The reason for such behavior is nevertheless not clear. This might be induced by the geometry of the hill, which has major axis in the orthogonal direction. At high frequencies, the variability of the H/V peak observed in **Figure 8** is noticeable also in its directionality (not shown here). As already introduced, this can be explained by the variability of the uppermost soil cover layer over the study area and will not be further discussed. It is interesting to notice the directionality of the two previously found harmonic signals which affect the recordings of configuration A2. These maxima are roughly aligned towards NW-SE direction (120~140°N).

The results of the H/V directional analysis are also confirmed by applying the wavelet polarization analysis techniques as described in Burjanek et al. (2008). Also in this case no sign of significant directionality (**Figure 10**A) and polarization (**Figure 10**B) of the wave-field is observable in the frequency band useful for f-k processing. Similarly, the low frequency resonance peak shows directionality similar to that found with H/V analysis, plus a moderate elliptical polarization.

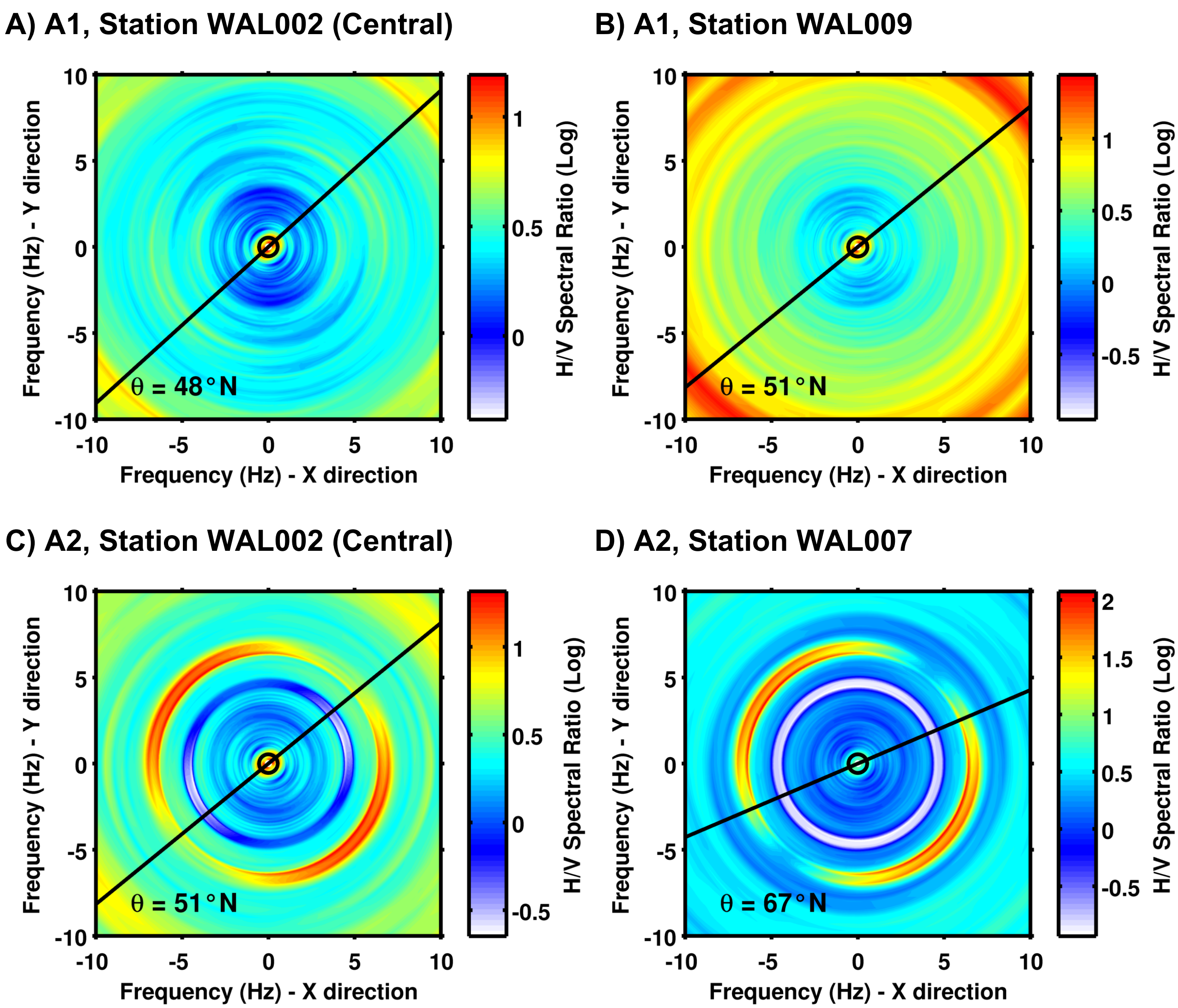

Figure 9 - *Example of directional H/V spectral ratios for the two concentric configurations A1 and A2. No consistent evidence of wave-field anisotropy is present in the intermediate frequency range (1-10Hz), while the low frequency resonance peak (f_0) is preferentially aligned perpendicularly to the hill major axis. Moreover, a strong directionality of the two harmonic disturbances (at 5Hz and 7Hz) is visible on the recordings of array configuration A2.*

A)

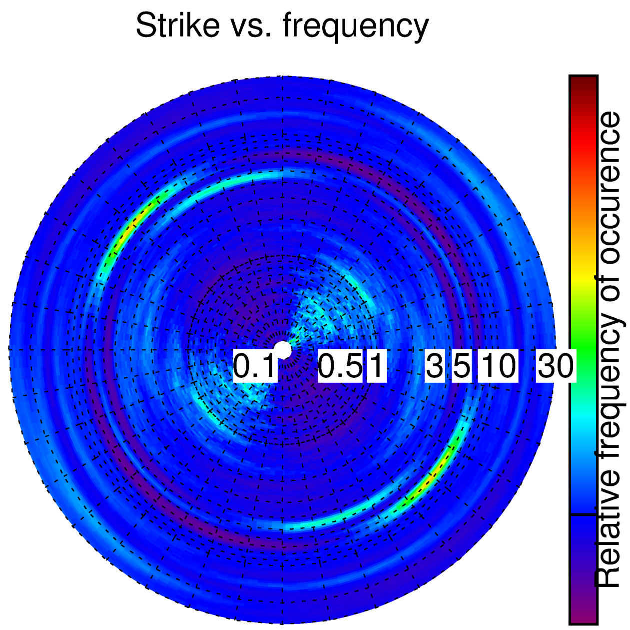

B)

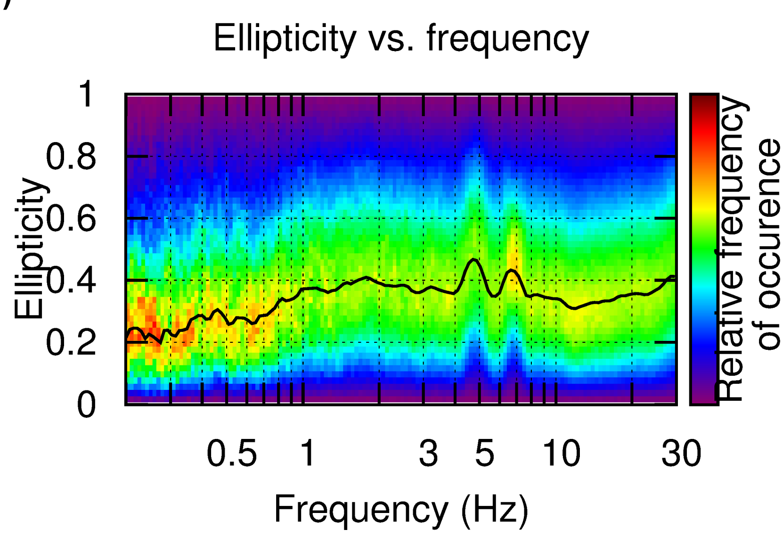

Figure 10 - *Wavelet-based polarization analysis at the central station of the array configuration A2. By analyzing the polarization over strike (A) and the particle motion ellipticity plot (B), no directional effect is visible in the frequency range of interest (roughly 1-10Hz), with the exception of the two anthropogenic disturbances, which are strongly directional.*

9. Three-component f-k analysis

The frequency-wavenumber analysis is a spectral technique based on seismic array recordings that allows retrieving direction and dispersion characteristics of the surface waves. We apply this technique to three-component ambient vibration recordings using a modification of the high-resolution method of Capon (1969) as described in Poggi et al. (2010). Using all the three-components of motion gives the possibility to retrieve information about the propagation of the Rayleigh waves (vertical and radial processing direction) as well as of the Love waves (transversal direction).

As in the case of the previous methods, the ambient vibration recordings are treated statistically by subdividing the traces in sub-windows. For each consecutive window a separated f-k analysis is performed, and the results are then averaged over the whole recording, increasing the robustness of the final estimation.

A) 2-4Hz

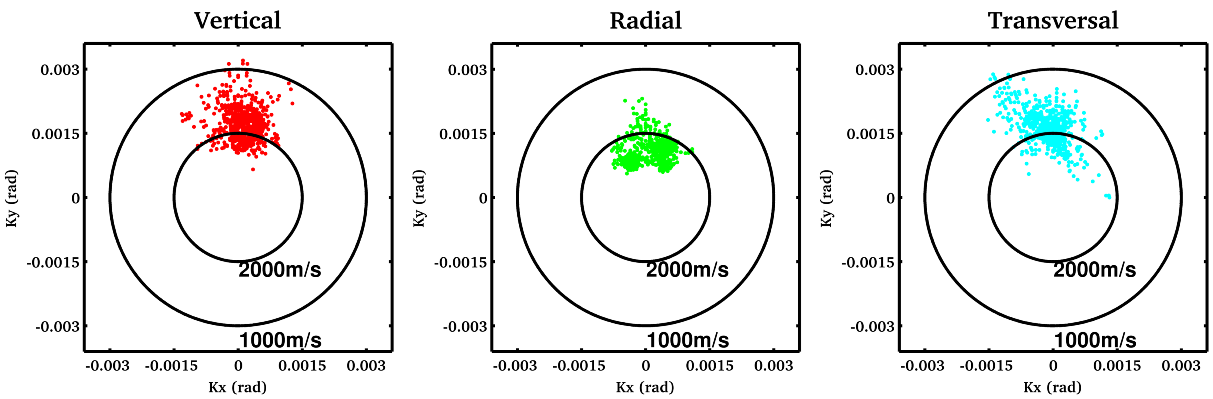

B) 4-8Hz

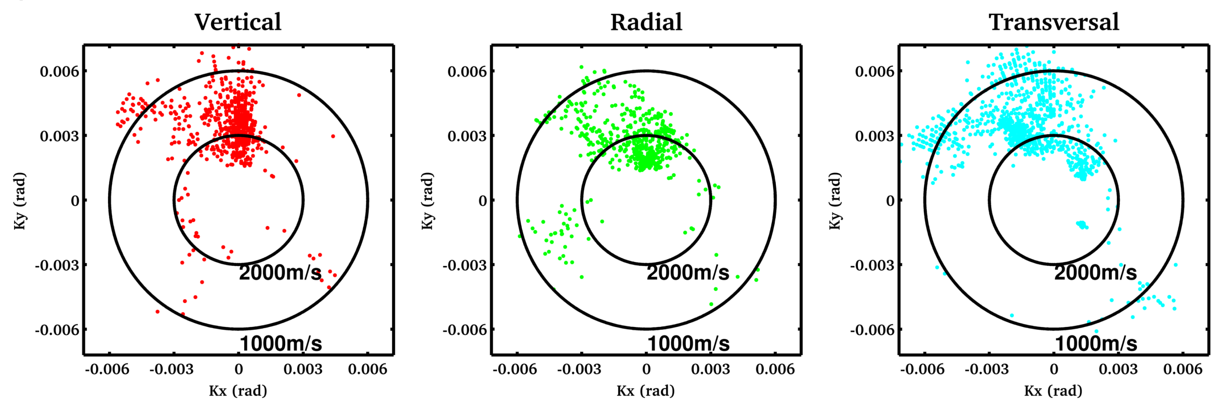

Figure 11 - *Example of distribution of noise sources in the low (2-4Hz) and intermediate frequency range (4-8Hz) obtained from three-component f-k analysis. The source distribution is strongly directional for all the propagation components.*

As first step, from the f-k analysis it is possible to assess the noise source azimuthal distribution over different ranges of frequencies (e.g. **Figure 11**) separately for the vertical, the radial and the transversal direction of polarization. From the analysis of the two geometries A1 and A2, source distribution appears to be strongly directional (anisotropic) in all the components, with major contribution from North. This condition is surprisingly rather stable on the whole analyzed frequency range, but has no direct explanation in terms of settlement location or local geomorphology.

As a second step, the surface-wave dispersion curves are extracted by visual inspection and manual picking of the f-k density plots (**Figure 12** and **Figure 13**), separately for the three polarization direction. Similar, but not identical results have been obtained for the two array configurations. In particular, Love wave dispersion can be well tracked in a broad frequency range (from 3~4Hz to about 20Hz) from both A1 and A2; velocity estimates are also consistent between the two geometries. Rayleigh wave dispersion is of more difficult to interpret. The vertical component shows indications of two modes, whose interpretation is quite clear on A2 (fundamental plus first higher mode), but doubtful on A1. Moreover, Rayleigh velocities are slightly mismatching between the two arrays configurations. This might be induced by the proximity of the two modes and the relatively high velocities of propagation, which can produce biased results especially when using small geometries. For this reason, the final interpretation of Rayleigh modal pattern is mostly based on the results from A2. Complementary, radial component processing confirms the presence of the first higher mode of Rayleigh waves, extending it to lower frequencies and higher velocities.

A summary of all the identified modes from vertical, radial and transversal direction of propagation is presented in **Figure 14**, while the final interpretation of Rayleigh and Love wave dispersion pattern is in **Figure 15**. The dispersion pattern is typical for a gradient velocity profile, with progressive decrease of velocity with increasing frequency.

10. Inversion of the dispersion curves

The surface wave dispersion curves (Rayleigh and Love) obtained from the three-component f-k analysis of the ambient vibrations are inverted to obtain an estimation of the velocity profile of the site (mainly S-wave velocity as function of depth, and to a lesser extend the P-wave velocity, due to the lower sensitivity). The analysis is performed using the software *Dinver* (www.geopsy.org), which implements a direct search approach (**Figure 16**) based on a conditional version of the neighborhood algorithm (Sambridge, 1999).

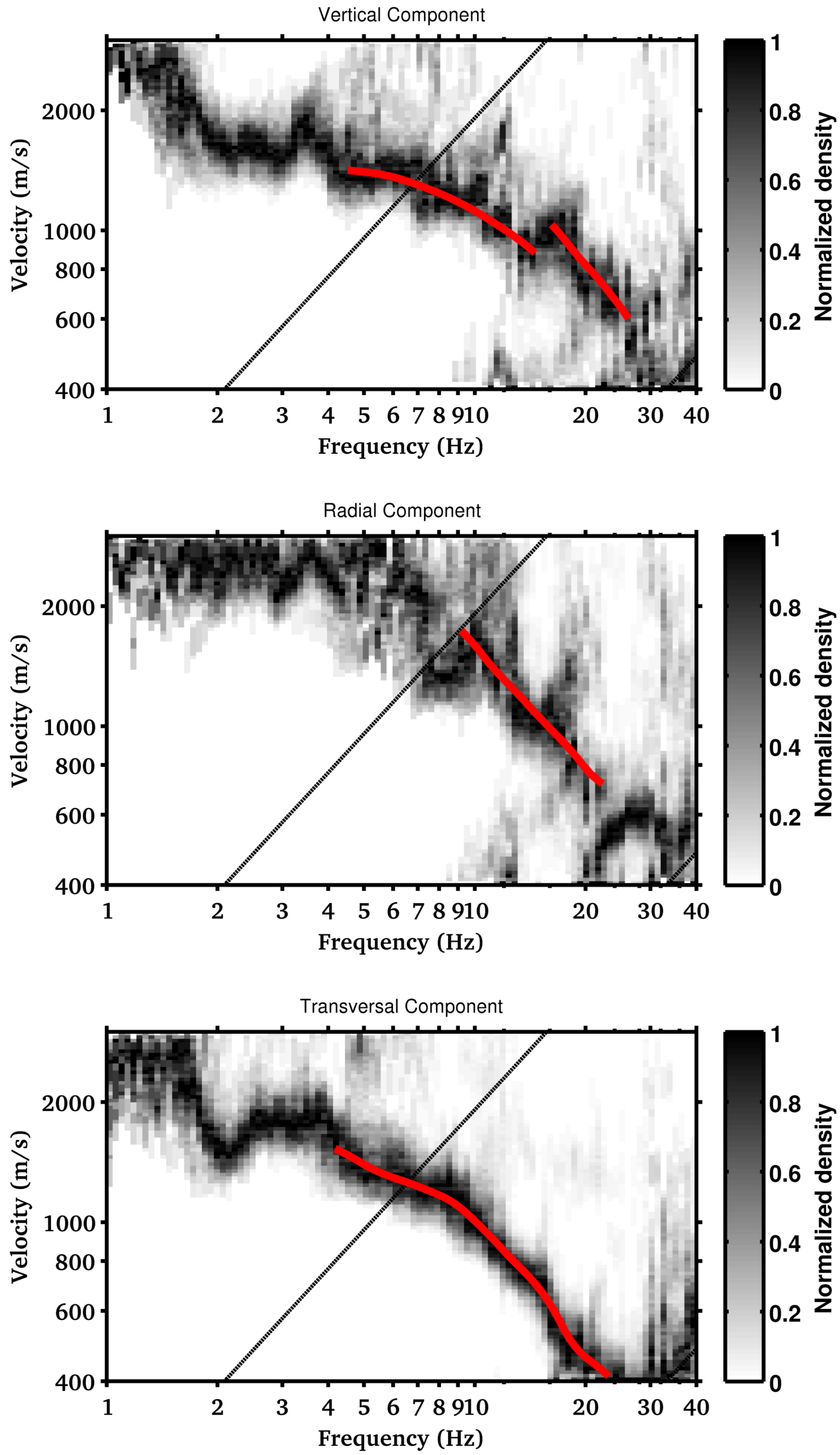

Figure 12 - *Density distribution of the surface wave signals obtained from the recording of the array configuration A1 using three-component f-k analysis. From top to bottom: Rayleigh vertical, Rayleigh radial and Love wave dispersion. In red the interpreted dispersion curves are given (manually selected).*

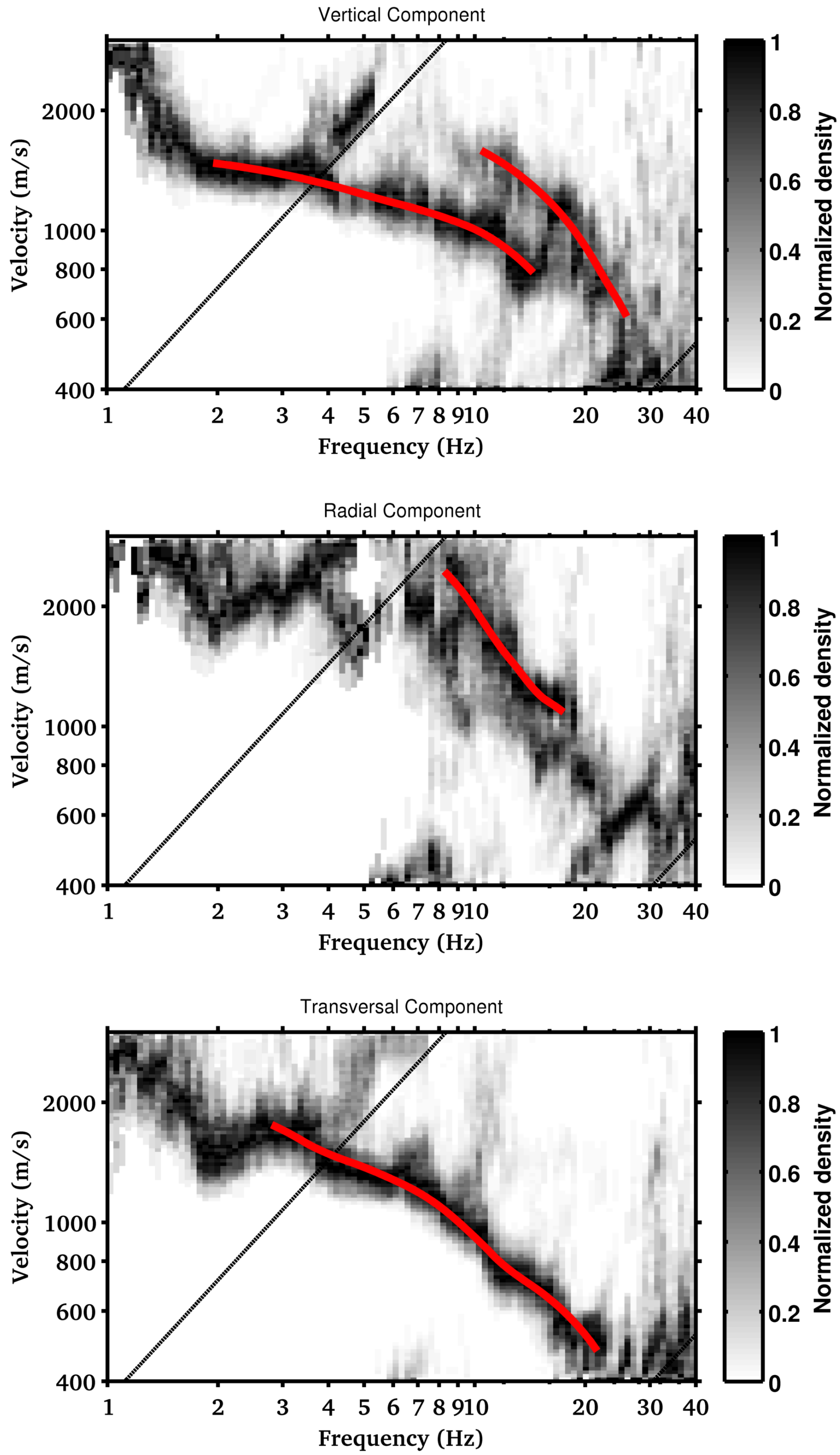

Figure 13 - *Density distribution of the surface wave signals obtained from the recording of the array configuration A2 using three-component f-k analysis. From top to bottom: Rayleigh vertical, Rayleigh radial and Love wave dispersion. In red the interpreted dispersion curves are given (manually selected).*

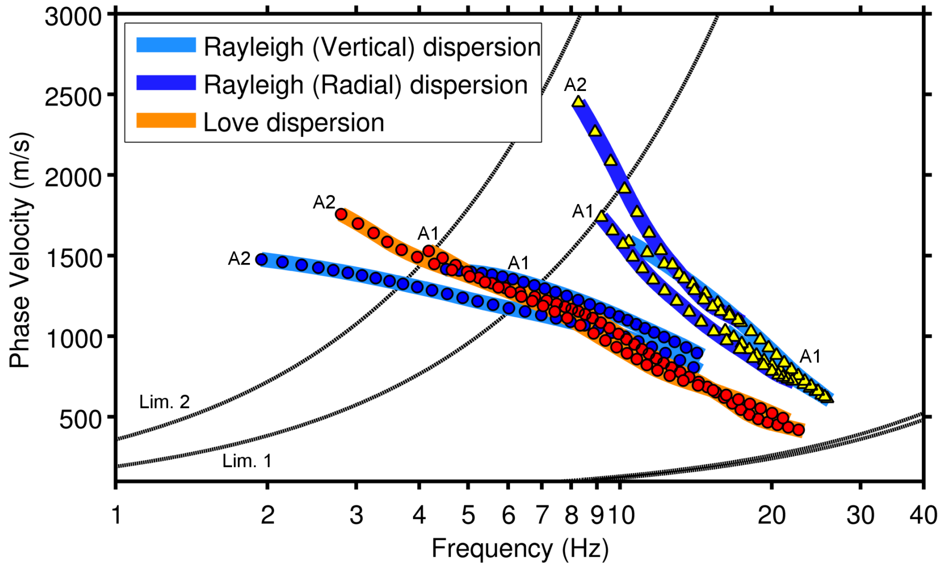

Figure 14 - *Summary of all dispersion curves obtained from three-component f-k analysis of the two array configurations A1 and A2. Minimum and maximum resolution bounds from the two geometries are indicated with black solid lines.*

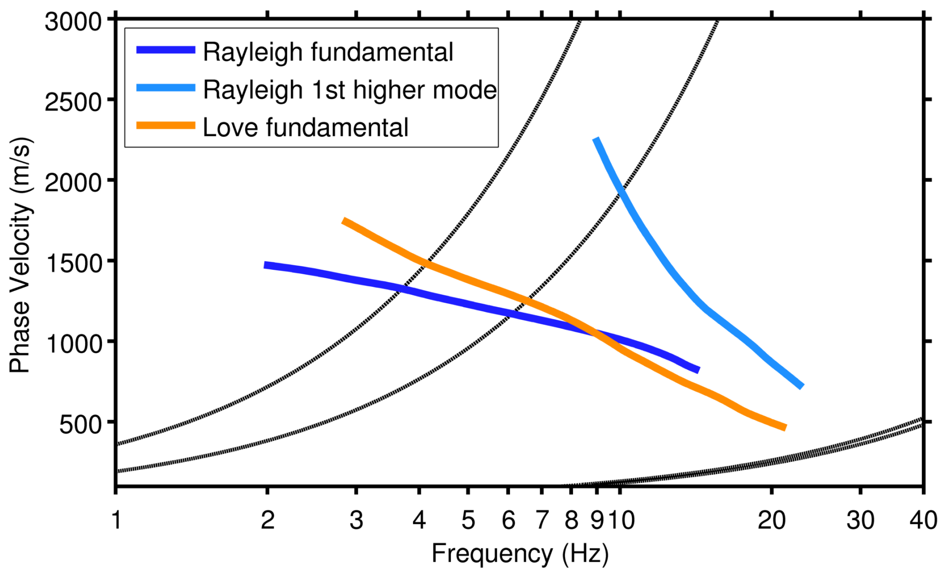

Figure 15 - *Final interpretation of the Rayleigh and Love dispersion curves for WALHA. Minimum and maximum resolution bounds from the full array are indicated with black solid lines.*

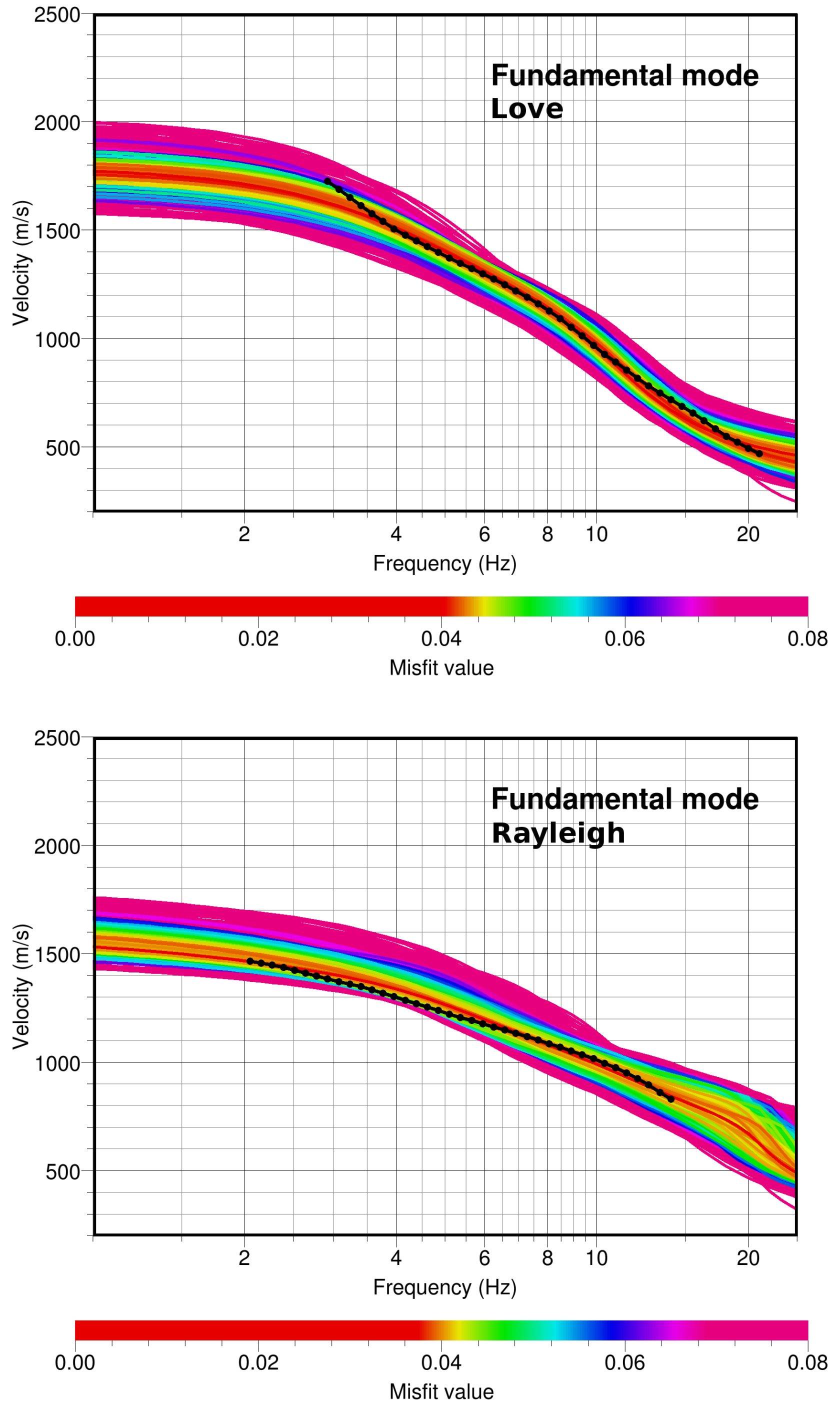

Figure 16 - *Fitting the surface dispersion data within the global optimization procedure; in this example, the Rayleigh and Love fundamental modes. Different colors represent different misfit between the observed (in black) and the modeled dispersion curves during the search.*

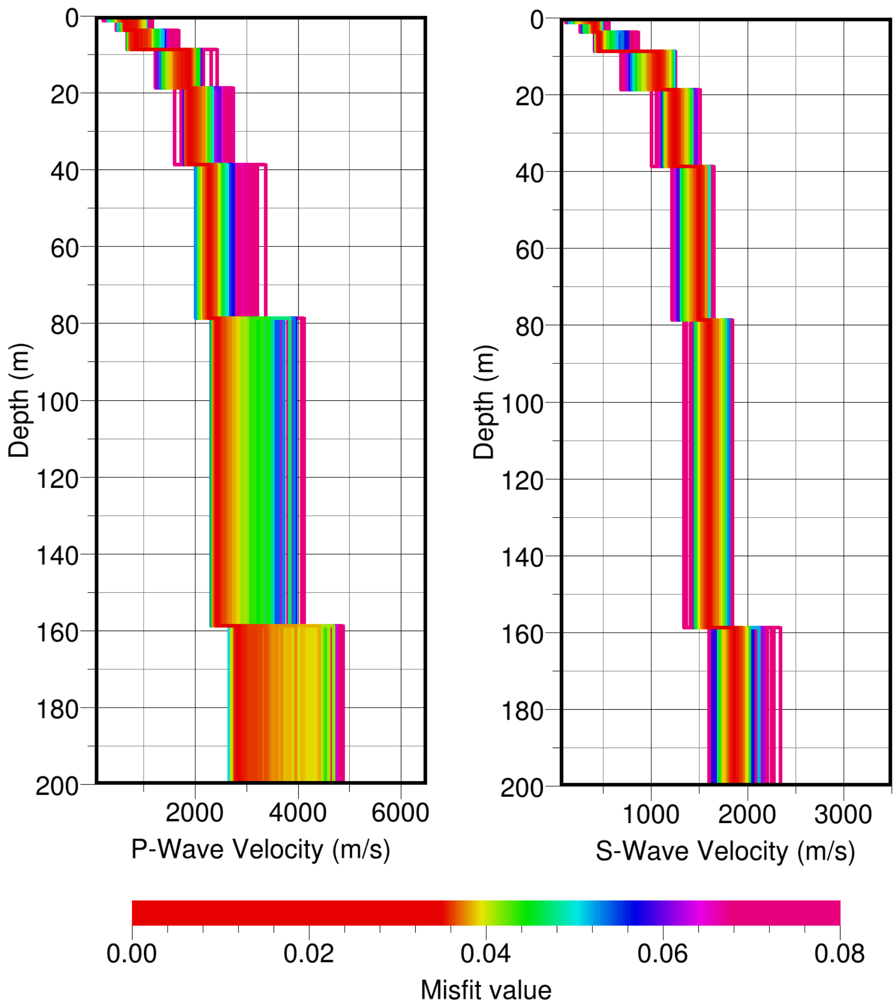

Figure 17 - *Distribution of the fix-layer velocity models generated during the inversion process and ordered by decreasing misfit, according to the color scheme of* **Figure 16***.*

To parameterize the velocity model, two different approaches were implemented. The first one consisted in setting up an eight-layer model with fix interface depths (**Figure 17**). In such a case the free inversion parameters are then the velocities (P and S) and layer thicknesses. In the second case, a free-thickness layer approach was used (**Figure 18**). The advantage of the former method stays in the possibility to better resolve sharp velocity interfaces, while the second is less unique and better constraints the seismic velocity. The two approaches have to be nevertheless considered complementary, and they should provide consistent results. Ten inversion tests (*runs*) were performed for each of the two model schemes, in order to minimize the effect related to a possible unfavorable initial randomization of the parameter space. The best fitting model from of each run was then collected (**Figure 19** and **Figure 21**) and used later on for the computation of the derived soil parameters.

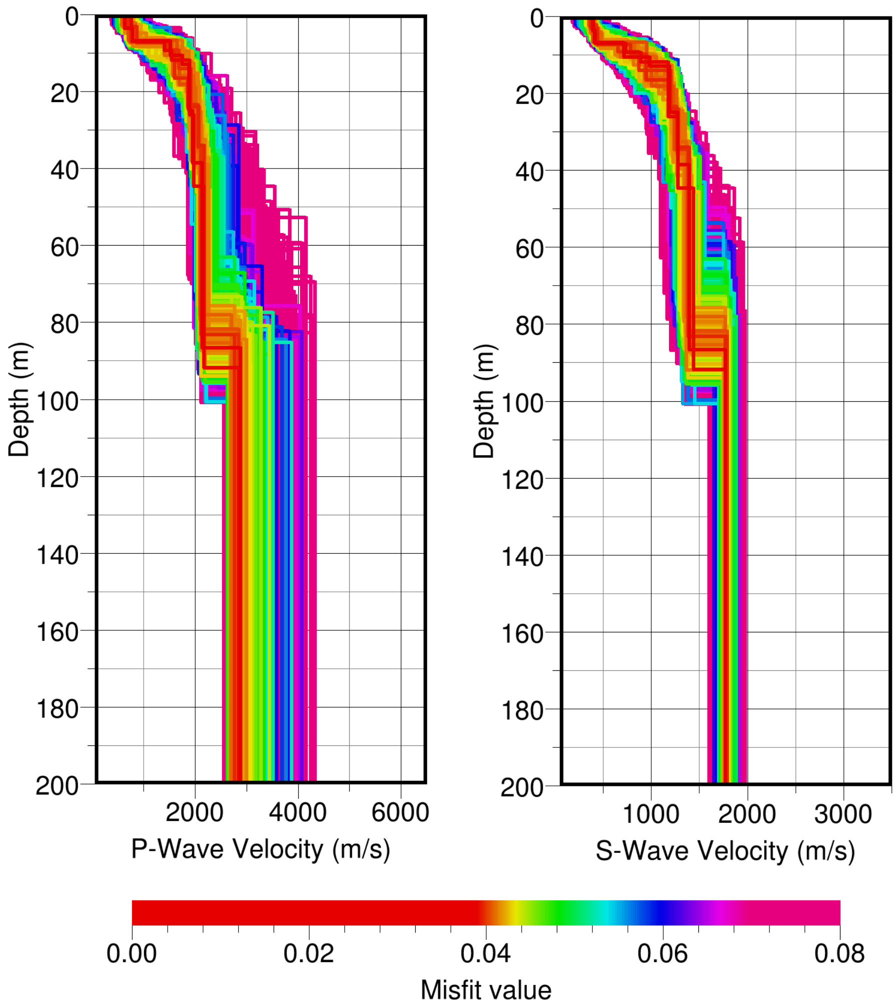

Figure 18 - *Distribution of the free-layer velocity models generated during the inversion process and ordered by decreasing misfit, according to the color scheme of* **Figure 16***.*

In more detail, the inverted velocity models (Vs and Vp) are gradient-like, with a faster increase in velocity in the first 20m, followed by a smoother part. This is generally expected for a rock velocity profile. The uppermost velocities of the profile, however, are not directly constrained by the data (**Figure 20**), because of the lack of information at high frequencies, and might be underestimating the true values for the topmost 10m. By considering the minimum available frequency of the surface-wave dispersion curves, and by analyzing the scattering of the inverted models (**Figure 21**), it is realistic to assume the velocity profiles to be reliable down to a depth of about ~120m. Below this value no direct constrain is available from f-k analysis, and the velocity values are obtained by pure extrapolation.

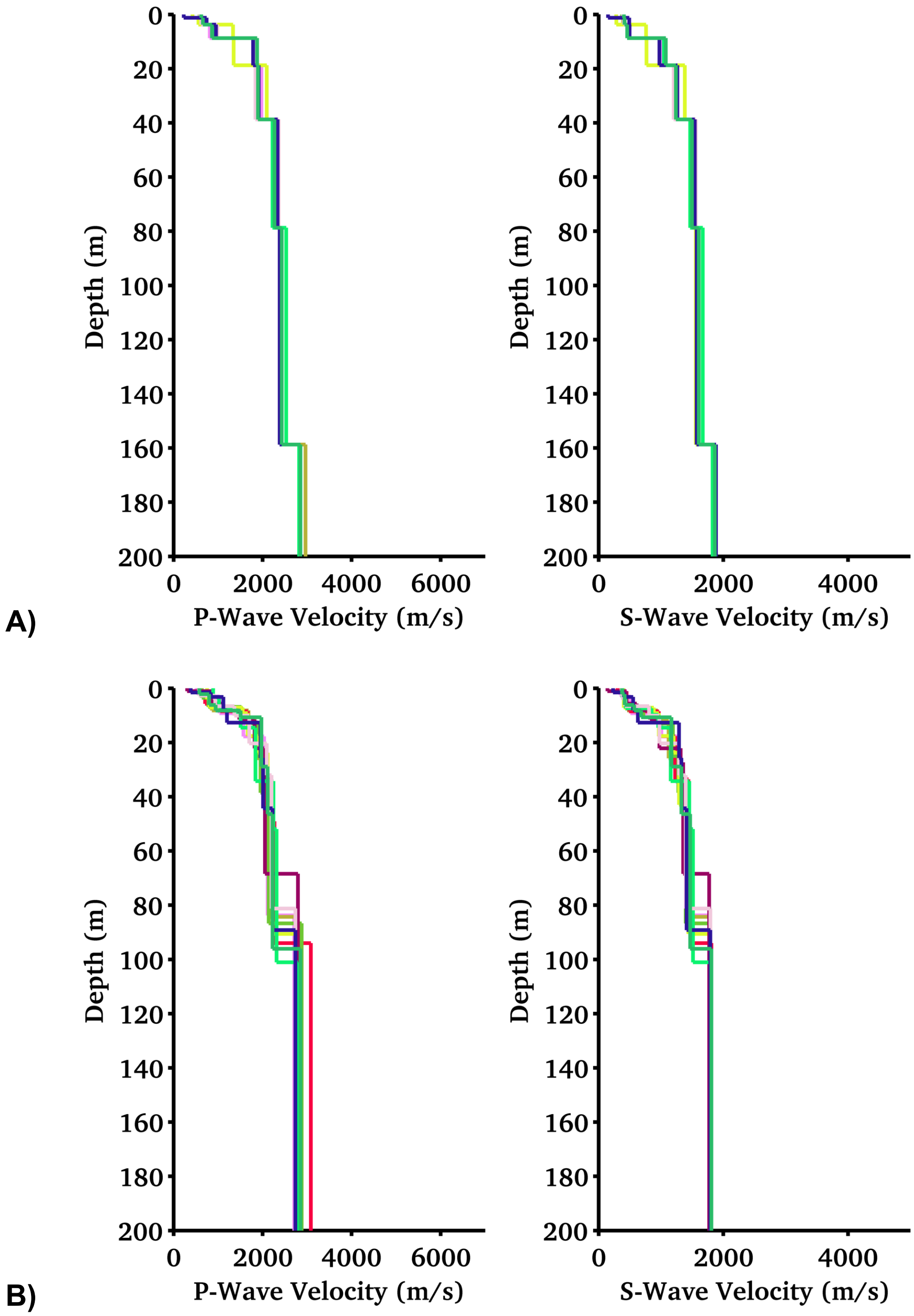

Figure 19 - *Collecting the best fitting models from the ten separated inversion runs using the free-layers (A, top) and fixed-layers (B, bottom) parameterization schemes.*

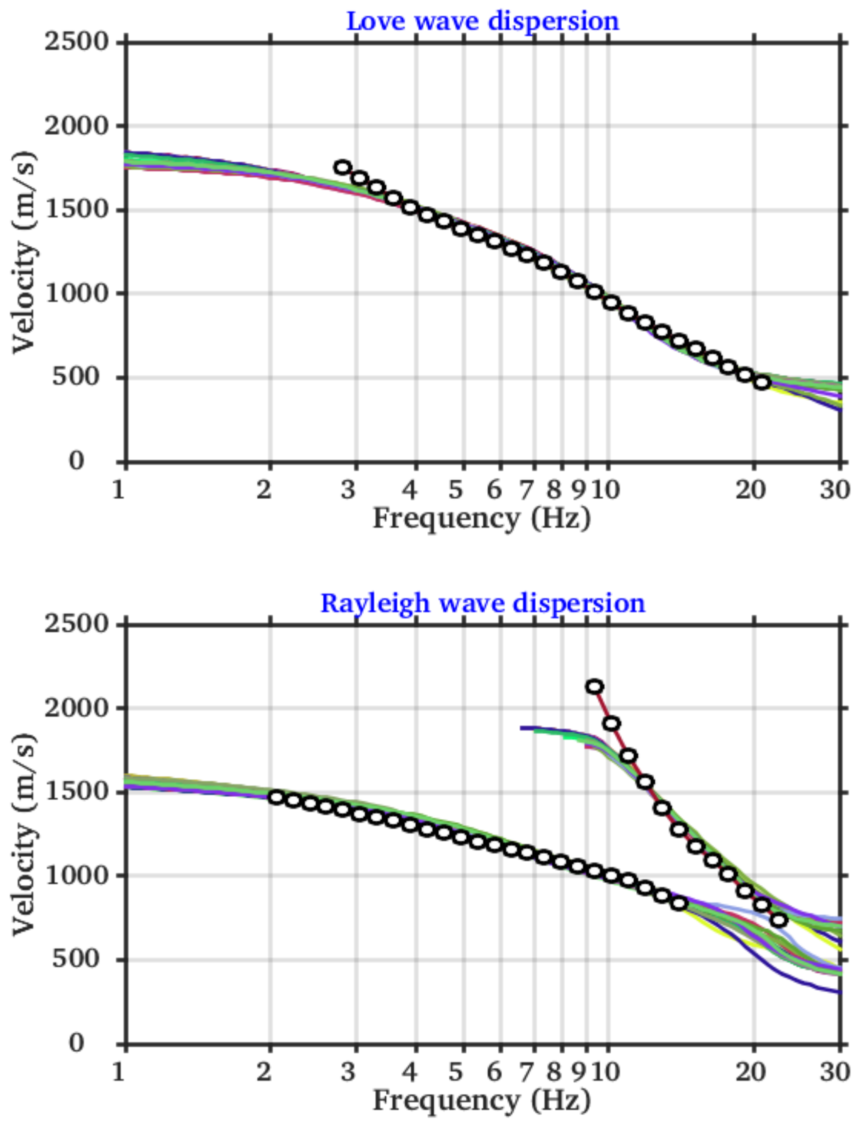

Figure 20 - *Rayleigh and Love dispersion curves computed from the 20 best fitting models of the two proposed interpretation schemes (free and fix layers). Fitting is good for both components, including the Rayleigh waves first overtone.*

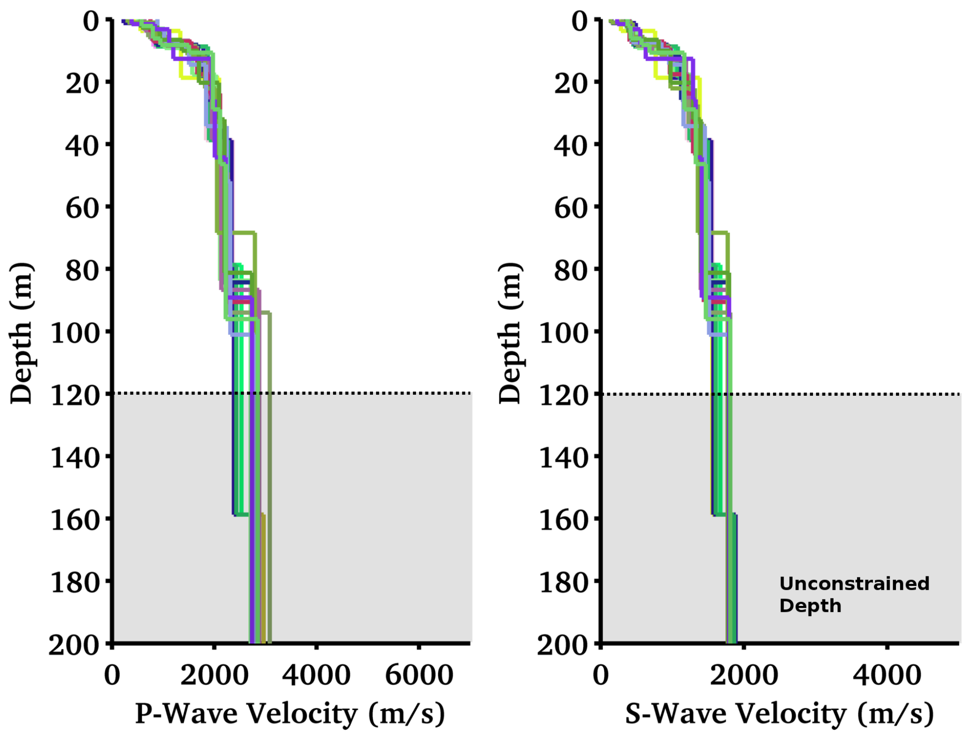

Figure 21 - *Comparison of all the best models from the two parameterization schemes (free and fixed layers). The two approaches produce consistent results. The depth of about 120m is considered approximately the maximum resolved depth.*

11. Engineering soil parameters

The ensemble of all the best inverted velocity profiles is then used to derive average soil parameters like the VsZ (average travel-time S-wave velocity over the depth Z, including Vs30, Table 1) and the quarter-wavelength (QWL) average velocities (Joyner et al., 1984) for a range of frequencies between 0.6 and 30Hz (**Figure 22**). The former is a standard parameter for the classification of ground-types in most building codes and in ground motion prediction equations. The latter is a parameter useful for the empirical estimation of the site-response and to assess the sensitivity of the seismic wave-field to the different depths. It has to be noticed that these two parameters are derived separately from all the best S-wave velocity models obtained from the inversion, and the results is finally averaged to improve statistics.

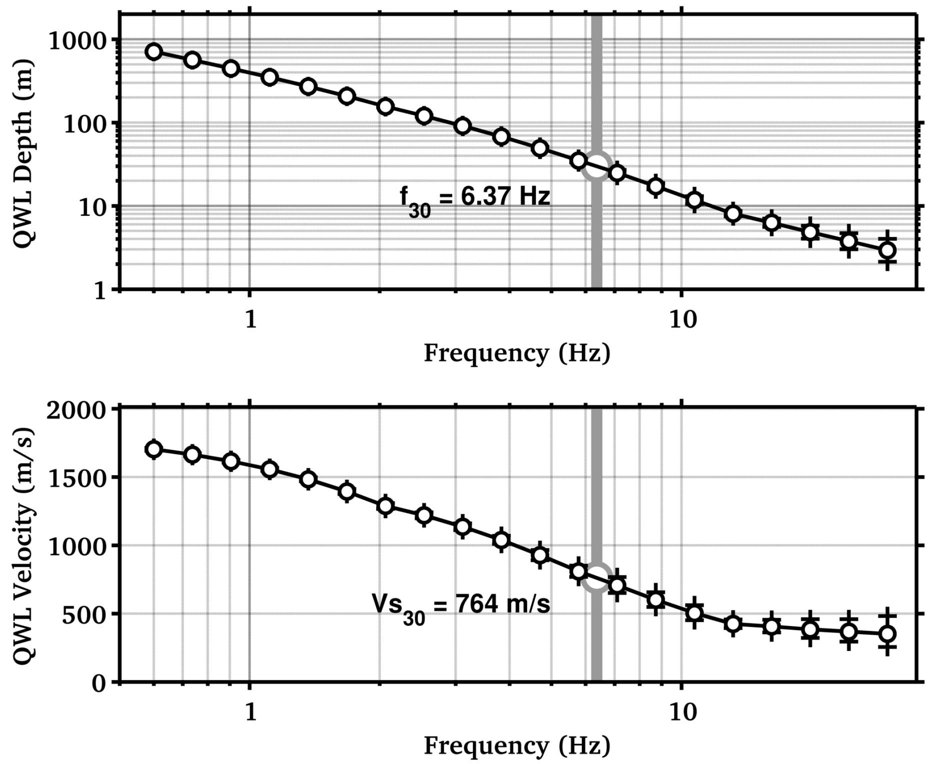

Figure 22 - *Quarter-wavelength representation of the inverted S-wave velocity profiles. Top: the depth-frequency dependency. Bottom: the QWL average velocity. The Vs30 value is indicated with its corresponding QWL frequency.*

12. Amplification models

Site amplification functions have been computed using two different approaches: the S-wave transfer function for vertical propagation and the quarter-wavelength amplification. In general the first method is used to evaluate the resonance characteristics of the site, while the second is more useful to assess the effect of the velocity contrasts between the lowermost rock layer (as reference) and the different QWL averaging depths. The two amplification functions are then corrected for the Swiss rock reference velocity profile as defined in Poggi et al. (2011), according to the procedure described in Edwards et al. (2013). Given the lower velocities in the uppermost part of the WALHA profile compared to the Swiss reference, the final corrected amplification function shows a lower average amplification level at high frequencies than the uncorrected (**Figure 23**).

Averaging depth (m)	Vs-mean (m/s)	St.Dev.
5	397.9305	38.9636
10	464.1567	21.22431
15	566.8519	26.29674
20	642.1789	30.5964
25	711.1462	28.47808
30	**766.062**	**26.13665**
40	851.3006	22.23505
50	933.7835	20.88589
75	1072.414	18.39015
100	1165.622	16.90059
150	1278.679	16.51862
200	1380.971	14.02402

Table 1 - *Average travel-time velocities at different depths. Vs30 is highlighted.*

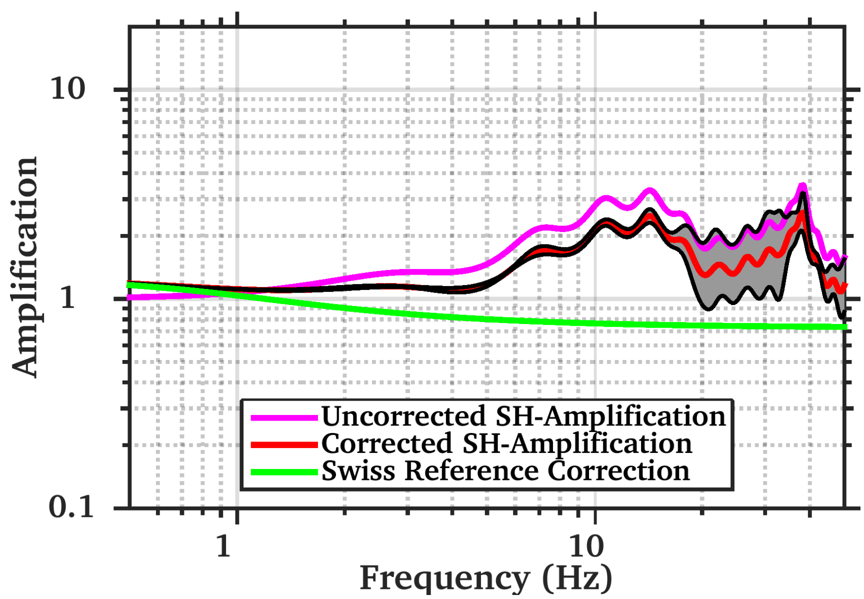

Figure 23 - *Correcting the SH-wave transfer function for the Swiss (rock) reference conditions (Poggi et al. 2011). The final corrected amplification function shows a lower (average) amplification at high frequencies than the uncorrected.*

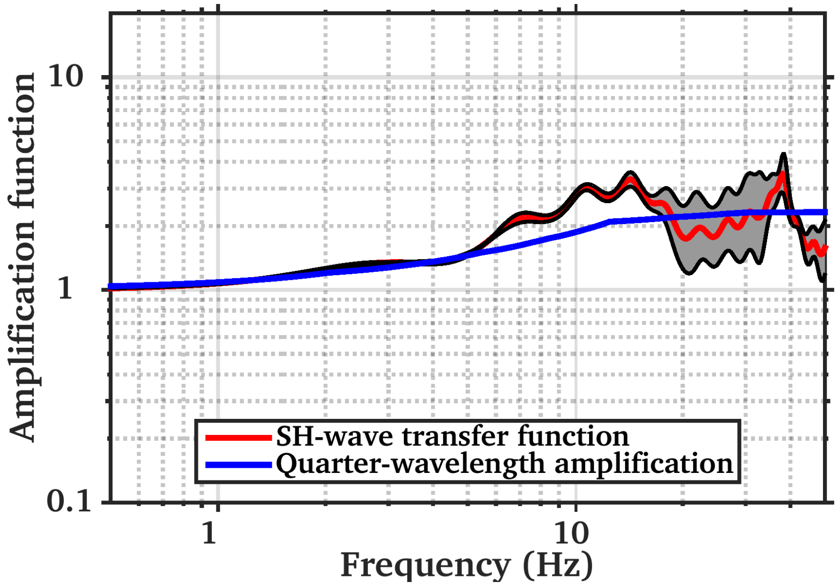

Figure 24 - *Comparison of amplification functions computed using the SH-wave transfer function and the quarter-wavelength formalism on the inverted velocity models.*

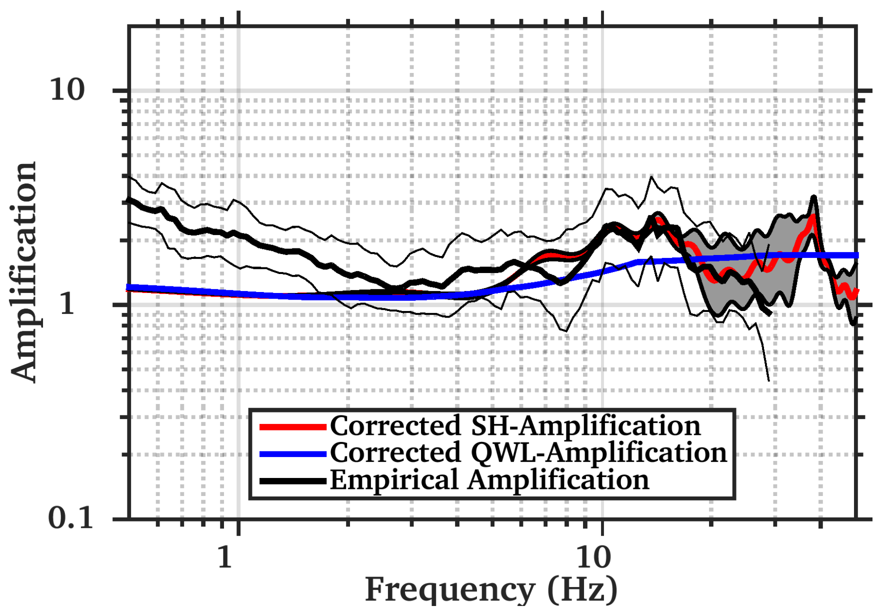

Figure 25 - *Comparison of amplification functions computed using the SH-wave transfer function and the quarter-wavelength approach with empirical observation from spectral modeling of low-magnitude earthquakes. All functions are referenced to the Swiss rock reference model (Poggi et al. 2011).*

Amplification functions using the transfer function and the quarter-wavelength approach are comparable (**Figure 24**), even if the transfer function provides a slightly larger amplification, because of the presence of some weak resonance peaks. At low frequencies both methods converge to the same amplification level. It has to be notice that the amplification functions do not include attenuation at this stage of the analysis, as the quality factors of the site are unknown.

A good matching is obtained by comparison between the one-dimensional transfer function and the empirical amplification from spectral modeling of low-magnitude earthquakes as described in Edwards et al., 2013 (**Figure 25**). Resonance peaks are mostly well reproduces by analytical solution, even though empirical amplification presents a positive shift at low frequency, which cannot be explained by the available data.

REFERENCES

Capon, J., 1969. High resolution frequency wavenumber spectrum analysis, Proc. IEEE, 57, 1408-1418.

Burjanek, J., G. Stamm, V. Poggi, J.R. Moore, and D. Fäh [2010], “Ambient vibration analysis of an unstable mountain slope”, Geophys. J. Int., Vol. 180, pp. 820-828.

Edwards, B., C. Michel, V. Poggi and D. Fäh (2013). Determination of Site Amplification from Regional Seismicity: Application to the Swiss National Seismic Networks. Accepted for publication in Seismological Research Letters.

Joyner, W. B., R. E. Warrick and T. E. Fumal (1981). The Effect of Quaternary Alluvium on Strong Ground Motion in the Coyote Lake, California, Earthquake of 1979, Bulletin of the Seismological Society of America, 71, 1333-1349.

Poggi, V., B. Edwards and D. Fäh (2011). Derivation of a Reference Shear-Wave Velocity Model from Empirical Site Amplification, Bulletin of the Seismological Society of America, 101, 258-274.

Poggi, V. and Fäh D., 2010. Estimating Rayleigh wave particle motion from three-component array analysis of ambient vibrations. Geophys. J. Int., 180-1, 251-267.

Eidgenössische Technische Hochschule Zürich
Swiss Federal Institute of Technology Zurich

SED
Schweizerischer Erdbebendienst
Swiss Seismological Service

Report on site characterization

Emmingen, Germany (EMING)

Poggi Valerio, Donat Fäh

Last modified - 24 / 12 / 2014

1. Introduction

In the framework of the NAGRA seismic network project, an array measurement of the ambient vibration wave-field was performed at the location of the SED station EMING (Emmingen, Germany). The scope of the survey is the seismic characterization of the area surrounding the installation (**Figure 1**), which consists in a broadband seismometer (Trillium Compact) with a high-resolution digitizer (Taurus 24Bit @200sps). Ambient vibration analysis has been used to infer the characteristics of the underground structure of the site, with special regard to the one-dimensional shear-wave velocity. Such profile is later used to assess the local seismic response of the station.

For the analysis, different spectral analysis techniques were implemented, consisting in both single and array methods, which are listed below:

- Time-frequency wavelet analysis
- Power-spectral density estimation
- Conventional horizontal to vertical spectral ratios
- Directional horizontal to vertical spectral ratios
- Wavelet polarization analysis
- Three-component high-resolution f-k analysis.

The results of all these analyses conformed to the definition of the final velocity model. In the following, the main results of these investigations are summarized and a final interpretation of the velocity profile is given. From this interpretation, engineering parameters are finally derived, e.g. the Qwl-Vs average velocity, VsZ (including Vs30) and the seismic amplification from the analytical SH-transfer function of the one-dimensional soil column.

2. Survey description

To characterize the seismic response of the site, an array measurement of ambient vibration was performed on 14/08/2014 (**Figure 1**). The array consists of three concentric measuring configurations (called “rings”, R1, R2 and R3) of 11 sensors each and increasing diameter (about 40m, 100m and 200m respectively). The three configurations were planned to partially overlap, with the aim of providing a continuous frequency resolution between the geometries. Configuration R1 recorded for a total of 40m, while configuration R2 for 1h and R3 for 2h30m. The differences in the recording length are due to the different resolution characteristics of the three geometries. As a general rule, larger arrays require longer recording time to produce a reasonable statistics of the ambient vibration processing results. Satisfactory results were obtained from the analysis of the first and last geometry. The second ring did not produce usable results, for reasons later explained. For the larger configuration, a penetration depth of about ~150m was initially expected.

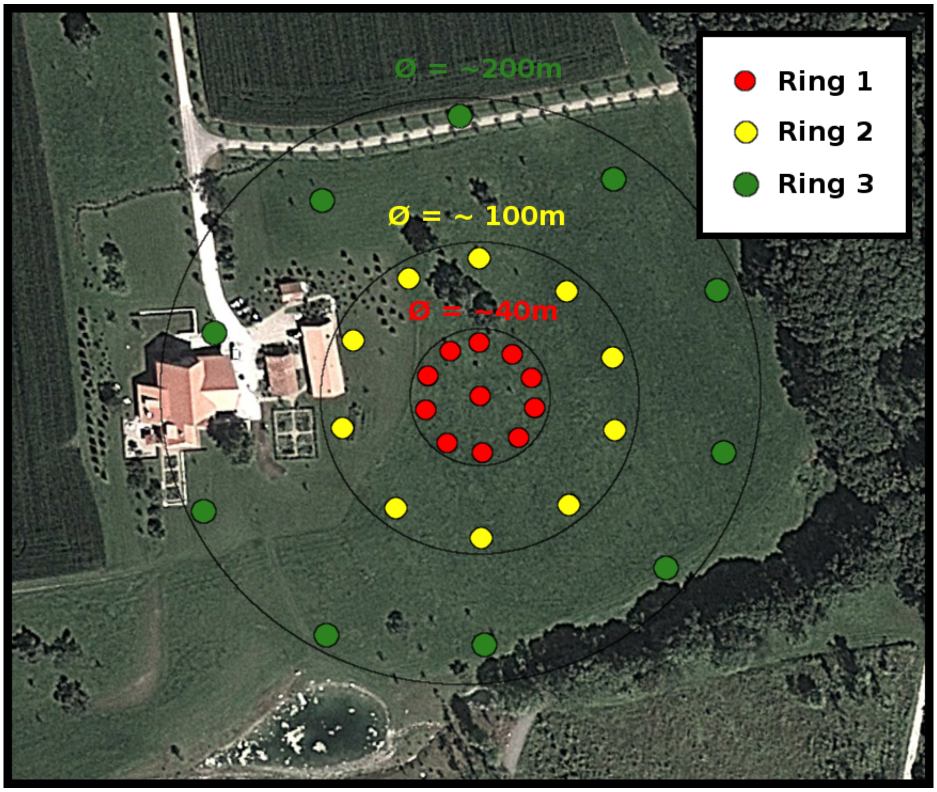

Figure 1 - *Location of the ambient vibration array survey performed in Emmingen (SED station EMING) on 14/08/2014. Three concentric configurations of increasing diameter were implemented (named R1, R2 and R3).*

3. Weather conditions

The weather conditions were good during great part of the measurement, with no precipitations an average temperature of 20 degrees. Some wind was experience during the acquisition of the third ring, as evident from recordings.

4. Soil type, topography and geology

The array has been set in open field conditions, in a rural area (**Figure 1**, **Figure 3**). The influence of buildings and anthropogenic disturbances is virtually negligible. Array sensors have been deployed on free soil. Good coupling with the ground was assured by means of digging small holes at the sensor's places, and by using a special support (*Trihedron*®) that facilitates the leveling of the device even for difficult soil conditions. The measurement area was located on a nearly flat area, and therefore no topographic correction was necessary before processing. The only relevant topographic issue was the presence of a narrow stream valley at the southern edge of the array.

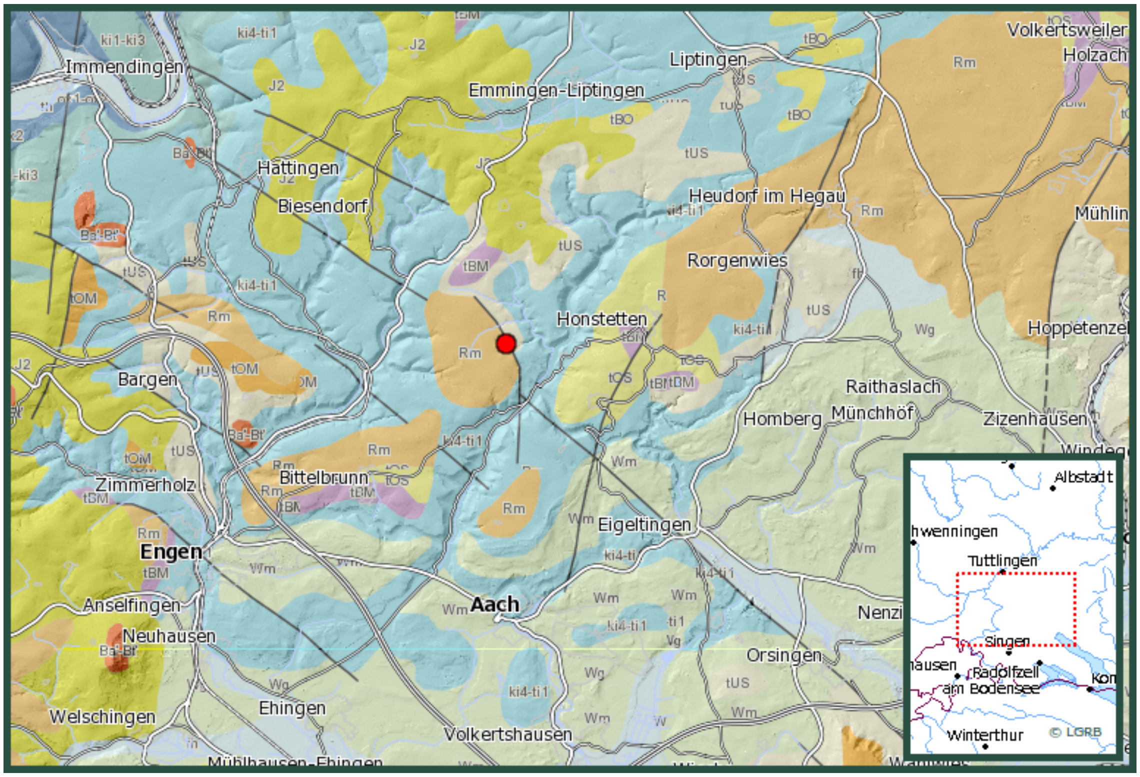

Figure 2 - *Geological map of the measuring area, in the surroundings of Emmingen (reproduced from Geological Atlas LGRB, Baden-Württemberg, modified). In red, the approximate location of the permanent station EMING.*

From the geological points of view (**Figure 2**) the target area sits on bedded limestone and cemented marls of Jurassic age (Kl4-tl1). Geological map shows that calcareous bedrock is in many areas outcropping, but discontinuously covered by spots of Tertiary Molasse sediments (lower Süsswassermolasse, tUS) and Quaternary moraine deposits (Rm). By visual survey, the surface morphology is considerably smooth and modeled by the action of glaciers during the Pleistocene. The station is likely located on top of a morainic deposit. Geophysical bedrock is never exposed at the target site, but likely shallow. A variable-thick cover of quaternary soil material is generally present. Such site can be classified as of rock ground-type A.

5. Acquisition equipment

Each acquisition point within the array consisted of a three components seismometer (Lennartz 3C with 5s eigenperiod) and a 24 bit data logger (Quanterra Q330). Synchronization between stations was assured by standard GPS, while a more accurate differential GPS (Leica Viva system) was used to precisely locate the sensor's coordinates with a tolerance of less than 5cm.

Figure 3 - *Overview of the measurement area taken from the central station of the array (EMN01). SED station EMING is located in background, close to the trees.*

6. Pre-processing and preliminary data-quality control

The three-component recording has been filtered prior to analysis using a band-pass 6^{th} order causal Butterworth filter with corners at 0.2Hz and 50Hz. Although it is not a strict requirement for spectral analysis techniques, such filtering was applied in order to facilitate the preliminary visual inspection of the noise traces and to evaluate the coherency of the wave-field (**Figure 4**). Such procedure gives essential information for the subsequent interpretation of the f-k analysis results.

To assess the quality of the ambient vibration recordings, spectral analysis was subsequently performed. Because of the stochastic nature of the ambient vibration wave-field, a statistical approach has to be used, such as the estimation of the power spectral density (*PSD*). This approach is useful to evaluate the average energy level of the recordings in the analyzed frequency range, and to access the presence of spurious spectral peaks, which might be related to human activity (machinery, pumps). By inspecting the PSD of all the three-component recordings of the array in the range between 0.5 and 40Hz, it is found that the average energy level of the spectrum fits well within the minimum and maximum bounds of the USGS noise model (**Figure 5**), with a progressive increase of energy at high frequency, although no significant peaks of possibly anthropogenic origin are visible.

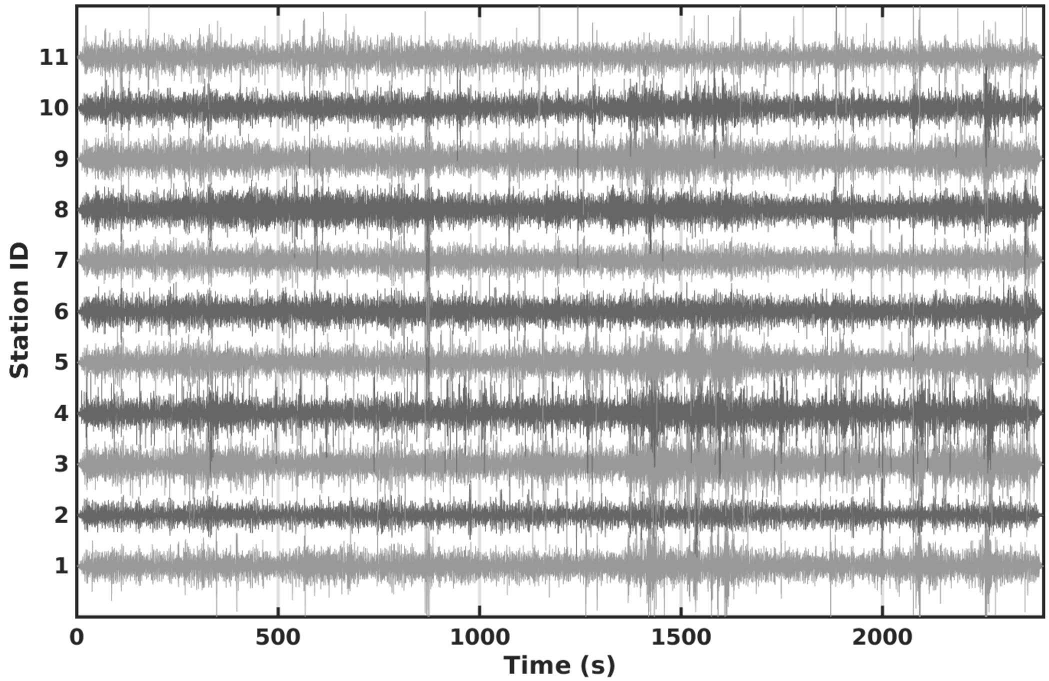

Figure 4 - *Inspection of the useful part of the ambient vibration recording of the Emmingen array (here configuration R1). A certain amount of short high-frequency transients were present during the acquisition, which nevertheless did not bias the subsequent f-k processing results.*

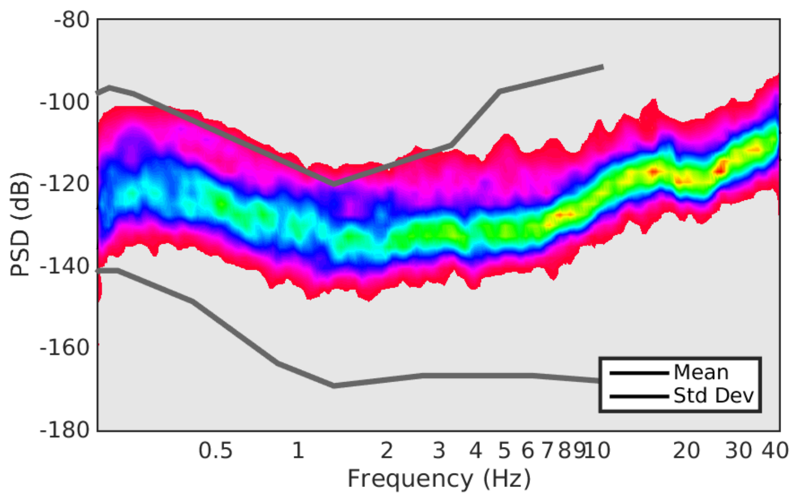

Figure 5 - *Power spectral density (PSD) computed for 40m recording at the central station of the array configuration R1, horizontal direction N-S. Similar results were obtained for the other stations of the array. In gray lines are the minimum and the maximum bounds of the USGS noise model, for comparison.*

Complementary to the aforementioned statistical methods, a spectral decomposition approach is more suitable to assess the stationarity of the ambient vibration wave-field over time. The wavelet time-frequency analysis was then performed over the whole recording time. From such analysis (**Figure 6**) an overall stability of the ambient-vibration wave-field over time is evident. No relevant harmonic signals can be identified in the frequency band useful for the processing, with the exception of a minor contribution at around 20Hz (nevertheless not always present over the whole recordings) and the 50Hz power line effect. These contributions won't likely affect the following processing steps.

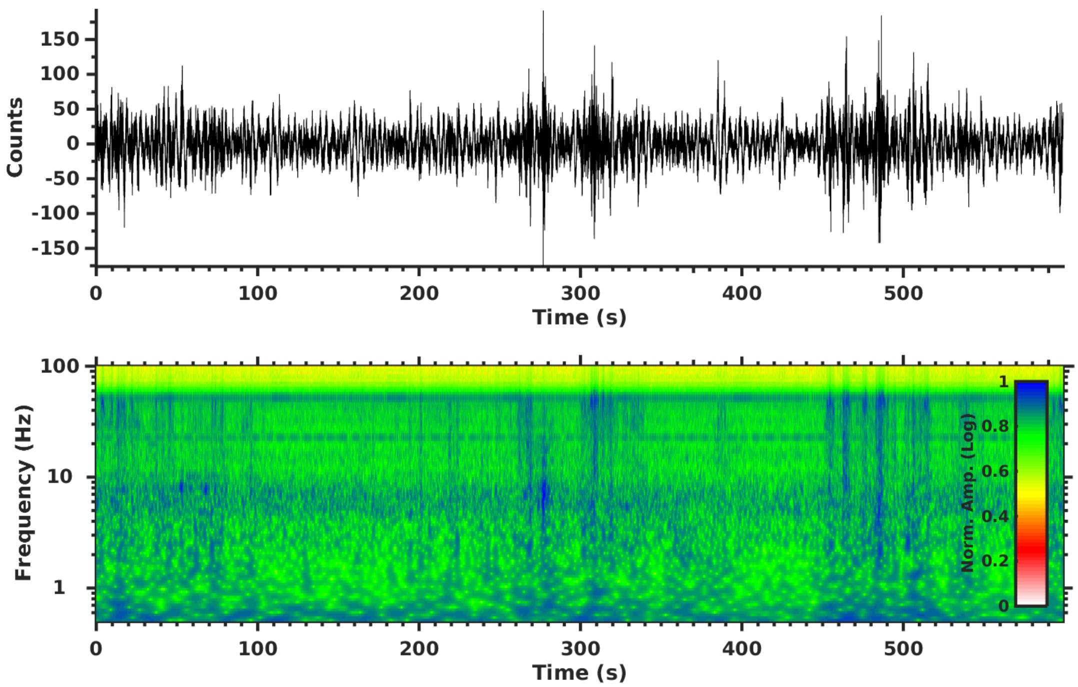

Figure 6 - *Example of spectrogram from 600s of recording of the central station (EMN01) of the array configuration R1, component N-S. No significant harmonic disturbances are visible on the whole spectrogram. Similar results were found for the other components. For the analysis, the cosine wavelet is used (wavelet parameter = 12).*

7. Conventional H/V spectral ratios

The horizontal-to-vertical (H/V) Fourier spectral ratio is a technique widely used in seismic site characterization because of its ability to provide an estimate of the SH wave fundamental frequency of resonance (f_0) of the site. Other than that, H/V ratios are useful to provide information on the Rayleigh wave ellipticity function, which can be used in surface wave dispersion inversion procedures to constrain large velocity contrasts at depth. In this study, we use the H/V technique also to map the variability of the subsoil structure along the investigated area; this is necessary to verify the fulfillment of the 1D structure assumption, which is necessary for the f-k method applied later.

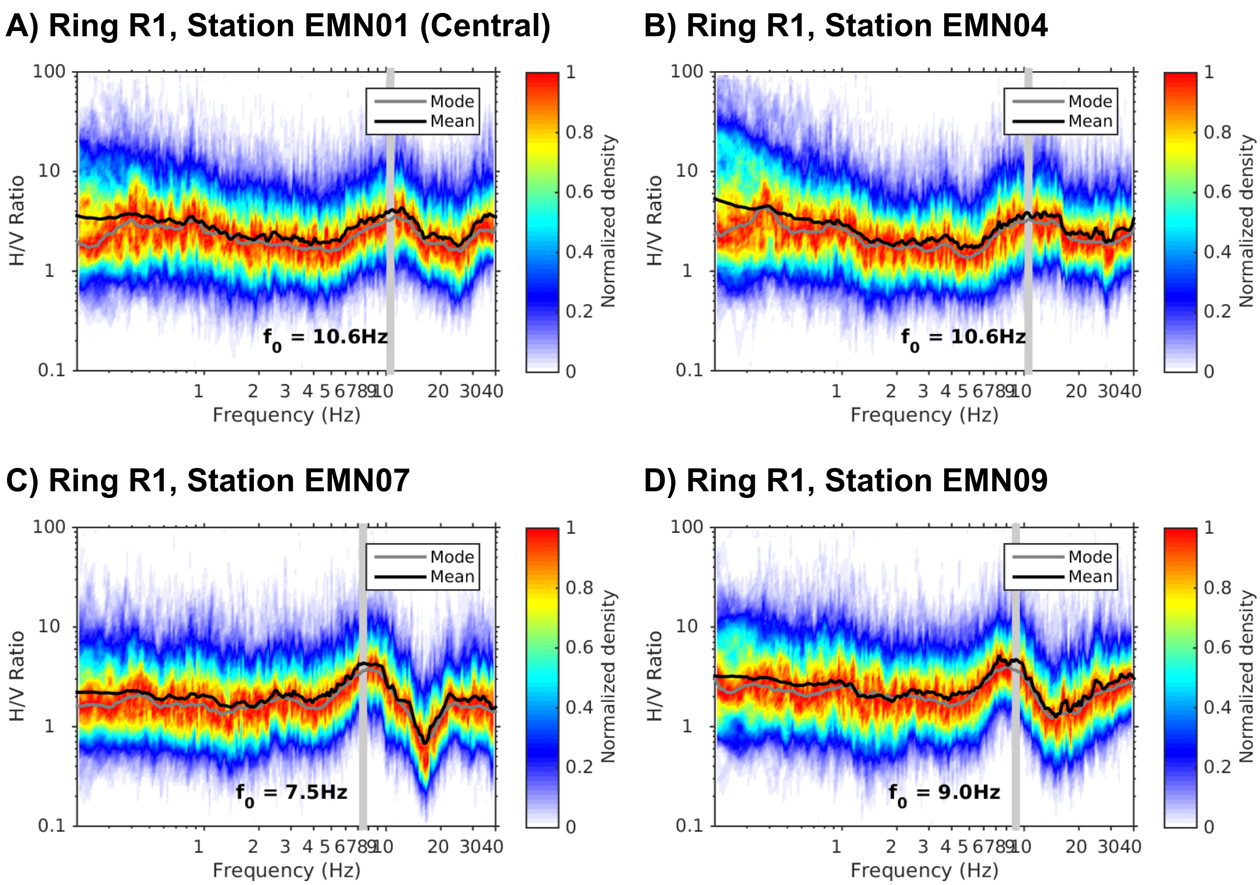

Figure 7 - *Example of H/V spectral ratios for the configurations R1. The resonance frequency of the soil cover is indicated with a light gray line (between about 7 and 11Hz). A very minor peak is visible at about 1Hz (better resolved on the average H/V curve of* **Figure 8***), however of more questionable interpretation.*

H/V spectral ratios have been computed for all the recordings at each station of the array and separately for configurations R1, R2 and R3 (e.g. **Figure 7**). The behavior of the noise wave-field at the different stations location is comparable at low to intermediate frequencies (roughly < 9Hz), while the high frequency region shows some variability, within and between array rings. This is likely due to variability of the top layer, which can be very heterogeneous over the measuring area. Only two stations from the larger configuration (close to the river) exhibited some significant difference with respect to average H/V ratio curves. However, removing these stations from the subsequent processing had no significant impact on the quality of the processing results. Such dissimilarity could then be interpreted as the effect of variability in the local sources, other than heterogeneities in soil conditions.

In average (**Figure 8**), spectral curves show a relatively stable high frequency peak (around 9Hz). Such maximum is likely induced by the presence of shallow bedrock, sheltered by a sediment cover of much lower velocity. An additional peak might be present at very low frequencies (around 1Hz), however of more questionable interpretation. We assume the high frequency peak as the fundamental frequency of the site. The behavior of the site can be considered laterally homogeneous for the f-k analysis.

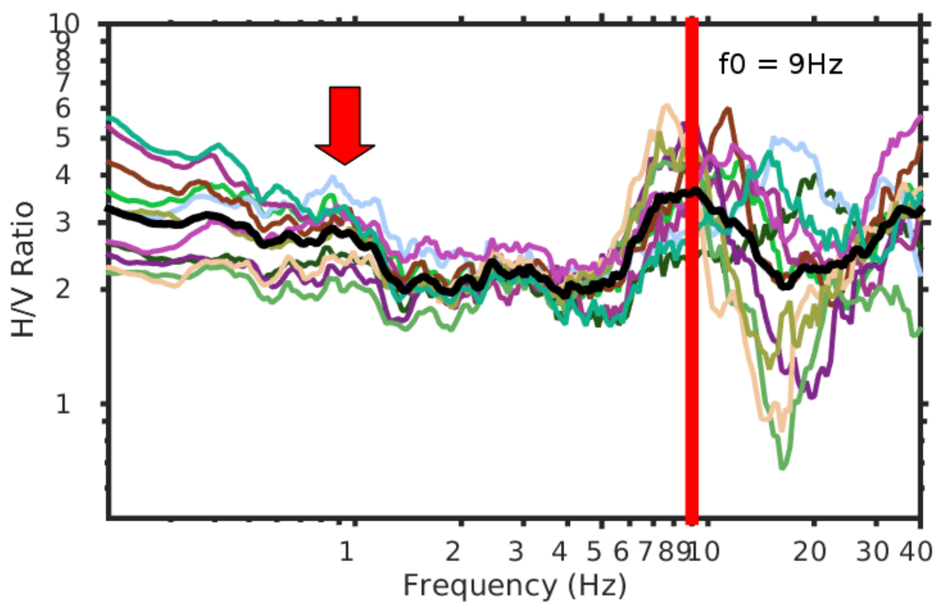

Figure 8 - *Comparison of the H/V spectral ratio curves of all the stations of the array (in this example for the array configuration R1). The curves are generally stable at low frequencies, confirming the lateral homogeneity of the underlying bedrock velocity structure of the site. High frequencies (> 10Hz) show more variability. The average fundamental peak of resonance is at about 9Hz.*

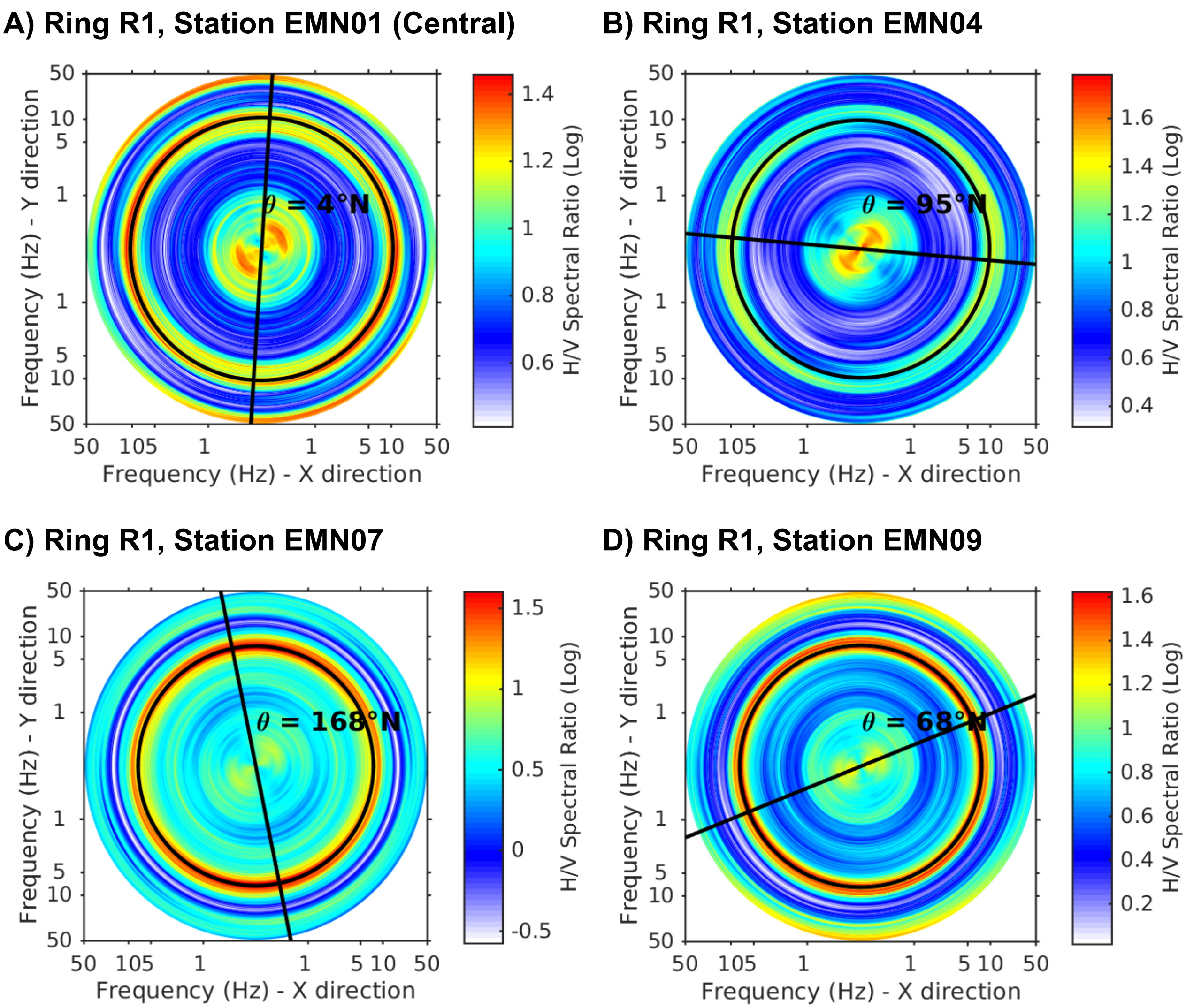

Figure 9 - *Example of directional H/V spectral ratios for configuration R1. No preferential direction of the resonance peak - as well as no evidence of wave-field anisotropy - is present.*

8. Directional analysis

The computation of directional H/V spectral ratio or polarization analysis is useful to reveal asymmetries in the ambient vibration wave-field. Different effects can induce such a behavior: 2D/3D structure, topographic effects or a non-homogeneous distribution of the noise sources. If a strong directionality is found by the analysis, it is generally recommended to carry out further investigations to properly address the origin of polarization. By processing the directional H/V ratios at all the recording stations of the two arrays (e.g. **Figure 9**) it is possible to observe an overall isotropy of the wave-field in the whole analyzed frequency range. In particular, the fundamental frequency peak at about 9 Hz does not show any preferential directionality pattern between the different station locations.

The results of the H/V directional analysis are confirmed by applying the wavelet polarization analysis technique (Burjanek et al., 2008). Here, the particle motion shows to be mostly elliptical, with a significant polarization only at the resonance frequency (**Figure 10**), nevertheless without any sign of azimuthal anisotropy (**Figure 11**A).

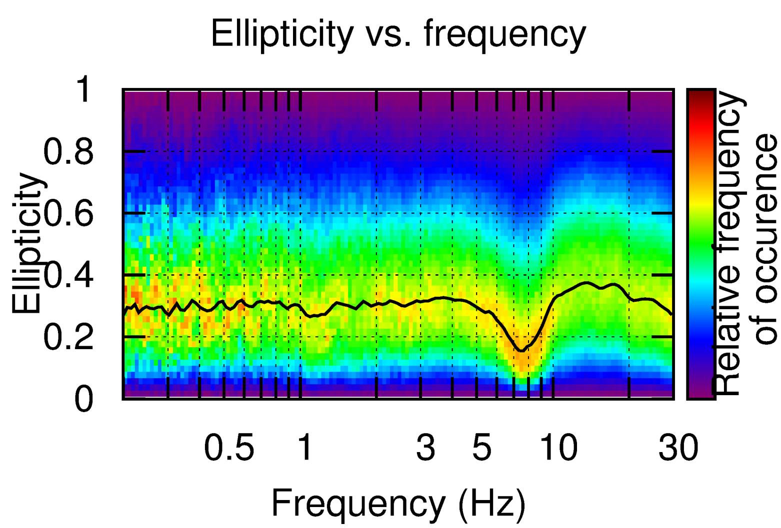

Figure 10 - *Ellipticity of the particle motion from wavelet-based polarization analysis at the central station of the array (EMN01). Similar results can be obtained for other stations of the arrays.*

A)

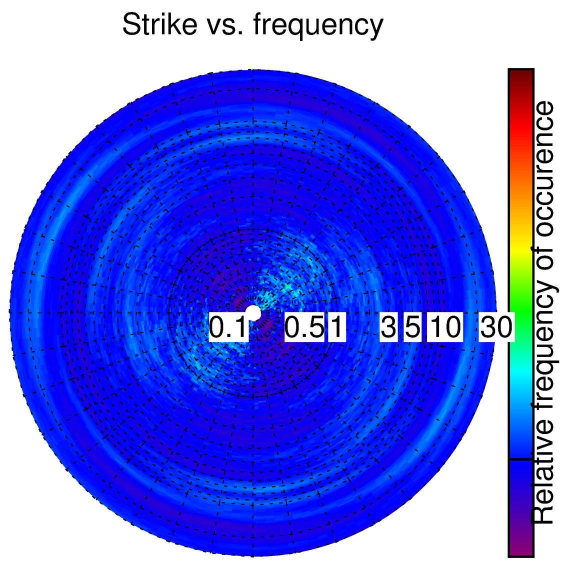

B)

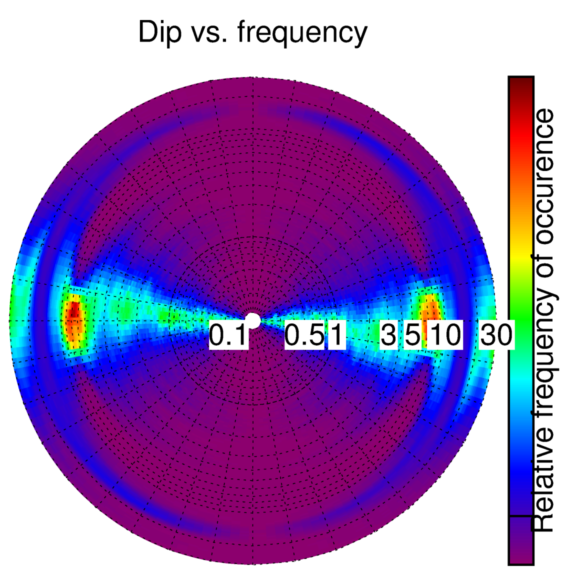

Figure 11 - *Directionality of the particle motion from wavelet-based polarization analysis (dip direction in B, strike in A) at the central station of the array (EMN01). Similar results can be obtained for other stations of the arrays.*

9. Three-component f-k analysis

The frequency-wavenumber analysis is a spectral technique based on seismic array recordings that allows retrieving direction and dispersion characteristics of the surface waves. We apply this technique to three-component ambient vibration recordings using a modification of the high-resolution method of Capon (1969) as described in Poggi et al. (2010). Using all the three-components of motion gives the possibility to retrieve information about the propagation of the Rayleigh waves (vertical and radial processing direction) as well as of the Love waves (transversal direction).

As in the case of the previous methods, the ambient vibration recordings are treated statistically by subdividing the traces in sub-windows. For each consecutive window a separated f-k analysis is performed, and the results are then averaged over the whole recording, increasing the robustness of the final estimation.

A) Ring 3, 5-10Hz

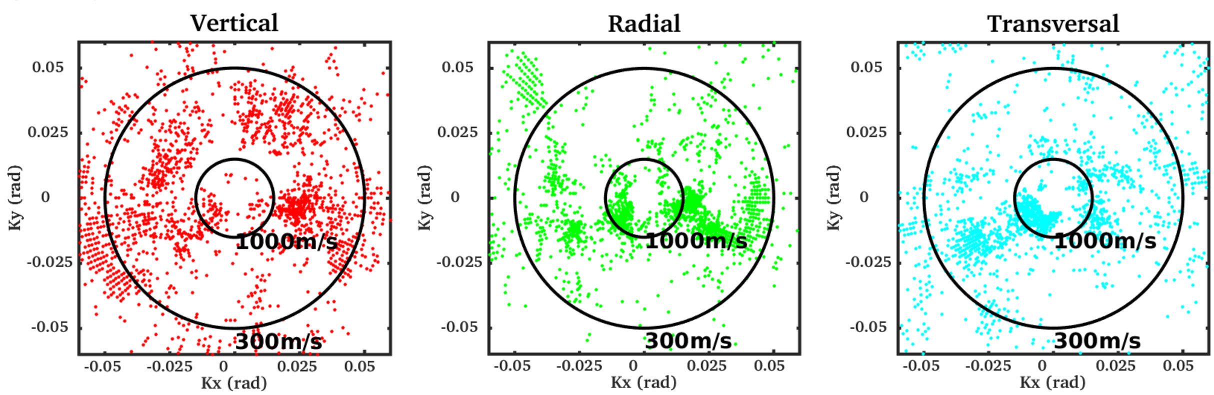

B) Ring1, 10-20Hz

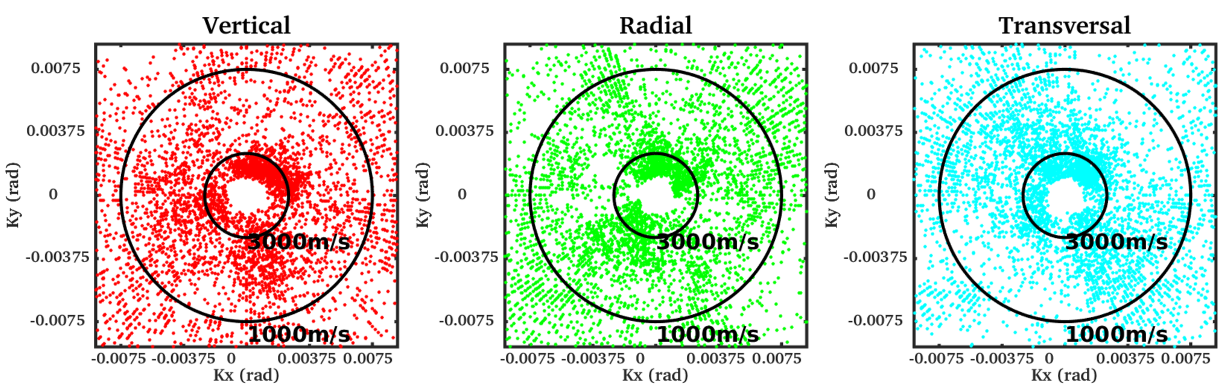

Figure 12 - *Example of distribution of noise sources in the low (5-10Hz) and high frequency range (10-20Hz) obtained from three-component f-k analysis. The source distribution is irregular but not strictly directional on all the propagation components.*

As first step, from the f-k analysis it is possible to assess the azimuthal distribution of noise sources over different frequency ranges (e.g. **Figure 12**) separately for the vertical, the radial and the transversal direction of polarization. From the analysis of the three geometries R1, R2 and R3, source distribution appears to be quite homogeneous in all the components, without displaying a clear directional pattern.

As a second step, the surface-wave dispersion curves are extracted by visual inspection and manual picking of the f-k density plots (**Figure 13** and **Figure 14**), separately for the three polarization directions. Complementary results have been obtained for the array configurations R1 and R3, while R2 did not produce usable results for reasons not yet clarified, but supposedly related to some lack of energy of the surface waves in the intermediate frequency range (as subsequently explained).

In particular, Love wave's fundamental mode dispersion can be well tracked in the frequency range between about 8Hz and 20Hz. Even though the picked dispersion curves present a discontinuity between the two geometries, velocity estimates are quite consistent, which allows extending the mode interpretation from R1 to R3. Same behavior is visible for the Rayleigh wave's fundamental mode, with the additional complication that the high frequency part is visible only on the radial component of R1, while the low frequencies are obtained from the vertical of R3. In a fist attempt we regarded such behavior as a modal jump. However, this hypothesis was later rejected because of incompatibility with the Love component during the inversion process. The running explanation is therefore a simple exchange of energy between vertical and radial directions in the vicinity of the frequency gap (9~10Hz).

A summary of all the identified modes from vertical, radial and transversal direction of propagation is presented in **Figure 15**, while the final interpretation of Rayleigh and Love wave dispersion pattern is in **Figure 16**.

10. Inversion of the dispersion curves

The surface wave dispersion curves (Rayleigh and Love) obtained from the three-component f-k analysis of the ambient vibrations and the fundamental frequency of resonance (f_0) from average H/V spectral ratios are inverted to obtain an estimation of the velocity profile of the site (mainly S-wave velocity as function of depth, and to a lesser extend the P-wave velocity, due to the lower sensitivity). The analysis is performed using the software *Dinver* (www.geopsy.org), which implements a direct search approach (**Figure 17**) based on a conditional version of the neighborhood algorithm (Sambridge, 1999).

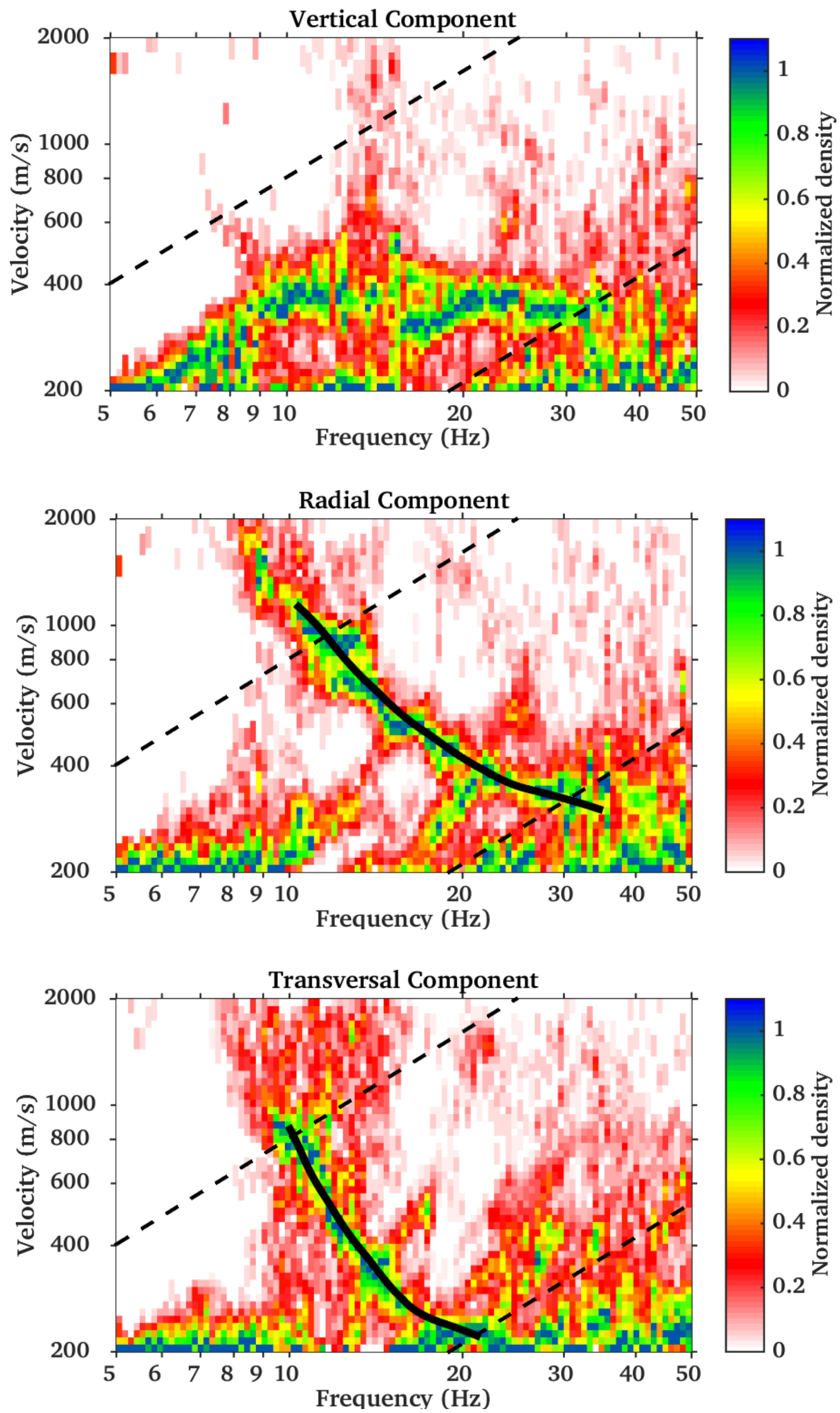

Figure 13 - *Density distribution of the surface wave signals obtained from the recording of the array configuration R1 using three-component f-k analysis. From top to bottom: Rayleigh vertical, Rayleigh radial and Love wave dispersion. In black the interpreted dispersion curves are given (manually selected).*

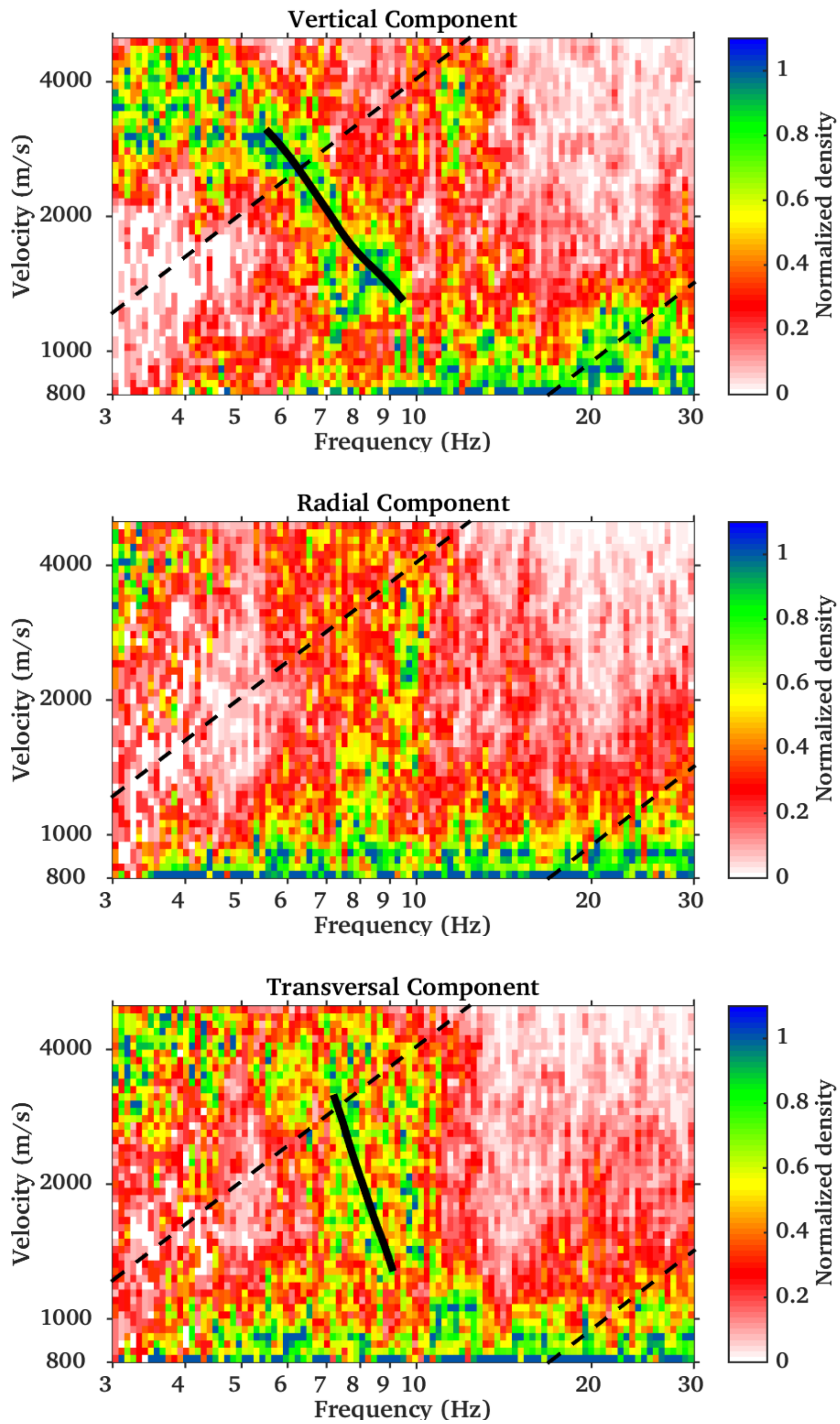

Figure 14 - *Density distribution of the surface wave signals obtained from the recording of the array configuration R3 using three-component f-k analysis. From top to bottom: Rayleigh vertical, Rayleigh radial and Love wave dispersion. In black the interpreted dispersion curves are given (manually selected).*

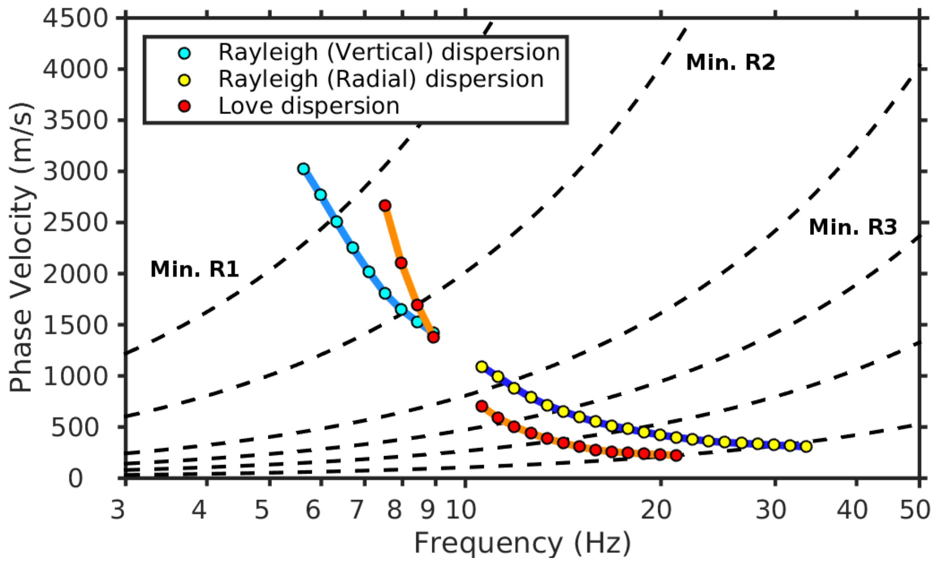

Figure 15 - *Summary of all dispersion curves obtained from three-component f-k analysis of the array configurations R1 and R3. Minimum and maximum resolution bounds from the two geometries are indicated with black dashed lines.*

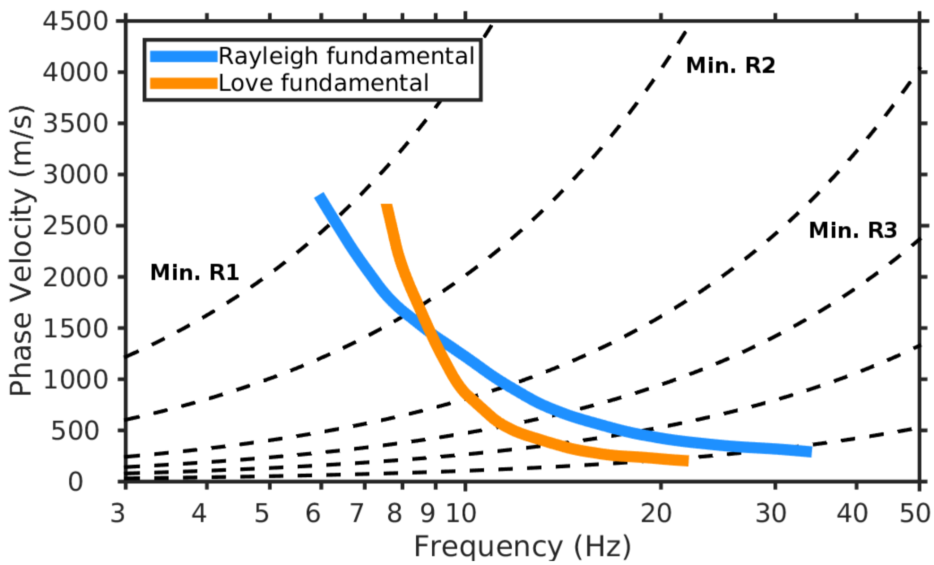

Figure 16 - *Final interpretation of the Rayleigh and Love dispersion curves for EMING. Minimum and maximum resolution bounds from the full array are indicated with black dashed lines.*

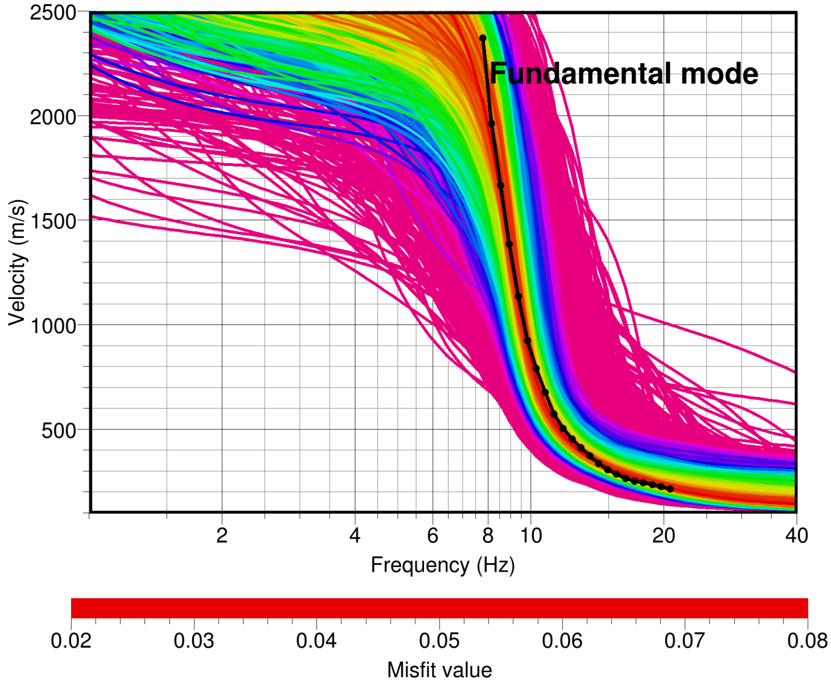

A)

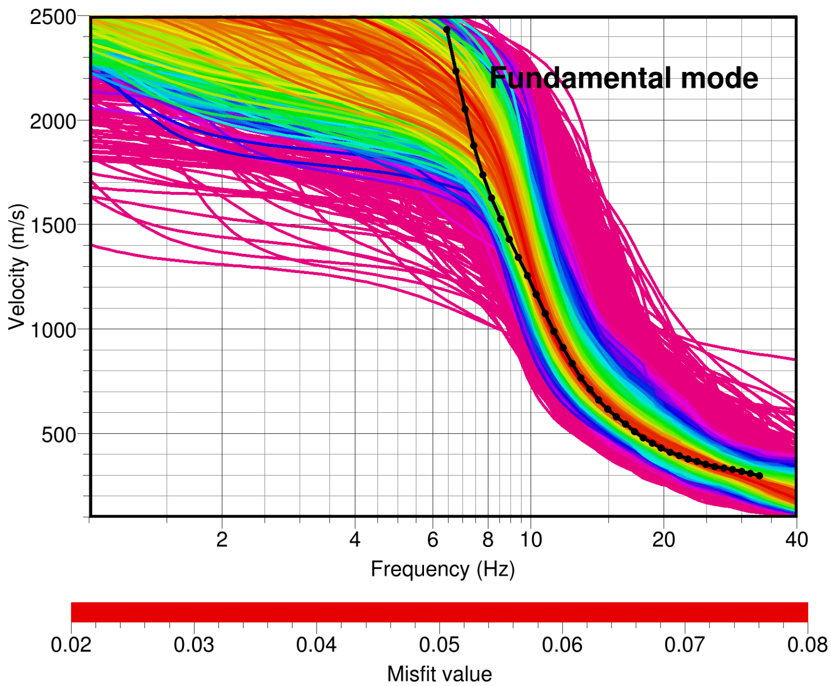

B)

Figure 17 - *Example of fitting the surface dispersion data within the global optimization procedure. Different colors represent different misfit between the observed (in black) and the modeled dispersion curves during the search (A, Rayleigh; B, Love).*

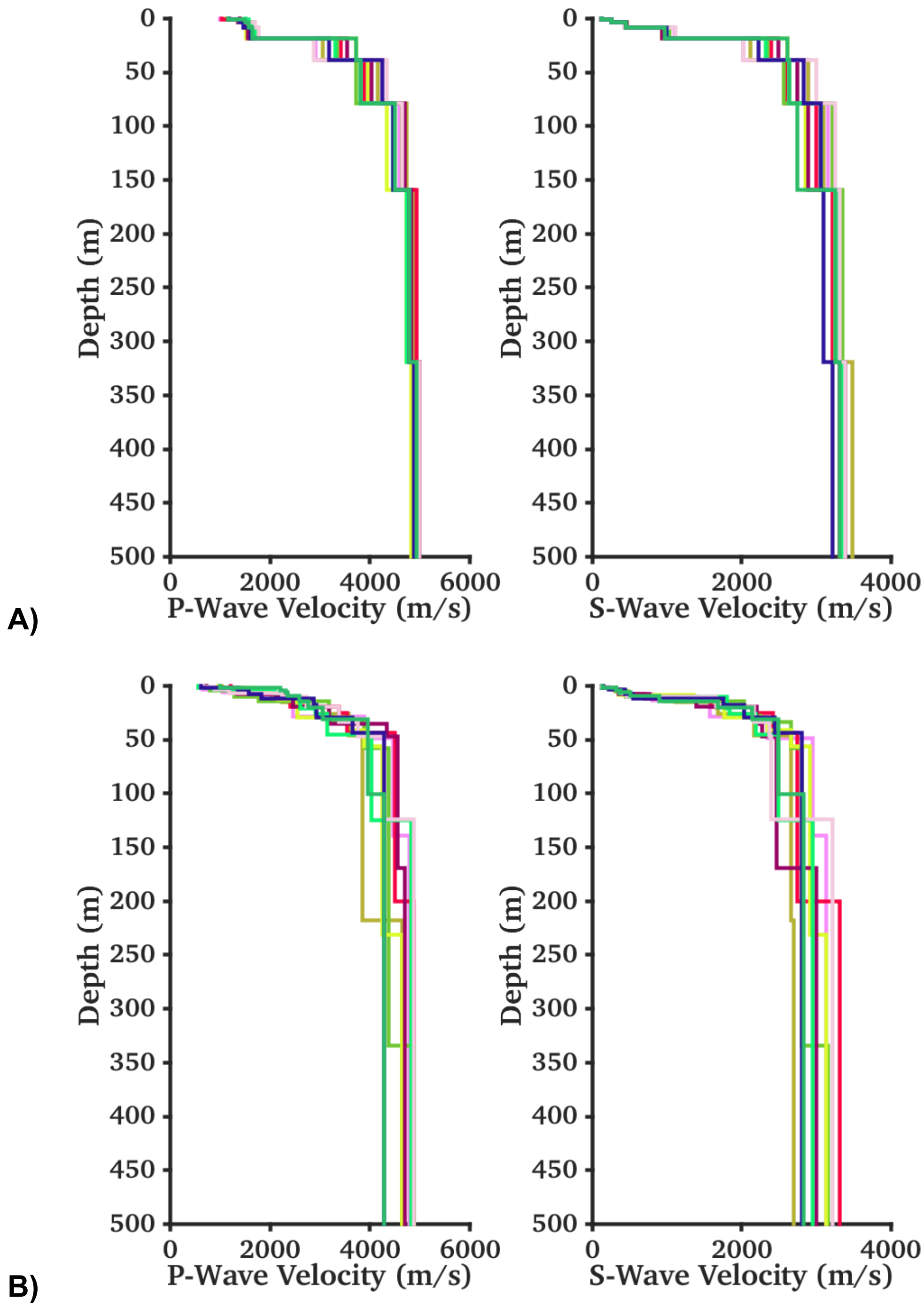

Figure 18 - *Collecting the best fitting models from the ten separated inversion runs using the free-layers (A, top) and fixed-layers (B, bottom) parameterization schemes.*

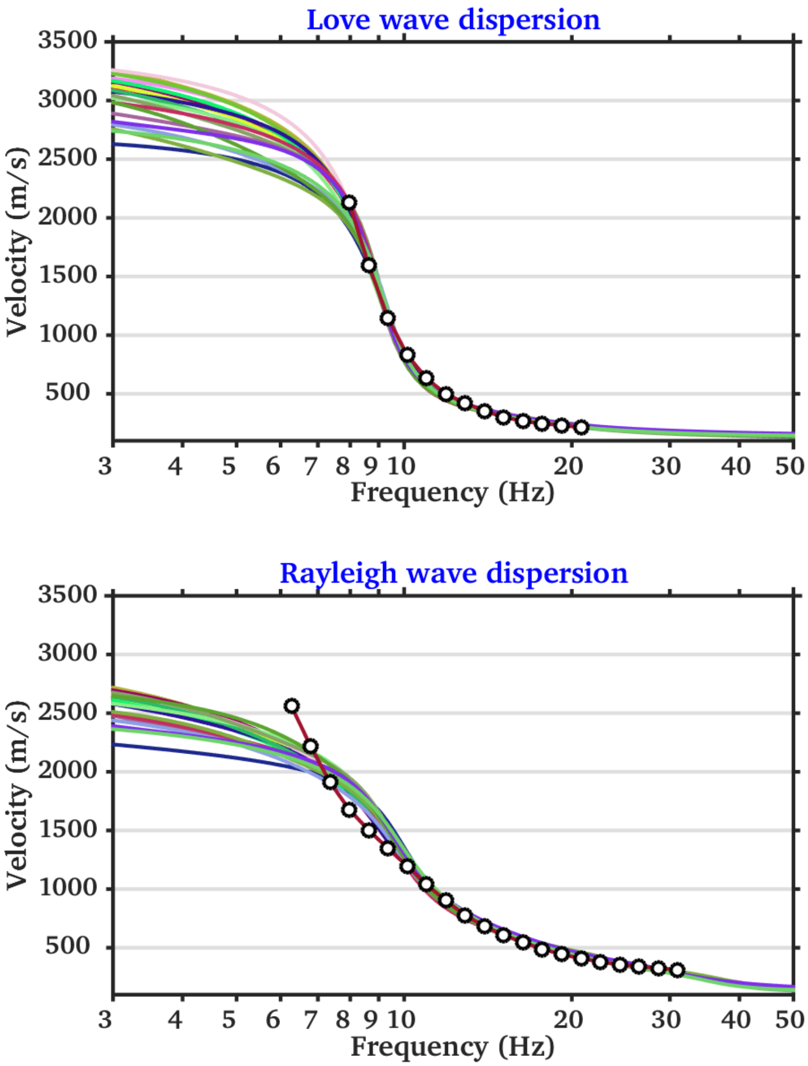

Figure 19 – *Rayleigh and Love dispersion curves computed from the 20 best fitting models of the two proposed interpretation schemes (free and fix layers).*

To parameterize the velocity model, two different approaches were implemented. The first one consisted in setting up an eight-layer model with fix interface depths. In such a case the free inversion parameters are then the velocities (P and S) and layer thicknesses. In the second case, a free-thickness layer approach was used. The advantage of the former method stays in the possibility to better resolve sharp velocity interfaces, while the second is less unique and better constraints the seismic velocity. The two approaches have to be nevertheless considered complementary, and they should provide consistent results.

Ten inversion tests (*runs*) were performed for each of the two model schemes, in order to minimize the effect related to a possible unfavorable initial randomization of the parameter space. The best fitting model from of each run was then collected (**Figure 18** and **Figure 21**) and used later on for the computation of the derived soil parameters.

In more detail, the inverted velocity models (Vs and Vp) are gradient-like, with a faster increase in velocity in the first 50m, followed by a more regular part of nearly constant velocity. This might be expected from the local geological information. The retrieved profile is well explained by both Love and Rayleigh dispersion curves (**Figure 19**) - which show a visible kink at about 10Hz - and by the high frequency part of the H/V spectral ratios (f_0 and right flank of the maximum), considered representative of the Rayleigh wave ellipticity function (**Figure 20**). Theoretical ellipticity doesn't nevertheless match the whole H/V function, likely due to the presence of additional wave contribution (e.g. SH waves) in the ambient vibration wave-field.

By considering the minimum available frequency of the surface-wave analysis, and by analyzing the scattering of the inverted models (**Figure 21**), it is realistic to assume the velocity profiles to be reliable down to a depth of about ~200m. Below this value no direct constrain is available from data, and the velocity values are obtained by pure extrapolation.

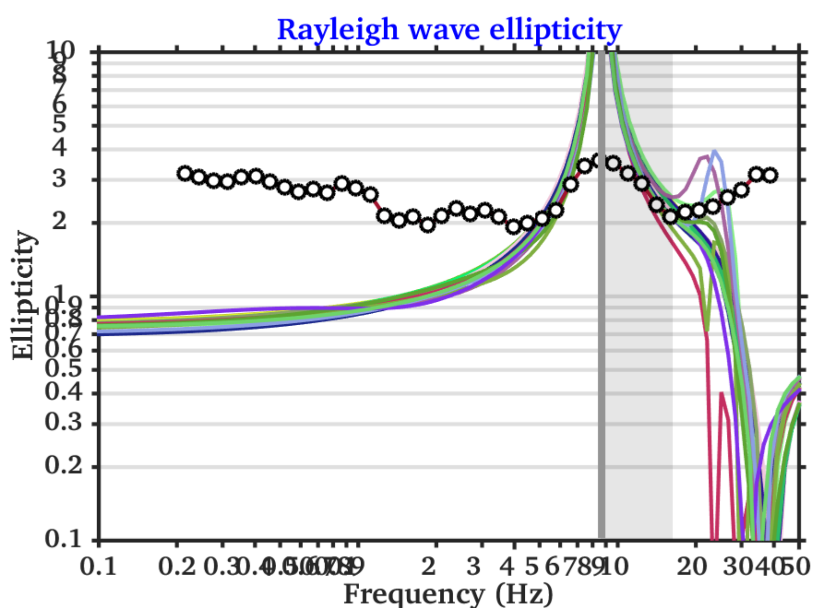

Figure 20 - *Rayleigh wave ellipticity curves computed from the best fitting models of the two proposed interpretation schemes (free and fixed layers), compared with average H/V spectral ratio from configuration R1 (scaled by sqrt(2)). Only the high frequency maximum (f_0) and the related right flank were used during the inversion.*

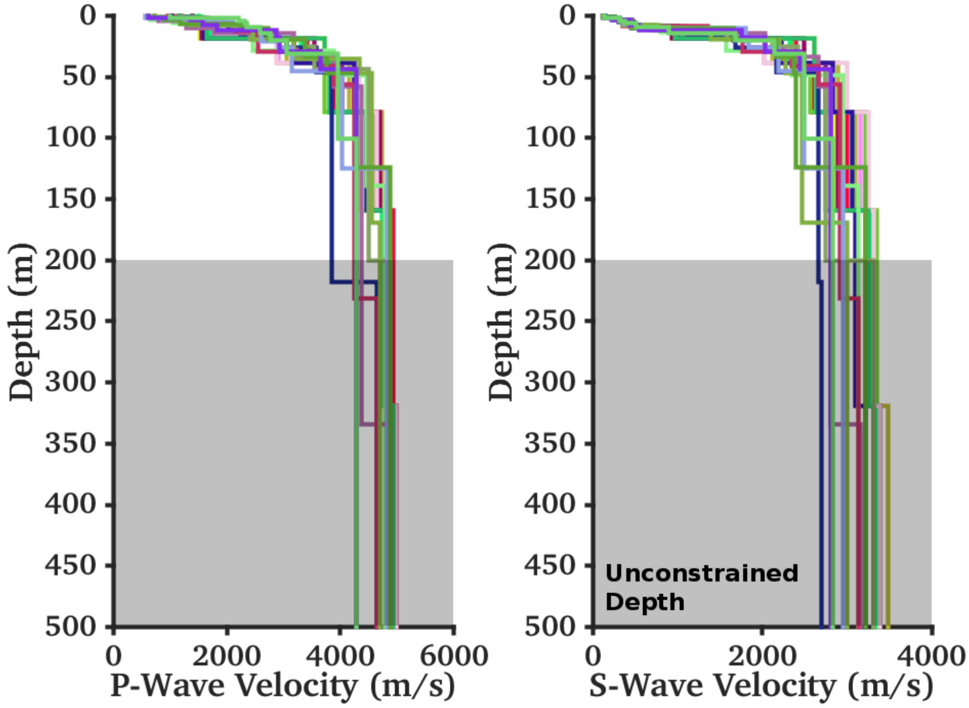

Figure 21 - *Comparison of all the best models from the two parameterization schemes (free and fixed layers). The two approaches produce consistent results. The depth of about 200m is considered approximately the maximum resolved depth.*

11. Engineering soil parameters

The ensemble of all the best inverted velocity profiles is then used to derive average soil parameters like the VsZ (average travel-time S-wave velocity over the depth Z, including Vs30, Table 1) and the quarter-wavelength (QWL) average velocities (Joyner et al., 1984) for a range of frequencies between 0.6 and 30Hz (**Figure 22**). The former is a standard parameter for the classification of ground-types in most building codes and in ground motion prediction equations. The latter is a parameter useful for the empirical estimation of the site-response and to assess the sensitivity of the seismic wave-field to the different depths. It has to be noticed that these two parameters are derived separately from all the best S-wave velocity models obtained from the inversion, and the results is finally averaged to improve statistics.

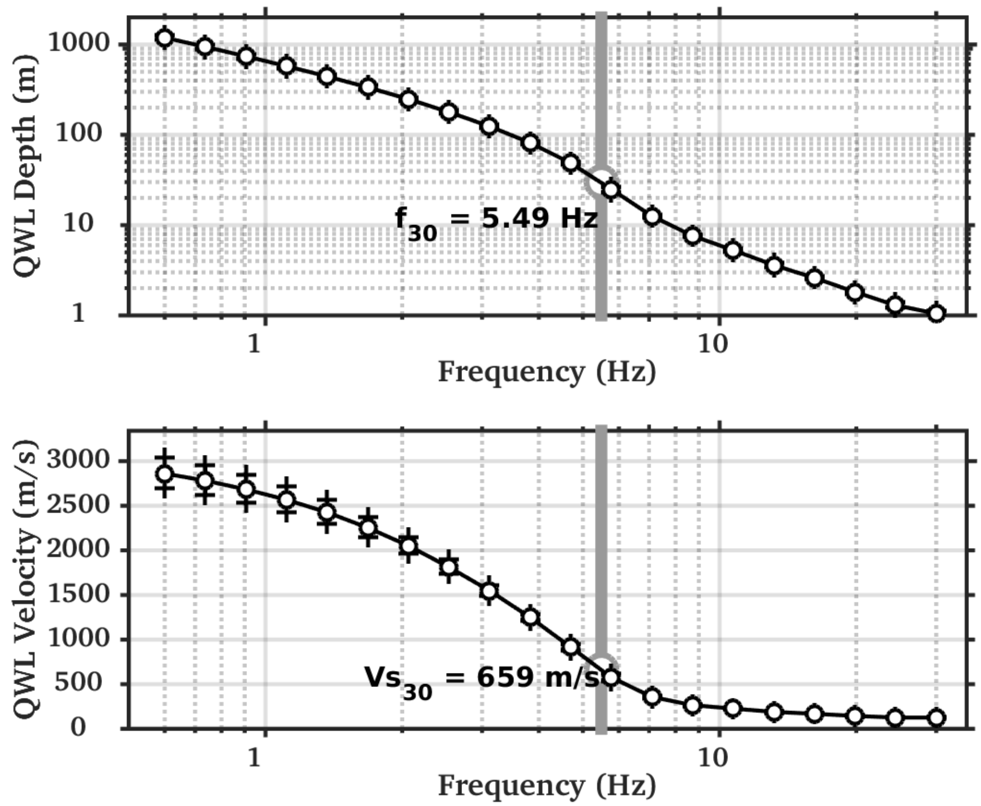

Figure 22 - *Quarter-wavelength representation of the inverted S-wave velocity profiles. Top: the depth-frequency dependency. Bottom: the QWL average velocity. The Vs30 value is indicated with its corresponding QWL frequency.*

12. Amplification models

Site amplification functions have been computed using two different approaches: the S-wave transfer function for vertical propagation and the quarter-wavelength amplification. In general the first method is used to evaluate the resonance characteristics of the site, while the second is more useful to assess the effect of the velocity contrasts between the lowermost rock layer (as reference) and the different QWL averaging depths. The two amplification functions are then corrected for the Swiss rock reference velocity profile as defined in Poggi et al. (2011), according to the procedure described in Edwards et al. (2013). Given the lower velocities in the uppermost part of the EMING profile compared to the Swiss reference, the final corrected amplification function shows a lower average amplification level at high frequencies than the uncorrected (**Figure 23**), while low frequency part is nearly asymptotic.

Averaging depth (m)	Vs-mean (m/s)	St.Dev.
5	220.99	5.10
10	306.21	4.43
15	402.68	5.70
20	489.82	12.72
25	578.41	11.79
30	**659.08**	**11.68**
40	803.27	13.97
50	932.00	13.75
75	1191.70	16.88
100	1392.32	24.76
150	1683.37	40.38
200	1895.09	52.10

Table 1 - *Average travel-time velocities at different depths. Vs30 is highlighted.*

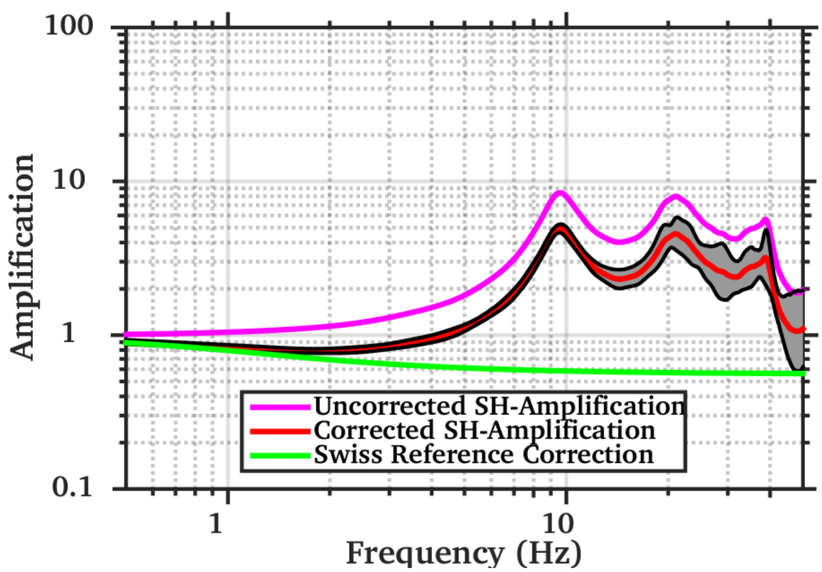

Figure 23 - *Correcting the SH-wave transfer function for the Swiss (rock) reference conditions (Poggi et al. 2011). The final corrected amplification function shows a lower (average) amplification at high frequencies than the uncorrected.*

Amplification functions using the transfer function and the quarter-wavelength approach are comparable (**Figure 24**), even if the transfer function provides a slightly larger amplification, because of the presence of some weak resonance peaks. At low frequencies both methods converge to the same amplification level. It has to be notice that the amplification functions do not include attenuation at this stage of the analysis, as the quality factors of the site are too uncertain.

A good matching is obtained by comparison between the one-dimensional transfer function and the empirical amplification from spectral modeling of low-magnitude earthquakes as described in Edwards et al., 2013 (**Figure 25**). This confirms the reliability of the inverted velocity profile in light of the current assumptions of one-dimensionality.

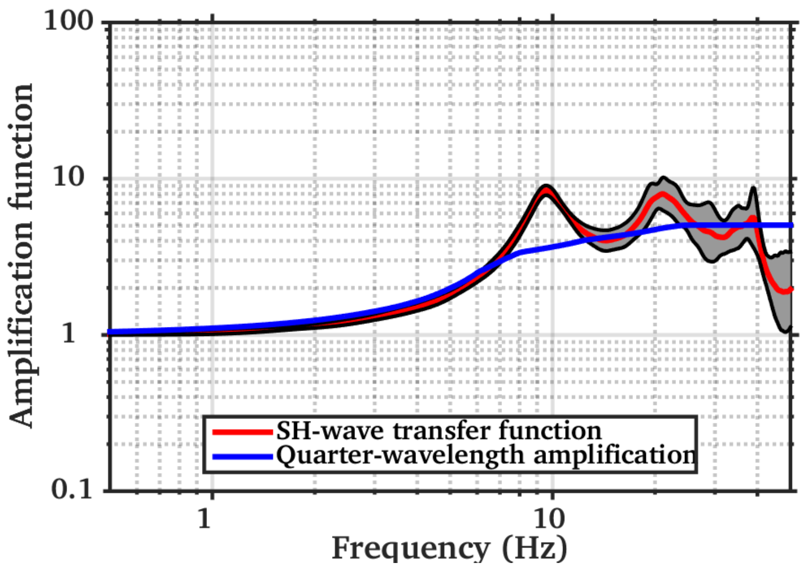

Figure 24 - *Comparison of amplification functions computed using the SH-wave transfer function and the quarter-wavelength formalism on the inverted velocity models.*

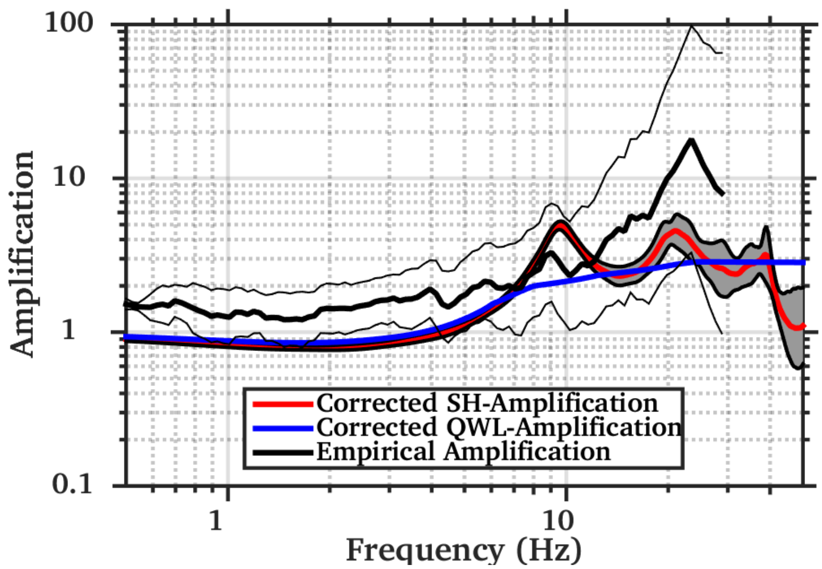

Figure 25 - *Comparison of amplification functions computed using the SH-wave transfer function and the quarter-wavelength approach with empirical observation from spectral modeling of low-magnitude earthquakes. All functions are referenced to the Swiss rock reference model (Poggi et al. 2011).*

REFERENCES

Capon, J., 1969. High resolution frequency wavenumber spectrum analysis, Proc. IEEE, 57, 1408-1418.

Burjanek, J., G. Stamm, V. Poggi, J.R. Moore, and D. Fäh [2010], “Ambient vibration analysis of an unstable mountain slope”, Geophys. J. Int., Vol. 180, pp. 820-828.

Edwards, B., C. Michel, V. Poggi and D. Fäh (2013). Determination of Site Amplification from Regional Seismicity: Application to the Swiss National Seismic Networks. Accepted for publication in Seismological Research Letters.

Joyner, W. B., R. E. Warrick and T. E. Fumal (1981). The Effect of Quaternary Alluvium on Strong Ground Motion in the Coyote Lake, California, Earthquake of 1979, Bulletin of the Seismological Society of America, 71, 1333-1349.

Poggi, V., B. Edwards and D. Fäh (2011). Derivation of a Reference Shear-Wave Velocity Model from Empirical Site Amplification, Bulletin of the Seismological Society of America, 101, 258-274.

Poggi, V. and Fäh D., 2010. Estimating Rayleigh wave particle motion from three-component array analysis of ambient vibrations. Geophys. J. Int., 180-1, 251-267.

Eidgenössische Technische Hochschule Zürich
Swiss Federal Institute of Technology Zurich

SED
Schweizerischer Erdbebendienst
Swiss Seismological Service

Report on site characterization

Emmethof, Switzerland
(EMMET)

Poggi Valerio, Donat Fäh

Last modified - 22 / 12 / 2014

1. Introduction

In the framework of the NAGRA seismic network project, an array measurement of the ambient vibration wave-field was performed at the location of the SED station EMMET (Emmethof, Switzerland). The scope of the survey is the seismic characterization of the area surrounding the installation (**Figure 1**), which consists in a broadband seismometer (Trillium Compact) with a high-resolution digitizer (Taurus 24Bit @200sps). Ambient vibration analysis has been used to infer the characteristics of the underground structure of the site, with special regard to the one-dimensional shear-wave velocity. Such profile was later used to assess the local seismic response of the station.

For the analysis, different spectral analysis techniques were implemented, consisting in both single and array methods, which are listed below:

- Time-frequency wavelet analysis
- Power-spectral density estimation
- Conventional horizontal to vertical spectral ratios
- Directional horizontal to vertical spectral ratios
- Wavelet polarization analysis
- Three-component high-resolution f-k analysis.

The results of all these analyses conformed to the definition of the final velocity model. In the following, the main results of these investigations are summarized and a final interpretation of the velocity profile is given. From this interpretation, engineering parameters are finally derived, e.g. the Qwl-Vs average velocity, VsZ (including Vs30) and the seismic amplification from the analytical SH-transfer function of the one-dimensional soil column.

2. Survey description

To characterize the seismic response of the site, an array measurement of ambient vibration was performed on 09/10/2014 (**Figure 1**). The array consists of two concentric measuring configurations (called “rings”, R1 and R2) of 12 sensors each and increasing diameter (about 20m and 40m respectively). Three configurations were initially planned, together with a larger configuration of about 100m, but dense vegetation and steep slopes toward north and south limited the available space. Ring 1 and 2 were partially overlapping, with the aim of providing a continuous frequency resolution between the geometries. Configuration R1 recorded for a total of 1h, while configuration R2 for 1h and 30m. The differences in the recording length are due to the different resolution characteristics of the three geometries. As a general rule, larger arrays require longer recording time to produce a reasonable statistics of the ambient vibration processing results. Satisfactory results were obtained from the analysis of the first geometry only, while the second did not produced usable results. A limited penetration depth of about ~50-80m was initially expected, increased by the use of ellipticity information.

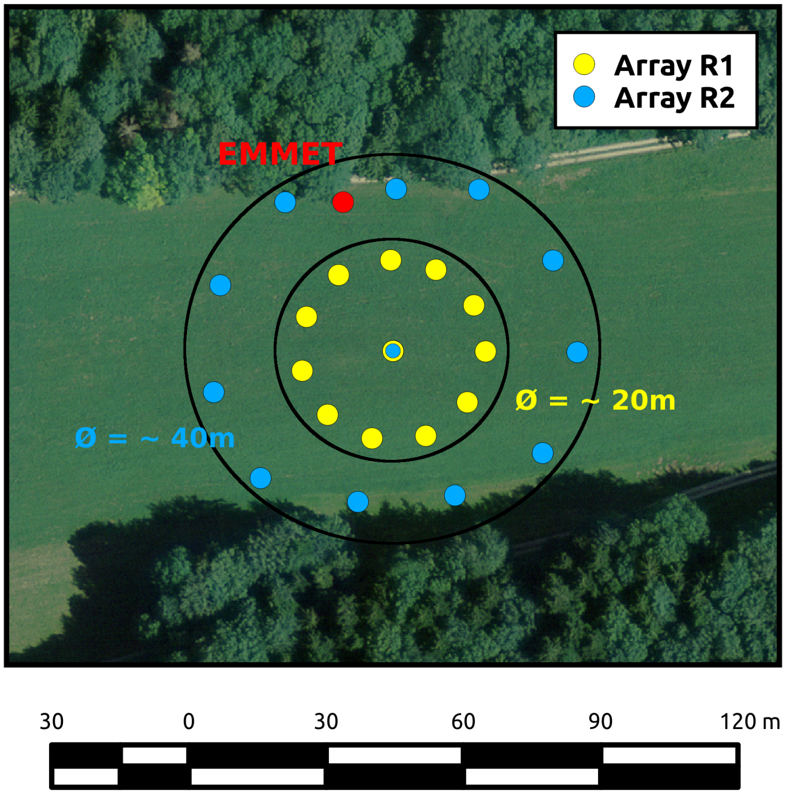

Figure 1 - *Location of the ambient vibration array survey performed in Emmethof (SED station EMMET) on 09/10/2014. Two concentric configurations of increasing diameter were implemented (named R1 and R2).*

3. Weather conditions

The weather conditions were optimal during the whole measurement, with no precipitations and an average temperature of 26 degrees.

4. Soil type, topography and geology

The array has been set in open field conditions, in a rural area (**Figure 1**, **Figure 3**). The influence of buildings and anthropogenic disturbances is virtually negligible. Array sensors have been deployed on free soil. Good coupling with the ground was assured by means of digging small holes at the sensor's places, and by using a special support (*Trihedron*®) that facilitates the leveling of the device even for difficult soil conditions. The measurement area was located on a gentle slope toward north; however no topographic correction was necessary before processing. Soil was mostly dry, with the exception of a limited zone at the southern edge of the array, which showed some evidence of water saturation.

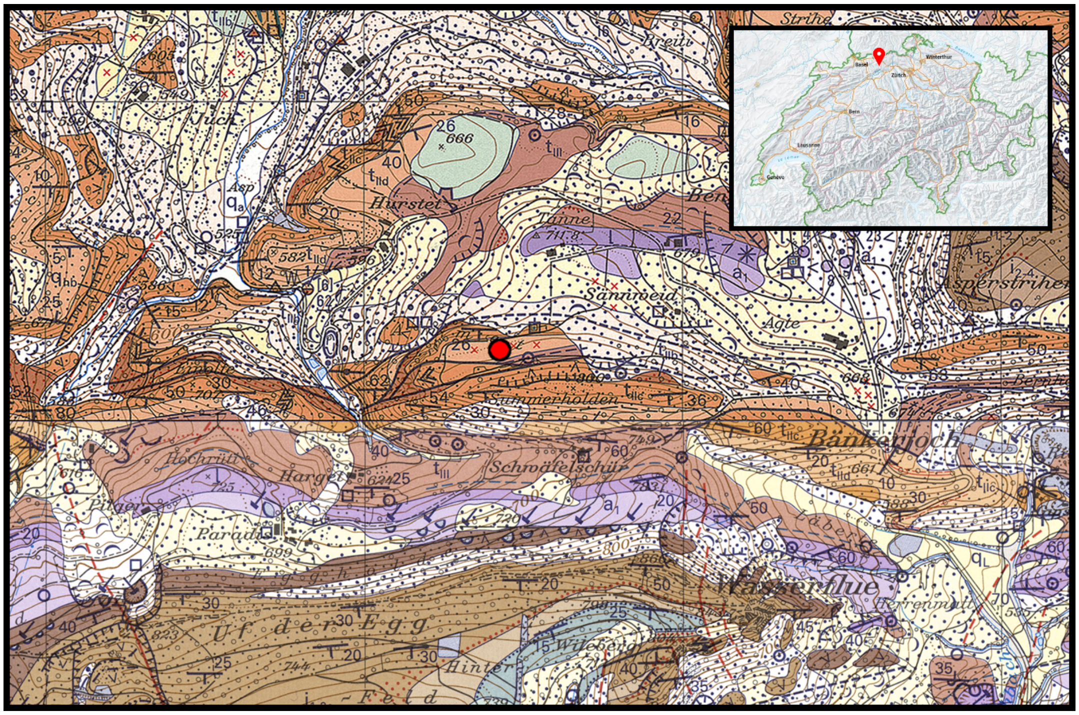

Figure 2 - *Geological map of the measuring area, in the surroundings of Emmethof (reproduced from Geological Atlas of Switzerland 1:25000, Swisstopo, modified). In red, the approximate location of the permanent station EMMET.*

From the geological points of view (**Figure 2**) the target area sits on outcropping calcareous (Muschelkalk) and dolomitic formations (Keuper) of Triassic age (t_{iid}-t_{iic}). Geological map shows that calcareous bedrock is in many areas exposed, but discontinuously covered by spots of Quaternary sediments. The region is nevertheless tectonically quite complex, with alternation of formation with different lithology over a relative short distance. By visual survey, the surface morphology is considerably smooth and modeled by the action of glaciers during the Pleistocene. Geophysical bedrock is never exposed at the measuring site, but likely very shallow. Such site can be classified as of rock ground-type A.

5. Acquisition equipment

Each acquisition point within the array consisted of a three components seismometer (Lennartz 3C with 5s eigenperiod) and a 24 bit data logger (Quanterra Q330). Synchronization between stations was assured by standard GPS, while a more accurate differential GPS (Leica Viva system) was used to precisely locate the sensor's coordinates with a tolerance of less than 5cm.

Figure 3 - *Overview of the measurement area during the acquisition of array configuration R1. SED station EMMET is located on the right side of the picture, close to the small path visible in background.*

6. Pre-processing and preliminary data-quality control

The three-component recording has been filtered prior to analysis using a band-pass 6^{th} order causal Butterworth filter with corners at 0.2Hz and 50Hz. Although it is not a strict requirement for spectral analysis techniques, such filtering was applied in order to facilitate the preliminary visual inspection of the noise traces and to evaluate the coherency of the wave-field (**Figure 4**). Such procedure gives essential information for the subsequent interpretation of the f-k analysis results. In particular, it was observed an anomalous behavior of station EMT02, whose recordings were affected by large high-frequency transients of unknown origin during great part of the R1 acquisition. Surprisingly, no sign of these transients is visible on other traces.

To assess the quality of the ambient vibration recordings, spectral analysis was subsequently performed. Because of the stochastic nature of the ambient vibration wave-field, a statistical approach has to be used, such as the estimation of the power spectral density (*PSD*). This approach is useful to evaluate the average energy level of the recordings in the analyzed frequency range, and to access the presence of spurious spectral peaks, which might be related to human activity (machinery, pumps). By inspecting the PSD of all the three-component recordings of the array in the range between 0.5 and 40Hz, it is found that the average energy level of the spectrum fits well within the minimum and maximum bounds of the USGS noise model (**Figure 5**A), with a progressive increase of energy at high frequency, although no significant peaks of possibly anthropogenic origin are visible.

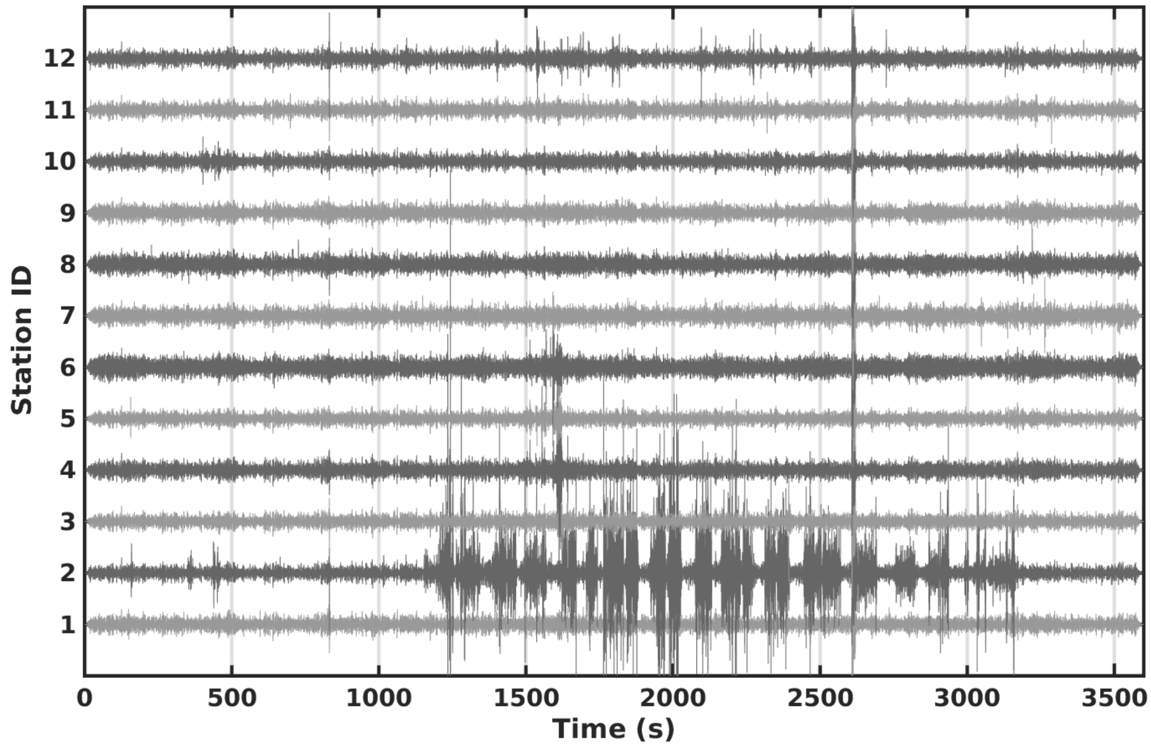

Figure 4 - *Inspection of the useful part of the ambient vibration recording of the Emmethof array (here configuration R1). A considerable amount of high-frequency transients of unknown origin affected station EMT02 during the acquisition, which was removed before subsequent f-k processing.*

Only for station EMT02, as previously mentioned, spectral analysis confirmed a contamination by rather high-frequency disturbances affecting all components (**Figure 5**B). The trace was therefore rejected from subsequent analysis.

Complementary to the aforementioned statistical methods, a spectral decomposition approach is more suitable to assess the stationarity of the ambient vibration wave-field over time. The wavelet time-frequency analysis was then performed over the whole recording time. From such analysis (**Figure 6**) an overall stability of the ambient-vibration wave-field over time is evident. No relevant harmonic signals can be identified in the frequency band useful for the processing, with the exception of few episodic contributions at very high-frequencies (>50 Hz), nevertheless discontinuous over the whole recordings and components. These contributions will not likely affect the following processing steps.

A) EMT01 (Central Station)

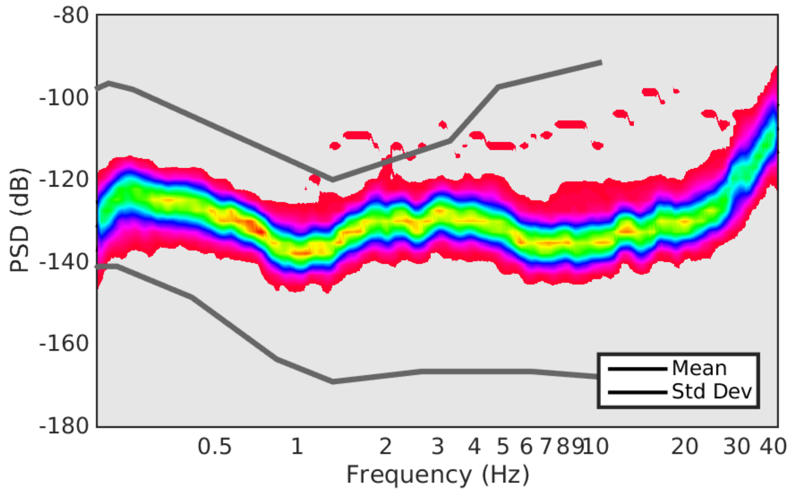

B) EMT02

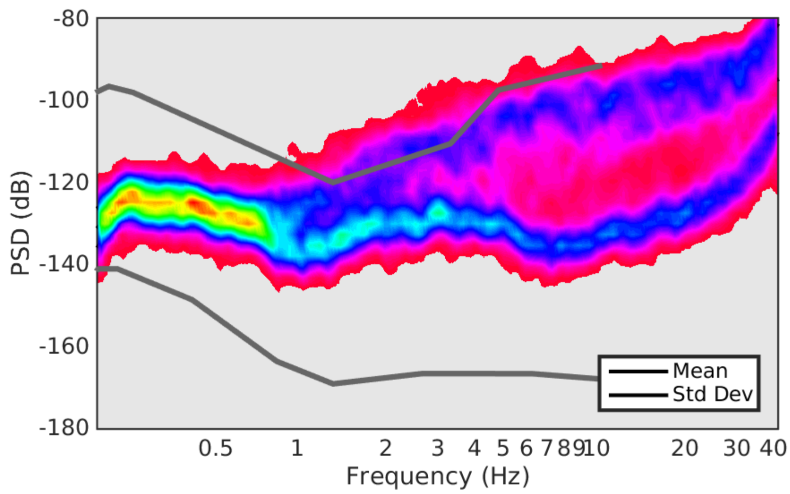

Figure 5 - *Power spectral density (PSD) computed for 1h recording at the central station of the array configuration R1 (EMT01, top) and at the station EMT02 (bottom). This last showed contamination of local high-frequency disturbances affecting the three components (in the plot horizontal direction N-S). Results similar to central station were nevertheless obtained for the other stations of the array. In gray lines are the minimum and the maximum bounds of the USGS noise model, for comparison.*

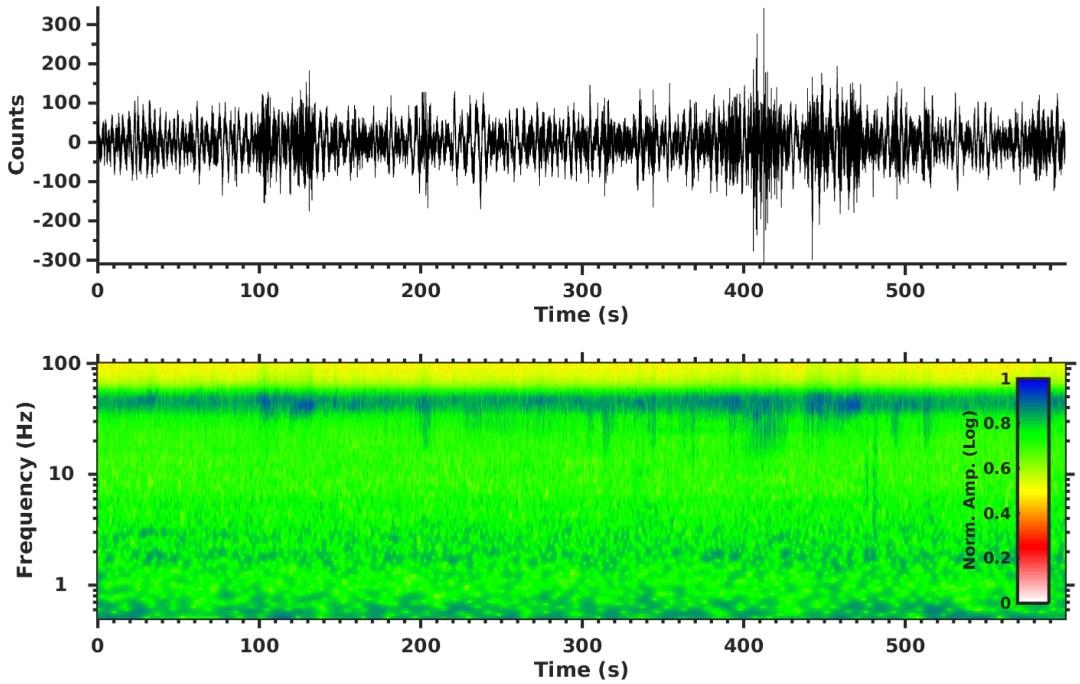

Figure 6 - *Example of spectrogram from 600s of recording of the central station (EMT01) of the array configuration R1, component N-S. No significant harmonic disturbances are visible on the whole spectrogram. Similar results were found for the other components. For the analysis, the cosine wavelet is used (wavelet parameter = 12).*

7. Conventional H/V spectral ratios

The horizontal-to-vertical (H/V) Fourier spectral ratio is a technique widely used in seismic site characterization because of its ability to provide an estimate of the SH wave fundamental frequency of resonance (f_0) of the site. Other than that, H/V ratios are useful to provide information on the Rayleigh wave ellipticity function, which can be used in surface wave dispersion inversion procedures to constrain large velocity contrasts at depth. In this study, we use the H/V technique also to map the variability of the subsoil structure along the investigated area; this is necessary to verify the fulfillment of the 1D structure assumption, which is necessary for the f-k method applied later.

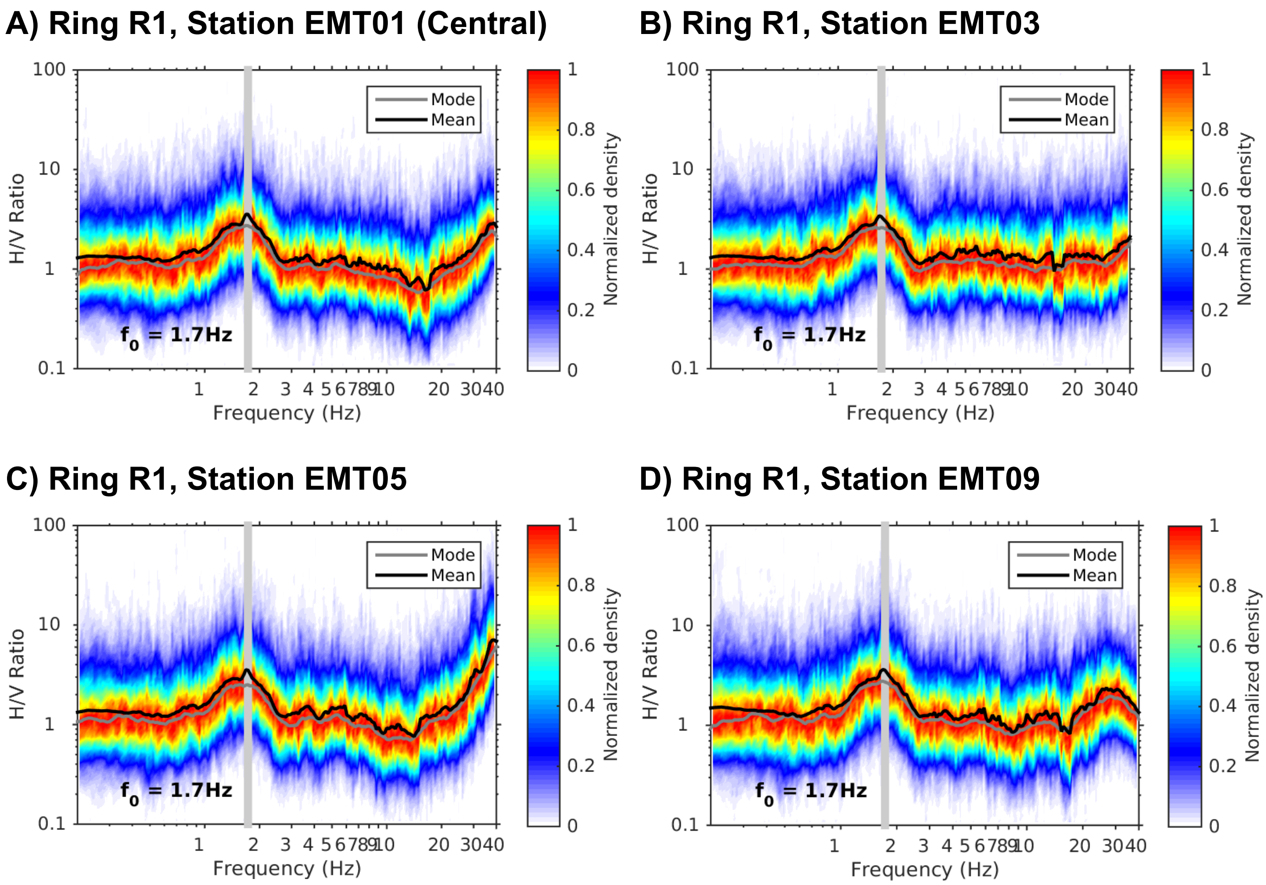

Figure 7 - *Example of H/V spectral ratios for the configurations R1. The resonance frequency of the cover is indicated with a light gray line (stable at 1.7Hz).*

H/V spectral ratios have been computed for all the recordings at each station of the array and separately for configurations R1 and R2 (e.g. **Figure 7**). The behavior of the noise wave-field at the different stations location is comparable at low to intermediate frequencies (roughly < 15Hz), while the high frequency region shows some variability, within and between array rings. This is likely due to variability of the top layers, which can show some heterogeneity over the measuring area. The behavior of the site can nevertheless be considered sufficiently homogeneous for the f-k analysis.

In average (**Figure 8**), spectral curves show a very stable low frequency peak at about 1.7Hz. Such maximum is likely induced by the presence of a deep interface, possibly between rocks of different competence. We assume such frequency peak to be the fundamental frequency of the site, later use as a constraint for the inversion of the deep portions of the velocity profile.

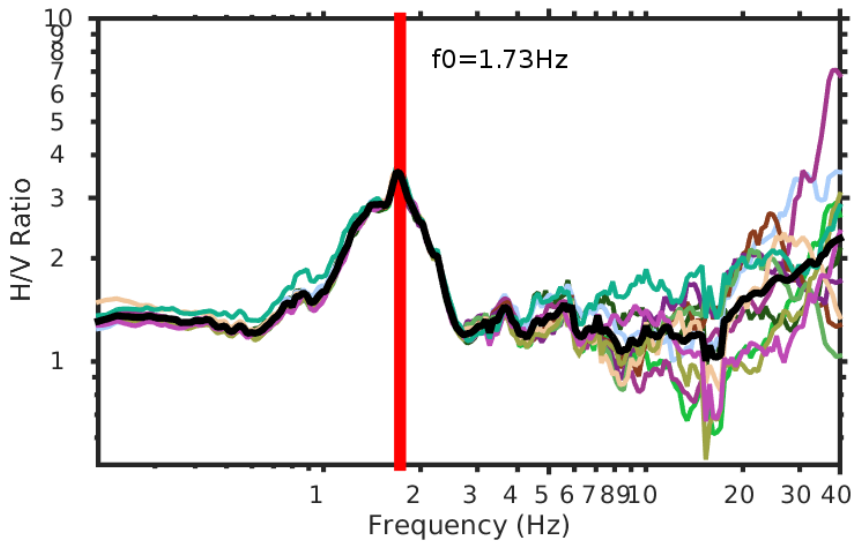

Figure 8 - *Comparison of the H/V spectral ratio curves of all the stations of the array (in this example for the array configuration R1). The curves are generally stable at low frequencies, confirming the lateral homogeneity of the underlying bedrock velocity structure. High frequencies (> 15Hz) show more variability, nevertheless in an acceptable range for the validation of one-dimensional assumption. The average fundamental peak of resonance is stable at about 1.7Hz.*

8. Directional analysis

The computation of directional H/V spectral ratio or polarization analysis is useful to reveal asymmetries in the ambient vibration wave-field. Different effects can induce such a behavior: 2D/3D structure, topographic effects or a non-homogeneous distribution of the noise sources. If a strong directionality is found by the analysis, it is generally recommended to carry out further investigations to properly address the origin of polarization. By processing the directional H/V ratios at all the recording stations of the two arrays (e.g. **Figure 9**) it is possible to observe an overall isotropy of the wave-field in the whole analyzed frequency range with the exception of the fundamental frequency peak (about 1.7 Hz), which shows a strong preferential alignment along NE-SW, stable between the different station locations of the array. Such behavior is of difficult interpretation; the hypothesis of dipping layer should be rejected by the confirmed stability of the resonance peak at the different measuring places. Topography features have no apparent relation with such directionality. The possibility of anisotropic noise source distribution will be later discussed in light of f-k analysis results.

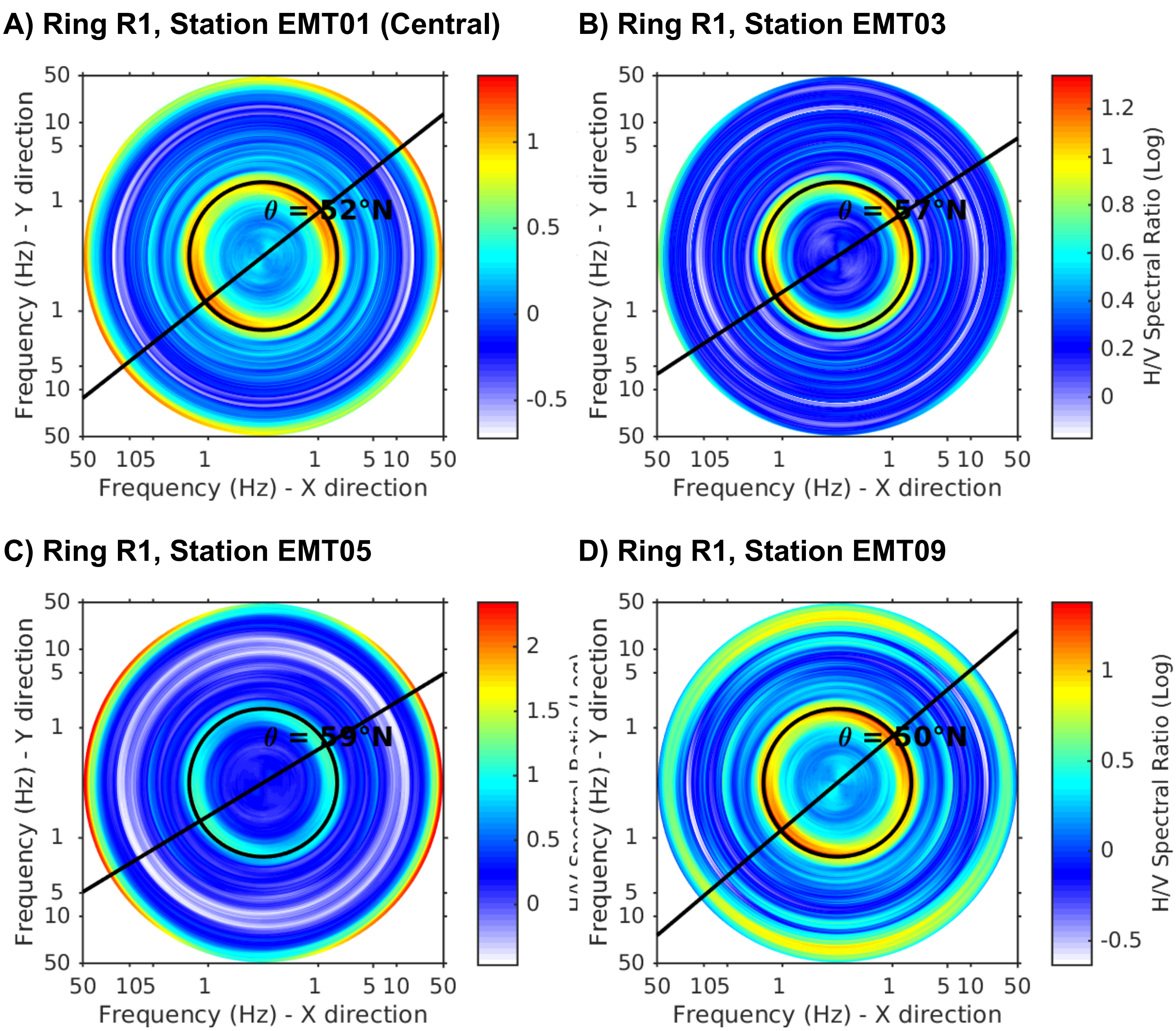

Figure 9 - *Example of directional H/V spectral ratios for configuration R1. A strong preferential direction of the resonance peak is present, roughly aligned NE-SW. However, other frequency bands show a more isotropic behavior of the noise wave-field.*

The results of the H/V directional analysis are confirmed by applying the wavelet polarization analysis technique (Burjanek et al., 2008). Here, the particle motion shows to be mostly elliptical, with a significant polarization only at the resonance frequency (**Figure 10**). As well, resonance frequency is associated with a mild azimuthal anisotropy, in agreement with previous H/V results (**Figure 11**A).

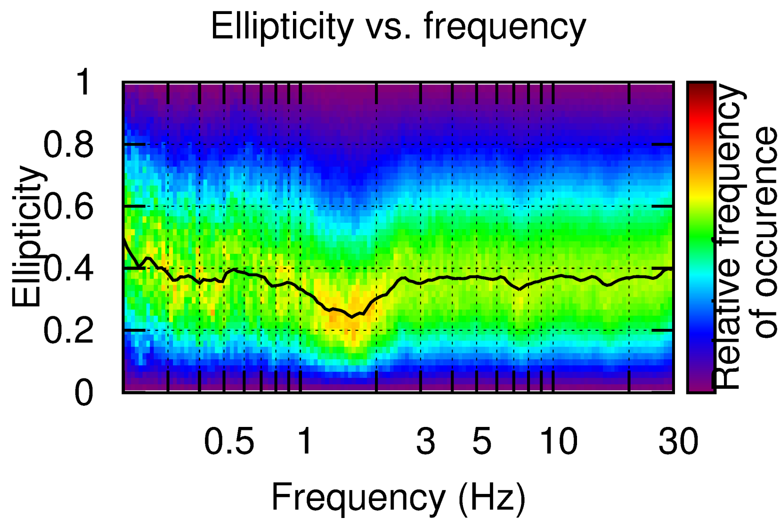

Figure 10 - *Ellipticity of the particle motion from wavelet-based polarization analysis at the central station of the array (EMT01). Similar results can be obtained for other stations of the arrays.*

9. Three-component f-k analysis

The frequency-wavenumber analysis is a spectral technique based on seismic array recordings that allows retrieving direction and dispersion characteristics of the surface waves. We apply this technique to three-component ambient vibration recordings using a modification of the high-resolution method of Capon (1969) as described in Poggi et al. (2010). Using all the three-components of motion gives the possibility to retrieve information about the propagation of the Rayleigh waves (vertical and radial processing direction) as well as of the Love waves (transversal direction). As in the case of the previous methods, the ambient vibration recordings are treated statistically by subdividing the traces in sub-windows. For each consecutive window, a separated f-k analysis is performed, and the results are then averaged over the whole recording, increasing the robustness of the final estimation.

As first step, from the f-k analysis it is possible to assess the azimuthal distribution of noise sources over different frequency ranges (e.g. **Figure 12**) separately for the vertical, the radial and the transversal direction of polarization. From the analysis of the two geometries R1 and R2, source distribution appears to be quite homogeneous for all the components, without displaying a clear directional pattern. Unfortunately, resolution limits of the two configurations do not allow investigating the source distribution at low frequencies (in particular at f_0), which would have been essential to understand the directionality pattern observed in H/V and polarization analysis.

A)

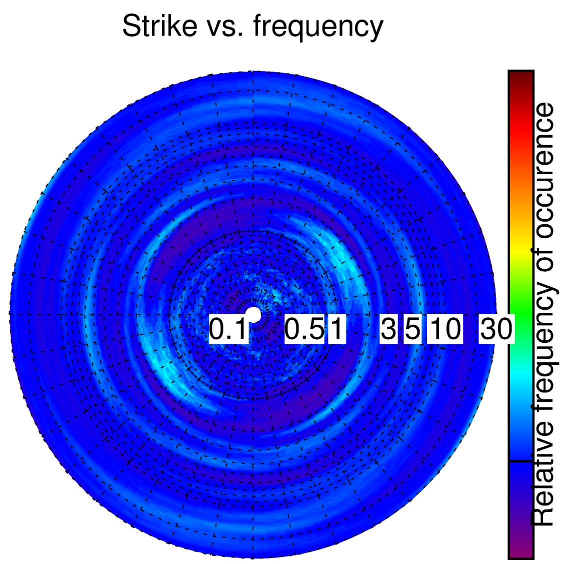

B)

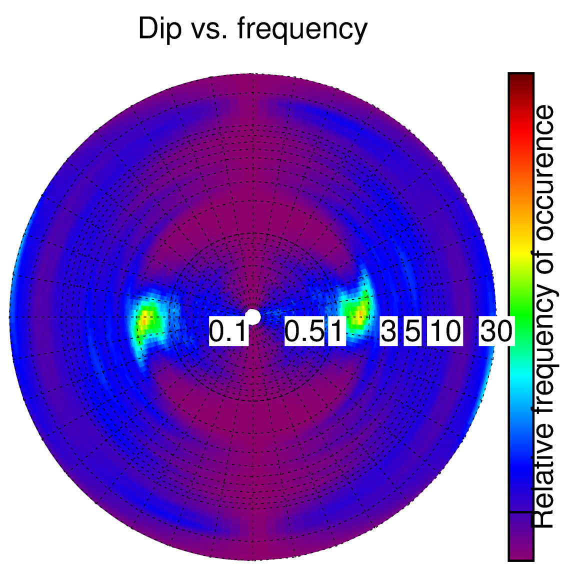

Figure 11 - *Directionality of the particle motion from wavelet-based polarization analysis (dip direction in A, strike in B) at the central station of the array (EMT01). Similar results can be obtained for other stations of the arrays.*

A) Ring 1, 12-20Hz

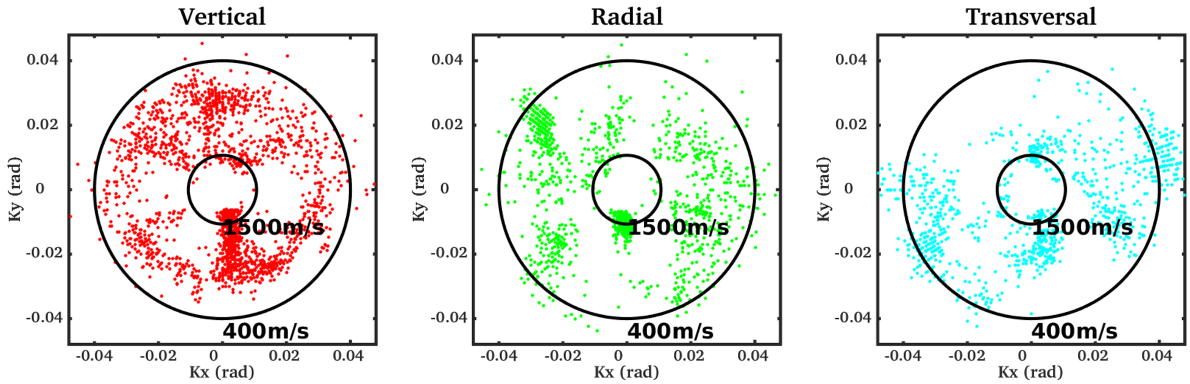

B) Ring1, 20-30Hz

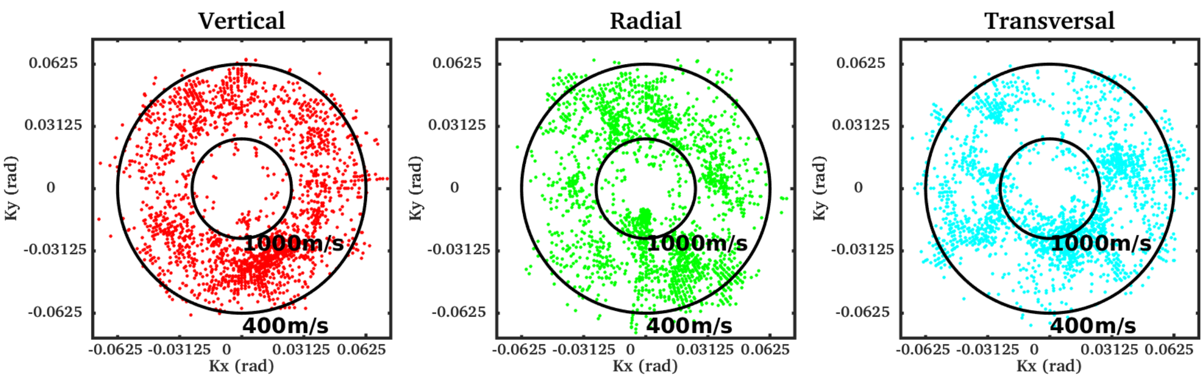

Figure 12 - *Example of distribution of noise sources in the intermediate (12-20Hz) and high frequency range (20-30Hz) obtained from three-component f-k analysis. The source distribution is irregular but not strictly directional on all the propagation components.*

As a second step, the surface-wave dispersion curves are extracted by visual inspection and manual picking of the f-k density plots (**Figure 13**), separately for the three polarization directions. Good results are obtained for the array configuration R1, while R2 did not show usable evidence of dispersion in the resolved frequency band. Given the high velocity of the site, results from R1 are nevertheless sufficient to provide a reasonable constraint for the inversion of the velocity profile of the site.

More in detail, Love wave's fundamental mode dispersion can be well tracked in the frequency range between about 18Hz and 35Hz. The Rayleigh wave's fundamental mode is also clearly visible on the vertical component of R1, between 12Hz and 40Hz, but of more problematic identification on the radial direction. The final interpretation of Rayleigh and Love wave dispersion pattern is given in **Figure 14**.

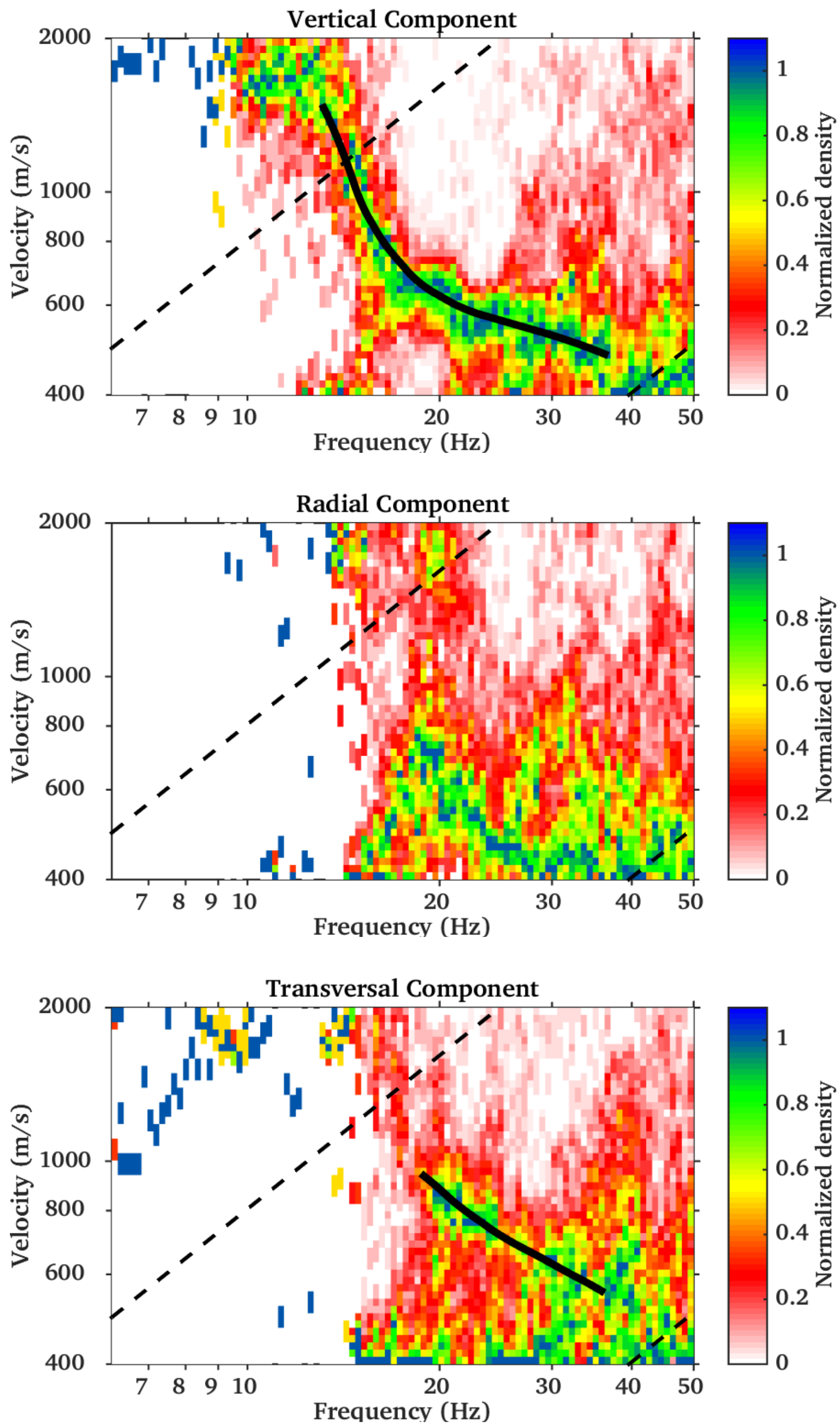

Figure 13 - *Density distribution of the surface wave signals obtained from the recording of the array configuration R1 using three-component f-k analysis. From top to bottom: Rayleigh vertical, Rayleigh radial and Love wave dispersion. In black, the interpreted dispersion curves are given (manually selected).*

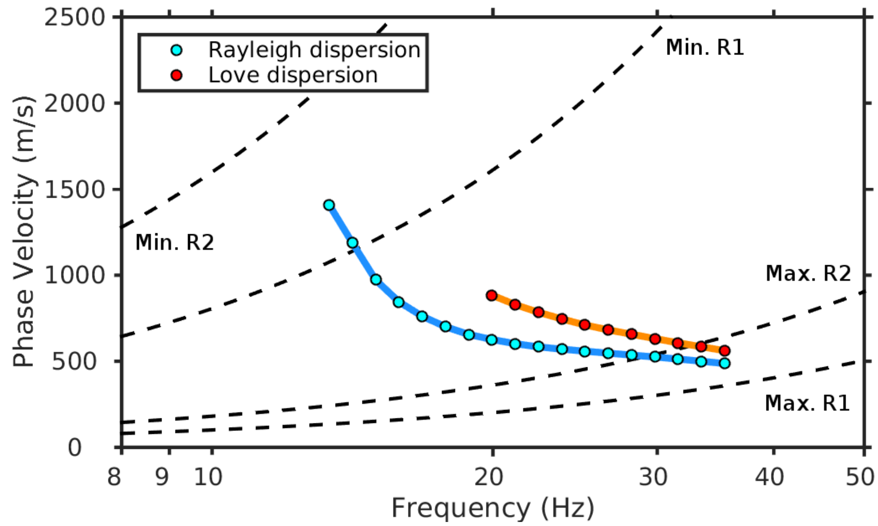

Figure 14 - *Summary of all dispersion curves obtained from three-component f-k analysis of the array configuration R1. Minimum and maximum resolution bounds from the two geometries are indicated with black dashed lines for comparison.*

10. Inversion of the dispersion curves

The surface wave dispersion curves (Rayleigh and Love) obtained from the three-component f-k analysis of the ambient vibrations and the fundamental frequency of resonance (f_0) from average H/V spectral ratios are inverted to obtain an estimation of the velocity profile of the site (mainly S-wave velocity as function of depth, and to a lesser extend the P-wave velocity, due to the lower sensitivity). The analysis is performed using the software *Dinver* (www.geopsy.org), which implements a direct search approach (**Figure 15**) based on a conditional version of the neighborhood algorithm (Sambridge, 1999).

To parameterize the velocity model, two different approaches were implemented. The first one consisted in setting up an eight-layer model with fix interface depths. In such a case, the free inversion parameters are then the velocities (P and S) and layer thicknesses. In the second case, a free-thickness layer approach was used. The advantage of the former method stays in the possibility to better resolve sharp velocity interfaces, while the second is less unique and better constraints the seismic velocity. The two approaches have to be nevertheless considered complementary, and they should provide consistent results.

Ten inversion tests (*runs*) were performed for each of the two model schemes, in order to minimize the effect related to a possible unfavorable initial randomization of the parameter space. The best fitting model from of each run was then collected (**Figure 16** and **Figure 19**) and used later on for the computation of the derived soil parameters.

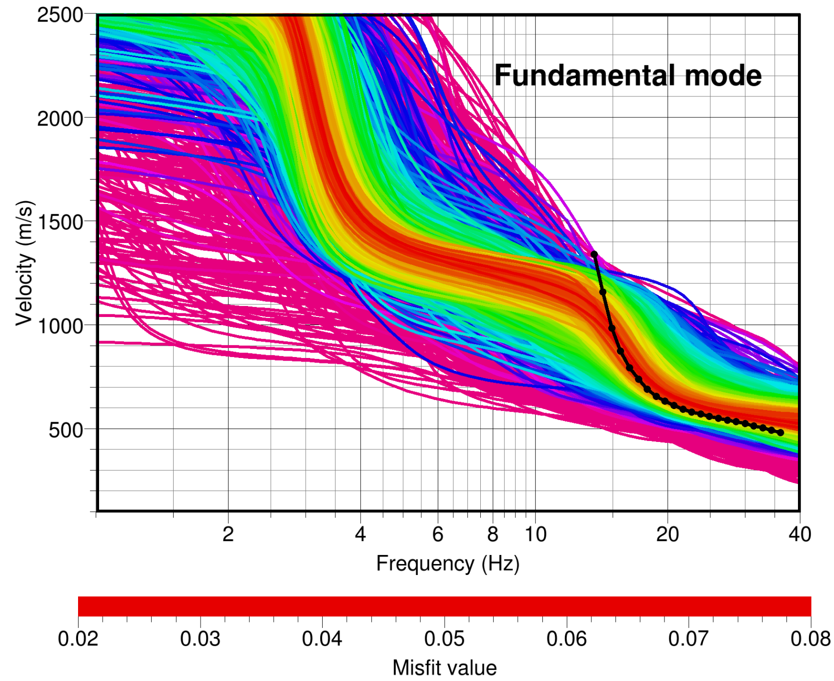

A)

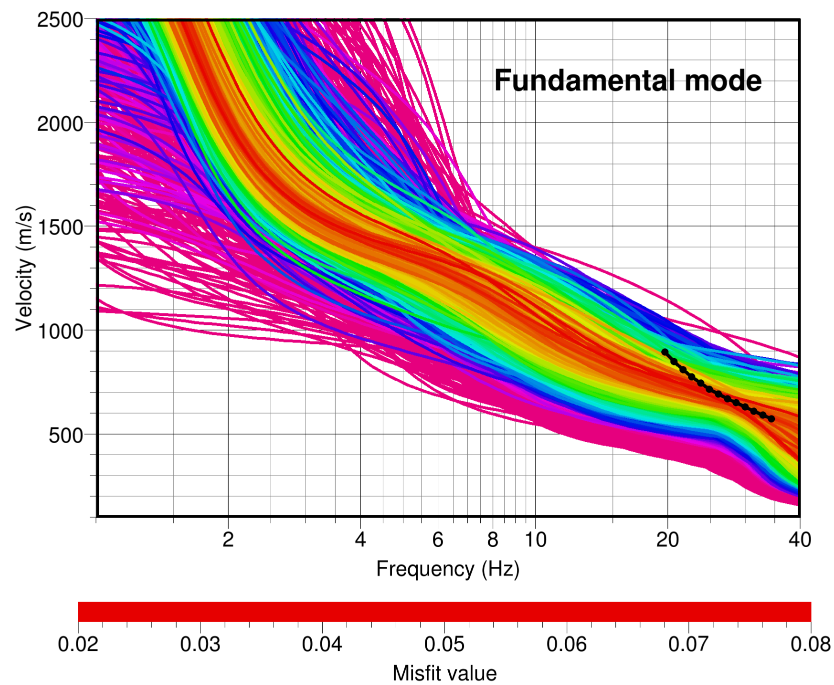

B)

Figure 15 - *Example of fitting the surface dispersion data within the global optimization procedure. Different colors represent different misfit between the observed (in black) and the modeled dispersion curves during the search (A, Rayleigh; B, Love).*

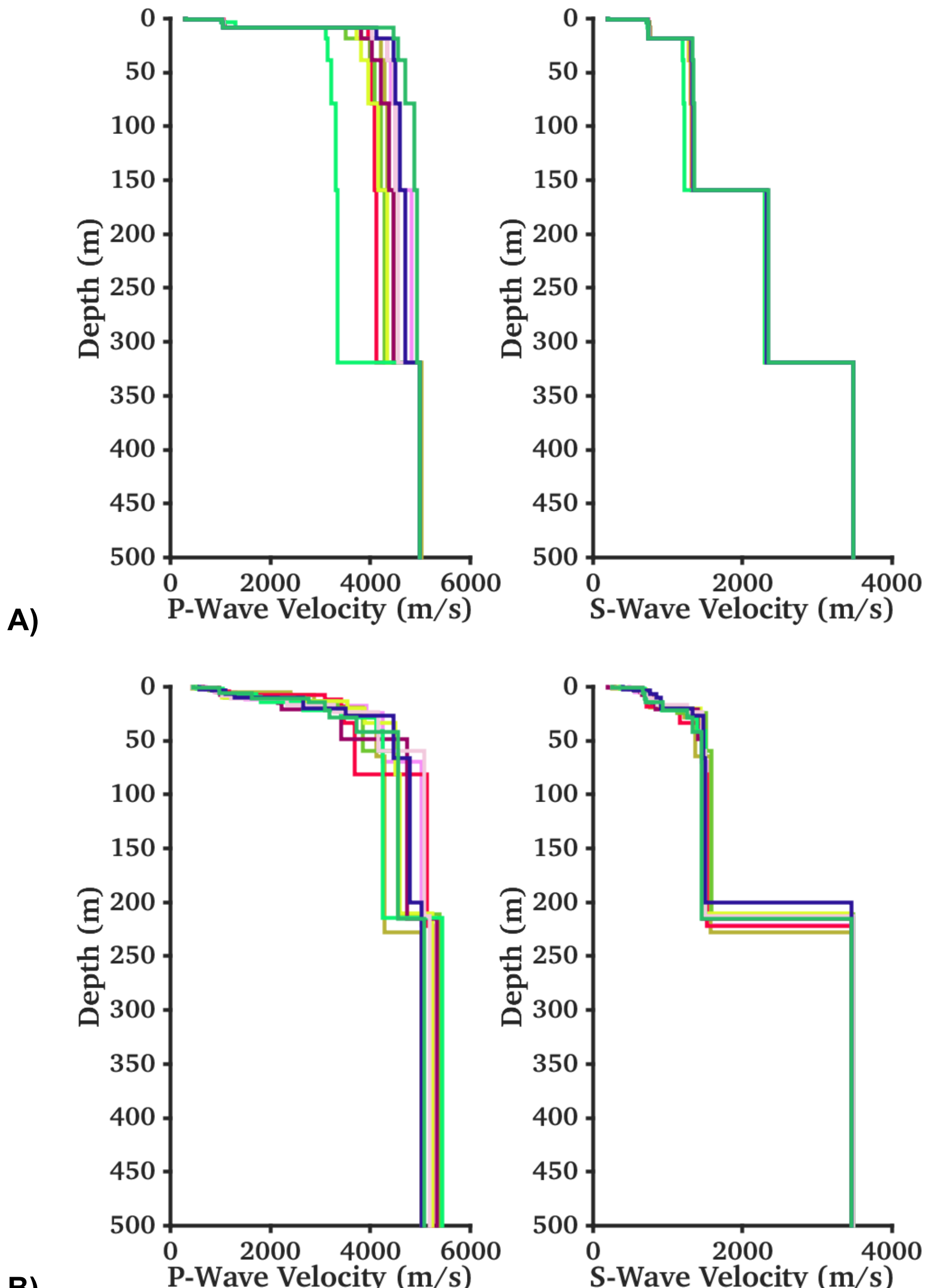

Figure 16 - *Collecting the best fitting models from the ten separated inversion runs using the free-layers (A, top) and fixed-layers (B, bottom) parameterization schemes.*

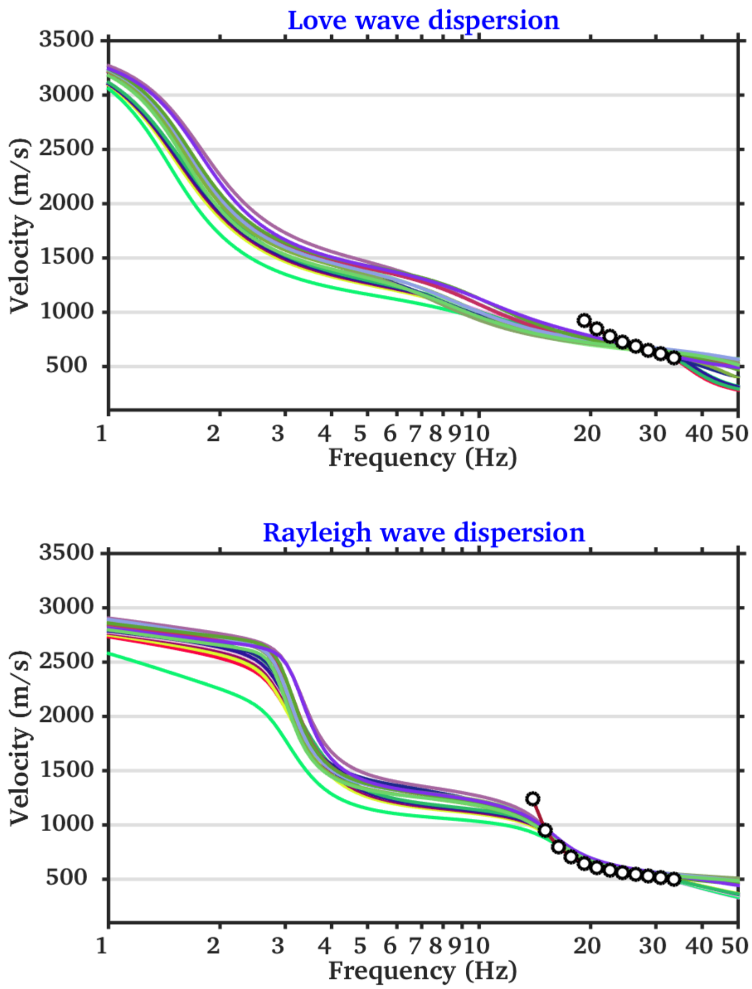

Figure 17 – *Rayleigh and Love dispersion curves computed from the 20 best fitting models of the two proposed interpretation schemes (free and fix layers).*

In more detail, the inverted velocity models (Vs and Vp) are gradient-like, with a faster increase in velocity in the first 100m, followed by a more regular part of nearly constant velocity. The large velocity contrast at about 200m (in the free layer approach) is constrained by the combined inversion with f_0 and the Rayleigh wave ellipticity right flank obtained from H/V spectral ratios (**Figure 18**). It is nevertheless interesting to notice that theoretical ellipticity match quite well the whole average H/V function, also at rather high frequencies.

By considering the minimum available frequency of the input data and by analyzing the scattering of the inverted models (**Figure 19**), it is realistic to assume the velocity profiles to be reliable down to a depth of about ~250m. Below this value no direct constrain is available from data, and the velocity values are obtained by pure extrapolation.

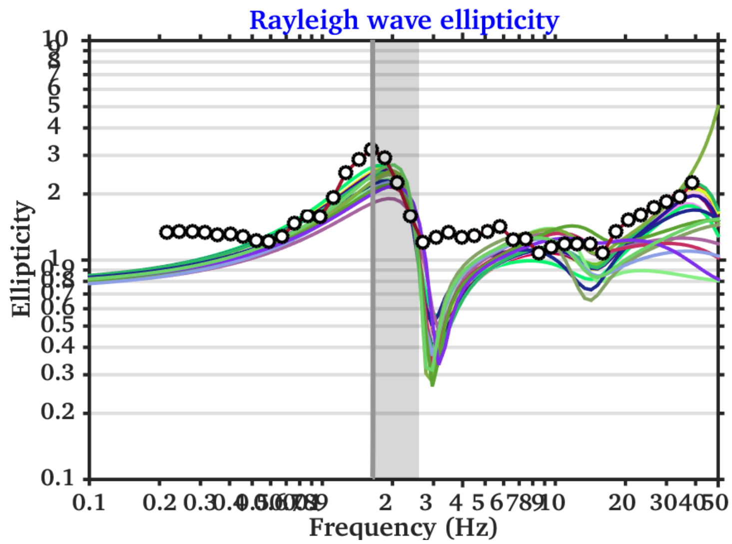

Figure 18 - *Rayleigh wave ellipticity curves computed from the best fitting models of the two proposed interpretation schemes (free and fixed layers), compared with average H/V spectral ratio from configuration R1 (scaled by sqrt(2)). Only the low frequency maximum (f_0) and the related right flank were used during the inversion.*

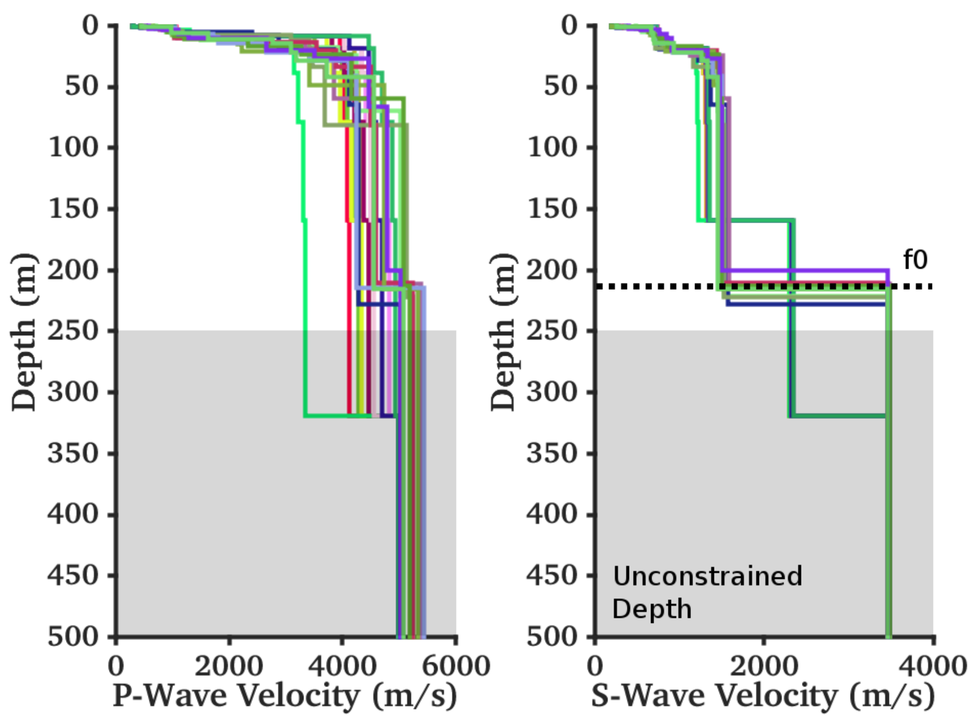

Figure 19 - *Comparison of all the best models from the two parameterization schemes (free and fixed layers). The two approaches produce consistent results. The depth of about 250m is considered approximately the maximum resolved depth.*

11. Engineering soil parameters

The ensemble of all the best inverted velocity profiles is then used to derive average soil parameters like the VsZ (average travel-time S-wave velocity over the depth Z, including Vs30, Table 1) and the quarter-wavelength (QWL) average velocities (Joyner et al., 1984) for a range of frequencies between 0.6 and 30Hz (**Figure 20**). The former is a standard parameter for the classification of ground-types in most building codes and in ground motion prediction equations. The latter is a parameter useful for the empirical estimation of the site-response and to assess the sensitivity of the seismic wave-field to the different depths. It has to be noticed that these two parameters are derived separately from all the best S-wave velocity models obtained from the inversion, and the results is finally averaged to improve statistics.

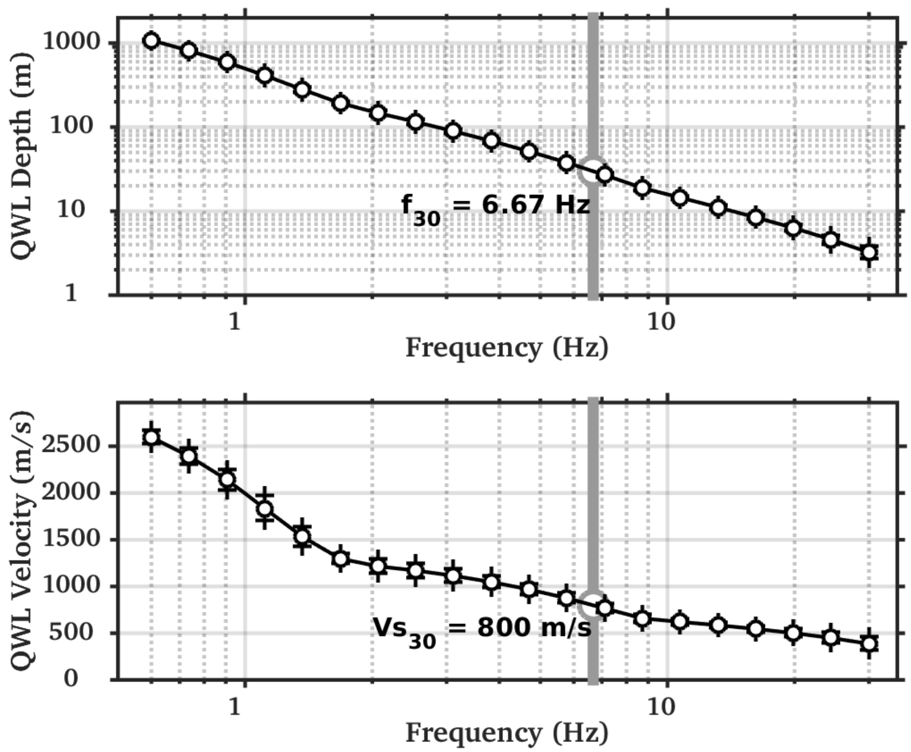

Figure 20 - *Quarter-wavelength representation of the inverted S-wave velocity profiles. Top: the depth-frequency dependency. Bottom: the QWL average velocity. The Vs30 value is indicated with its corresponding QWL frequency.*

Averaging depth (m)	Vs-mean (m/s)	St.Dev.
5.00	468.12	36.01
10.00	571.58	24.65
15.00	625.89	26.81
20.00	672.68	28.93
25.00	741.49	27.91
30.00	800.73	31.30
40.00	892.53	36.96
50.00	960.55	41.12
75.00	1071.72	50.56
100.00	1140.80	58.26
150.00	1220.08	68.98
200.00	1316.13	32.38

Table 1 - *Average travel-time velocities at different depths. Vs30 is highlighted.*

12. Amplification models

Site amplification functions have been computed using two different approaches: the S-wave transfer function for vertical propagation and the quarter-wavelength amplification. In general the first method is used to evaluate the resonance characteristics of the site, while the second is more useful to assess the effect of the velocity contrasts between the lowermost rock layer (as reference) and the different QWL averaging depths. The two amplification functions are then corrected for the Swiss rock reference velocity profile as defined in Poggi et al. (2011), according to the procedure described in Edwards et al. (2013). Given the lower velocities in the uppermost part of the EMMET profile compared to the Swiss reference, the final corrected amplification function shows a lower average amplification level at high frequencies than the uncorrected (**Figure 21**), while low frequency part is nearly asymptotic.

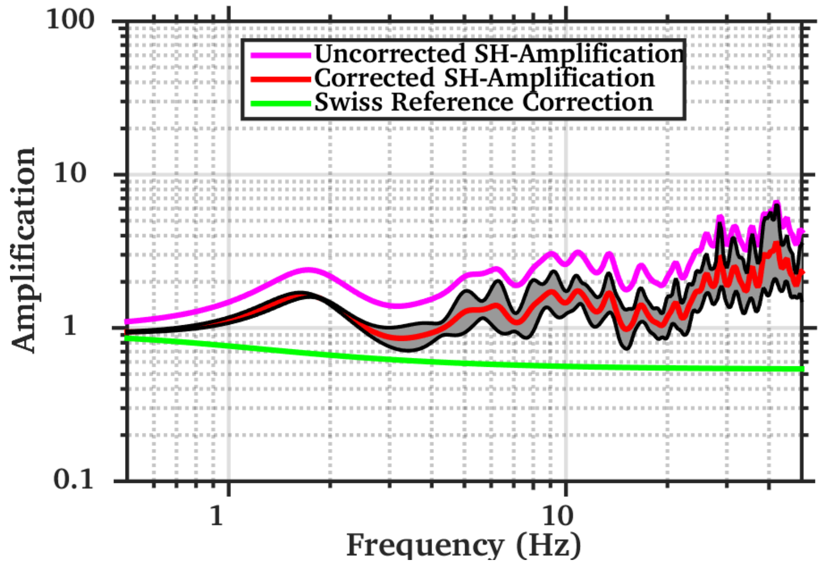

Figure 21 - *Correcting the SH-wave transfer function for the Swiss (rock) reference conditions (Poggi et al. 2011). The final corrected amplification function shows a lower (average) amplification at high frequencies than the uncorrected.*

Amplification functions using the transfer function and the quarter-wavelength approach are comparable (**Figure 22**), even if the transfer function provides a slightly larger amplification, because of the presence of some weak resonance peaks. At low frequencies both methods converge to the same average amplification level. It has to be notice that the amplification functions do not include attenuation at this stage of the analysis, as the quality factors of the site are too uncertain.

A good matching is obtained by comparison between the one-dimensional transfer function and the empirical amplification from spectral modeling of low-magnitude earthquakes as described in Edwards et al., 2013 (**Figure 23**). Resonance peaks are mostly well reproduces by analytical solution, even though empirical amplification presents a minor positive offset at low frequency, which cannot be explained by the available data.

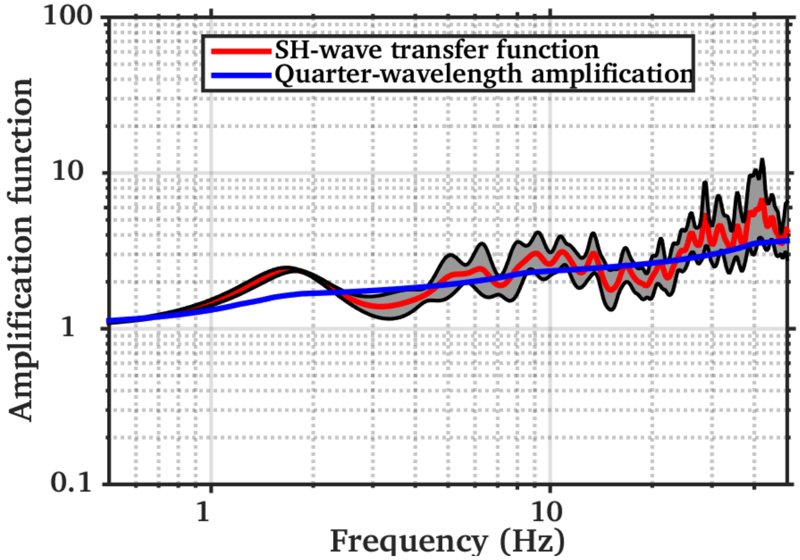

Figure 22 - *Comparison of amplification functions computed using the SH-wave transfer function and the quarter-wavelength formalism on the inverted velocity models.*

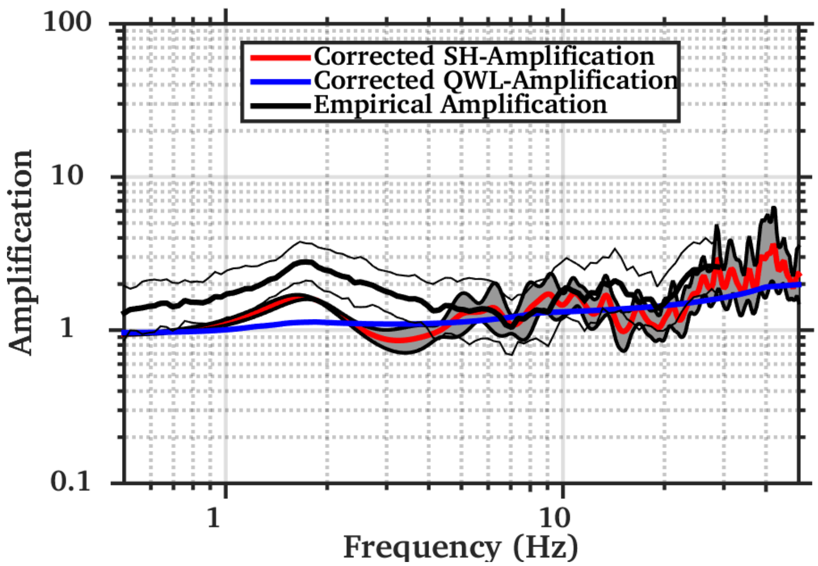

Figure 23 - *Comparison of amplification functions computed using the SH-wave transfer function and the quarter-wavelength approach with empirical observation from spectral modeling of low-magnitude earthquakes. All functions are referenced to the Swiss rock reference model (Poggi et al. 2011).*

REFERENCES

Capon, J., 1969. High resolution frequency wavenumber spectrum analysis, Proc. IEEE, 57, 1408-1418.

Burjanek, J., G. Stamm, V. Poggi, J.R. Moore, and D. Fäh [2010], “Ambient vibration analysis of an unstable mountain slope”, Geophys. J. Int., Vol. 180, pp. 820-828.

Edwards, B., C. Michel, V. Poggi and D. Fäh (2013). Determination of Site Amplification from Regional Seismicity: Application to the Swiss National Seismic Networks. Accepted for publication in Seismological Research Letters.

Joyner, W. B., R. E. Warrick and T. E. Fumal (1981). The Effect of Quaternary Alluvium on Strong Ground Motion in the Coyote Lake, California, Earthquake of 1979, Bulletin of the Seismological Society of America, 71, 1333-1349.

Poggi, V., B. Edwards and D. Fäh (2011). Derivation of a Reference Shear-Wave Velocity Model from Empirical Site Amplification, Bulletin of the Seismological Society of America, 101, 258-274.

Poggi, V. and Fäh D., 2010. Estimating Rayleigh wave particle motion from three-component array analysis of ambient vibrations. Geophys. J. Int., 180-1, 251-267.